

**Capture Solar Energy and Reduce Heat-Island Effect from Asphalt Pavement**

by

Bao-Liang Chen

A Dissertation

Submitted to the Faculty

of the

WORCESTER POLYTECHNIC INSTITUTE

in partial fulfillment of the requirements for the

Degree of Doctor of Philosophy

in

Civil Engineering

December 15, 2008

APPROVED:



Dr. Rajib B. Mallick, Associate Professor (Major Advisor)

Civil Engineering Department



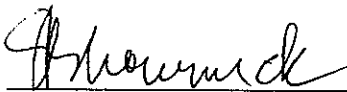
Dr. Tahar El-Korchi, Professor (Chair)

Civil Engineering Department



Dr. Mingjiang Tao, Assistant Professor

Civil Engineering Department



Dr. Sankha Bhowmick, Associate Professor

Mechanical Engineering Department, UMASS (Dartmouth)

## **ABSTRACT**

Asphalt pavements are made up of several layers of materials and different types of materials are being used as base courses in these pavements. The properties of these pavement layers are affected significantly by temperature, and all of the layers are made up of heterogeneous mixtures of a wide variety of materials whose thermal properties are not readily available. Therefore, laboratory experiments were carried out with samples of pavements with different base course materials to determine temperature profiles along the depth, and finite element analysis was used to backcalculate thermal properties of the materials in the different layers of the different samples.

The concept of extracting heat energy from asphalt pavements was evaluated by finite element modelling and testing small and large scale asphalt pavement samples. Water flowing through copper tubes inserted within asphalt pavements samples were used as heat exchangers in the experiments. The rise in temperature of water as a result of flow through the asphalt pavement was used as the indicator of efficiency of heat capture. The results of small scale testing show that the use of aggregates with high conductivity can significantly enhance the efficiency of heat capture. The efficiency can also be improved by using a reflectivity reducing and absorptivity increasing top layer over the pavement. Tests carried out with large scale slabs show that a larger surface area results in a higher amount of heat capture, and that the depth of heat exchanger is critical

Heat-Islands are formed as a result of construction that replaces vegetation with absorptive surfaces (asphalt pavement). One suggested method to reduce the emitted heat from asphalt pavement surfaces is to reduce the temperature of the surface by flowing a suitable fluid through the pavement. Laboratory experiments were carried out using hand-compacted hot mix asphalt samples with quartzite and metagranodiorite aggregates. Pipes with different surface area were used to flow water through the samples, and the processes were modeled using finite element method. The results clearly show the feasibility of the proposed method, and indicate the beneficial effects of higher thermal conductivity of aggregates and larger surface area of pipes.

## **DEDICATION**

This dissertation is dedicated to my parents

Mrs. Shu-Feng Chen

and

Mr. Matzuda Kazyuki

for giving me invaluable opportunities in life and for their inspiration, constant

encouragement and tremendous belief in me.

## **ACKNOWLEDGEMENTS**

I would like to express my profound gratitude to my advisor Dr. Rajib Basu Mallick for giving me the research opportunity and his thorough guidance and encouragement in every aspect of my research work.

I also thank my committee members Dr. Tahar El-Korchi, Dr. Mingjiang Tao, and Dr. Shnkha Bhowmick (University of Massachusette, Dartmouth) for their suggestions, comments, and assistances.

I would also like to thank Mr. Mike Hulen, President of Novotech Inc. Massachusetts Technology Collaborative Inc., and Faculty Advancement Research (FAR) for their funding supports, and Gerard Moulzolf of American Engineering Testing, Inc., for providing the most valuable information, and Mr. Ron Tardiff of Aggregate Industries and Mr. Jeff Carlstrom of New Ulm Quartzite Quarries for providing the samples.

Finally, this study would not have been possible without the laboratory and shop help from, Mr. Don Pellegrino, Mr. Dean Daigneault, Ms. Laura Rockett, Mr. Daniel Martel, Mr. Yanxuan Xiu, and Ms. Karen O’Sullivan of the Civil and Environmental Engineering department at Worcester Polytechnic Institute (WPI).

## TABLE OF CONTENTS

CHAPTER	PAGE
<b>1. INTRODUCTION</b>	<b>1</b>
1.1 Background	1
1.2 Objective of Research	2
1.3 Scope of Research	3
<b>2. LITERATURE REVIEW</b>	<b>4</b>
2.1 Prediction and validation of temperature at the surface and any depth of asphalt and concrete pavements	4
2.2 Evaluation of effect of temperature change on material properties, such as modulus	5
2.3 Modification of design procedures to consider the effect of temperature change on pavement material properties	5
2.4 Investigate the feasibility of using heat from solar heated asphalt pavements	11
2.5 Evaluation of Heat-Island Effect on reducing pavement temperature	11
2.6 Discussion	12
<b>3. HEAT TRANSFER</b>	<b>15</b>
3.1 Analytical Approach	15
3.2 Energy Balance of Asphalt Pavement	22
3.3 Finite Element Analysis Approach	26
<b>4. DETERMINE THERMAL PROPERTIES OF EXISTING ASPHALT PAVEMENT</b>	<b>30</b>
4.1 Introduction	30
4.2 Objective	30
4.3 Methodology	30
4.4 Laboratory Parameters Measurement	34
4.5 Experiment Results	39
4.6 Statistical Approach of Determining Temperature at Specific Location	46

<b>CHAPTER</b>	<b>PAGE</b>
4.7 Finite Element Analysis/Modeling	48
4.8 Discussion	56
<b>5. SMALL SCALE ASPHALT PAVEMENT TESTING</b>	<b>59</b>
5.1 Introduction	59
5.2 Objective	59
5.3 Methodology	59
5.4 Experiment Results	62
5.5 Robustness Test	80
5.6 Finite Element Analysis/Modeling	81
5.7 Discussion	87
<b>6. HAND-COMPACTED ASPHALT PAVEMENT TESTING</b>	<b>88</b>
6.1 Introduction	88
6.2 Objective	88
6.3 Methodology	88
6.4 Experiment Results	91
6.5 Finite Element Analysis/Modeling	94
6.6 Discussion	96
<b>7. DETERMINE EFFECTIVE PIPE LENGTH AND SPACING</b>	<b>97</b>
8.1 Introduction	97
6.2 Objective	97
6.3 Methodology	97
6.4 Experiment Results	100
6.5 Finite Element Analysis/Modeling	103
6.6 Discussion	107
<b>8. REDUCE URBAN HEAT-ISLAND EFFECT</b>	<b>108</b>
7.1 Introduction	108
7.2 Objective	108
7.3 Methodology	108
7.4 Experiment Results	110
7.5 Discussion	123

<b>CHAPTER</b>	<b>PAGE</b>
<b>9. LARGE SCALE ASPHALT PAVEMENT TESTING</b>	124
9.1 Introduction	124
9.2 Objective	127
9.3 Methodology	127
9.4 Experiment Results	129
9.5 Finite Element Analysis/Modeling	140
9.6 Discussion	150
<b>10. CONCLUSION</b>	151
<b>11. FUTURE STUDY RECOMMENDATION</b>	153
11.1 What is the effect of water outlet temperature by using different pipe materials?	153
11.2 How to increase the water temperature to meet the minimum temperature requirement of turbine to generate electric?	153
11.3 How much pavement life can be extended by using asphalt pavement as solar collector?	154
<b>12. REFERENCE</b>	156
<b>APPENDIX</b>	
<b>A SIX HIGHTWAY PAVEMENT THERMOCOUPLE</b>	160
<b>B DETERMINE THMERAL PROPERTIES OF R, P401, M, AND FR SAMPLES</b>	163
<b>C EXPERIMENT SETUP FOR EACH SCENARIO</b>	173
<b>D DETERMINE THERMAL PROPERTIES OF QUARTZITE , LIMESTONE, AND METAGRANODIORTE (SMALL SCALE)</b>	177
<b>E LARGE SCALE PAVEMENT PREPARATION</b>	183
<b>F SKETCH AND DIMENSION OF HAND-COMPACTED SAMPLES</b>	187
<b>G DETERMINE THERMAL PROPERTIES OF METAGRANODIORITE AND QUARTZITE (HAND-COMPACTED)</b>	190

## LIST OF TABLES

<b>TABLE</b>	<b>PAGE</b>
4-1 Types of pavements considered	32
4-2 Measured heat parameters	37
4-3 Measured emissivity values	38
4-4 G Sample - Highway-HMA layers over HMA base with different NMAS	39
4-5 S Sample -HMA layers over PMRAP base	40
4-6 M Sample- HMA layers over Foamed Asphalt base	41
4-7 R Sample- HMA layers over cement treated base	42
4-8 P401 Sample- HMA layers of same NMAS	43
4-9 FR Sample- HMA layers of different types two lifts	44
4-10 Equation from statistical analysis	47
4-11 Back-calculated thermal conductivity and heat capacity values	57
5-1 Quartzite and Limestone mix temperature difference	63
5-2 Quartzite mix with and without placement of tinted glass temperature difference	63
5-3 100% Quartzite with iced water (3mL/min) temperature difference	64
5-4 100% Quartzite mix with trapped iced water inside of cooper pipe temperature difference	64
5-5 Complied of 5 quartzite samples with 0.01905m (3/4") copper pipe temperature difference	64
5-6 100% Quartzite mix temperature difference	67
5-7 100% Metagranodiorite mix temperature difference	67
5-8 100% RAP mix temperature difference	67
5-9 Quartzite with 22% copper mix temperature difference	70
5-10 Quartzite with 30% aluminum mix temperature difference	70
5-11 Quartzite with 50% RAP mix temperature difference	72
5-12 Quartzite with 75% RAP mix temperature difference	72
5-13 67% quartzite with 33% limestone mix temperature difference	72
5-14 Tinted glass on the surface of quartzite with 22% copper mix temperature difference	75



<b>TABLE</b>	<b>PAGE</b>
5-15 Acrylic paint on the surface of quartzite with 22% copper mix temperature difference	75
5-16 Tinted glass on the surface of quartzite with 30% aluminum mix temperature difference	76
5-17 Chipped glass with asphalt mix on the quartzite with 30% aluminum mix temperature difference	76
5-18 Repetitive test of 67% quartzite and 33% limestone mix	80
5-19 Thermal properties of quartzite and limestone sample mix (Appendix D)	81
5-20 Thermal properties of quartzite and metagranodiorite mix (Appendix D)	86
6-1 Description of compacted samples (Appendix E)	89
6-2 Temperature difference at time= 60 minutes (Lab Data); water flowing at 10 ml/minute	92
6-3 Temperature difference at time= 180 minutes (Lab Data)	93
6-4 Quartzite mix back-calculated thermal properties	94
6-5 Metagranodiorite mix back-calculated thermal properties	94
6-6 Laboratory and FE temperature difference at time = 60 minutes comparison	95
6-7 Laboratory and FE temperature difference at time = 180 minutes comparison	95
7-1 The typical Nusselt number for fully developed flow	98
7-2 Required pipe length at wall temperature= 50 °C	98
7-3 Average water temperature difference at time= 60 minutes	101
7-4 Average water temperature difference at time= 180 minutes	102
7-5 Water temperature comparison	107
8-1 Average Reduction in surface temperature due to flowing water	118
9-1 Metagranodiorite slab water temperature (all pipe open)	132
9-2 Quartzite slab water temperature (all pipe open)	133
9-3 Quartzite slab temperature profile with 1L/min (1 pipe)	134
9-4 Quartzite slab temperature profile with 2L/min (1 pipe)	135
9-5 Quartzite slab temperature profile with 3L/min (1 pipe)	136

<b>TABLE</b>	<b>PAGE</b>
9-6 Quartzite slab temperature profile with 4L/min (1 pipe)	137
9-7 Quartzite slab temperature profile with 1L/min (2 pipes open)	138
9-8 Thermal conductivity and heat capacity of two slab mix	142
9-9 Quartzite slab 1L/min (35mins)	145
9-10 Quartzite slab 2L/min (35mins)	146
9-11 Quartzite slab 3L/min (36mins)	147
9-12 Quartzite slab 4L/min (15mins)	148

## LIST OF FIGURES

FIGURE	PAGE
2-1 Energy balance on asphalt surface	6
3-1 Energy balance on the surface of a grey body	22
4-1 Six existing highway samples	33
4-2 Laboratory testing setup	34
4-3 Location of thermocouples in different samples	35
4-4 Halogen lamp heat radiation measurement	36
4-5 Laboratory testing setup with fan and anemometer	37
4-6 G Sample temperature distribution (7-days cycle)	39
4-7 S Sample temperature distribution (7-days cycle)	40
4-8 M Sample temperature distribution (7-days cycle)	41
4-9 R Sample temperature distribution (7-days cycle)	42
4-10 P401 Sample temperature distribution (7-days cycle)	43
4-11 FR Sample temperature distribution (7-days cycle)	44
4-12 6 Samples temperature distribution at end of 7 <sup>th</sup> heating cycle	45
4-13 Mesh generated from COMSOL	49
4-14 COMSOL simulation result	49
4-15 G sample temperature at T2 (finite element predicted vs. laboratory results)	51
4-16 G sample temperature at T3 (finite element predicted vs. laboratory results)	51
4-17 G sample temperature at T4 (finite element predicted vs. laboratory results)	52
4-18 G sample temperature at T5 (finite element predicted vs. laboratory results)	52
4-19 G sample temperature at T6 (finite element predicted vs. laboratory results)	53
4-20 S sample temperature at T2 (finite element predicted vs. laboratory results)	53

<b>FIGURE</b>	<b>PAGE</b>
4-21 S sample temperature at T3 (finite element predicted vs. laboratory results)	54
4-22 S sample temperature at T4 (finite element predicted vs. laboratory results)	54
4-23 S sample temperature at T5 (finite element predicted vs. laboratory results)	55
4-24 S sample temperature at T6 (finite element predicted vs. laboratory results)	55
5-1 Small scale testing (Scenario I) temperature difference $\Delta T$	63
5-2 Small scale testing (Scenario II) temperature difference $\Delta T$	65
5-3 Small scale testing (Scenario II) power generated	65
5-4 Typical asphalt sample with thermocouples	66
5-5 Small scale testing (Scenario III) temperature vs. flow rate	68
5-6 Small scale testing (Scenario III) temperature difference $\Delta T$	69
5-7 Small scale testing (Scenario III) power generated	69
5-8 Small scale testing (Scenario VI) effect of copper powder	71
5-9 Small scale testing (Scenario VI) effect of aluminum powder	71
5-10 Small scale testing (Scenario VI) temperature vs. flow rate	73
5-11 Small scale testing (Scenario VI) temperature difference $\Delta T$	74
5-12 Small scale testing (Scenario VI) power generated	74
5-13 Small scale testing (Scenario VI) temperature vs. flow rate	76
5-14 Small scale testing (Scenario V) temperature difference $\Delta T$	77
5-15 Small scale testing (Scenario V) power generated	77
5-16 Effective of Acrylic Paint	78
5-17 Small scale testing temperature difference $\Delta T$	79
5-18 5-days repetitive test of 67% quartzite and 33% limestone mix	80
5-19 Steady-state finite element model	82
5-20 Transient finite element model	82
5-21 Water temperature distribution along the length of copper pipe (Quartzite)	84

<b>FIGURE</b>	<b>PAGE</b>
5-22 Water temperature distribution along the length of copper pipe (Metagranodiorite)	84
5-23 Water temperature distribution along the depth of copper pipe (Quartzite)	85
5-24 Water temperature distribution along the depth of copper pipe (Metagranodiorite)	85
5-25 Quartzite mix temperature profile	86
6-1 Copper pipe with 6 rings	90
6-2 Placed thermocouples on top layer	90
6-3 Drilled vs. compacted sample temperature distribution	91
6-4 Average water temperature difference at time = 60 minutes	92
6-5 Average water temperature difference at time = 180 minutes	93
7-1 Effective pipe diameter, length, and flow rate chart	99
7-2 Serpentine pipe being placed and compacted	100
7-3 Average water temperature difference at time = 60 minutes	101
7-4 Average water temperature difference at time = 180 minutes	102
7-5 Temperature variation between two pipes	103
7-6 Finite element model for temperature variation between various pipe spacing	104
7-7 Straight pipe 0.1524m (6") (temperature distribution)	105
7-8 Serpentine pipe 0.3556m (14") (temperature distribution)	105
7-9 Serpentine pipe 0.7112m (28") (temperature distribution)	106
8-1 Samples with three thermocouples	110
8-2 Quartzite and metagranodiorite mixes for 8 hour heating and 8 hour no heating data for surface temperature (T2 thermocouple)	111
8-3 Heating with water flow data for surface temperature (T2 thermocouple) for quartzite and metagranodiorite mixes	112
8-4 Schematic of thermocouple locations on the surface of asphalt sample	113
8-5 Thermocouple locations on the surface of asphalt sample	113
8-6 Plot of time versus temperature (T1)	114
8-7 Plot of time versus temperature (T2)	115

<b>FIGURE</b>	<b>PAGE</b>
8-8 Plot of time versus temperature (T3)	115
8-9 Plot of time versus temperature (T4)	116
8-10 Plot of time versus temperature (T5)	116
8-11 Plot of time versus temperature (T6)	117
8-12 Plot of time versus temperature (T7)	117
8-13 Serpentine pipe in a sample (during compaction)	119
8-14 Plot of time versus temperature (T1)	119
8-15 Plot of time versus temperature (T2)	120
8-16 Plot of time versus temperature (T3)	120
8-17 Plot of time versus temperature (T4)	121
8-18 Plot of time versus temperature (T5)	121
8-19 Plot of time versus temperature (T6)	122
8-20 Plot of time versus temperature (T7)	122
9-1 Schematics of slab with thermocouple, copper pipes, and water flow direction	125
9-2 Dimension of slab and copper frame	125
9-3 Metagranodiorite mix slab thermocouple location	126
9-4 Quartzite mix slab thermocouple location	126
9-5 Two slabs tests under the real environmental conditions	128
9-6 Metagranodiorite mix slab temperature profile	129
9-7 Quartzite mix slab temperature profile	130
9-8 Metagranodiorite slab thermocouple locations	131
9-9 Water temperature measured at 3ft pipe outlet for both slabs	132
9-10 Water temperature measured at 6ft pipe outlet for both slabs	133
9-11 Quartzite mix slab temperature profile (1L/min)	134
9-12 Quartzite mix slab temperature profile (2L/min)	135
9-13 Quartzite mix slab temperature profile (3L/min)	136
9-14 Quartzite mix slab temperature profile (4L/min)	137
9-15 Quartzite mix slab temperature profile (1L/min at 2 3ft pipes)	138
9-16 Quartzite slab temperature profile (1 pipe with 1L/min)	139

<b>FIGURE</b>	<b>PAGE</b>
9-17 Quartzite slab temperature profile (2 pipe s with 1L/min)	139
9-18 Solar Radiation	140
9-19 Finite element mesh model	141
9-20 Finite element model of heating period	141
9-21 Quartzite slab temperature profile of heat-up period	142
9-22 Finite element model with various water flow rates	143
9-23 Finite element mesh model	143
9-24 Water temperature distribution along the length of copper pipe	144
9-25 Water temperature distribution along the depth of copper pipe	144
9-26 Quartzite slab temperature profile 1L/min (laboratory vs. finite element analysis)	145
9-27 Quartzite slab temperature profile 2L/min (laboratory vs. finite element analysis)	146
9-28 Quartzite slab temperature profile 3 L/min (laboratory vs. finite element analysis)	147
9-29 Quartzite slab temperature profile 4L/min (laboratory vs. finite element analysis)	148
9-30 Quartzite slab water temperature at various water flow rate (laboratory vs. finite element analysis)	149
11-1 Extended service life of pavement by reducing pavement temperature	155
A-1 G Sample - Highway-HMA layers over HMA base with different NMAS	160
A-2 S Sample -HMA layers over PMRAP base	160
A-3 M Sample- HMA layers over Foamed Asphalt base	161
A-4 R Sample- HMA layers over cement treated base	161
A-5 P401 Sample- HMA layers of same NMAS	162
A-6 FR Sample- HMA layers of different types two lifts	162
B-1 R sample temperature at T2 (finite element predicted vs. laboratory results)	163
B-2 R sample temperature at T3 (finite element predicted vs. laboratory results)	163

<b>FIGURE</b>	<b>PAGE</b>
B-3 R sample temperature at T4 (finite element predicted vs. laboratory results)	164
B-4 R sample temperature at T5 (finite element predicted vs. laboratory results)	164
B-5 R sample temperature at T6 (finite element predicted vs. laboratory results)	165
B-6 P401 sample temperature at T2 (finite element predicted vs. laboratory results)	165
B-7 P401 sample temperature at T3 (finite element predicted vs. laboratory results)	166
B-8 P401 sample temperature at T4 (finite element predicted vs. laboratory results)	166
B-9 P401 sample temperature at T5 (finite element predicted vs. laboratory results)	167
B-10 P401 sample temperature at T6 (finite element predicted vs. laboratory results)	167
B-11 M sample temperature at T2 (finite element predicted vs. laboratory results)	168
B-12 M sample temperature at T3 (finite element predicted vs. laboratory results)	168
B-13 M sample temperature at T4 (finite element predicted vs. laboratory results)	169
B-14 M sample temperature at T5 (finite element predicted vs. laboratory results)	169
B-15 M sample temperature at T6 (finite element predicted vs. laboratory results)	170
B-16 FR sample temperature at T2 (finite element predicted vs. laboratory results)	170
B-17 FR sample temperature at T3 (finite element predicted vs. laboratory results)	171



<b>FIGURE</b>	<b>PAGE</b>
B-18 FR sample temperature at T4 (finite element predicted vs. laboratory results)	171
B-19 FR sample temperature at T5 (finite element predicted vs. laboratory results)	172
B-20 FR sample temperature at T6 (finite element predicted vs. laboratory results)	172
C-1 Steady-state setup	173
C-2 Steady-state setup with halogen lamp on	173
C-3 Complied 5 asphalt pavement testing	174
C-4 Complied 5 asphalt pavements testing without halogen lamp on	174
C-5 Transient testing setup	175
C-6 Glass chips-Asphalt mix placed on top of asphalt sample	175
C-7 Tinted glass placed on top of asphalt sample	176
D-1 Quartzite sample temperature at T2 (finite element predicted vs. laboratory results)	177
D-2 Quartzite sample temperature at T3 (finite element predicted vs. laboratory results)	177
D-3 Quartzite sample temperature at T4 (finite element predicted vs. laboratory results)	178
D-4 Quartzite sample temperature at T5 (finite element predicted vs. laboratory results)	178
D-5 Limestone sample temperature at T3 (finite element predicted vs. laboratory results)	179
D-6 Limestone sample temperature at T4 (finite element predicted vs. laboratory results)	179
D-7 Limestone sample temperature at T5 (finite element predicted vs. laboratory results)	180
D-8 Metagranodiorite sample temperature at T2 (finite element predicted vs. laboratory results)	180

<b>FIGURE</b>	<b>PAGE</b>
D-9 Metagranodiorite sample temperature at T3 (finite element predicted vs. laboratory results)	181
D-10 Metagranodiorite sample temperature at T4 (finite element predicted vs. laboratory results)	181
D-11 Metagranodiorite sample temperature at T5 (finite element predicted vs. laboratory results)	182
E-1 100% Metagranodiorite mix	183
E-2 100% Quartzite mix	183
E-3 50% Quartzite on the top and 50% Metagranodiorite on the bottom	184
E-4 35% Metagranodiorite on the top, 30% quartzite in the center layer, and 35% Metagranodiorite on the bottom	184
E-5 100% Metagranodiorite mix with Portland cement placed around copper pipe	185
E-6 100% Quartzite mix with a copper pipe consists 6 rings	185
E-7 100% Quartzite mix with a rough surface copper pipe	186
F-1 Metagranodiorite sample temperature at T2 (finite element predicted vs. laboratory results)	187
F-2 Metagranodiorite sample temperature at T6 (finite element predicted vs. laboratory results)	187
F-3 Metagranodiorite sample temperature at T7 (finite element predicted vs. laboratory results)	188
F-4 Quartzite sample temperature at T4 (finite element predicted vs. laboratory results)	188
F-5 Quartzite sample temperature at T6 (finite element predicted vs. laboratory results)	189
F-6 Quartzite sample temperature at T7 (finite element predicted vs. laboratory results)	189
G-1 Cart with thermocouple at the bottom	190
G-2 Lay down of mix	190
G-3 Compaction	191

<b>FIGURE</b>		<b>PAGE</b>
G-4	Fixing thermocouples	191
G-5	Copper pipe frame	192
G-6	Close-up of slab showing copper tube and thermocouples at different depths	192
G-7	Completed slab ready for testing	193

# CHAPTER 1

## INTRODUCTION

### 1.1 Background

Asphalt pavements consist 95% of major roadway in the United States, and their performance and longevity are greatly affected by the change of temperature. Research has shown that there is a temperature distribution inside asphalt pavements, in the different layers, which are in many cases made up of different materials. The temperature distribution along the depth actually depends on the properties of these different layers – the temperature at any layer is affected significantly by the thermal properties of the layers above and below it. Thus, the temperature distribution in a full depth asphalt pavement will be different from, for example, an asphalt pavement with an aggregate base, even though the asphalt mixtures/materials in the two pavements are the same. This is of practical significance considering the wide variety of materials that are currently being used as base material in both highway and airfield pavements.

The sun provides a cheap and abundant source of clean and renewable energy. Solar cells have been used to capture this energy and generate electricity. A useful form of “cell” could be asphalt pavements, which get heated up by solar radiation. The “road” energy solar cell concept takes advantage of a massive acreage of installed parking lots, tarmacs and roadways.

The heat retained in the asphalt mixture can continue to produce energy after nightfall when traditional solar cells do not function. The idea of capturing energy from pavement not only turns areas such as parking lots into an energy source, but also could cool the asphalt pavements, thus reducing the Urban Heat-Island Effect.

The significance of this concept lies in the fact that the massive installed base of parking lots and roadways creates a low cost solar collector an order of magnitude more productive than traditional solar cells. The significantly high surface area can offset the expected lower efficiency (compared to traditional solar cells) by several orders of magnitude, and hence result in significantly lower cost per unit of power produced.

The system uses an existing lot, so does not require purchase or lease of new real estate (as would be needed for a solar “farm” installation). The system has no visible signature — that is, the parking lot looks the same. This compares well against rooftop silicon panels that are often bulky and unattractive. The fact that roads and parking lots are resurfaced on a 10-12 year cycle could be a good selling point for the road energy system - any time the pavement is replaced, the energy system can be installed.

The captured energy from heated asphalt pavements can be used for relatively simple applications, such as heating of water, to sophisticated applications, such as generating electricity through thermoelectric generators. In addition, the benefit of lower asphalt pavement temperature can also reduce Urban Heat-Island Effect to improve the human comfort level in the major cities.

## **1.2 Objective of Research**

The objectives of this research were to:

1. Investigate the temperature distribution along the depth of asphalt pavements with laboratory experiments.
2. Build statistical models to predict the temperature in different base layers.
3. Model the temperature distribution, using principles of heat transfer in different pavements and determine appropriate values of thermal properties of the different layers
4. Investigate the feasibility of enhancing the amount and rate of flow of heat energy from heated asphalt pavements by using appropriate primary construction materials, additives, and modification of top layer of the pavement.
5. Use theoretical approach to develop a relationship among flow rate, pipe diameter, and pipe length.
6. Investigate different pipe geometries to increase heat transfer from asphalt pavement to water.
7. Investigate the possibility of reducing Urban Heat-Island Effect.

### 1.3 Scope of Research

The scope of this research consists of

1. Performing a series of literature review on prediction of asphalt pavement temperature, extraction of heat energy from asphalt pavement, and reducing Urban Heat-Island Effect by lowering asphalt pavement temperature.
2. Determining thermal properties of the existing highway and airport samples with different materials layers.
3. Developing the statistical models to predict the temperature relationship of 1-inch above surface, surface, and 1-inch below surface for six existing highway and airport samples.
4. Evaluating the heat energy transfer of different small scale asphalt mix samples with high conductive fillers, aggregates, and modified surface conditions.
5. Evaluating the heat energy transfer ability by using different asphalt mix layers and copper pipe layouts, and increase contact of asphalt mix and copper pipe in hand-compacted asphalt samples.
6. Determining the effective copper pipe length, spacing, and water flow rate for asphalt solar collector systems by using analytical approach.
7. Evaluating the feasibility of reducing Urban Heat-Island Effect by using higher thermal conductivity aggregate and different pipe layouts.
8. Evaluating the feasibility of heat energy transfer by performing field tests with two large scale asphalt pavements.
9. Analyzing and evaluating the experiment data with backcalculated thermal properties from finite element analysis, and determine the effect of thermal conductivity, asphalt composition, pipe layout, and water flow rate.

## **CHAPTER 2**

### **LITERATURE REVIEW**

Studies have been carried out on different aspects of temperature change and its effect on pavements. These studies can be broadly classified into five types: 1. Prediction and validation of temperature at the surface and any depth of asphalt and concrete pavements; 2. Evaluation of effect of temperature change on material properties, such as modulus; 3. Modification of design procedures to consider the effect of temperature change on pavement material properties; 4. Investigation of the feasibility of using heat from solar heated asphalt pavements. 5. Evaluation of Urban Heat-Island Effect on reducing pavement temperature.

Since the focus of this study is on topics 1, 4, and 5, the literature review will be restricted to that pertinent topics only.

#### **2.1 Prediction and validation of temperature at the surface and any depth of asphalt and concrete pavements**

The earliest published work is that by Southgate (1) who presented a method for predicting temperatures in asphalt pavement layers, as a function of depth, time of the day, and the 5-day mean air temperature.

Hermansson (2) presented a procedure based on finite difference procedure to determine pavement temperatures. This procedure estimates pavement temperatures at different depths using formulas that consider convection, short and long-wave radiation, and a finite difference approximation for the calculation of heat transfer into the pavement through the subsurface layers. For calculating heat transfer, the pavement is divided into cells, each of which is assigned a different value for temperature, porosity and degree of saturation. The proposed model can, according to comparisons with field experiments, calculate temperatures of pavement at different depths during summer days using hourly solar radiation, air temperature and wind velocity as weather input. The model proved to be accurate, having errors around 2°C for different parameters.

## **2.2 Evaluation of effect of temperature change on material properties, such as modulus**

In their study on asphalt pavement layer temperature prediction, Park, Dong-Yeob, et al. (3) collected a large amount of temperate data and deflection profiles from various sites in Michigan to investigate how temperature affects the in-place strength of asphalt mixes. The goal was to develop a model that could cover all seasons and various climatic and geographic regions. Previous methods have utilized temperature data from 5 days and did not take into consideration temperature gradients due to heating and cooling cycles. Results yielded the following temperature model, which was validated by using data from other sites, proving the model is applicable to various regions ( $z$  = pavement depth,  $t$  = time).

$$T_s = T_{suf} + (-0.3451z - 0.0432z^2 + 0.00196z^3) \times \sin(-6.3252t + 5.0967)$$

A correction factor was calculated for the asphalt mix layer modulus to correct for the difference between predicted and actual temperatures at the mid-depth of the pavement. The measured and predicted temperature values were consistent, meaning that the temperature prediction model and correction procedures were valid. Using prediction of rutting, the effects of error between the calculated and measured temperatures were determined to be very minimal. The newly formed temperature model accounted for temperature gradients, which varied depending on the time of day due to the heating and cooling cycle.

## **2.3 Modification of design procedures to consider the effect of temperature change on pavement material properties**

Yavuzturk et al (4) presented the results of a study on the use of finite difference method to predict pavement temperature. They mention that thermal conditions which pavements are exposed to greatly affect the performance and longevity of the pavement, and current models to predict temperature gradient could be inaccurate because they fail to account for the thermal history and thermal interaction between asphalt of varying grades and contents. This paper proposes a new method to predict pavement temperatures at various depths and horizontal locations using a transient, two-dimensional finite-



difference model of a pavement section. Figure 2-1 shows the primary modes of heat transfer that have been considered in a pavement. Sensitivity analyses were conducted in order to assess the dependency of the predicted temperature on the thermal properties.

The highest discrepancy occurred at the pavement's surface because of more heat dissipation as it is exposed to open air. The longer the asphalt section, the more heat is transferred from it because the wind over the surface in longer segments is more likely to assume a turbulent fluid flow regime, allowing for lower temperatures because of increased cooling from heat transfer. Temperature difference ranges were found to be much larger in the summer than in the winter. Temperature predictions using the proposed model were most sensitive to (in decreasing order) variations in absorptivity, volumetric specific heat capacity, emissivity, and thermal conductivity of the mix. They conclude that further work could be done on bridge segments as the bridge deck does not allow for an adiabatic boundary causing a cooling convection from underneath.

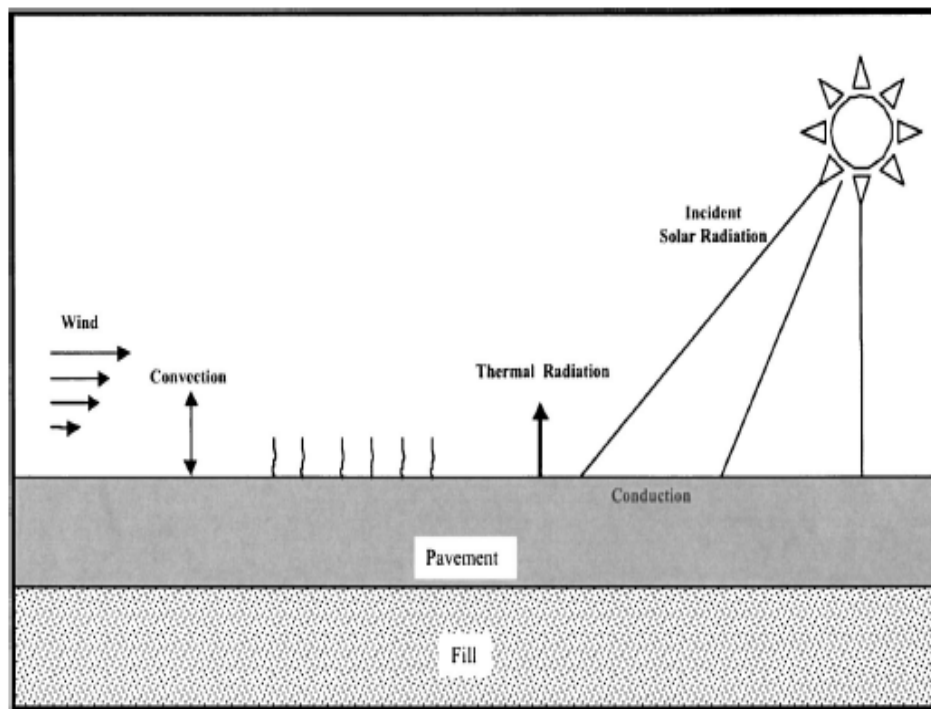


**Figure 2-1 Energy balance on asphalt surface**

Currently, the most widely cited temperature prediction equations for asphalt pavements are those based on the work by Solaimanian and Kennedy (5) and from SHRP and LTPP studies (6, 7). Solaimanian and Kennedy developed a method to be used mainly for Strategic Highway Research Program binder and mixture specifications to calculate the maximum pavement temperature profile. The method was based on energy balance and temperature equilibrium at the pavement surface by using the measured data of hourly solar radiation, wind velocity, and emissivity from various test locations. The proposed equation was able to predict the maximum pavement temperature at specific location within 3 °C error, which was within the reasonable limit- considering various environmental factors and measurement uncertainty.

SHRP high temperature model equations for Superpave Mixes are:

$$T_{surf} = T_{air} - 0.00618lat^2 + 0.2289lat + 24.4$$

$$T_{(depth,in)} = T_{(surf)}(1 - 0.063d + 0.007d^2 - 0.0004d^3)$$

$$T_{20mm} = (T_{air} - 0.00618lat^2 + 0.2289lat + 42.4)(0.9545) - 17.78$$

LTPP high temperature model equations are:

$$T_{pav} = 54.32 + 0.78T_{air} - 0.0025lat^2 - 15.14 \log_{10}(H + 25) + z(9 + 0.61S_{air}^2)^{0.5}$$

Where  $T_{pav}$  is high asphalt pavement temperature below surface (°C);  $T_{air}$  is high air temperature (°C);  $lat$  is latitude of the section (degrees);  $H$  is depth to surface (mm);  $S_{air}$  is standard deviation of the high 7-day mean air temperature (°C);  $z$  is Standard normal dist. table,  $z$  is 2.055 for 98% reliability Statistics:  $R^2 = 76\%$ ,  $N = 309$ ,  $SEE = 3.0$ .

SHRP low temperature model equations are:

$$T_{(d,mm)} = T_{(surf)} + 0.51d - 0.000063d^2$$

50% reliability:  $T_{pav} = T(d) - z \times S_{air}$

Where  $T_{pav}$  is low asphalt pavement temperature with reliability ( $^{\circ}\text{C}$ );  $T_{(d)}$  is Low asphalt pavement temperature at calculated depth ( $^{\circ}\text{C}$ );  $S_{air}$  is Standard deviation of the low air temperature ( $^{\circ}\text{C}$ );  $z$  is standard normal dist. table,  $z = 2.055$  for 98% reliability.

LTTP low temperature model equations are:

$$T_{pav} = -1.56 + 0.72T_{air} - 0.004lat^2 + 6.26\log_{10}(H + 25) - z(4.4 + 0.52S_{air}^2)^{0.5}$$

Where  $T_{pav}$  is low asphalt pavement temperature below surface ( $^{\circ}\text{C}$ ),  $T_{air}$  is low air temperature ( $^{\circ}\text{C}$ ),  $lat$  is latitude of the section (degrees),  $H$  is depth below surface (mm),  $S_{air}$  is Standard deviation of the mean low air temperature ( $^{\circ}\text{C}$ ),  $z$  is standard normal dist. table,  $z = 2.055$  for 98%, and  $z = 0.0$  for 50% Statistics:  $R_z = 96\%$ ,  $N = 411$ ,  $SEE = 2.1$ .

The most recent validation of these equations has been from the NCAT test track (8). The study concluded that:

1. At 20, 35, 50 and 100 mm below the pavement surface, SHRP high temperature model closely predicted actual temperatures in 2001 and slightly under-predicted temperatures in 2002.
2. LTTP high temperature closely predicted temperatures in 2001 but underestimated in 2002 as much as  $5.5^{\circ}\text{C}$  ( $10^{\circ}\text{F}$ ).
3. Both low temperature models over predicted temperatures at both 50 and 98% reliability.
4. Mix type (open/dense graded, for example) on the surface has an effect on the temperature on underlying layers.
5. The thicker the surface, the cooler the underlying layers.
6. Pavement temperatures varied by as much  $28^{\circ}\text{C}$  ( $50^{\circ}\text{F}$ ) during a 24-hour period.

Diefenderfer et. al. (9) developed an equation on the basis of work conducted on the Virginia Smart Road project. The following model was developed to predict temperature at a depth (maximum depth below the surface = 0.188m):

$$T_p = a + bT_m + cY + dP_d$$

Where  $T_p$  is predicted pavement temperature ( $^{\circ}\text{C}$ ),  $a$  is intercept coefficient,  $b$  is ambient temperature coefficient,  $T_m$  is measured ambient temperature ( $^{\circ}\text{C}$ ),  $c$  is day of year coefficient,  $Y$  is day of year (1 to 183),  $d$  is depth coefficient; and  $P_d$  is depth within the pavement (m).

The day of year coefficient was used in the early stages of the model instead of solar radiation and increased linearly from January 1 to July 2, then decreased linearly from July 3 to December 31.

Initial model to predict maximum pavement temperatures

(RMSE = 3.54, adjusted  $R^2 = 91.36\%$ ) is:

$$T_{ps\max} = 3.2935 + 0.6356T_{\max} + 0.1061Y - 27.7975P_d$$

Initial model to predict minimum pavement temperature

(RMSE = 2.79,  $R^2 = 91.41\%$ ) is:

$$T_{ps\min} = 1.6472 + 0.6504T_{\min} + 0.08611Y - 7.2385P_d$$

Calculated solar radiation is introduced to predict pavement temperatures at all locations where latitude is known. (The paper describes the steps to calculate solar radiation at any location on any day. From that new temperature models are derived)

The equation to predict the maximum pavement temperature using solar radiation is (RSME = 5.76,  $R^2 = 77.07\%$ ):

$$T_{p\max} = 2.78752 + 0.6861T_{\max} + 5.6736 \times 10^{-4} \times R_s - 27.8739P_d$$

Where  $T_{ps\max}$  is predicted pavement temperature ( $^{\circ}\text{C}$ ),  $T_{\max}$  is maximum daily ambient temperature ( $^{\circ}\text{C}$ ),  $R_s$  = calculated daily solar radiation ( $\text{kJ}/\text{m}^2\text{-day}$ ); and  $P_d$  is depth from the surface (m).

The equation to predict minimum pavement temperature using solar radiation is (RSME = 4.28,  $R^2 = 79.79\%$ ):

$$T_{ps\min} = -1.2097 + 0.6754T_{\min} + 3.764 \times 10^{-4} \times R_s + 7.2043P_d$$

Data from two randomly selected LTTP-SMP sites was used to validate the equations above. Using the data, new models were formulated which incorporated the day of year and latitude.

While most of the studies have been conducted on the basis of field data, a series of laboratory studies have been conducted by Mrawira and his colleagues at the University of New Brunswick. In several papers they describe the use of a laboratory set up to observe temperatures at different depths of HMA samples, and another equipment to determine thermal/heat properties of HMA.

In their 2002 TRB paper (10), the authors describe an approach in which thermal diffusivity and corresponding thermo-physical properties are measured. These properties were found to be affected by density, saturation and temperature. Using the estimated thermal conductivities, the authors predicted the transient temperature conditions in an asphalt pavement under changing environmental conditions. They used energy balance equation and Fourier heat transfer equation. They show from their results that the asphalt pavement goes through daily temperature cycles, and the relative amplitude of such cycles decrease with an increase in depth.

Subsequently, in their 2004 TRB paper (11) Luca and Mrawira describe a laboratory device to observe temperature changes inside a 150 mm diameter asphalt mix sample when subjected to heat from a halogen lamp. Varying wind speeds were created with the help of a fan positioned close to the sample. For the configuration, the authors predicted the time-temperature data with a finite difference approach. And the predicted and actual data were found to be in good agreement. The authors conclude that thermal radiation is the most critical factor affecting the rate of change in temperature, which was higher at depths closer to the surface.

In their 2005 paper (12), Luca and Mrawira point out the importance of getting reliable thermo-physical data for the proper implementation of transient temperature models, and that the existing ASTM C177-85 is not suitable for testing HMA. They present a new method for determination of thermal properties of HMA. They used the new device to determine thermal conductivity in steady state and thermal diffusivity in transient state. They compared their obtained values with those found in the literature.

Based on their studies they conclude that there is no correlation between thermal properties and resilient modulus and Marshal stability

#### **2.4 Investigate the feasibility of using heat from solar heated asphalt pavements**

As summarized by Bijsterveld et al (13) there are three potential ways of utilizing the heat from pavements. The heat can either be used to provide heating energy to buildings, or used to melt snow on the pavement during winter and keep its temperature at a higher than natural level, or can be extracted away from the pavement during the summer time to reduce the potential of permanent deformation (or rutting). In their paper, Bijsterveld et al describes a finite element modeling study to investigate the effects of providing a heat exchanger system inside the pavement on the temperature distribution, as well as stress, strains inside the pavement. They conclude on the basis of results obtained from the models that locating the heat exchanger tubes at shallow depths would allow extraction of more energy but would result in higher stresses in the pavement, which could reduce the durability of the pavement. They mention that there is a need to determine the effect of different materials on the thermal and structural properties of the pavement. Hasebe et al (14) has reported a study on the use of energy from heated pavements to produce electricity, and use the heat flux away from the pavement to lower high pavement temperatures during summer. Their study involved conducting experiments and modeling to evaluate the effect of the flow rate and temperature of the heat exchanger. They confirmed the significant effect of the temperature of the heat exchanger fluid and the resistance of the thermoelectric modules on the peak power output.

#### **2.5 Evaluation of Urban Heat-Island Effect on reducing pavement temperature**

Heat-islands are formed as vegetation is replaced by asphalt and concrete for roads, buildings, and other structures, which absorb - rather than reflect - the sun's heat, causing surface temperatures and overall ambient temperatures to rise (15). The heat from asphalt pavements is a major contributor to the rise in temperature in areas with asphalt pavements, resulting in what is known as the Urban Heat-Island Effect (16). The Urban Heat-Island effect is created by the high absorptivity of the pavement surface

which subsequently leads to an elevated surface temperature and therefore higher emission from the pavement (17).

In their recent paper Gui et al (18) have presented a mathematical model to calculate the pavement near-surface temperatures using hourly measured solar radiation, air temperature, dew-point temperature, and wind velocity data. Their objective was to determine optimum combination of material properties and/or paving practices to lower air temperature rise caused by paving materials in urban areas. They point out that reflectivity and emissivity have the highest positive effects on pavement maximum and minimum temperatures, respectively, while increasing the thermal conductivity, diffusivity, and volumetric heat capacity is effective in lowering maximum temperatures.

Various techniques have been proposed to lower the heat island effect. For asphalt pavements, one prominent method proposed is to use specialized reflective coating so that the albedo is significantly increased (19). This approach has allowed significant lowering of surface temperature. Increased surface reflectivity may increase visibility problems during the daytime. Also, there is a possibility that the reflected light may be absorbed by other surfaces.

## **2.6 Discussion**

1. Studies have been conducted both in the laboratory and with field data for predicting pavement temperature at different depths.
2. Studies have primarily focused on steady state conditions, although some work on transient conditions has been conducted.
3. The main drawback in conducting transient condition analysis is the lack of appropriate thermal properties of HMA.
4. A laboratory set up has been proposed for conducting tests to observe temperatures at different depths of a pavement, and relate those temperatures to surface temperature.
5. A laboratory set up has been developed to estimate thermal properties of HMA in the laboratory – this procedure is proposed as a better method compared to the current ASTM standard test procedure.

6. Based on limited studies it has been shown that physical properties such as saturation, density and temperature affect thermal properties. However, no correlation has been observed between thermal properties and mechanical properties such as stability and modulus.
7. A significant amount of work has been conducted to develop models to predict temperatures at different depths of asphalt pavements.
8. A number of significant factors affecting heat flow in asphalt pavements have been identified.
9. The feasibility of using heat from solar heated asphalt pavements has been investigated.
10. The studies have been showed that the Urban Heat-Island Effect is created by high absorptivity of the pavement surface and asphalt pavement is a major contributor.

Note that so far the most of the studies have been conducted assuming full depth HMA pavements, and temperatures at different depths of HMA have been predicted. However, in practice, in many cases, the pavement structure consists of layers of different materials, and the effect of such materials on the temperature distribution within the pavement has not been studied. The feasibility of using heat from heated asphalt pavements has been investigated, however, how to improve the performance of heat exchanger (asphalt pavement) such as effective of pipe location, length and spacing, water flow rate, geometry of pipe layout, enhancing thermal conductivity materials, and how to reduce the Urban Heat Island Effect by utilizing heat exchanger design have not been studied

This study was carried out in an attempt to answer these questions:

1. What is the effect of using different materials in different layers on the temperature distribution inside the pavement structure?
2. Is the effect similar to or different from the case of a full depth asphalt pavement?
3. How to predict the temperature in the base layers, specifically when those layers are made up of different materials?



4. What is the effect of heat transfer capability of asphalt mix when the overall thermal conductivity is increased?
5. What is the effective design of heat exchanger to generate higher  $\Delta T$ ?
6. What is the effect of higher thermal conductivity of aggregates on reducing Urban Heat-Island Effect?

## CHAPTER 3

### HEAT TRANSFER

#### 3.1 Analytical Approach

Heat transfer is when the energy transfer from one substance to another substance without work done and only result in temperature difference. Heat transfer can be classified into three categories, conduction, convection, and radiation (20).

##### Conduction

The heat transfer by conduction is the energy transfer through a substance, a solid or a fluid as result of the presence of a temperature gradient within the substance. This process is also referred to as the diffusion of energy or heat. Fourier's law is used to calculate the conduction or diffusion energy in a substance; and it states that the heat flux is directly proportional to the magnitude of the component of the temperature gradient in the direction of the flux.

$$\dot{q}_x = -k \frac{\partial T}{\partial x}, \dot{q}_y = -k \frac{\partial T}{\partial y}, \dot{q}_z = -k \frac{\partial T}{\partial z}$$

Another way to express the speed of heat transfer propagating from one point to another is thermal diffusivity, which is the ratio of thermal conductivity to volumetric heat capacity.

$$\alpha = \frac{k}{\rho c_p}$$

Where  $k$  is thermal conductivity,  $\rho$  is density, and  $C_p$  is the specific heat of the material.

It measures the ability of a material to conduct thermal energy relative to its ability to store thermal energy. Materials of large  $\alpha$  will response quickly to changes in their thermal environment, while materials of small  $\alpha$  will response slowly, taking longer to reach a new equilibrium condition.

The thermal conductivity ( $k$ ) is a thermophysical property of the substance through which the heat flows and has the units of  $\text{W/m}\cdot\text{K}$ . It is directly related to the microscopic mechanism involved in the transfer of heat within the matter.

Heat capacity, also known simply as specific heat ( $C$ ) is the measure of the heat energy required to raise the temperature of a given amount of a substance by one degree Kelvin (or Celsius). The term specific in the physical sciences often refers to quantities divided by a specified reference quantity or amount, and in the case of specific heat capacity, the term usually means that the heat capacity is mass-specific, or "per unit of mass."

### Convection

The heat transfer by convection is the energy transfer between a fluid and a solid surface. There are two different types of heat convection, the first type is when the diffusion or conduction of energy through the air or fluid because of the presence of a temperature gradient within the fluid or called natural convection.

The second type is the transfer of the energy within the fluid due to the movement of the fluid from one thermal environment, temperature field, to another or called forced convection.

The magnitude ( $Q$ ) of the rate of energy transfer by convection can be expressed by Newton's law of cooling:

$$\dot{Q} = hA\Delta T$$

Or

$$h = \frac{\dot{q}}{\Delta T}$$

Where  $A$  is the surface area of the body which is in contact with the fluid,  $\Delta T$  is the appropriate temperature difference,  $\dot{q}$  is the heat flux, and  $h$  is the convection heat transfer coefficient.

Natural heat transfer coefficient can be calculated based on Rayleigh number and Grashof number. The different parameters are defined below in the order in which the calculations for the natural heat transfer coefficient are to be done.

Rayleigh number is the product of Grashof and Prandtl numbers

$$Ra_L = Gr_L Pr$$

Where Gr is Grashof number and Pr is Prandtl number.

$$Gr_L = \frac{g\beta(T_w - T_\infty)L^3}{\nu^2}$$

Where  $Gr_L$  is Grashof number,  $g$  is gravitational acceleration,  $T$  is the absolute film temperature,  $L$  is characteristic length, and  $\nu$  is viscosity

$$\beta = -\frac{1}{\rho} \frac{\partial \rho}{\partial T} \Big|_p$$

Where  $\beta$  is the coefficient of volumetric expansion, and  $\beta = 1/T$  for an ideal gas, and  $\rho$  is the density of the material. The value of Pr,  $\beta$ ,  $\rho$ , and  $\nu$  can be obtained from typical material property table

Rayleigh number ( $Ra$ ) identifies the transition of the flow characteristic from laminar flow to turbulent flow occur at  $Ra \approx 10^9$ , and for a vertical plate with a uniform surface temperature: the Nusselt number can be defines as:

Laminar flow  $< Ra \approx 10^9$

$$\bar{Nu} = 0.68 + 0.67[Ra_L \Psi(Pr)]^{\frac{1}{4}}$$

Where Nu is the Nusselt number and  $Ra_L$  is Rayleigh number.

$$\Psi(Pr) = \left[ 1 + \left( \frac{0.492}{Pr} \right)^{\frac{9}{16}} \right]^{\frac{-16}{9}}$$

Where Pr is Prandtl number.

Turbulent flow  $> Ra \approx 10^9$

$$\bar{Nu} = 0.15[Ra_L \Psi(\text{Pr})]^{1/3}$$

Where Nu is the average Nusselt number and  $Ra_L$  is Rayleigh number.

When the heat transfer from the horizontal flow plate; the Nusselt number can be calculated based on correlation of Rayleigh number

Hot surface up or cold surface down

$$\bar{Nu}_L = 0.54Ra_L^{1/4} \quad 10^4 \leq Ra_L \leq 10^7$$

$$\bar{Nu}_L = 0.15Ra_L^{1/3} \quad 10^7 \leq Ra_L \leq 10^{11}$$

Cold surface up or hot surface down

$$\bar{Nu}_L = 0.27Ra_L^{1/4} \quad 10^5 \leq Ra_L \leq 10^{10}$$

Average natural heat transfer coefficient h can be calculated based on Nusselt number

$$\bar{h} = \frac{Nu k}{L}$$

Where Nu is Nusselt number, k is thermal conductivity of the material, L is characteristic length.

Force heat transfer coefficient can be calculated based on Reynolds and Nusselt number

$$Re_L = \frac{UL}{\nu}$$

Where, U is wind velocity, L is characteristic length, and  $\nu$  is viscosity of the material.

Reynolds number identifies the transition of the flow characteristic from laminar flow to turbulent flow occur at  $Re = 5 \times 10^5$ , and the heat transfer over a flat plate can be calculated based on Nu

Laminar flow  $< Re = 5 \times 10^5$

$$\bar{Nu} = 0.664(Re_L)^{\frac{1}{2}} Pr^{\frac{1}{3}}$$

Where Re is Reynolds number and Pr is Prandtl number.

Turbulent flow  $> Re = 5 \times 10^5$

$$\bar{Nu} = \frac{0.037 Re_L^{0.8} Pr}{1 + 2.443 Re_L^{-0.1} (Pr^{\frac{2}{3}} - 1)}$$

Where Re is Reynolds number and Pr is Prandtl number.

The convective heat transfer coefficient ( $h_c$ ) can be calculated by using the empirical equation developed by Vehrencamp and Dempsey (21):

$$h_c = 698.24 \left[ 0.00144 T_m^{0.3} U^{0.7} + 0.00097 (T_s - T_{air})^{0.3} \right]$$

Where  $h_c$  is the radiation loss to the air in  $W/m^2$ , which depends on the surface temperature  $T_s$ ,  $T_{air}$  is the air temperature,  $T_m$  is average temperature of  $T_s$  and  $T_{air}$ , and  $U$  is wind velocity.

## Radiation

The transfer of energy by electromagnetic waves is called radiation heat transfer. All matter at temperature greater than absolute zero will radiate energy. Energy can be transferred by thermal radiation between a gas and solid surface or between two or more surface. The rate of energy emitted by an ideal surface (black body) with emissivity equals to 1 is given by the Stefan-Boatman law:

$$E_b = \epsilon \sigma T^4$$

Where  $E_b$  is the rate of black body radiation energy,  $\epsilon$  is the emissivity of the material, and  $\sigma = \text{Stefan-Boltzmann constant} = 5.68 \times 10^{-8} \text{W}/(\text{m}^2\text{K}^4)$ , and  $T$  is temperature.

### Heat transfer in internal pipe flow

When heat is added or removed from a fluid flowing through a pipe. The energy content of the fluid will change as it moves through the pipe. The amount of heat transferred and the temperature distribution in the fluid will depend on the thermodynamic state of the fluid entering the pipe, the velocity of the fluid, and the thermal boundary conditions at the wall of the pipe.

The value of the convection heat transfer coefficient for laminar flow is dependent on the geometrical cross section of the pipe, the thermal boundary condition at the pipe wall, and the distance from pipe entrance. The Nusselt number is defined as

$$Nu = \frac{hd_h}{k}$$

Where  $d_h$  is the hydraulic diameter of the section and  $k$  is the thermal conductivity of the fluid.

There are two types of boundary conditions used in convection heat transfer, uniform wall flux and uniform wall temperature.

Uniform wall flux  $\dot{q}_w''$  is when the heat flux at the wall of the pipe is uniform,

$$T_b = \frac{\dot{q}_w'' A}{\dot{m} C_p} + T_i$$

$$\dot{q}_w'' = h_x (T_w - T_b)$$

Where  $T_b$  is the exit temperature,  $A$  is the surface area of the pipe,  $\dot{m}$  is the mass flow rate,  $C_p$  is heat capacity,  $T_i$  is the initial temperature at the entrance,  $h_x$  is the local heat transfer coefficient, and  $T_w$  is the wall temperature.

Uniform wall temperature is when the temperature at the wall is uniform; the local heat flux is replaced by  $h_x(T_w - T_b)$ , the equation can be rearranged as

$$\frac{T_w - T_b}{T_w - T_i} = \exp \left[ -\frac{hA}{\dot{m}C_p} \right]$$

Where  $h$  is the heat transfer coefficient.

The velocity profile of the fluid  $U$ , can be identified and calculated based on the Reynolds's number and Power Law of Velocity (22).

Laminar flow  $Re \leq 2300$

$$U = V_{max} \left( 1 - \left( \frac{r}{R} \right)^2 \right)$$

Turbulent flow  $Re \geq 2300$

$$U = V_{max} \left( 1 - \left( \frac{r}{R} \right)^7 \right)$$

Where  $V_{max}$  is maximum velocity,  $r$  is any point at the diameter of pipe, and  $R$  is the diameter of the pipe.



### 3.2 Energy Balance of Asphalt Pavement

The heat energy transfers from sun radiation to asphalt pavement can be defined by using energy balance theory, the Figure 3-1 shows the energy balance on the surface of the asphalt pavement (grey body) and the parameters are defined as following.

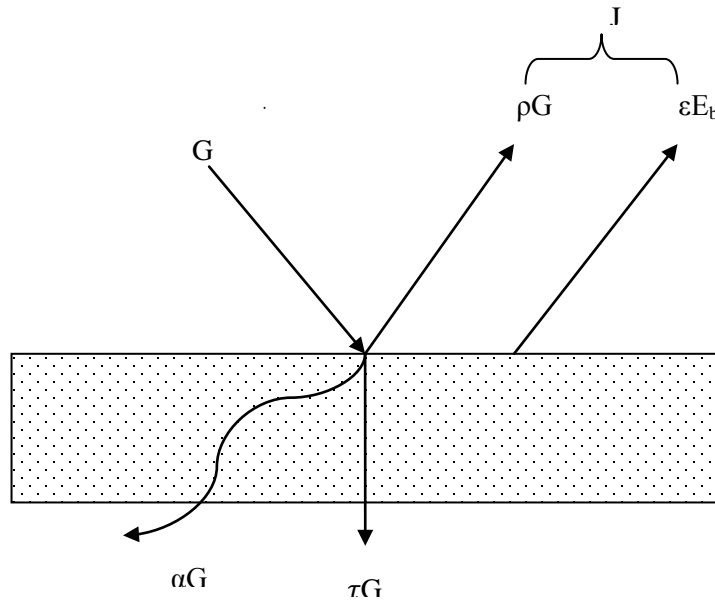


**Figure 3-1 Energy balance on the surface of a grey body**

Irradiation ( $G$ )

The rate at which radiation strikes a surface is called irradiation. Directional characteristics of the radiation are important. The irradiation per unit area is identified by  $G$ , in watts per meter squared. The subscript  $\lambda$  will be used to denote the monochromatic rate of radiant energy striking the surface. The total radiation incident on a surface is obtained by integrating over the complete range of wavelengths.

$$G = \int_0^{\infty} G_{\lambda} d\lambda$$

### Absorptivity ( $\alpha$ )

Absorptivity is the fraction of the total incident radiation that is absorbed by the surface. For a real body, the absorptivity usually varies with wavelength; the monochromatic absorptivity is denoted by  $\alpha_\lambda$ . The absorptivity is expressed in terms of the monochromatic absorptivity by

$$\alpha = \frac{\text{absorbed radiation}}{\text{incident radiation}} = \frac{1}{G} \int_0^\infty \alpha_\lambda G_\lambda d\lambda$$

Typical  $\alpha$  for asphalt mixtures varies from 0.85 to 0.93 (Solaimanian and Kenndey)

### Reflectivity ( $\rho$ )

The fraction of the total incident radiation that is reflected by the surface. Again, this property is a function of wavelength so that  $\rho_\lambda$  is used to represent the monochromatic reflectivity of a surface and

$$\rho = \frac{\text{reflected radiation}}{\text{incident radiation}} = \frac{1}{G} \int_0^\infty \rho_\lambda G_\lambda d\lambda$$

There are two types of reflection of the electromagnetic waves, specular and diffuse. Specular reflections are present when the angle of incidence is equal to the angle of reflection. Diffuse radiation is present when the reflection is uniformly distributed in all directions.

### Transmissivity ( $\tau$ )

Transmissivity is the fraction of the total incident radiation that is transmitted through the body. It also has a wavelength dependency. The monochromatic transmissivity is designated by  $\tau_\lambda$  and the total transmissivity is

$$\tau = \frac{\text{transmitted radiation}}{\text{incident radiation}} = \frac{1}{G} \int_0^\infty \tau_\lambda G_\lambda d\lambda$$

For most solid surfaces the transmissivity is equal to the zero, since the bodies are usually opaque to the incident radiation.

The sum of the absorptivity, reflectivity, and transmissivity is equal 1.

$$\alpha + \rho + \tau = 1$$

For an opaque body

$$\tau = 0$$

hence

$$\alpha + \rho = 1$$

Emissivity ( $\varepsilon$ )

The emissivity of a material (usually written  $\varepsilon$ ) is the ratio of energy radiated by the material to energy radiated by a black body ( $E_b$ ) at the same temperature. It is a measure of a material's ability to absorb and radiate energy. A true black body would have  $\varepsilon = 1$  while any real object would have  $\varepsilon < 1$ . Emissivity is a numerical value and does not have units. This emissivity depends on factors such as temperature, emission angle, and wavelength.

$$\varepsilon = \frac{1}{E_b} \int_0^{\infty} \varepsilon_{\lambda} E_{\lambda,b} d\lambda$$

$$E_b = \sigma T^4$$

$\sigma$  = Stefan-Boltzmann constant =  $5.68 \times 10^{-8} \text{ W}/(\text{m}^2 \cdot \text{K}^4)$

Gray body

A body whose surface monochromatic emissivity and absorptivity are independent of wavelength and direction is called a gray body, so that the emissivity is a constant. This is known as the grey body assumption. When dealing with non-black surfaces, the deviations from ideal black body behavior are determined by both the geometrical structure and the chemical composition, and follow Kirchhoff's law of thermal radiation: emissivity equals absorptivity (for an object in thermal equilibrium), so

that an object that does not absorb all incident light will also emit less radiation than an ideal black body.

### Radiosity (J)

The amount of thermal radiation leaving a body is called the Radiosity, it is the sum of the incident radiation that is reflected and that which is emitted by the body. The radiosity, denoted by  $J$ , may be expressed in terms of the emissivity and the reflectivity of the surface as

$$J = \varepsilon E_b + \rho G$$

Therefore, the total energy that the object can absorb can be calculated based on incident radiation and back-radiation measurement; and for most solid surfaces the transmissivity is equal to zero, since the bodies are usually opaque to the incident radiation.

### Albedo

The surface condition of the ground and pavement of the road- involving color, texture (roughness), absorptivity, the angle of the sun and solar elevation, and exposure, for example, is of practical significance because it has a considerable influence on how much in-radiation is reflected back to the atmosphere and how much radiation is actually absorbed by the ground. The ratio of in-radiation and reflected radiation (percentage of reflection) per unit of surface and time is called albedo of the medium. For example, fresh paved asphalt is 0.05 to 0.1 and aged asphalt pavement is 0.1 to 0.2

### 3.3 Finite Element Analysis Approach

The finite element analysis is a numerical method for solving problems of engineering and mathematical physics. For the problems involving complicated geometries, loadings, and materials properties, it is generally not possible to obtain analytical mathematical solutions. The finite element formulation of the problem results in a system of simultaneous algebraic equation for simulation, rather than requiring the solution of differential equations. These numerical methods yield approximate values of the unknowns at discrete numbers of points in the continuum (23).

The heat transfer problem can be analyzed based on conservation of energy and Fourier's law of heat conduction.

Heat Conduction (Without Convection)

By conservation of energy

$$E_{in} + E_{generated} = \Delta U + E_{out}$$

or

$$q_x A dt + Q A dx dt = \Delta U + q_{x+dx} A dt$$

Where  $E_{in}$  is the energy entering the control volume,  $\Delta U$  is the change in stored energy,  $q_x$  is the heat conducted (heat flux) into the control volume at surface edge  $x$ ,  $q_{x+dx}$  is the heat conducted out of control volume at the surface edge  $x+dx$ ,  $t$  is time,  $Q$  is the internal heat source, and  $A$  is the cross-sectional area.

By Fourier's law of heat conduction,

$$q_x = -K_{xx} \frac{dT}{dx}$$

Where  $K_{xx}$  is the thermal conductivity in the  $x$  direction,  $T$  is the temperature,  $\frac{dT}{dx}$  is the temperature gradient.

The change in stored energy can be expressed by

$$\Delta U = c(\rho A dx) dT$$

Where  $c$  is the specific heat and  $\rho$  is the mass density.

One-dimensional heat conduction equation as

$$\frac{\partial}{\partial x} \left( K_{xx} \frac{\partial T}{\partial x} \right) + Q = \rho c \frac{\partial T}{\partial t}$$

For steady state, any differentiation with respect to time is equal zero,

$$\frac{\partial}{\partial x} \left( K_{xx} \frac{\partial T}{\partial x} \right) + Q = 0$$

For constant thermal conductivity and steady state,

$$\left( K_{xx} \frac{\partial^2 T}{\partial x^2} \right) + Q = 0$$

The boundary conditions are of the form

$$T = T_B \text{ on } S_1$$

Where  $T_B$  represents a known boundary temperature and  $S_1$  is a surface where temperature is known, and

$$q_x^* = -K_{xx} \frac{dT}{dx} = \text{constant on } S_2$$

Where  $S_2$  is a surface where the prescribed heat flux  $q_x^*$  or temperature gradient is known, and on an insulated boundary  $q_x^* = 0$ .

Convective heat transfer

For a conducting solid in contact with a fluid, if heat transfer is taking place, the fluid will be in motion either through external pumping action (forced convection) or through the buoyancy forces created within the fluid by the temperature differences within it (natural or free convection).

For conservation of energy

$$q_x Adt + QAdxdt = c(\rho Adx)dT + q_{x+dx} Adt + q_h Pdxdt$$

Heat transfer convection is

$$q_h = h(T - T_\infty)$$

Where h is the heat-transfer or convection coefficient, T is the temperature of the solid surface,  $T_\infty$  is the temperature of the fluid, P is the perimeter around the constant cross-sectional area A.

Heat Conduction (with convection)

$$\frac{\partial}{\partial x} \left( K_{xx} \frac{\partial T}{\partial x} \right) + Q = \rho c \frac{\partial T}{\partial t} + \frac{hP}{A} (T - T_\infty)$$

With possible boundary conditions on (1) temperature, (2) temperature gradient, and/or (3) loss of heat by convection from the ends of the one-dimensional body,

$$-K_{xx} \frac{dT}{dx} = h(T - T_\infty)$$

Total heat transfer from simulated heat flux into the object (asphalt pavement) can be defined as

$$(k\Delta T) = -q_{irradiant} + h_c (T_{air} - T_s) + \epsilon\sigma(T_{air}^4 - T_s^4)$$

Conduction heat transfer

$$q_{conduction} = -k \frac{T_d - T_s}{d}$$

Where  $q_{irradiant}$  incident radiation, k is thermal conductivity of the material,  $T_d$  is the temperature at distance x,  $T_s$  is the surface temperature, d is the total length.

## Heat Radiation

The emitted radiation intensity from the object (pavement) surface to its surroundings is calculated as

$$q_{radiation} = h_r (T_s - T_{air})$$

$$h_r = \varepsilon \sigma (T_s - T_{air})(T_s^2 + T_{air}^2)$$

$$q_{radiation} = \varepsilon \sigma (T_s^4 - T_{air}^4)$$

Where  $q_{radiation}$  = incident radiation,  $h_r$  is heat transfer coefficient,  $\varepsilon$  is the emissivity of the material,  $\sigma$  = Stefan-Boltzmann constant =  $5.68 \times 10^{-8} \text{W}/(\text{m}^2 \cdot \text{K}^4)$ ,  $T_s$  is surface temperature in Kelvin,  $T_{air}$  is air temperature Kelvin.



## **CHAPTER 4**

### **THERMAL PROPERTIES AND TEMPERATURE OF EXISTING ASPHALT PAVEMENT**

#### **4.1 Introduction**

It is a common knowledge that asphalt pavements get heated up by sunlight, and the thermal conditions which the pavements are exposed to greatly affect the performance and longevity of the pavement. Research has shown that there is a temperature distribution inside asphalt pavements, in the different layers, which are in many cases made up of different materials.

The temperature distribution along the depth actually depends on the properties of these different layers – the temperature at any layer is affected significantly by the thermal properties of the layers above and below it. Thus, the temperature distribution in a full depth asphalt pavement will be different from, for example, an asphalt pavement with an aggregate base, even though the asphalt mixtures/materials in the two pavements are the same.

This is of practical significance considering the wide variety of materials that are currently being used as base material in both highway and airfield pavements.

#### **4.2 Objective**

The objectives of this chapter were to:

1. Investigate the temperature distribution along the depth of asphalt pavements with six different base layers with laboratory experiments.
2. Build statistical models to predict the temperature in different base layers.
3. Model the temperature distribution, using principles of thermodynamics in different pavements and determine appropriate values of thermal properties of the different layers.

#### **4.3 Methodology**

The six existing pavement samples used were described in Table 4-1 and Figure 4-1 shows photos of the samples. The different base layer materials considered in this phase were conventional Hot Mix Asphalt (HMA) – one with a bigger Nominal Maximum Aggregate Size (NMAS) compared to the surface course and another with the same NMAS, Plant Mixed Reclaimed Asphalt Pavement (PMRAP, RAP mixed with

asphalt emulsion), foamed asphalt mix, cement treated base and a polymer modified HMA. Two of the samples were from airport pavements, while the rest were from highway pavements. The highway pavements consist of standard wearing and binder course HMA and different reclaiming material as base course, with one HMA base course. Of the two airport pavement samples, one consists of standard FAA specified P401 mix wearing, binder and base courses (these are actually a number of overlays), while the other consists of Fuel Resistant (FR) wearing course over polymer modified binder course.

A typical test consisted of the followings steps.

1. Set up the halogen lamp with a timer programmed to operate on 12 hours on and 12 hours off cycle.
2. Position the sample over the base and make all the appropriate connections for thermocouples.
3. Start the data acquisition system.
4. Switch on the halogen lamp.
5. Continuously collect temperature data from all thermocouple locations.
6. Repeat the above steps to go through several cycles of temperature.

**Table 4-1 Types of pavements considered**

<b>Pavements</b>	<b>Sample/description</b>	<b>Thickness</b>	<b>Bulk Specific Gravity</b>
Highway-HMA layers over HMA base with different NMAS	G – Wearing (9.5 NMAS) and two base courses (12.5 and/or 19mm); 9.5mm NMAS mix with 6% PG 64-28 binder; 12.5 NMAS mix with 5.9 % PG 64-28 binder; 19mm NMAS mix with 5.1% PG 64-28 binder	(35mm over 40mm over 125mm) Sample - 72mm of wearing +binder HMA over 115mm of base	Top layer: 2.277 Middle Layer: 2.342 Bottom Layer: 2.321
Highway-HMA layers over PMRAP base	S (9.5mm over 12.5mm NMAS over PMRAP base); PMRAP – RAP with 3.5% emulsion and 1.3% cement; 9.5 and 12.5mm mixes as described for G sample	(30mm over 40mm over 75mm) Sample – 63 mm of HMA over 75 mm of PMRAP	Top layer+ Middle Layer 2.377 Bottom Layer: 2.084
Highway-HMA layers over Foamed Asphalt base	M– (9.5 mm over 9.5 mm over foamed asphalt base); foamed asphalt contained 3.1 % binder and 1.4% cement; 9.5 mm mix as described for G sample	(30mm over 30mm) over 150mm Sample – 55 mm of HMA over 135 mm of foamed asphalt	Top layer+ Middle Layer 2.284 Bottom Layer 2.067 1.975
Highway-HMA layers over cement treated base	R (9.5mm over 12.5 mm over Cement treated base); full depth reclaimed base with 4% cement; 9.5 and 12.5mm mixes as described for G sample	(32mm over 45mm over 200mm) Sample – 70mm of HMA over 165mm of cement treated base	Top layer: 2.386 Middle Layer: 2.209 Bottom Layer: 2.033
Airport-HMA layers of same NMAS – three lifts of P 401	P401-Three layers of RAP-P401 layers; 19mm maximum size mix with 18 % RAP, 1% lime, and 5.2% PG 64-28 binder	Sample - 54mm over 70mm over 80mm over 94mm	Top layer: 2.472 Middle Layer: 2.517 Bottom Layer: 2.467
Airport-HMA layers of different types two lifts -	(FR) Fuel Resistant ½ inch NMAS mix over ¾ inch NMAS polymer modified (PM) binder mix over existing HMA or Macadam; FR – 12.5 mm maximum size mix with 7% PG 88-22 Fuel Resistant binder PM – 19 mm maximum size mix with 6% PG 82-22 PM binder	Sample – 40 mm of FR over 53mm of PM over 59 mm of existing P401 mix	Top layer: 2.549 Middle Layer: 2.557 Bottom Layer: 2.467

Note: All binders are PG 64-28 grade, unless mentioned otherwise



**Figure 4-1 Six existing highway samples**

#### 4.4 Laboratory Parameters Measurement

##### Heat Flux Measurement

The basic test set up first proposed by Luca and Mrawira (11) and used by Nazarian and Alvarado (24) has been utilized in this study. It consists of a pavement sample encapsulated within Styrofoam (thermal conductivity =  $0.029 - 0.033\text{W/m}\cdot\text{K}$ ).

A halogen lamp positioned over the sample was used to raise the temperature of the sample (Figure 4-2), and temperatures were recorded constantly over the duration of the tests. Each sample was fitted with thermocouples at different depths as well as on the surface. Figure 4-3 shows the location of the thermocouples for the different samples (Appendix A).

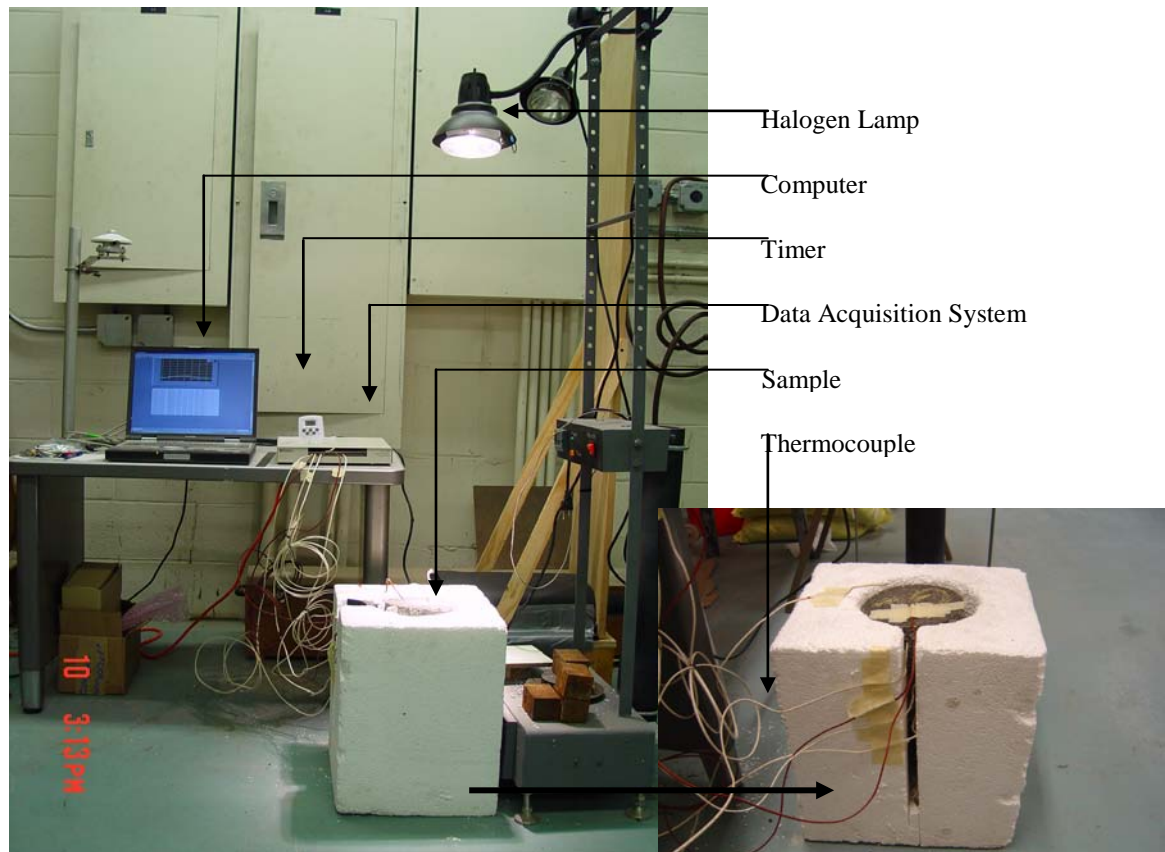
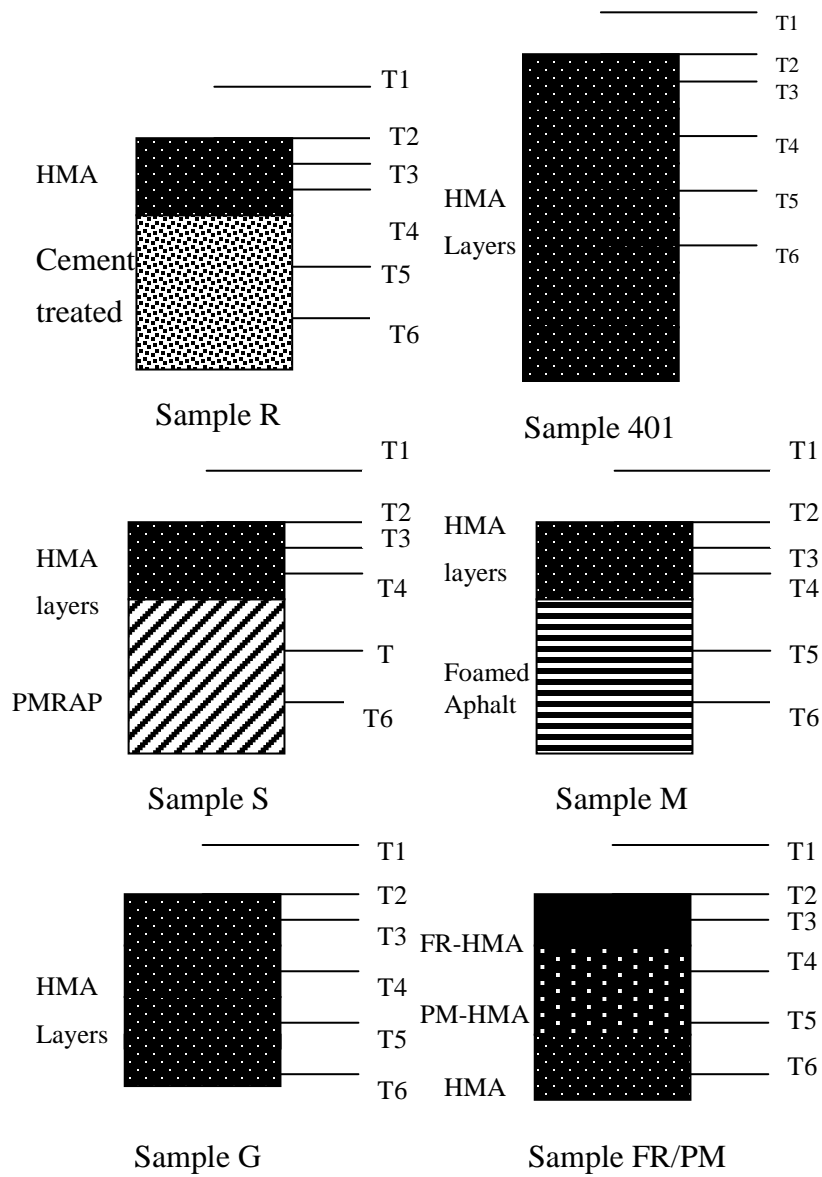


Figure 4-2 Laboratory testing setup



Note: T1-T6 – thermocouples 1 through 6; PMRAP- plant mixed RAP with emulsion; FR-HMA- fuel resistant HMA; PM-HMA- polymer modified HMA

**Figure 4-3 Location of thermocouples in different samples**

Radiation from the halogen lamp was measured by using a CMP-3 pyranometer, and the radiation was measured indirectly by placing a piece of aluminum foil on the surface of the HMA sample to measure the reflected radiation. The emissivity of the aluminum foil is 0.03 which means it would reflect 97% of radiation emitted from the halogen lamp Figure 4-4.

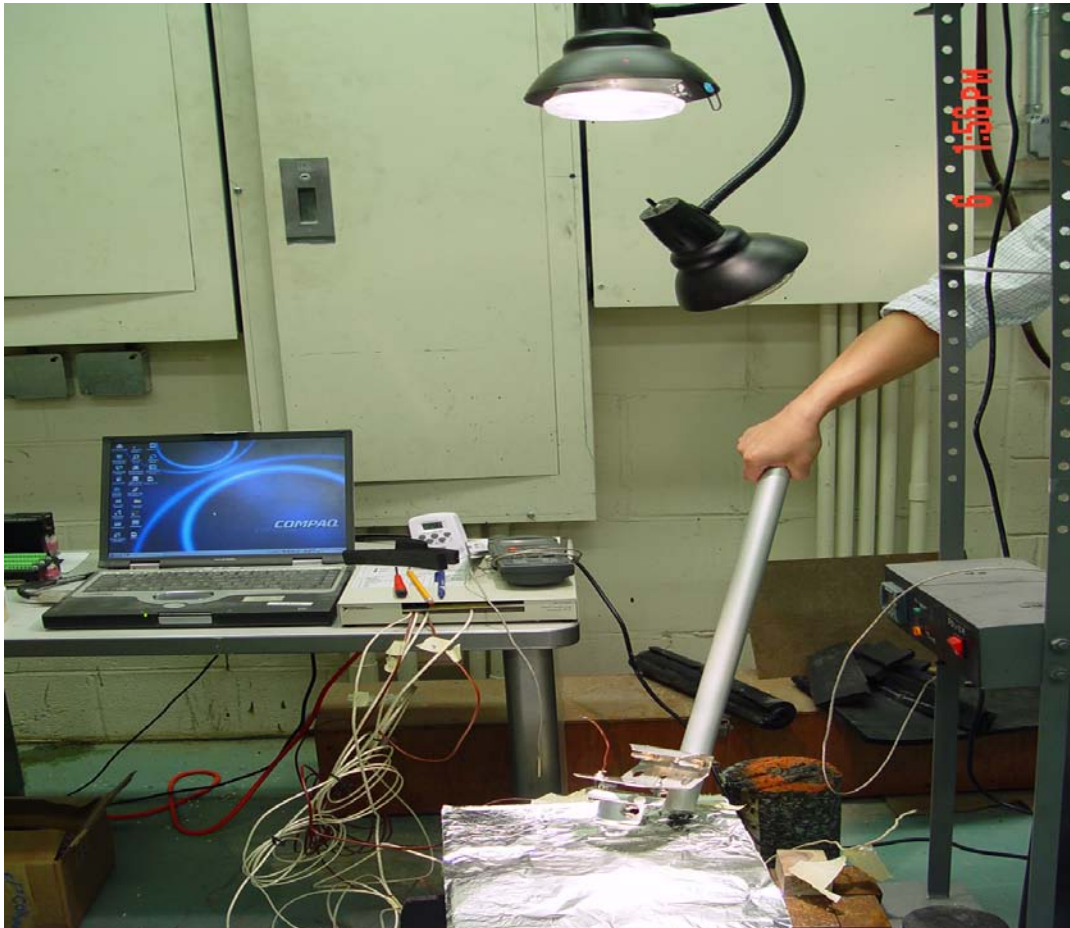


**Figure 4-4 Halogen lamp heat radiation measurement**

The halogen lamp (100W) was positioned 1.1m above the sample, primarily on the basis of convenience in setting up the experiment. The incident radiation from the lamp at this level was found to be  $500\text{W/m}^2$ , as measured with a pyranometer.

Two samples were also tested with wind, using a fan held close to the sample. The position of the fan was adjusted to produce a wind speed of  $4.45\text{m/s}$  (10mph), as measured with an anemometer (Figure 3-4).



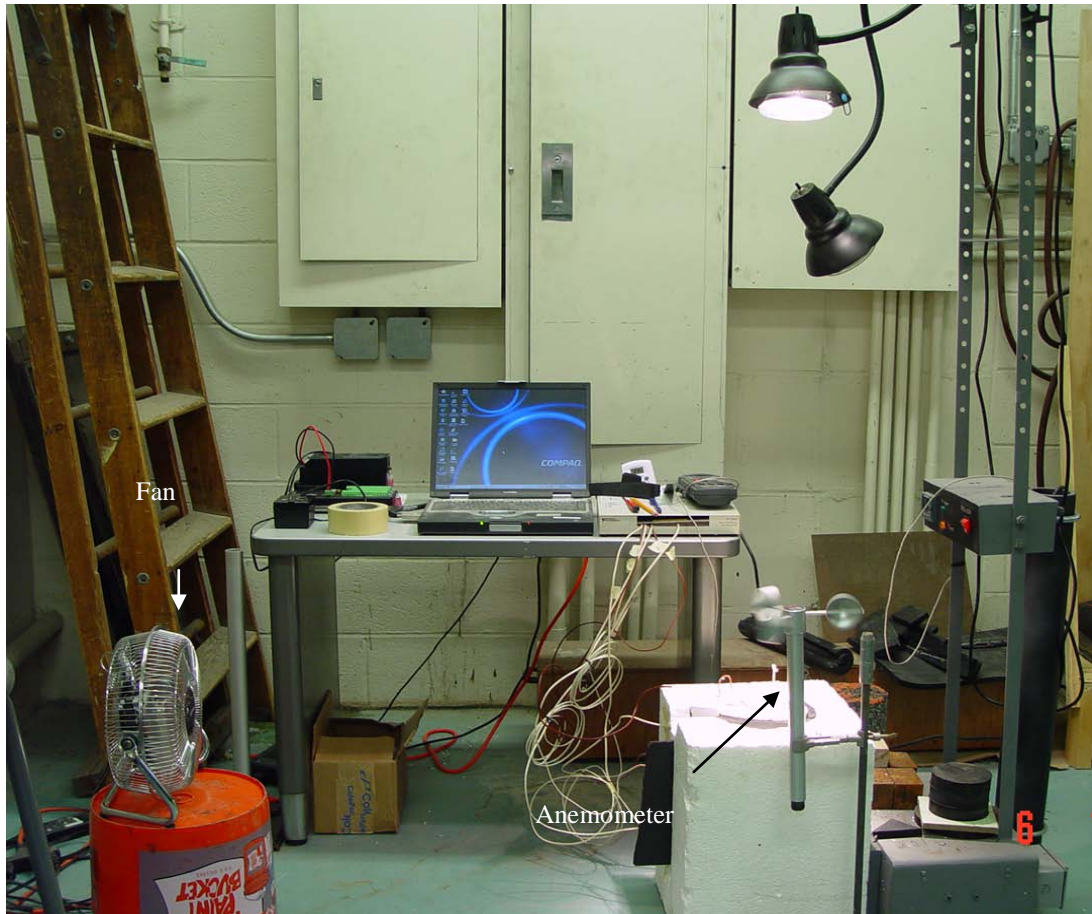


**Figure 4-5 Laboratory testing setup with fan and anemometer**

**Emissivity Measurement**

The emissivity or the back-radiation reflected from surface was measured by the pyranometer; the hemispherical surface of the pyranometer was turned to face the HMA samples

The different values obtained from the laboratory and a parking lot pavement in Worcester, MA (Latitude: 42.27, Longitude: 71.87) were shown in Table 4-2.

**Table 4-2 Measured heat parameters**

	Incident Radiation (W/m <sup>2</sup> )	Emitted Radiation (W/m <sup>2</sup> )	Emissivity	Calculated Absorptivity (%)
Field	1050	95	0.91	91
Laboratory	500*	-	-	-

\*The halogen radiation measurement was performed by placing a piece of aluminum foil on the surface of the HMA sample to measure the reflected radiation of halogen lamp. The emissivity of the aluminum foil is 0.03 which would reflect 97% of radiation emitted from the halogen lamp.



The total reflected radiation can be calculated as

$$\rho = \frac{485}{x} \Rightarrow 0.97 = \frac{485}{x}$$

$$Radiation(x) = 500W / m^2$$

Absorptivity calculation:

Field radiation:

$$\rho = \frac{95}{1050} = 0.09$$

$$\alpha + \rho = 1$$

$$\alpha = 1 - 0.09 = 0.91$$

The emissivity  $\epsilon$  can be obtained by Kirchoff's law of thermal radiation: emissivity equals absorptivity (for an object in thermal equilibrium). Therefore, emissivity of field pavement is 0.91, and this was used for laboratory samples.

This value was checked by testing each sample for emissivity. The pyranometer was positioned to face the surface of the HMA and the back radiation was measured. The results are shown in Table 4-3. Note that the measured values are fairly close to 0.91. The 0.91 value was used instead of the different measured values since it was suspected that during this testing the pyranometer created a small shadow on the surface of the samples and hence the measured values could be slightly different than real values.

**Table 4-3 Measured emissivity values**

Sample	Temperature (°C)		Radiation (W/m <sup>2</sup> )	$\epsilon$ (air)	$\epsilon$ (HMA)
	T1	T2			
G	29.14	41.08	79.35	0.16	0.84
S	33.00	44.89	82.01	0.16	0.84
M	31.53	41.45	66.81	0.13	0.87
R	34.04	42.17	55.61	0.11	0.89
P401	29.36	39.63	67.84	0.14	0.86
FR	30.08	41.3	74.99	0.15	0.85

T1- thermocouple 25 mm above the surface in air, T2- thermocouple on the surface

#### 4.5 Experiment Results

The temperature data from each sample was analyzed to determine the temperature profile along the depth and different times. For all of the samples, the maximum temperature along the depth was recorded by the thermocouple located 25mm below the surface.

**Table 4-4 G Sample - Highway-HMA layers over HMA base with different NMAS**

	1st	2nd	3rd	4th	5th	6th	7th		
Time (mins)	720	2160	3600	5040	6480	7920	9360		
Depth (m)	T (°C)	T (°C)	T (°C)	T (°C)	T (°C)	T (°C)	T (°C)	MEAN	STDev
0	41.21	39.07	41.23	39.08	37.98	39.07	38.85	39.50	1.24
-0.0254	47.87	47.79	47.40	45.92	44.19	44.29	44.23	45.96	1.73
-0.05715	44.21	44.25	43.97	42.91	41.47	41.33	41.09	42.75	1.43
-0.1016	38.25	38.34	38.22	37.49	35.89	36.07	35.68	37.13	1.21
-0.1524	35.19	35.15	35.33	34.54	33.10	33.16	32.98	34.21	1.09

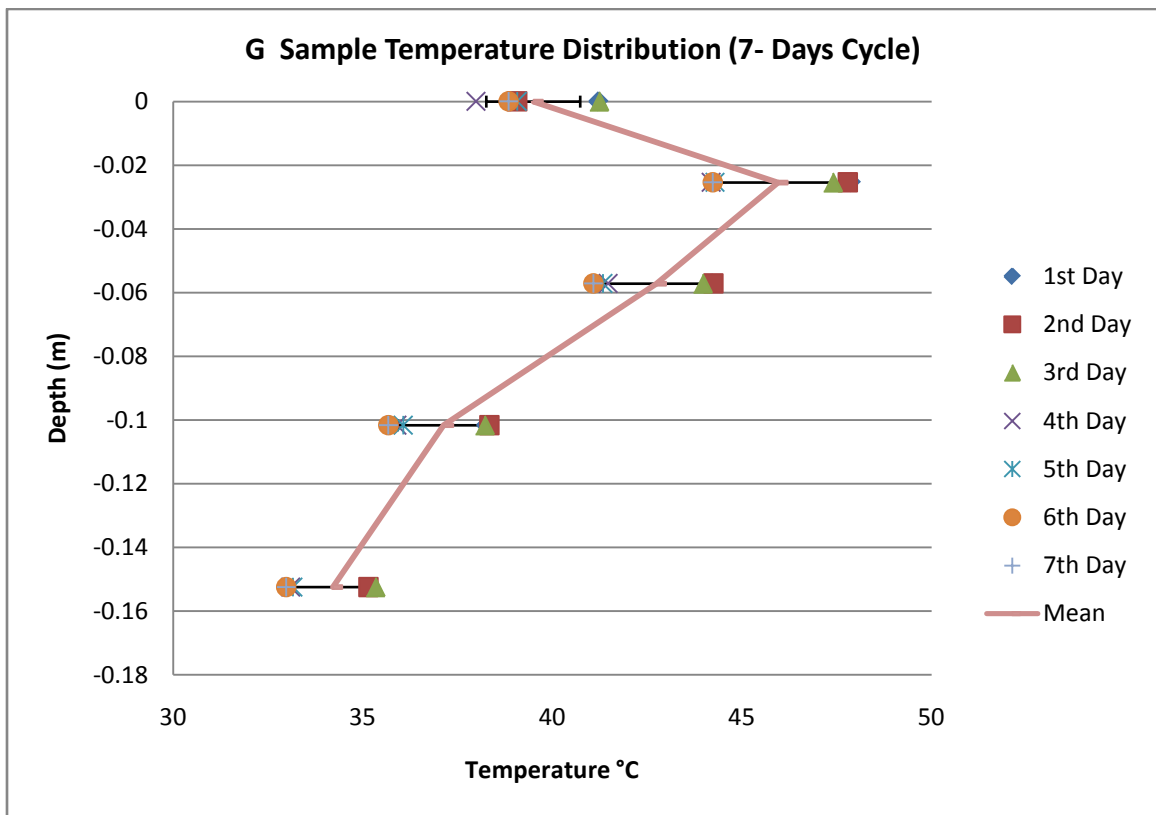


**Figure 4-6 G Sample temperature distribution (7-days cycle)**

**Table 4-5 S Sample -HMA layers over PMRAP base**

	1st	2nd	3rd	4th	5th	6th	7th		
Time (mins)	720	2160	3600	5040	6480	7920	9360		
Depth (m)	T(°C)	T(°C)	T(°C)	T(°C)	T(°C)	T(°C)	T(°C)	Mean	STDev
0	47.44	48.50	48.15	48.70	46.68	47.42	46.45	47.62	0.87
-0.0254	47.31	50.28	49.91	49.53	49.17	49.10	48.15	49.06	1.03
-0.041275	46.01	49.49	49.10	48.81	48.51	48.33	47.41	48.24	1.18
-0.079375	40.87	45.91	45.52	45.26	45.08	44.90	43.71	44.46	1.73
-0.10795	38.39	43.99	43.82	43.43	43.17	43.07	41.99	42.55	1.95

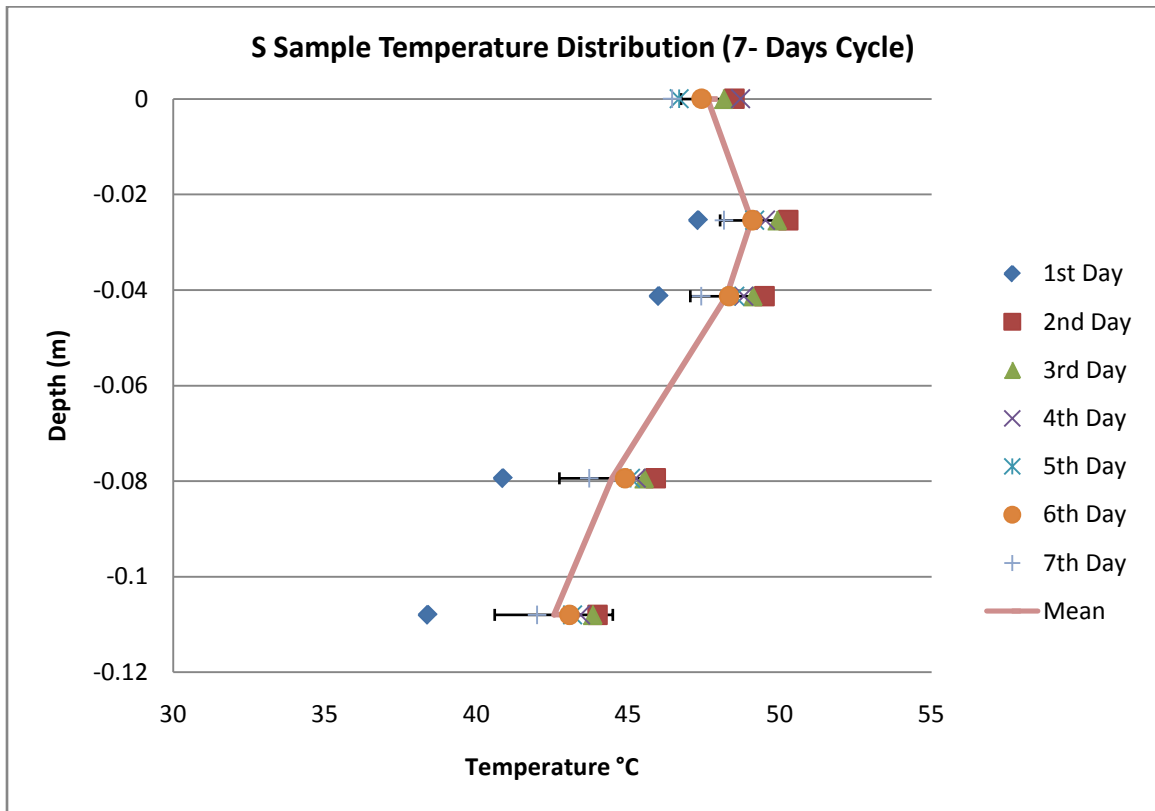


**Figure 4-7S Sample temperature distribution (7-days cycle)**

**Table 4-6 M Sample- HMA layers over Foamed Asphalt base**

	1st	2nd	3rd	4th	5th	6th	7th		
Time (mins)	720	2160	3600	5040	6480	7920	9360		
Depth (m)	T(°C)	T(°C)	T(°C)	T(°C)	T(°C)	T(°C)	T(°C)	Mean	STDev
0	43.88	44.13	46.10	44.72	44.47	43.26	43.27	44.26	0.98
-0.0254	47.02	48.46	51.83	50.78	50.57	49.92	49.75	49.76	1.59
-0.0508	45.90	47.42	49.85	48.68	48.49	47.95	47.76	48.01	1.22
-0.06985	40.23	41.90	43.31	42.31	42.11	41.55	41.41	41.83	0.94
-0.10795	36.72	38.15	39.54	38.65	38.35	37.98	37.86	38.18	0.85

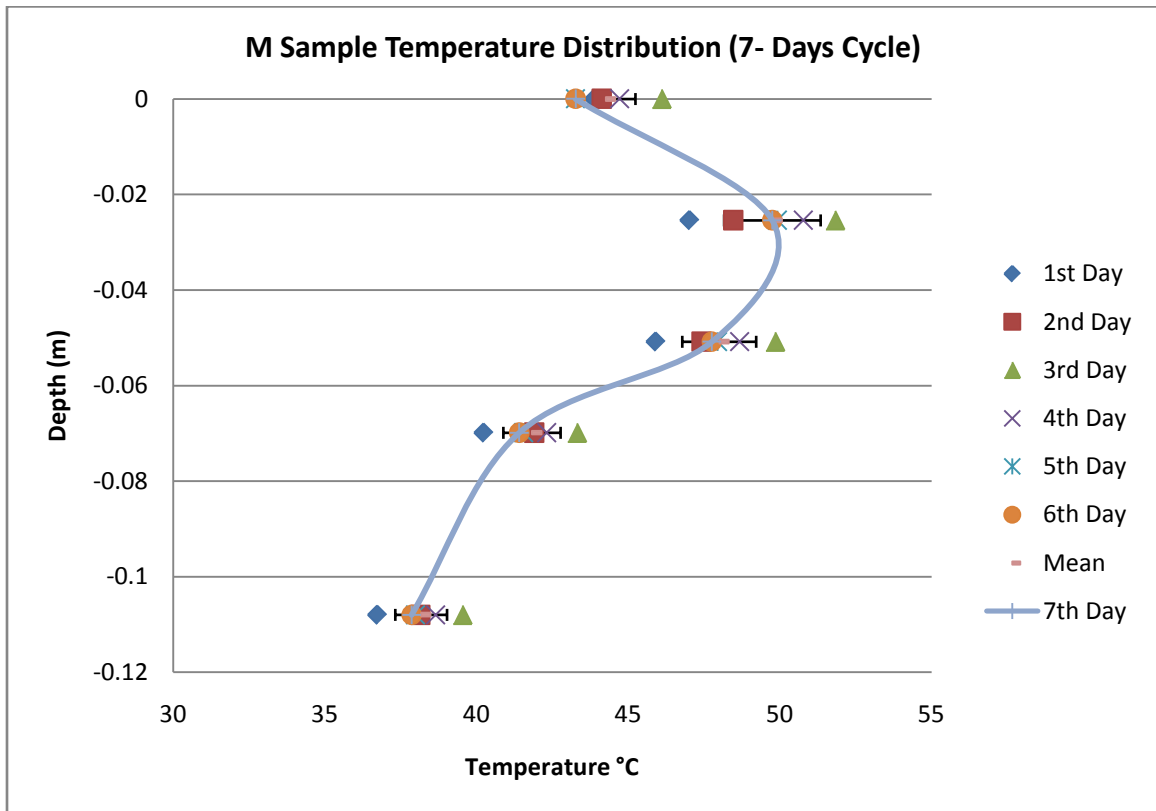


**Figure 4-8 M Sample temperature distribution (7-days cycle)**

**Table 4-7 R Sample- HMA layers over cement treated base**

	1st	2nd	3rd	4th	5th	6th	7th		
Time (mins)	720	2160	3600	5040	6480	7920	9360		
Depth (m)	T(°C)	T(°C)	T(°C)	T(°C)	T(°C)	T(°C)	T(°C)	Mean	STDev
0	44.80	43.88	42.19	42.86	42.97	44.21	41.78	43.24	1.10
-0.0254	47.68	47.83	48.43	48.05	48.84	48.38	48.50	48.25	0.41
-0.0508	46.60	46.89	47.52	47.12	47.85	47.50	47.44	47.28	0.43
-0.107995	42.47	42.93	43.61	43.03	43.69	43.50	43.33	43.22	0.44
-0.17145	38.61	39.13	39.82	39.17	39.85	39.69	39.60	39.41	0.46

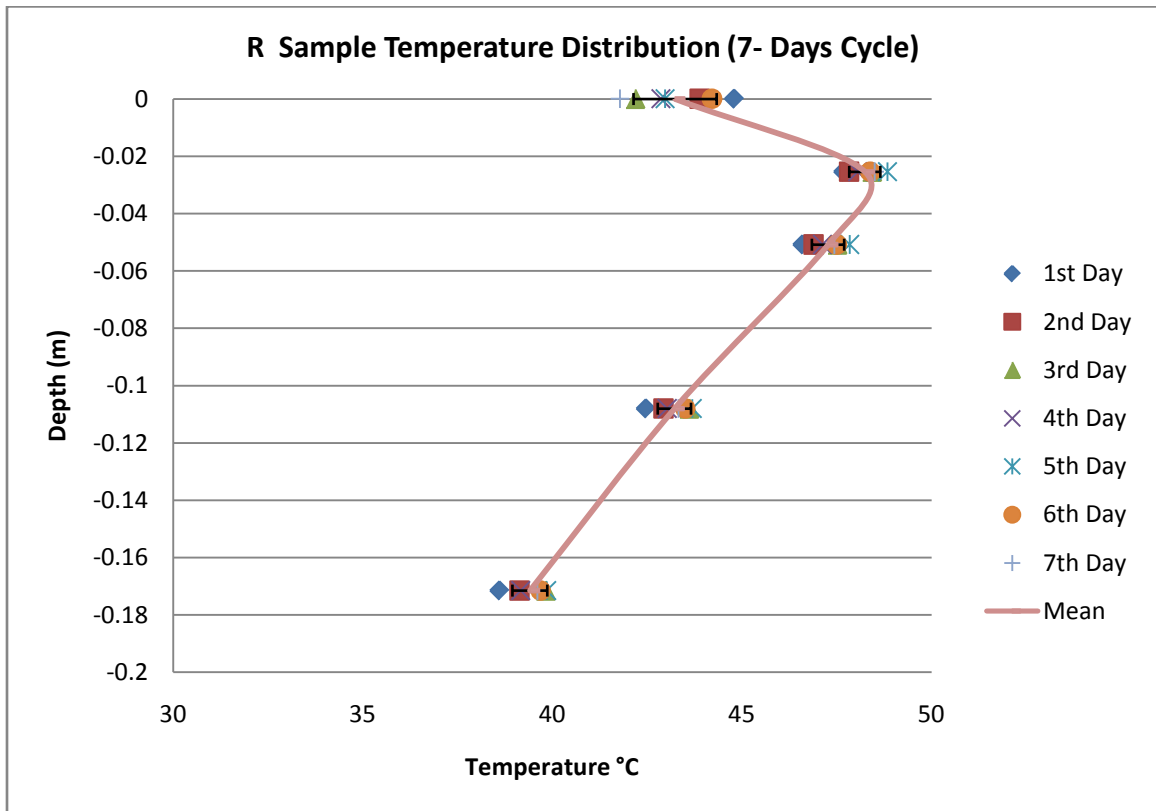


**Figure 4-9 R Sample temperature distribution (7-days cycle)**

**Table 4-8 P401 Sample- HMA layers of same NMAS**

	1st	2nd	3rd	4th	5th	6th	7th		
Time (mins)	720	2160	3600	5040	6480	7920	9360		
Depth (m)	T(°C)	T(°C)	T(°C)	T(°C)	T(°C)	T(°C)	T(°C)	Mean	STDev
0	41.86	42.40	42.55	44.76	45.01	44.43	44.73	43.68	1.34
-0.0254	45.70	44.38	45.36	46.83	46.52	46.21	46.67	45.95	0.87
-0.09525	37.09	36.00	36.93	37.92	37.85	37.75	37.96	37.36	0.73
-0.1651	33.10	32.23	32.98	33.63	33.67	33.60	33.76	33.28	0.55
-0.2286	31.38	30.77	31.37	31.83	32.07	31.95	32.03	31.63	0.48

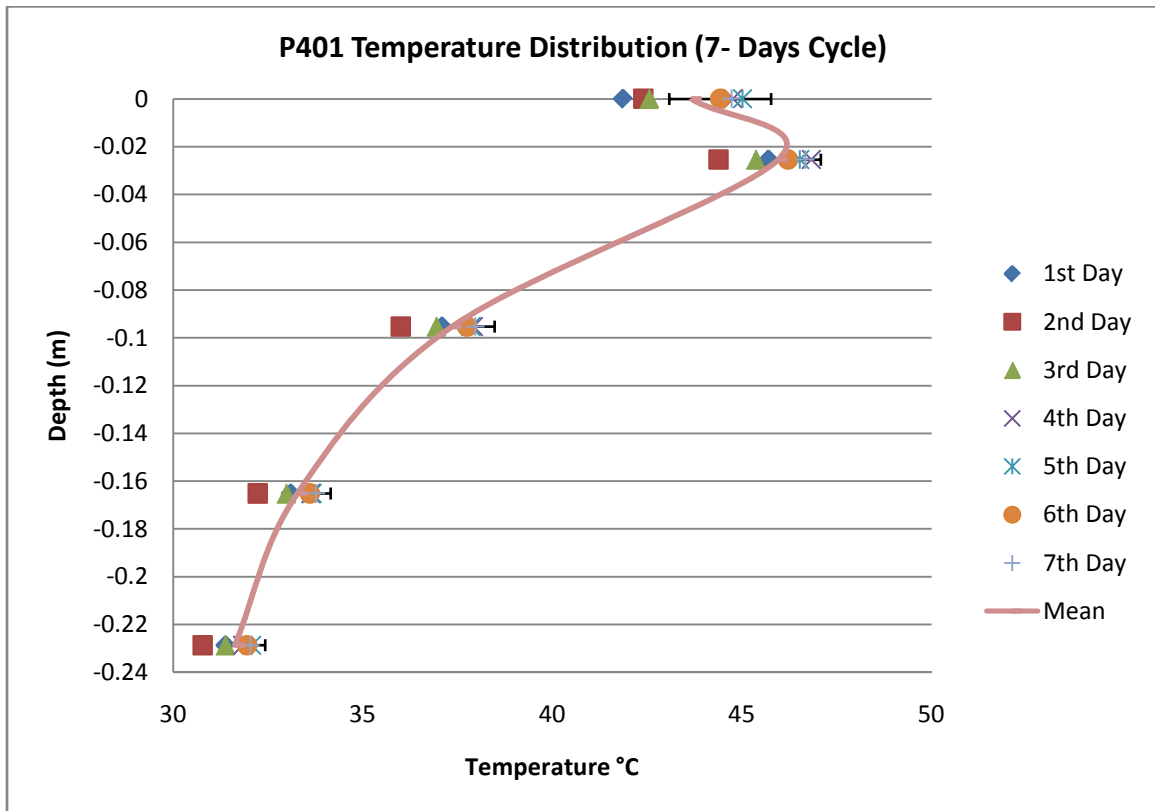


**Figure 4-10 P401 Sample temperature distribution (7-days cycle)**

**Table 4-9 FR Sample- HMA layers of different types two lifts**

	1st	2nd	3rd	4th	5th	6th	7th		
Time (mins)	720	2160	3600	5040	6480	7920	9360		
Depth (m)	T(°C)	T(°C)	T(°C)	T(°C)	T(°C)	T(°C)	T(°C)	Mean	STDev
0	43.12	44.86	43.16	45.35	43.27	41.27	42.62	43.38	1.37
-0.0254	47.54	47.99	47.31	48.58	47.87	47.14	47.20	47.66	0.52
-0.0508	44.67	45.19	44.82	45.82	45.06	44.51	44.47	44.93	0.47
-0.06985	43.42	44.24	43.75	44.73	43.87	43.38	43.36	43.82	0.51
-0.10795	41.31	41.98	41.77	42.37	41.73	41.06	41.21	41.63	0.47

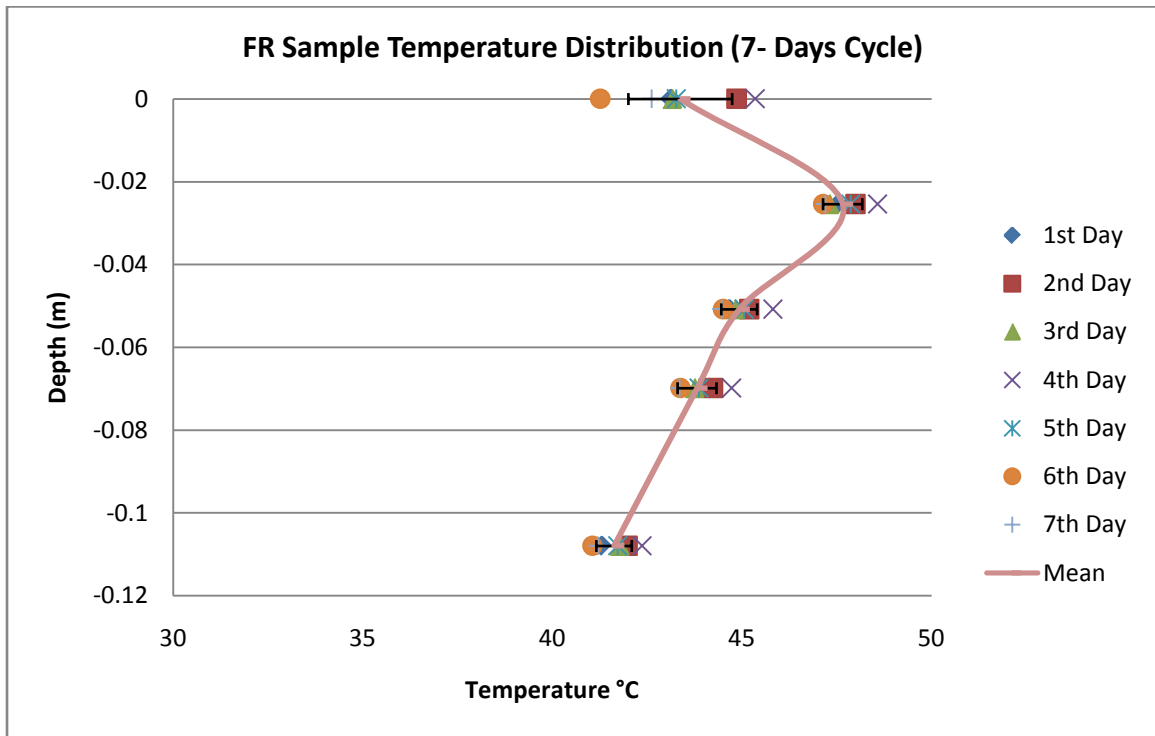


**Figure 4-11 FR Sample temperature distribution (7-days cycle)**

Figure 4-12 showed a plot of temperatures versus depth for the different samples at the end of the seventh heating cycle.

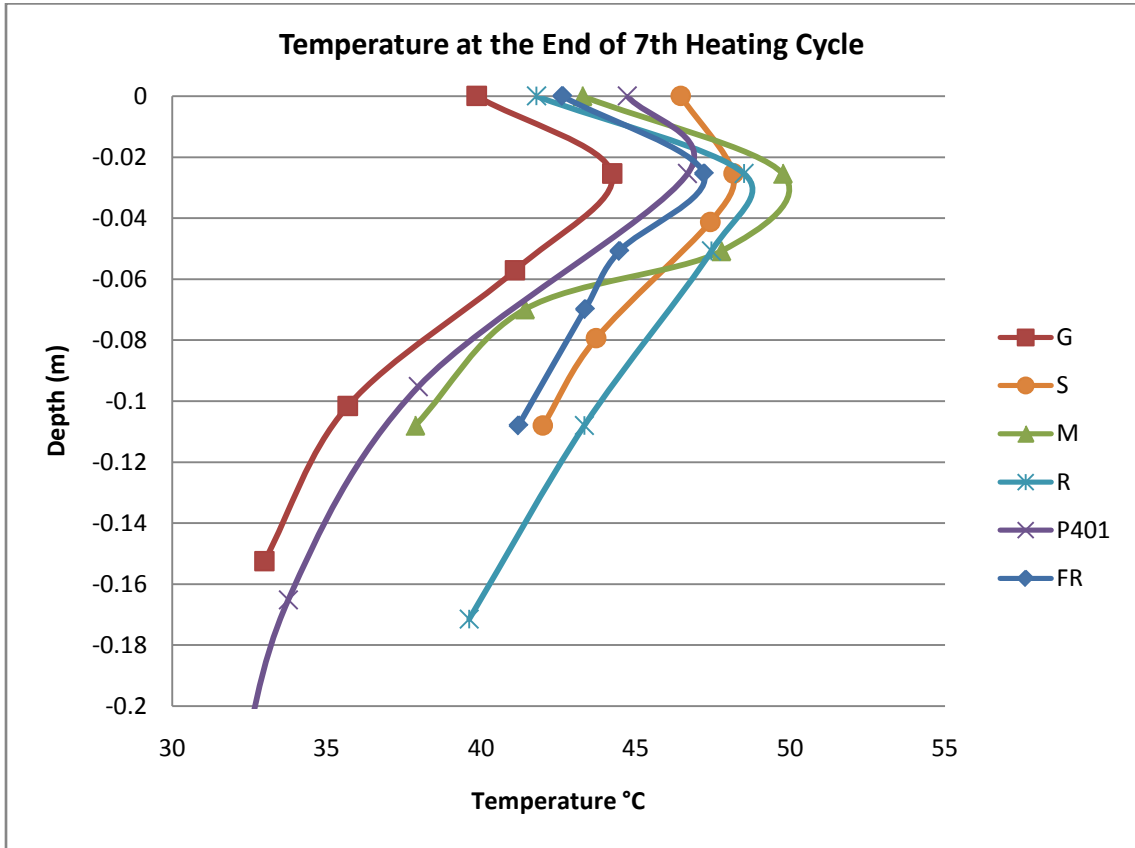


Figure 4-12 6 Samples temperature distribution at end of 7<sup>th</sup> heating cycle



#### **4.6 Statistical Approach of Determining Temperature at Specific Location**

To predict the maximum temperature for each sample (mix) on the basis of “known” or “measurable” temperatures, statistical analyses were conducted to build models relating the maximum subsurface temperature to air and surface temperature. These models were developed on the basis of one heating cycle data only. The equations were shown in Table 4-10, which also included the equations developed for P401 and M samples, with and without wind.

To predict the temperature in the “base” course, statistical models were developed relating the base temperature to surface and air temperatures for each sample. These were also shown in Table 4-10. Temperature limits of each equation were also shown. Note that no attempt was made to compare the maximum temperatures for the different samples, since the air temperatures in the laboratory were slightly different for the different samples.

As expected, for each sample, the model for the temperature at a depth of 25mm was different from the model for the temperature at the midpoint of the base. Also, the coefficients for the equations for the different samples for temperature at a depth of 25mm were quite different. The different temperature profiles were no doubt affected by the thermal properties of the different materials. The primary objective of presenting the equation in Table 4-10 was to show the differences in the coefficients.

**Table 4-10 Equation from statistical analysis**

Sample	Model for prediction of maximum temperature, in the HMA layer, based on one heating cycle	Model for prediction of temperature at the mid-point of base layer, based on one heating cycle
P401/no wind T <sub>A</sub> :25.8 to 36.2 °C T <sub>S</sub> :25.8 to 41.9 °C	$T_{20\text{mm}} = 1.700.92 \cdot T_A + 1.81 \cdot T_S$	$T_{\text{base}} = 14.15 - 1.00 \cdot T_A + 1.36 \cdot T_S$
P401/10 mph wind T <sub>A</sub> :26.1 to 27.5 °C T <sub>S</sub> :25.9 to 33.3 °C	$T_{20\text{mm}} = 2.48 - 0.73 \cdot T_A + 1.52 \cdot T_S$	$T_{\text{base}} = -7.52 - 0.02 \cdot T_A + 1.12 \cdot T_S$
R T <sub>A</sub> :26.6 to 38.5 °C T <sub>S</sub> :27.6 to 45.3 °C	$T_{20\text{mm}} = 0.16 - 1.50 \cdot T_A + 2.36 \cdot T_S$	$T_{\text{base}} = -3.69 - 1.48 \cdot T_A + 2.28 \cdot T_S$
S T <sub>A</sub> :26.9 to 37.3 °C T <sub>S</sub> :26.7 to 47.9 °C	$T_{20\text{mm}} = 6.05 - 0.91 \cdot T_A + 1.56 \cdot T_S$	$T_{\text{base}} = 18.35 - 1.29 \cdot T_A + 1.47 \cdot T_S$
G T <sub>A</sub> :23.3 to 36.4 °C T <sub>S</sub> :25.4 to 51.2 °C	$T_{20\text{mm}} = -18.41 - 0.45 \cdot T_A + 1.59 \cdot T_S$	$T_{\text{base}} = -22.23 - 0.35 \cdot T_A + 1.52 \cdot T_S$
FR over PM T <sub>A</sub> :24.7 to 36.2 °C T <sub>S</sub> :25.3 to 43.9 °C	$T_{20\text{mm}} = -2.65 - 1.19 \cdot T_A + 2.11 \cdot T_S$	$T_{\text{base}} = 0.18 - 1.45 \cdot T_A + 2.19 \cdot T_S$
M T <sub>A</sub> :24.6 to 33.9 °C T <sub>S</sub> :24.5 to 43.9 °C	$T_{20\text{mm}} = -0.97 - 0.98 \cdot T_A + 1.87 \cdot T_S$	$T_{\text{base}} = 9.02 - 1.57 \cdot T_A + 1.95 \cdot T_S$
M/10 mph wind T <sub>A</sub> :23.9 to 26.9 °C T <sub>S</sub> :24.5 to 31.9 °C	$T_{20\text{mm}} = -8.97 - 0.46 \cdot T_A + 1.66 \cdot T_S$	$T_{\text{base}} = -28.46 + 1.09 \cdot T_A + 0.86 \cdot T_S$

Where T<sub>A</sub>= air temperature, °C; and T<sub>S</sub>= surface temperature, °C.

#### **4.7 Finite Element Analysis/Modeling**

The heating of each sample was modeled using the finite element analysis. The objective of finite element modeling was to “backcalculate” the unknown thermal conductivity and heat capacity of the different layers for existing highway and airport samples. These parameters were required as inputs for consideration of the effect of the environment in the mechanistic-empirical pavement design process, using the Enhanced Integrated Climatic Model (EICM) (25).

Heat transfer module from COMSOL Multiphysics software (26) was used for simulating the heat transfer process and predicting the thermal properties of the asphalt mix samples.

There were four main components that required to be identified in order to model the heat transfer process: sub-domain, boundary condition, mesh size, and solver parameter. Subdomains were defined based on the thermal properties, densities and initial temperatures of each layer. The boundary conditions for the samples were assumed as fully insulated except the top surface boundary, where natural convection with laminar air flow condition was assumed. The model allowed heat energy transfer in the downward (-z) direction. There were five parameters that were required for boundary condition inputs: heat flux, heat transfer coefficient, ambient temperature, surface temperature, and surface emissivity.

For modeling, the global mesh size was set to predefined normal size which consisted of 3,436 elements for sub-domains, boundaries, edges, and nodes. The solver parameters were set to time dependant analysis with steps of 900 seconds from 0 to 43,200 seconds for one heating cycle. Examples of a model and results were shown in Figure 4-13 and 4-14.

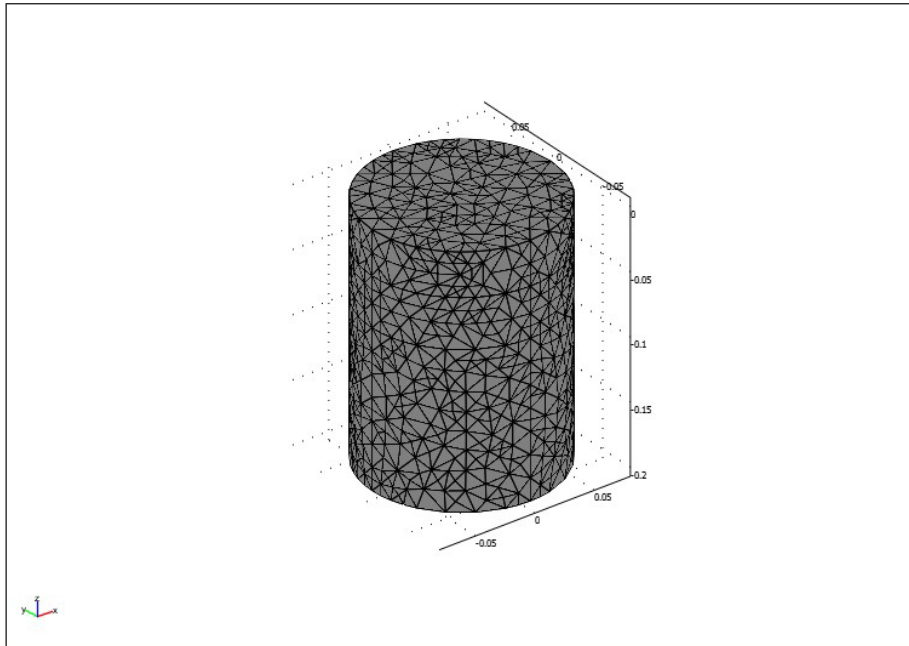


**Figure 4-13 Mesh generated from COMSOL**

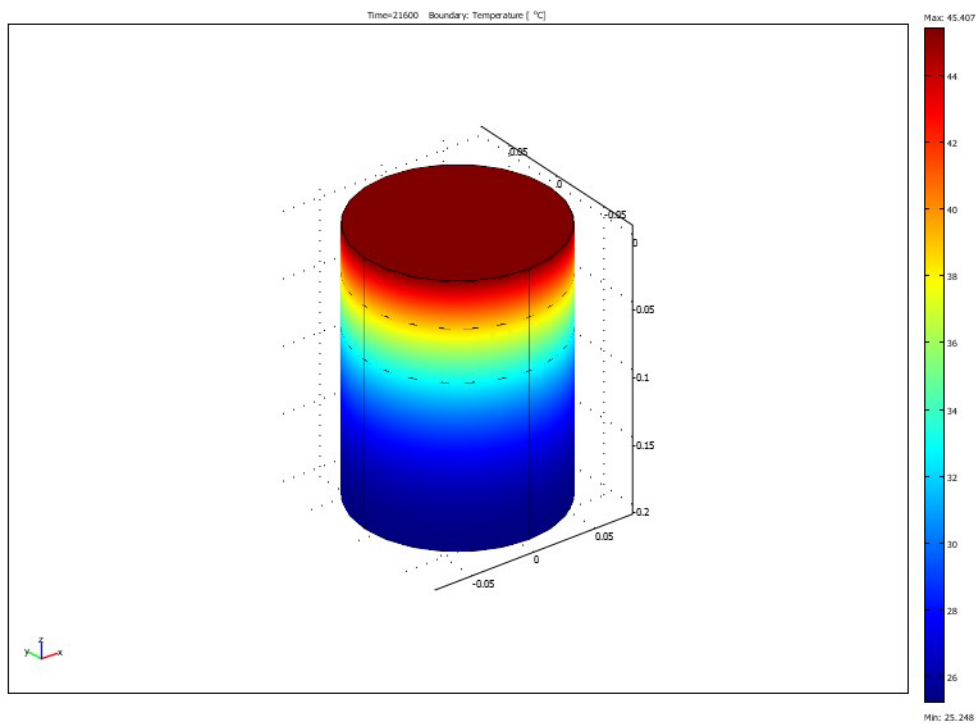


**Figure 4-14 COMSOL simulation result**

The analysis for prediction of thermal properties consisted of the following steps:

1. Put “seed” values of  $k$  and  $C$  for all the layers.
2. Model each sample and simulate heating.
3. Obtain finite element model output and plot the predicted temperature; compare them with laboratory obtained temperatures at different thermocouple located at different material layers.
4. Rerun the simulations by changing  $k$  values to match predicted and measured temperature at thermocouple T2 and T3 locations for which the second layer is different from the first layer, and to match predicted and measured temperatures for T2, T3 and T4, for those samples for which the first and second layers are the same.
5. For the samples for which the second layer is different from the first, then run simulations by changing  $k$  of the second layer, or  $k$  of the second layer as well as the first layer to match predicted and measured temperatures at T4 as well as T2 and T3.
6. Rerun the simulations by changing the  $k$  of the bottom layer to match predicted and measured temperatures for T5 and T6.
7. Repeated steps 1 through 5 for determining  $C$  values by matching predicted and measured temperatures.

The input values of thermal properties were based on the currently recommended values from the literature. First, the values provided in the recently released NCHRP mechanistic-empirical design guide (25) were considered. The ranges for asphalt materials are  $0.76$  to  $1.4\text{W}/(\text{m}\cdot\text{K})$  for thermal conductivity and  $921$  to  $1,674\text{J}/(\text{kg}\cdot\text{K})$  for heat capacity (for Portland cement they are  $1.7$  to  $2.6\text{W}/(\text{m}\cdot\text{K})$  and  $837$  to  $1,172\text{J}/(\text{kg}\cdot\text{K})$  for thermal conductivity and heat capacity, respectively). Wider ranges were found in Reference 10 and were therefore used for initial values (thermal conductivity ranges from  $0.8$  to  $2.89\text{W}/(\text{m}\cdot\text{K})$  and heat capacity ranges from  $800$  to  $1,853\text{J}/(\text{kg}\cdot\text{K})$ ).

Figure 4-15 to 4-24 showed the plots of finite element analysis predicted as well as laboratory measured (for five thermocouples for each of the samples) time versus temperature data. Note that for G, R and P401 samples (Appendix B), it was possible to get predicted values within 10% of the measured values by using 12 hour heating cycle.

For the S, M and FR samples (Appendix B) this was not possible, and the back-calculation was done by remodeling and reanalyzing the predicted data for 6 hours of heating.

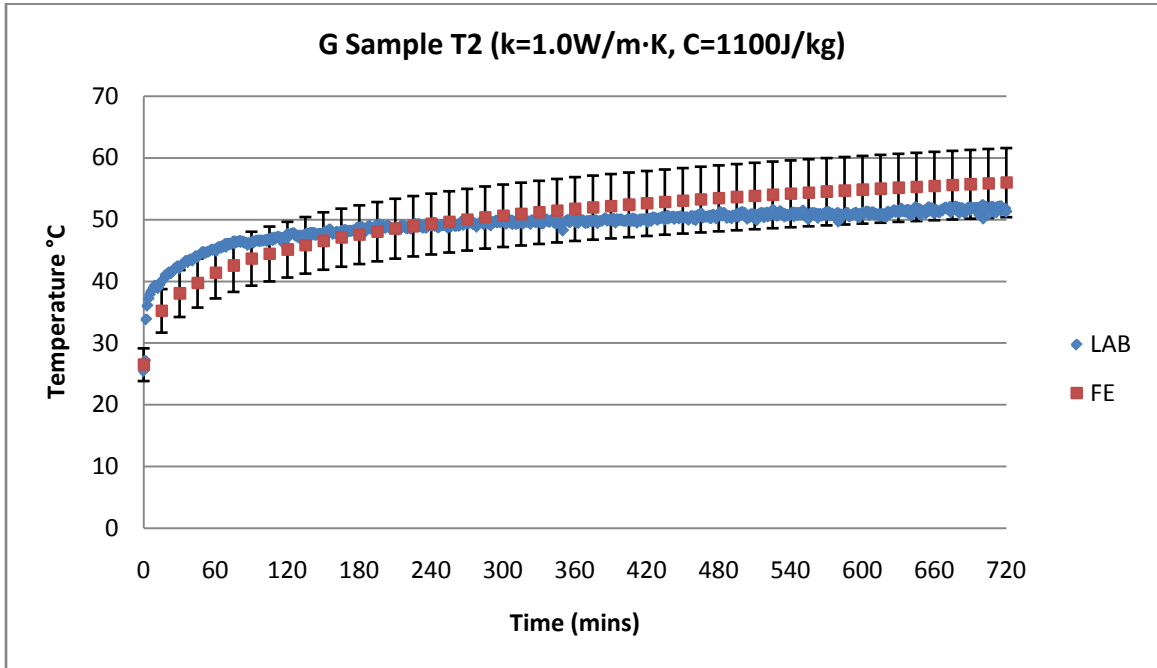


Figure 4-15 G sample temperature at T2 (finite element analysis vs. laboratory results)

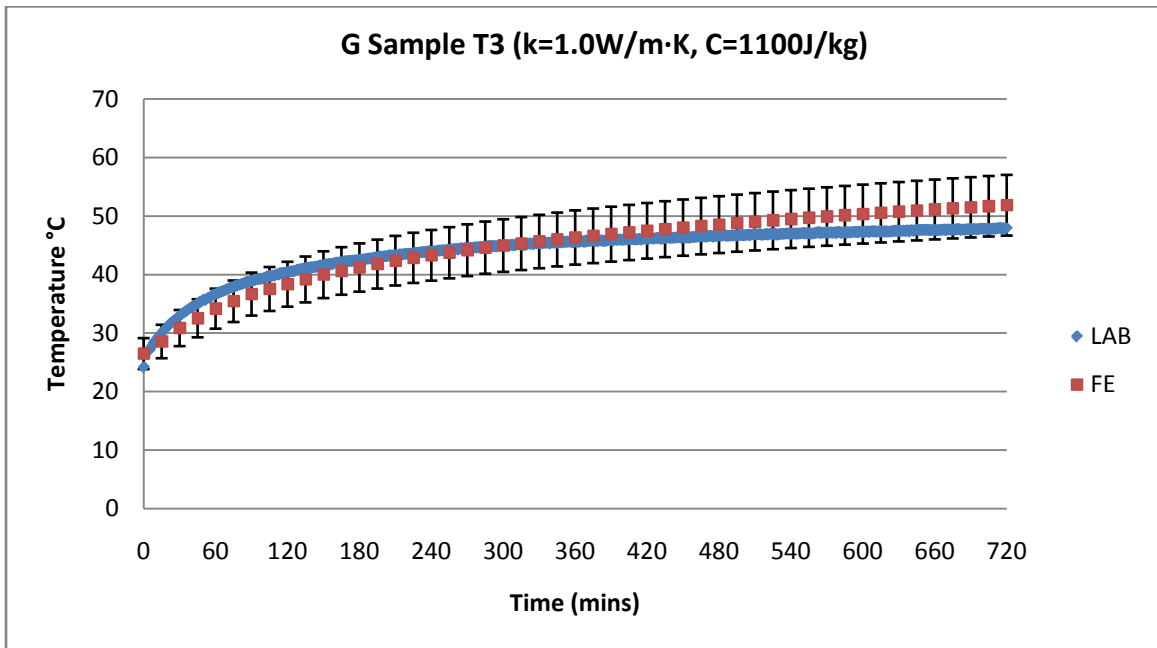
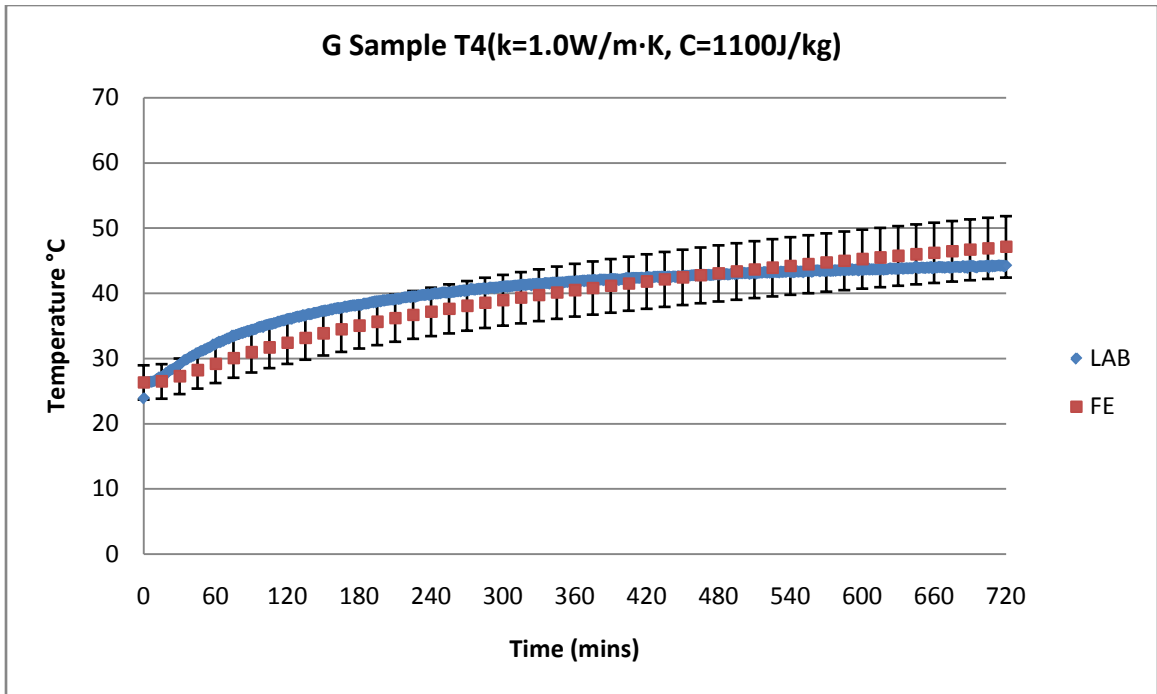
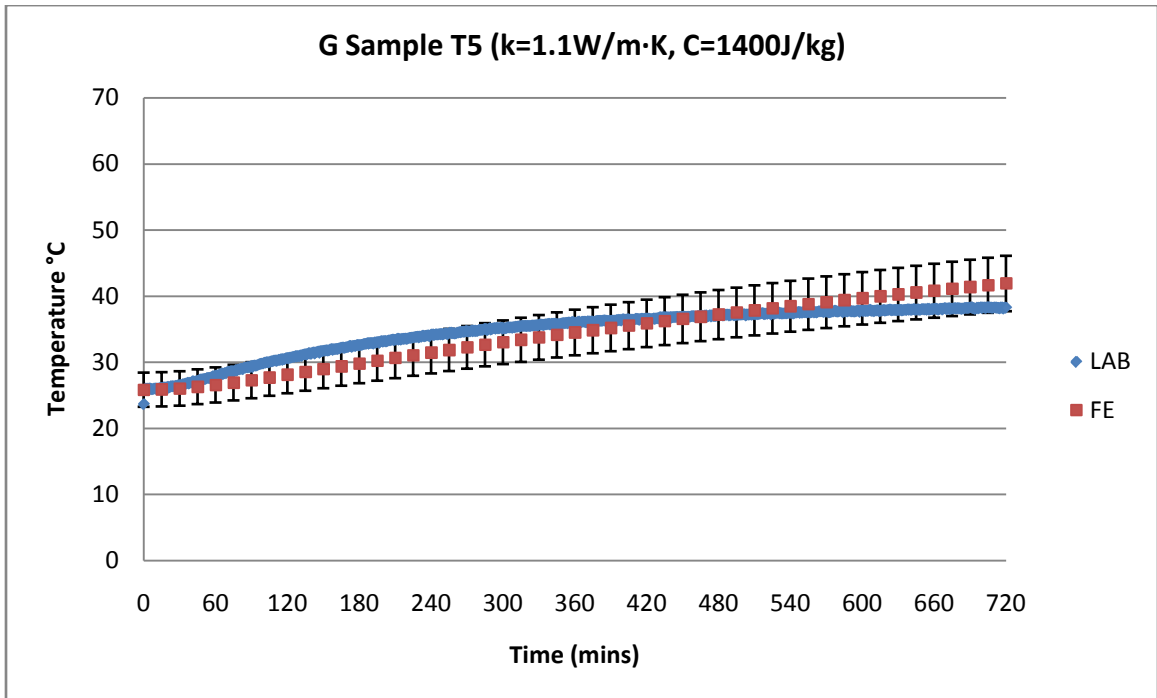


Figure 4-16 G sample temperature at T3 (finite element analysis vs. laboratory results)



**Figure 4-17 G sample temperature at T4 (finite element analysis vs. laboratory results)**



**Figure 4-18 G sample temperature at T5 (finite element analysis vs. laboratory results)**

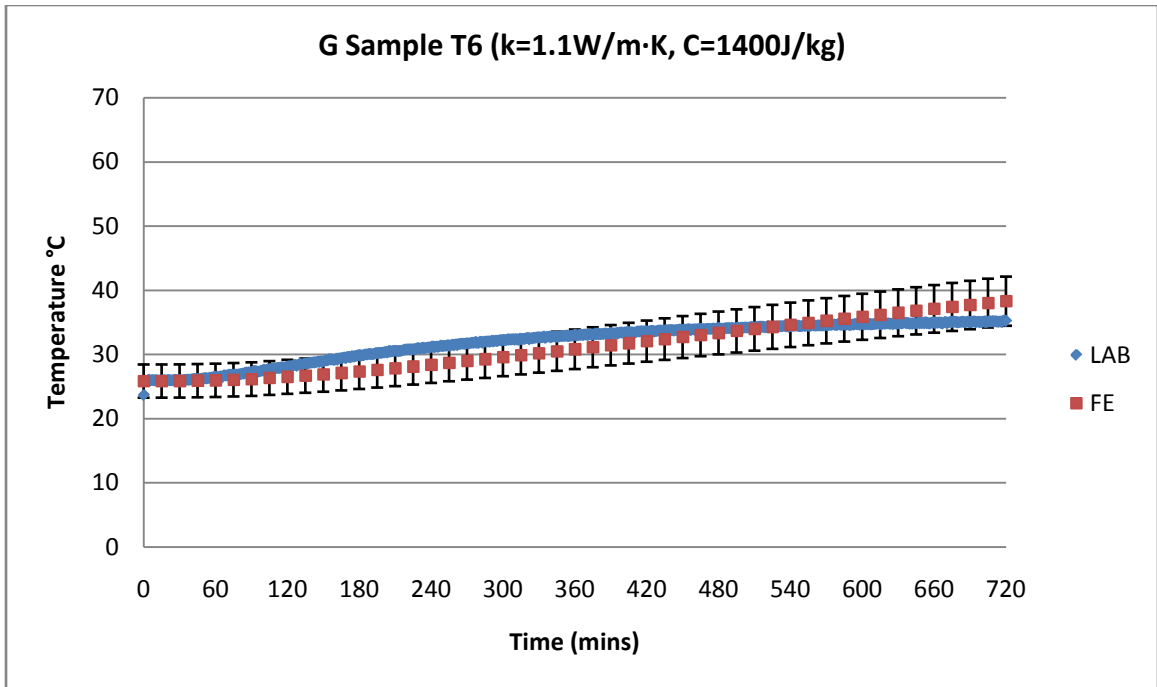


**Figure 4-19 G sample temperature at T6 (finite element analysis vs. laboratory results)**

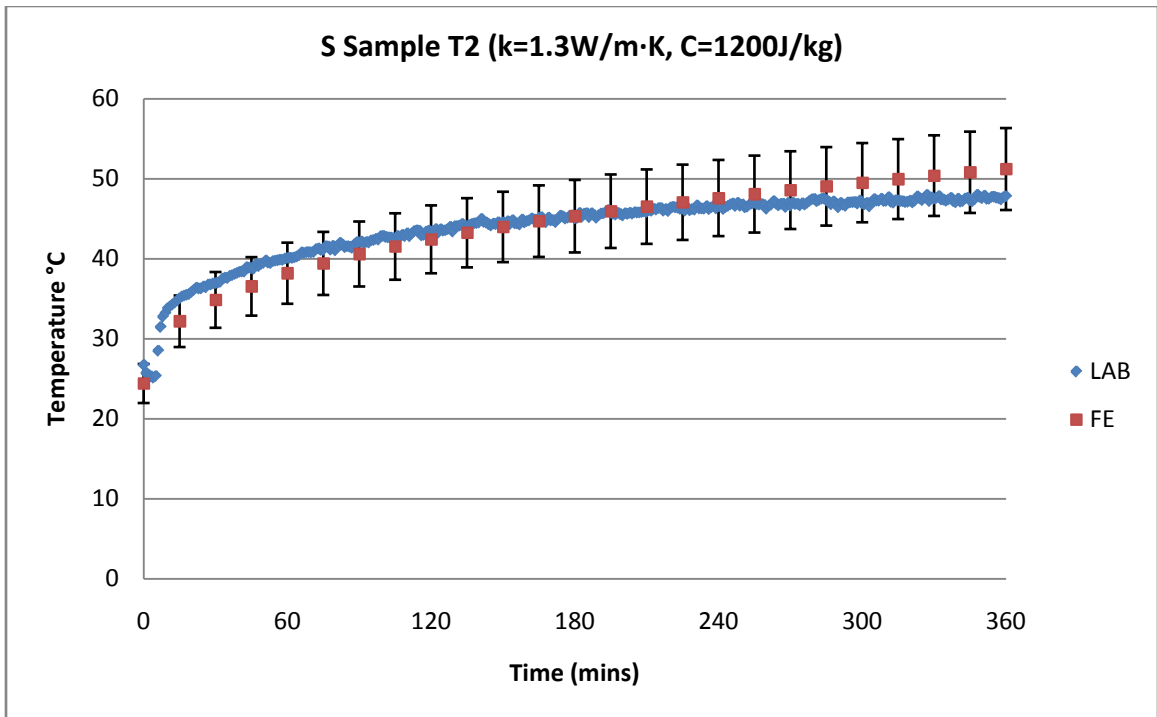


**Figure 4-20 S sample temperature at T2 (finite element analysis vs. laboratory results)**



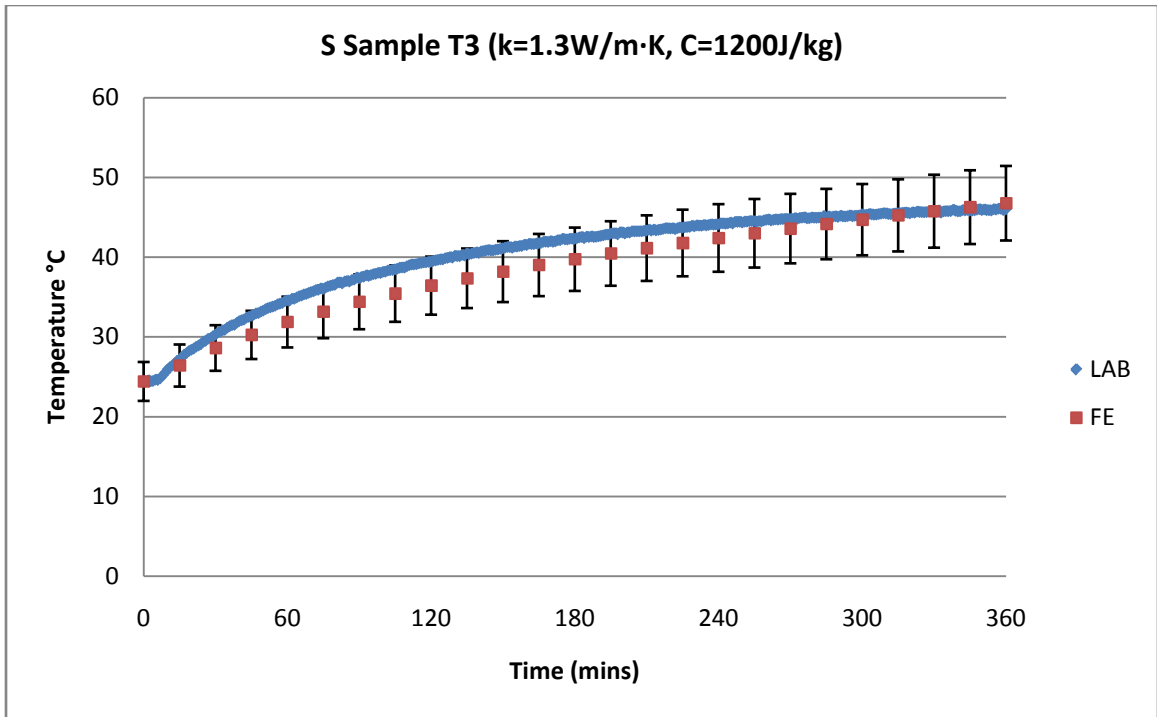


**Figure 4-21 S sample temperature at T3 (finite element analysis vs. laboratory results)**

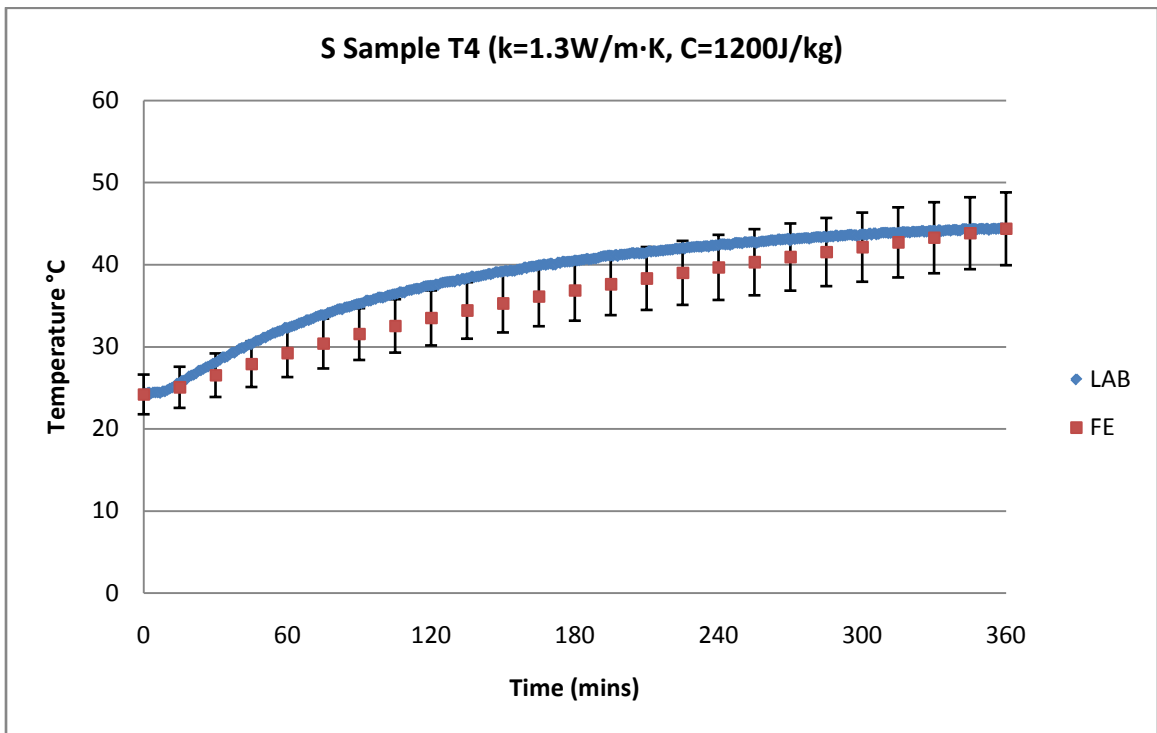


**Figure 4-22 S sample temperature at T4 (finite element analysis vs. laboratory results)**

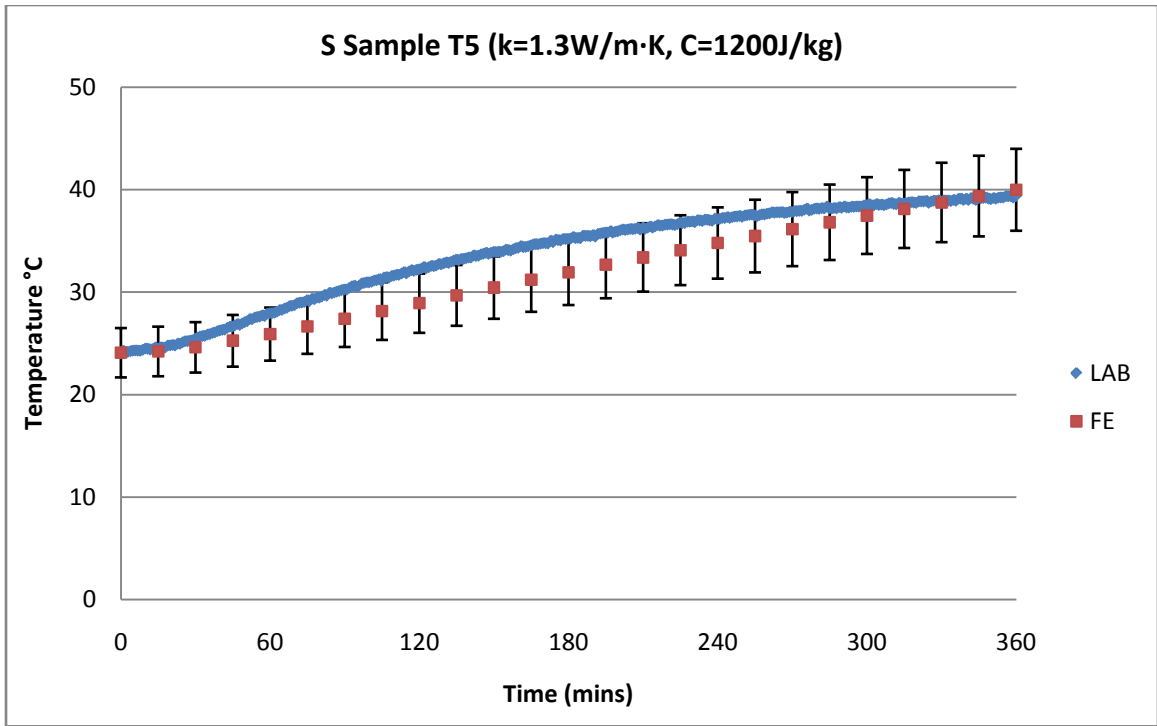


**Figure 4-23 S sample temperature at T5 (finite element analysis vs. laboratory results)**

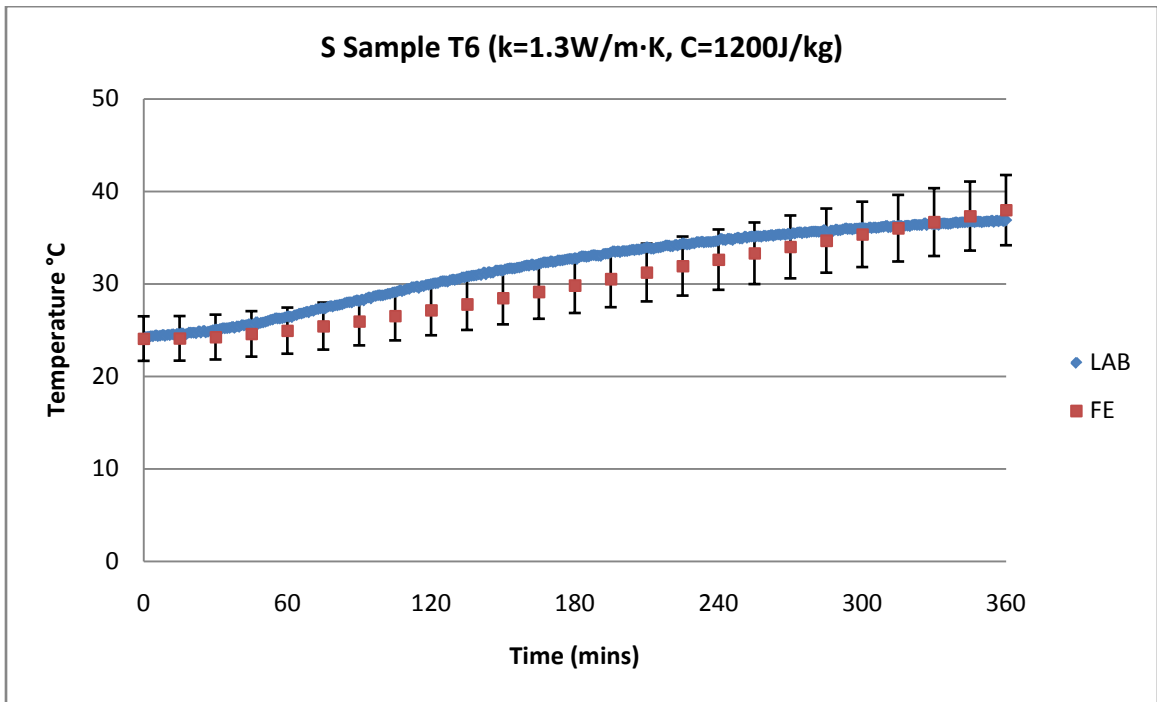


**Figure 4-24 S sample temperature at T6 (finite element analysis vs. laboratory results)**

## 4.8 Discussion

The back-calculated thermal conductivity ( $k$ ), heat capacity ( $C$ ), and thermal diffusivity ( $\alpha$ ) values for the different materials (layers) were shown on the respective samples in Table 4-11. Note that HMA and the other materials are all anisotropic and therefore the thermal properties are not the same in any direction – the estimated thermal properties indicated the effective and overall thermal property for the different layers.

The lengths of the different samples were different; this had affected the results from modeling as well as laboratory measurements. The study was carried out to estimate thermal properties of different layers in typical pavements. Therefore, these results are valid for the different materials and layers as long as they are present in a structure/thickness similar to those used in this chapter.

It was interesting to note from Table 4-11 that similar HMA mixes presented in different structures (that is with different base layers) showed different “effective” thermal properties. In their 2006 paper, Côté and Konrad (27) presented a practical approach of estimating thermal conductivity of pavement granular materials. Their method linked dry and saturated thermal conductivities through a set of empirical parameters, and one could estimate the thermal conductivity by using these parameters, as well as saturation and thermal conductivity of the solid particles, which could be estimated by considering the proportion of different minerals presented in the granular particles and their respective thermal conductivities. They also provided data which showed that thermal conductivities were inversely related to porosity of the soil particles.

One important point they noted was that for dry soils, the thermal conductivity was more sensitive to microstructure and/or particle type and less on the thermal conductivity of the solid particles. Since all of the mixes considered here were dry, it could be expected that mixes with similar aggregates, but different gradations and densities would show different thermal conductivities.

**Table 4-11 Backcalculated thermal properties of existing asphalt pavement samples**

Materials	Thermal Conductivity W/(m·K)	Heat Capacity J/(kg·K)	Thermal Difussivity (m <sup>2</sup> /s)
Surface+Binder			
HMA over similar HMA base (G)	1.6	1200	5.77e-07
HMA over Emulsion treated RAP base (S)	1.3	1200	4.55e-07
HMA over Cement treated base (R)	1.8	1800	4.59e-07
HMA over foamed asphalt (M)	1.5	1800	3.62E-07
HMA over coarser HMA base (P401)	1.0	1100	3.64E-07
Fuel resistant HMA over Polymer Modified HMA Base (FR)	1.5	1200	4.89e-07
Base			
HMA Base (G)	1.6	1200	5.60e-07
Emulsion treated RAP Base (S)	1.3	1200	5.19e-07
Cement Treated Base (R)	1.5	1400	5.42e-07
Foamed Asphalt Base (M)	1.5	1800	4.09e-07
HMA Base (P401)	1.1	1400	3.18e-07
Polymer Modified HMA Base (FR)	1.6	1200	5.40e-07

Note that because of the presence of asphalt binder in significant amount (5-7%), the use of the procedure outlined in Reference 24 may be somewhat impractical at this time, especially since the empirical parameters that are needed in this procedure have not been developed yet.

In this chapter, the backcalculated thermal conductivity and heat capacity values at the different thermocouple locations were adjusted until the predicted and measured temperatures at all thermocouple were within  $\pm 10\%$  of each other. Therefore, the analysis was affected significantly by the thermocouple locations – which were the same for the surface layers of all of the samples (surface, and 25mm below the surface), but not in the base layers. The base thermocouples were placed in the base layers at the third points – one third and two third down from the surface+binder layer. The temperature distribution throughout the depth of the base layer was measured. Therefore, the back-

calculated values were strictly valid for pavement structures which have the respective materials at the depths which are present in the sampled pavements.

This could be considered as a drawback, but more importantly, it pointed out the importance of estimating thermal properties of similar materials in conjunction with base materials in different pavement structures. Thermal conductivity or heat capacity testing (in the way conducted in this chapter) of surface+binder or base course only samples would not yield the same values as obtained in this chapter, and would most likely be also further away from the “effective” values. Obviously the best approach is using data from in-place instrumentation. Since in-place instrumentation is relatively costly and involves a significant amount of installation work, testing full-depth (or at least with base layer) samples as done in this study is an alternative option. Furthermore, even though Reference 22 recommends ASTM E1952, direct validation of thermal conductivity of a composite material as HMA is very difficult.

## CHAPTER 5

### SMALL SCALE ASPHALT PAVEMENT TESTING

#### 5.1 Introduction

The heat transfer from a pavement heated by solar energy can be enhanced by using a high conductivity material as well as by using an insulating layer on the top that would reduce reflectivity and emissivity. The amount of energy generated can also be increased significantly by increasing the surface area exposed to the sun. To ensure that the pavement is constructed using conventional equipment and techniques, and it is sufficiently durable, the materials that can be used are mineral aggregates, asphalt binder and additives, and the insulating layer on the top has to be either in the form of a powder or a liquid. Accordingly, the effect of higher conductivity material, layers on the surface, and surface area were evaluated in this chapter.

#### 5.2 Objective

The objectives of this chapter were to evaluate:

1. Aggregate with high conductivity.
2. Partial replacement of granite aggregate with quartzite.
3. High conductivity material as additives.
4. Absorptivity enhancing paint.
5. Modified surface conditions.
6. Increased surface area of sample and copper pipe.
7. Controlled water inlet temperature and volume.

#### 5.3 Methodology

The methodology of this chapter included finite element modeling, experiments with small 150 mm diameter, 114 mm thick pavement samples (henceforth referred to as small scale tests) (Hot Mix Asphalt, HMA samples, compacted using Superpave gyratory compactor in the laboratory, and a dense graded HMA mix gradation and asphalt content; all HMA used in this study had PG 64-28 grade asphalt binder).

The relative positions of the heating lamp over the HMA sample were selected to provide  $1,000\text{W/m}^2$  of radiation (Appendix C). The radiation  $1,000\text{W/m}^2$  was used for simulating the maximum summer time radiation in Worcester, MA area. The objective

was to investigate change of temperature in the water caused by conduction of heat from a heated HMA sample for a time span of 6 hours, and as well to evaluate the effect of thermal conductivity. The finite element analysis was used along with these preliminary tests.

This chapter was a continuation of investigating of temperature distributions in 150 mm diameter pavement samples, which were subjected to heat radiation from a halogen lamp. The experiment setup and test were categorized into five scenarios.

- I. A 0.0508m (½”) diameter copper pipe was inserted inside the sample; the other end of the copper pipe was placed in a small bath of water. Initially, the copper pipe was used as the “heat exchanger” between the heated HMA sample and the water in the bath. Thermocouples were positioned to the sample at different heights, and the bath/inlet and outlets were connected to a data acquisition system, which allowed continuous recording of temperature (Appendix C). The following samples were analyzed:
  1. 100% Quartzite mix.
  2. 100% Limestone mix.
  3. 100% Quartzite mix with tinted glass on the surface.
- II. Modified initial water temperature and flow rate and complied asphalt samples with increased diameter of copper pipe (Appendix C). The following samples were analyzed:
  4. 100% Quartzite with iced water (3mL/min).
  5. 100% Quartzite mix with trapped iced water inside of cooper pipe.
  6. Complied of 5 quartzite samples with 0.01905m (¾”) copper pipe.
- III. Uniform granite and quartzite aggregate with various water flow rate was pumped through the 0.00635m (¼”) diameter copper pipe, and used as the heat exchanger. Thermocouples were positioned to the sample at different heights, and the bath/inlet and outlets were connected to a data acquisition system, which allowed continuous recording of temperature. (Appendix C). The following samples were analyzed:
  7. 100% Quartzite mix.

8. 100% Metagranodiorite mix.
  9. 100% RAP mix.
- IV. Partial replacement of granite aggregate with quartzite with various water flow rate was pumped through the 0.00635m (¼") diameter copper pipe. Thermocouples were positioned to the sample at different heights, and the bath/inlet and outlets were connected to a data acquisition system, which allowed continuous recording of temperature. The following samples were analyzed:
10. Quartzite with 22% copper mix.
  11. Quartzite with 30% aluminum mix.
  12. Quartzite with 50% RAP mix.
  13. Quartzite with 75% RAP mix.
  14. 67% Quartzite with 33% limestone mix.
- V. Modified surface conditions on partial replacement of granite aggregate with quartzite with various water flow rate was pumped through the 0.00635m (¼") diameter copper pipe. Thermocouples were positioned to the sample at different heights, and the bath/inlet and outlets were connected to a data acquisition system, which allowed continuous recording of temperature. The following samples were analyzed:
15. Tinted glass on the surface of 78% quartzite with 22% copper mix.
  16. Acrylic paint on the surface of 78% quartzite with 22% copper mix.
  17. Tinted glass on the surface of 70% quartzite with 30% aluminum mix.
  18. Chipped glass with asphalt mix on the 70% quartzite with 30% aluminum mix.



## 5.4 Experiment Results

The 10, 20, 40, 60, 80, and 100mL/min water flow rate were used to determine the temperature difference between initial water temperature and outflow water temperature except scenario I.

The delta T of each scenario used for comparison was based on 10mL/min with 60 minutes of time period because the temperature showed most significant difference at this flow rate. The heat energy (power) generated from each flow rate can be calculated by:

$$Q = mC_p \Delta T$$

Where m is mass of water,  $C_p$  is heat capacity of water;  $\Delta T$  is temperature difference between water inlet and outlet.

### Scenario I

The quartzite aggregate, consisting of approximately 95% quartz and with traces of hematite (giving it a pink color) was obtained from New Ulm quarry, MN. This aggregate is currently used mainly for poultry and traction grit as well as for railroad ballast and surface seal mix aggregates. The limestone aggregate, typically used in HMA mixtures, was obtained from Calera, AL.

Two HMA samples were prepared, one each with quartzite and limestone aggregates. Rise of temperature in water was noted from tests conducted with the small scale experimental setup described above. The results (Table 5-1 and Figure 5-1) showed that the sample with quartzite aggregate had a significantly higher temperature difference (between original water temperature and final water temperature) compared to the limestone aggregate mix. The comparison revealed that the higher heat capacity of quartzite (1.5 times higher) and conductivity (2.5 times higher) were clearly beneficial in heating water by extracting heat from depth inside the pavement (via copper pipe inserted at a depth of 25mm). The water was heated by 10.13°C for the quartzite sample over 6 hours as opposed to 5.02°C for the limestone sample. This showed preliminary evidence that altering the pavement material would allow higher amount of heat energy from the pavement to be extracted for similar radiation conditions.

**Table 5-1 Quartzite and Limestone mix temperature difference**

	T <sub>initial</sub> (°C)	T <sub>final</sub> (°C)	ΔT (°C)	Watt, W
100% Quartzite mix	24.11	34.24	10.13	1.12
100% Limestone mix	23.81	28.83	5.02	0.55

The quartzite mix was then placed a tinted glass on its surface, and performed the same test procedure to investigate the improving heat transfer by modifying the surface condition. The results (Table 5-2 and Figure 5-1) showed the delta T from quartzite with tinted glass was slightly higher than just quartzite sample by 0.34°C, which meant that the tinted glass would reduce the convective heat transfer from the surface of the sample, and increased the heat transfer from asphalt sample to the water.

**Table 5-2 Quartzite mix with and without placement of tinted glass temperature difference**

	T <sub>initial</sub> (°C)	T <sub>final</sub> (°C)	ΔT (°C)	Watt, W
100% Quartzite mix	24.11	34.24	10.13	1.12
100% Quartzite + Glass	23.39	33.87	10.47	1.16

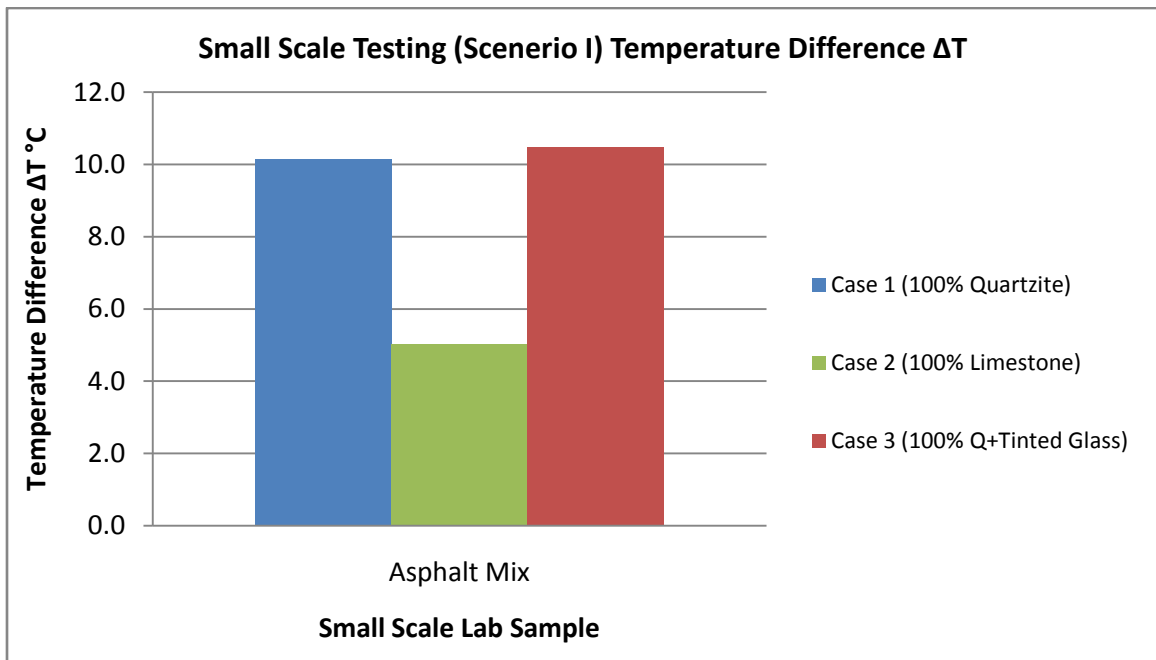


**Figure 5-1 Small scale testing (Scenario I) temperature difference ΔT**

## Scenario II

The Figure 5-2 showed the most temperature difference was trapped iced water inside of copper pipe; however, it did not generate the most power due to its small volume. On the other hand, the compiled quartzite samples (Table 5-5) generated approximately 6 times of power than other two samples (Table 5-3 and 5-4) because it had most large surface area which increased higher heat transfer rate (Figure 5-3).

## Scenario II

**Table 5-3 100% Quartzite with iced water (3mL/min) temperature difference**

Time (min)	T <sub>initial</sub> (°C)	T <sub>final</sub> (°C)	ΔT (°C)
5	2.69	8.37	5.67
10	3.73	12.29	8.56
20	5.21	18.94	13.73
40	5.07	26.49	21.42
60	5.51	30.60	25.09
80	5.67	33.28	27.61
100	5.95	34.80	28.85
120	7.20	35.47	28.27

**Table 5-4 100% Quartzite mix with trapped iced water inside of cooper pipe temperature difference**

Time (min)	T <sub>initial</sub> (°C)	T <sub>final</sub> (°C)	ΔT (°C)
5	8.62	44.65	36.03
10	14.12	43.05	28.93
15	11.27	43.19	31.92
20	13.27	42.43	29.16
30	16.2	43.52	27.32

**Table 5-5 Complied of 5 quartzite samples with 0.01905m (¾”) copper pipe temperature difference**

Flow Rate (mL/min)	T <sub>initial</sub> (°C)	T <sub>final</sub> (°C)	ΔT (°C)
10	24.50	58.43	33.93
20	24.50	54.49	29.99
30	24.50	47.90	23.40
40	24.50	44.35	19.85
60	24.50	39.59	15.09
80	24.50	37.03	12.53
100	24.50	36.81	12.31

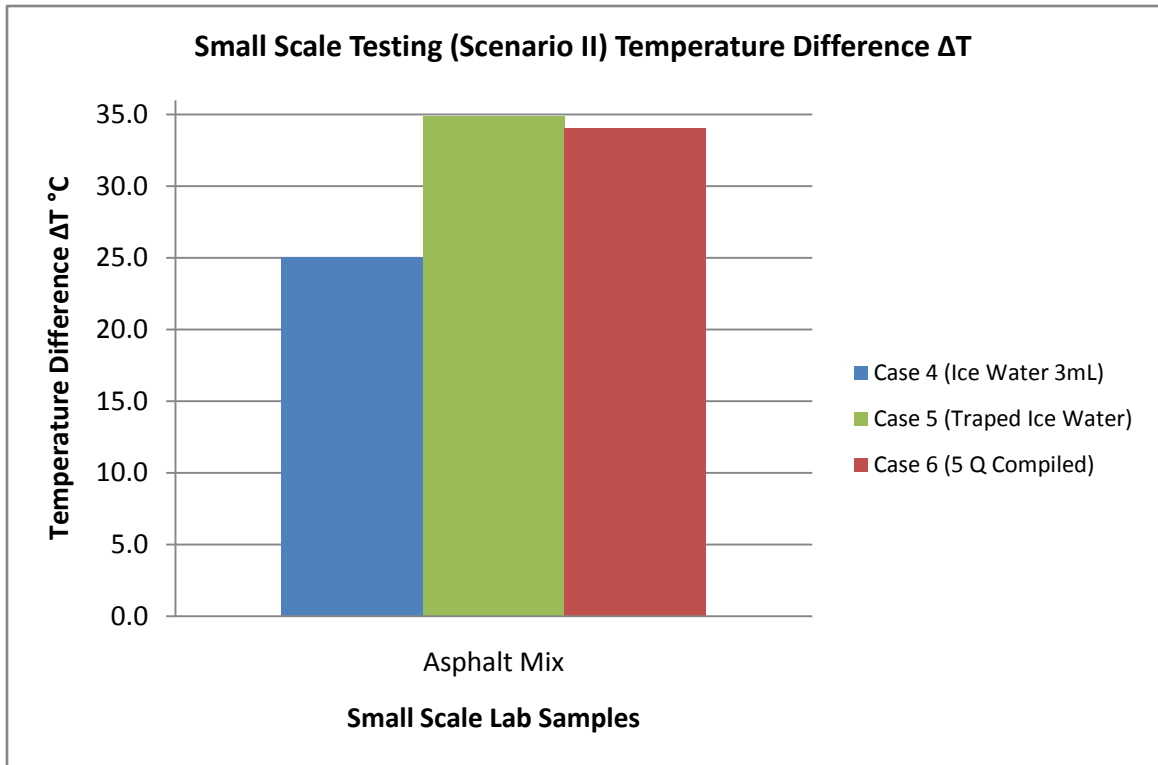


**Figure 5-2 Small scale testing (Scenario II) temperature difference  $\Delta T$**

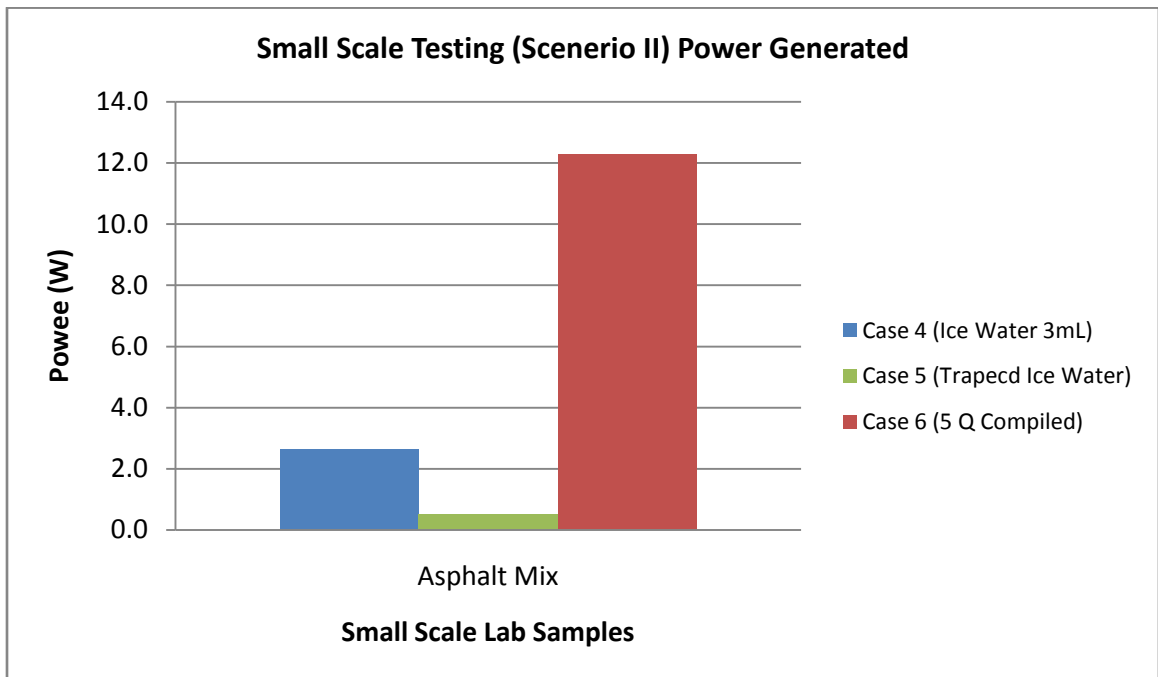


**Figure 5-3 Small scale testing (Scenario II) power generated**

### Scenario III

Three HMA samples were prepared, one with 100% quartzite mix, one with metagranodiorite mix, and one with 100 % locally available reclaimed asphalt pavement (RAP) materials (with aggregate from bedrock characterized as biotite-quartz-plagioclase granofels)). The Figure 5-4 showed the typical sample with thermocouple locations. The final temperature readings of each flow rate were recorded when water temperature remained stabilized. The results (Figure 5-5) showed that the delta T of 100% quartzite mix (Table 5-6) from various flow rate were the highest among three. The Figure 5-6 showed that the most significant difference was at 10mL/min; even though the delta T of 100% RAP (Table 5-8) was slightly higher than 100% Wrentham (Table 5-7) at higher flow rates, but the temperature difference is less than 1°C which could not be taken into consideration. The Figure 5-7 also showed the power generated from 10mL/min for three samples.

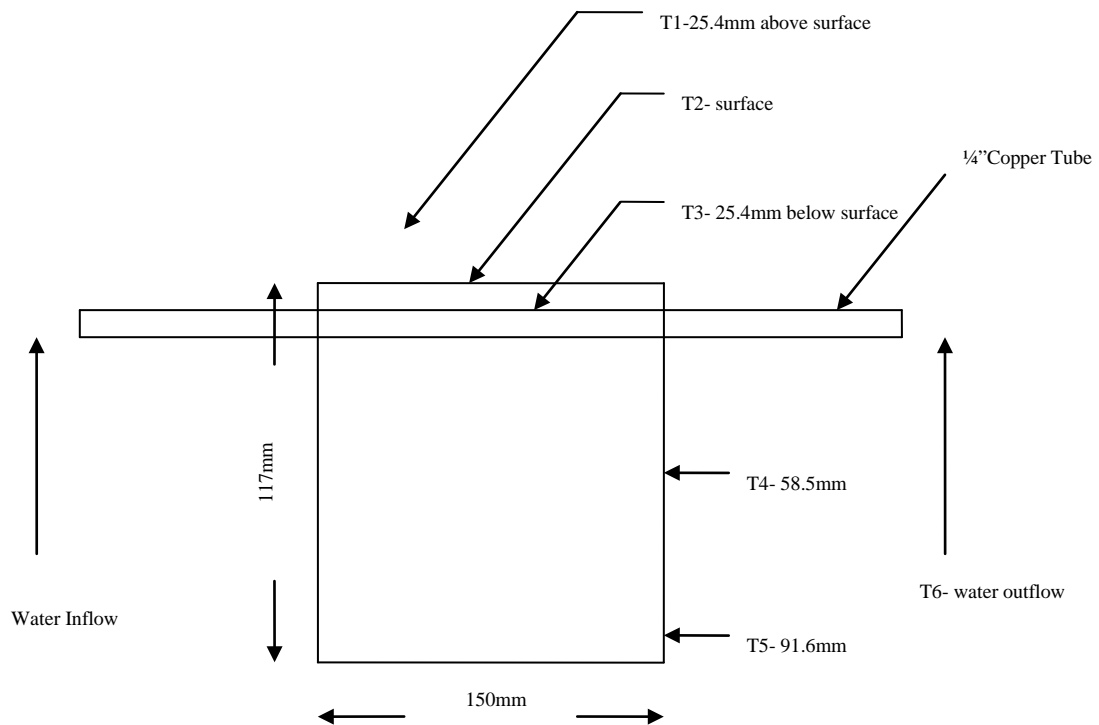


**Figure 5-4** Typical asphalt sample with thermocouples

**Table 5-6 100% Quartzite mix temperature difference**

Flow Rate (mL/min)	T <sub>initial</sub> (°C)	T <sub>final</sub> (°C)	ΔT (°C)
10	24.95	33.59	8.64
20	25.08	30.25	5.17
40	25.07	27.78	2.72
60	24.68	26.64	1.96
80	24.89	26.37	1.49
100	24.98	26.48	1.49

**Table 5-7 100% Metagranodiorite mix temperature difference**

Flow Rate (mL/min)	T <sub>initial</sub> (°C)	T <sub>final</sub> (°C)	ΔT (°C)
10	24.33	31.31	6.98
20	24.14	27.45	3.31
40	24.69	25.71	1.03
60	24.67	24.94	0.27
80	24.66	24.60	0.06
100	24.72	24.53	0.18

**Table 5-8 100% RAP mix temperature difference**

Flow Rate (mL/min)	T <sub>initial</sub> (°C)	T <sub>final</sub> (°C)	ΔT (°C)
10	24.50	30.60	6.10
20	24.50	28.08	3.58
40	24.50	26.15	1.65
60	24.50	25.59	1.09
80	24.50	25.39	0.89
100	24.50	25.24	0.74

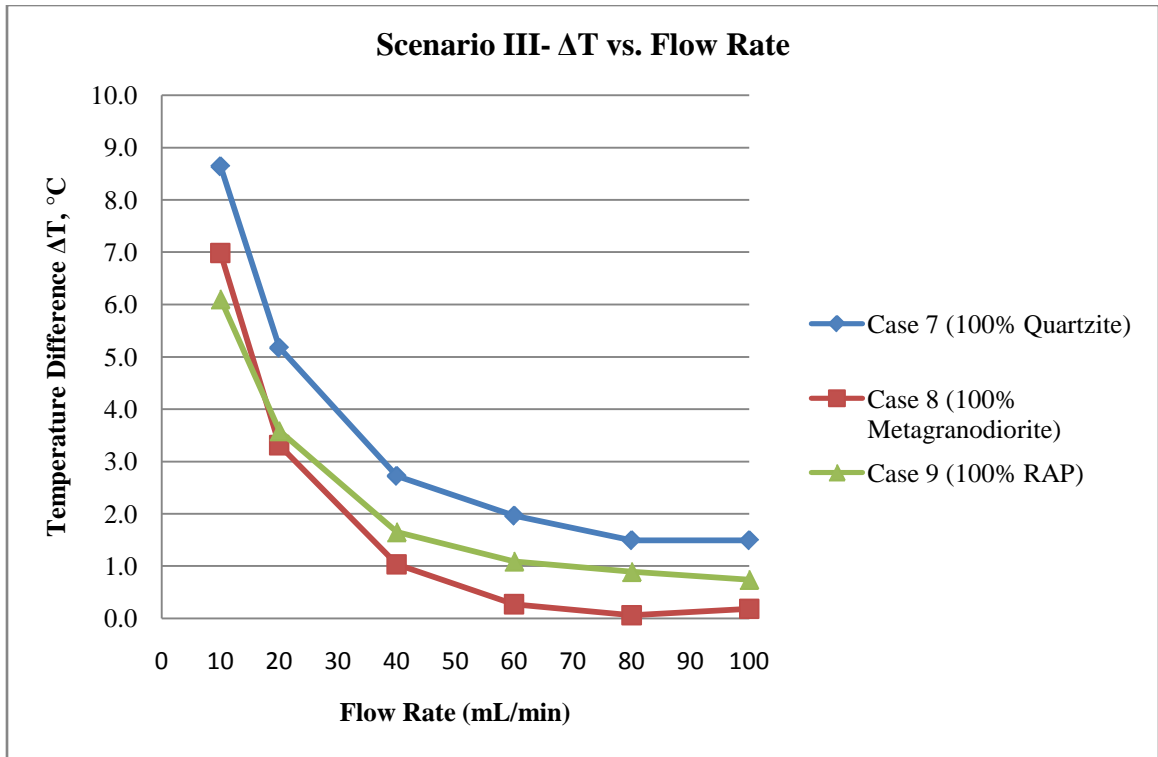


**Figure 5-5 Small scale testing (Scenario III) temperature vs. flow rate**

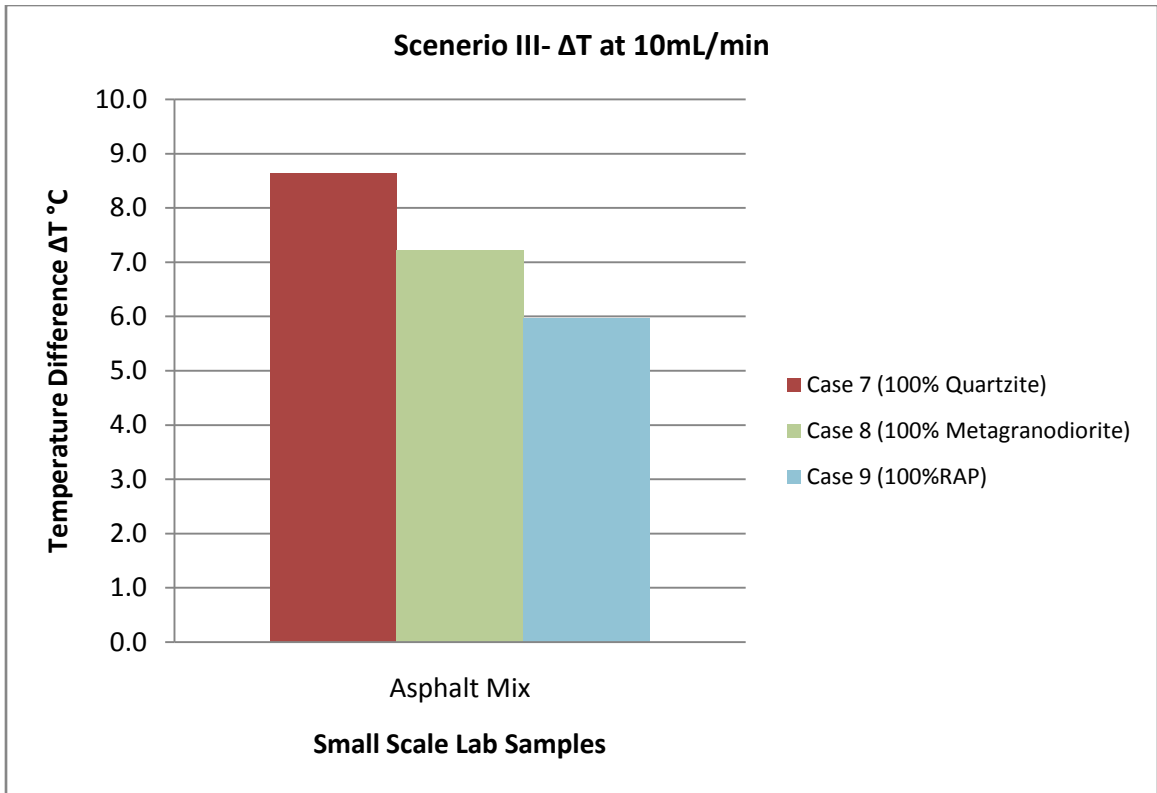


**Figure 5-6 Small scale testing (Scenario III) temperature difference ΔT**

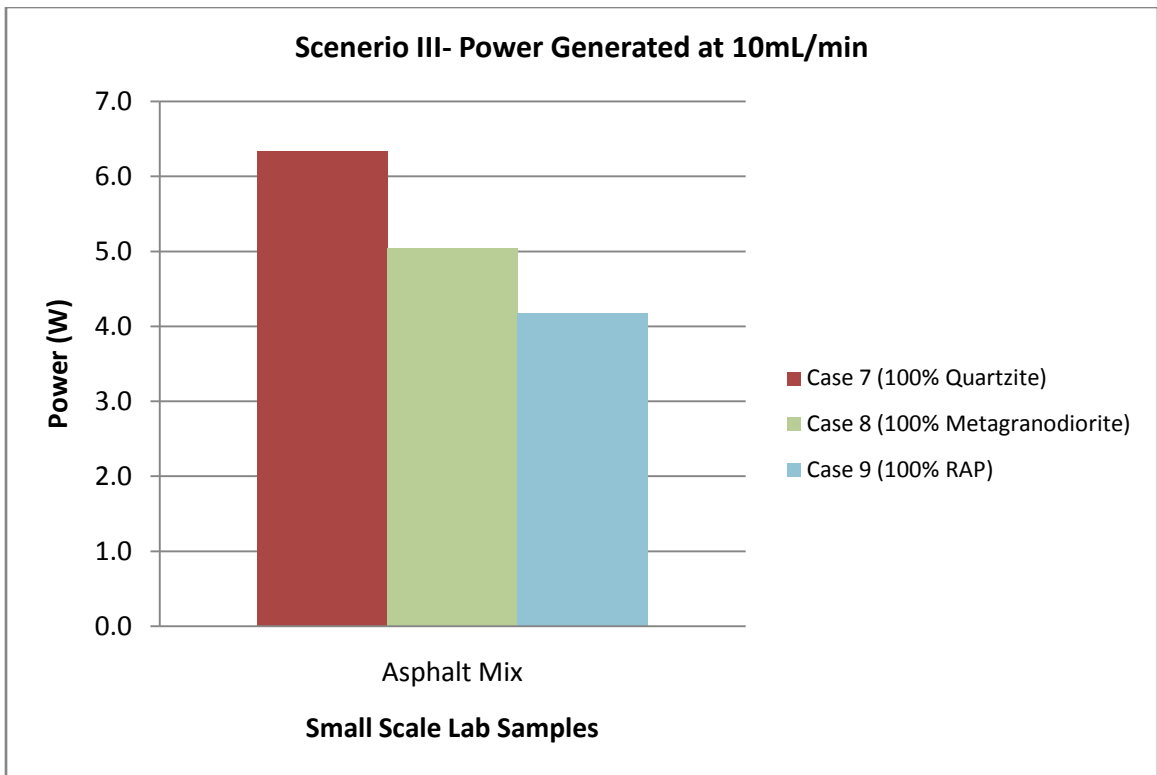


**Figure 5-7 Small scale testing (Scenario III) power generated**



#### Scenario IV

Since a higher conductivity would help in obtaining a higher rate of energy transfer, the metal with high conductivity, copper ( $k= 401 \text{ W/m}\cdot\text{K}$ ) and aluminum powder ( $k=250 \text{ W/m}\cdot\text{K}$ ) were used by replacing about 22% and 30% of the quartzite aggregate respectively. The both powders were mixed with the aggregates prior to mixing with the asphalt binder. The samples were tested at different flow rates of water. A comparison of delta T for samples with and without copper and aluminum was shown in Figure 5-8 and 5-9. No significant increase in delta T was observed for the copper-HMA and aluminum-HMA samples (Table 5-9 and 10). In fact, the delta T was reduced with the introduction of copper and aluminum. This could be due to the fact that the copper and aluminum powder were covered with asphalt during mixing and also was partially oxidized during the heating of the aggregates prior to mixing.

Based on the results obtained, it was argued that a partial replacement of locally available aggregates with quartzite aggregates would significantly increase delta T. Two samples were prepared and tested to investigate one with 75% RAP and 25 % quartzite aggregate and another one is with 50% RAP with 50% quartzite (Table 5-11 and 5-12). As Figure 5-10, 5-11, 5-12 shows the addition of quartzite has a significant positive effect on delta T.

**Table 5-9 Quartzite with 22% copper mix temperature difference**

Flow Rate (mL/min)	T <sub>initial</sub>	T <sub>final</sub>	$\Delta T$
10	24.50	31.46	6.96
20	24.50	28.65	4.15
40	24.50	26.84	2.34
60	24.50	26.35	1.85
80	24.50	26.17	1.67
100	24.50	26.16	1.66

**Table 5-10 Quartzite with 30% aluminum mix temperature difference**

Flow Rate (mL/min)	T <sub>initial</sub>	T <sub>final</sub>	$\Delta T$
10	24.50	31.06	6.56
20	24.50	28.85	4.35
40	24.50	27.40	2.90
60	24.50	27.03	2.53
80	24.50	26.82	2.32
100	24.50	26.82	2.32

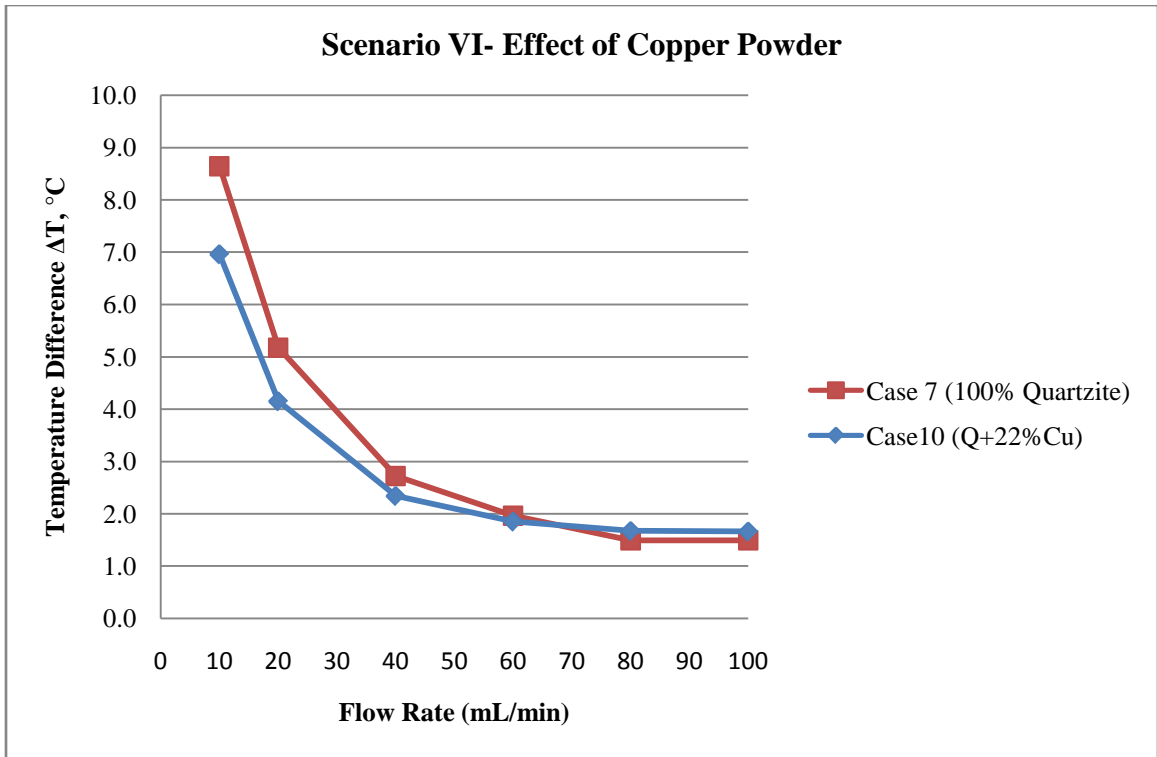


**Figure 5-8 Small scale testing (Scenario VI) effect of copper powder**

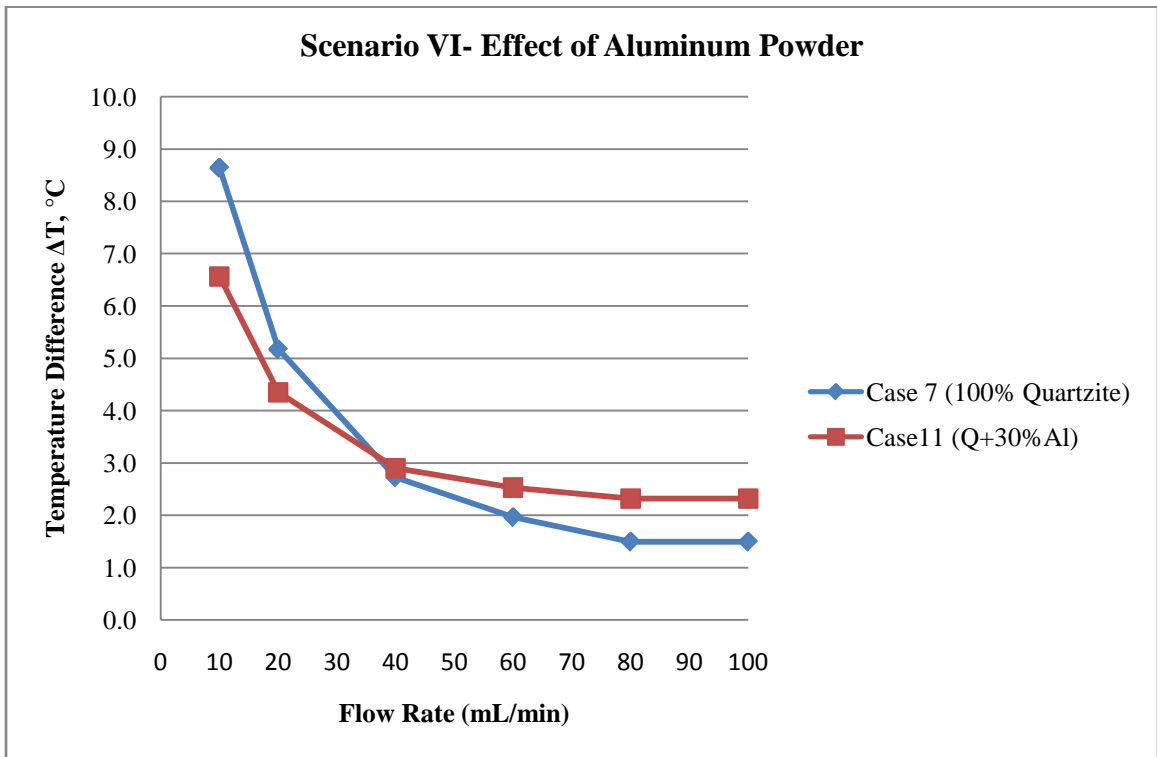


**Figure 5-9 Small scale testing (Scenario VI) effect of aluminum powder**

**Table 5-11 Quartzite with 50% RAP mix temperature difference**

Flow Rate (mL/min)	T <sub>initial</sub>	T <sub>final</sub>	ΔT
10	23.17	31.48	8.31
20	22.99	27.40	4.41
40	23.26	25.41	2.14
60	23.25	24.75	1.50
80	23.29	24.36	1.07
100	23.35	24.31	0.96

**Table 5-12 Quartzite with 75% RAP mix temperature difference**

Flow Rate (mL/min)	T <sub>initial</sub>	T <sub>final</sub>	ΔT
10	24.50	33.02	8.52
20	24.50	29.25	4.75
40	24.50	27.03	2.53
60	24.50	26.39	1.89
80	24.50	26.20	1.70
100	24.50	26.04	1.54

**Table 5-13 67% quartzite with 33% limestone mix temperature difference**

Flow Rate (mL/min)	T <sub>initial</sub>	T <sub>final</sub>	ΔT
10	25.29	31.48	6.19
20	25.51	28.24	2.73
40	25.50	26.35	0.85
60	25.18	25.97	0.80
80	24.68	25.34	0.66
100	24.24	24.91	0.67

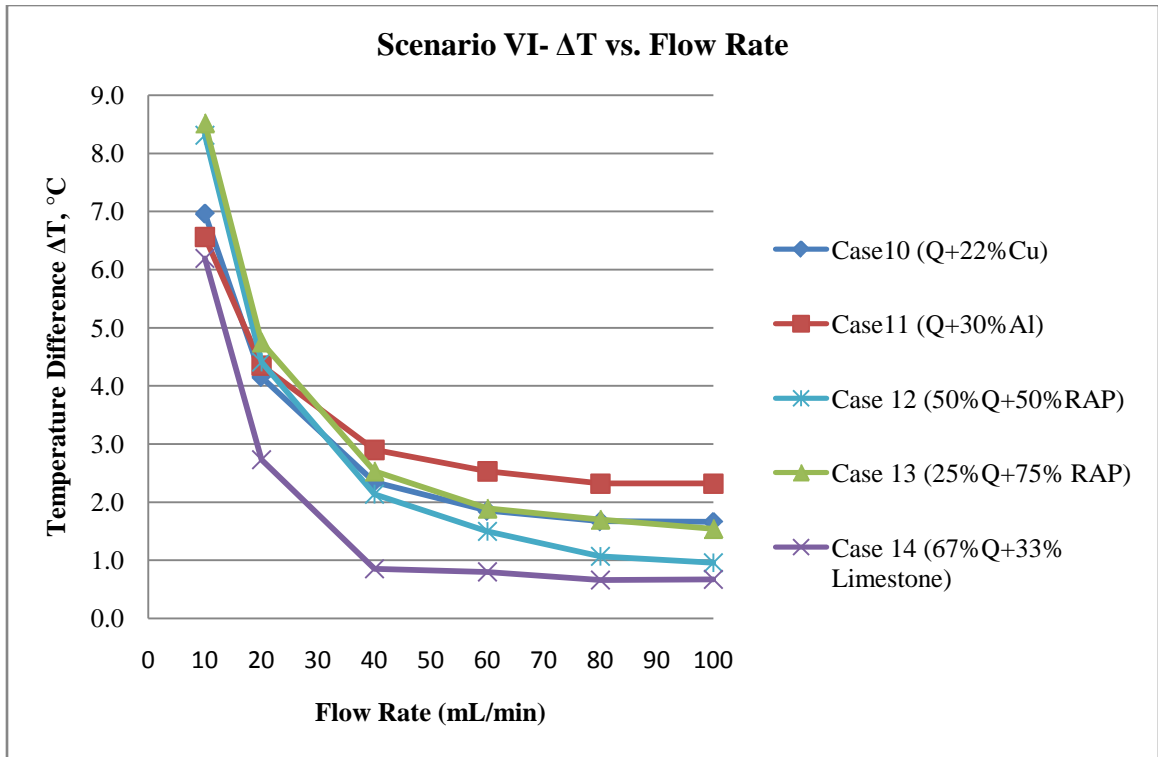


**Figure 5-10 Small scale testing (Scenario VI) temperature vs. flow rate**

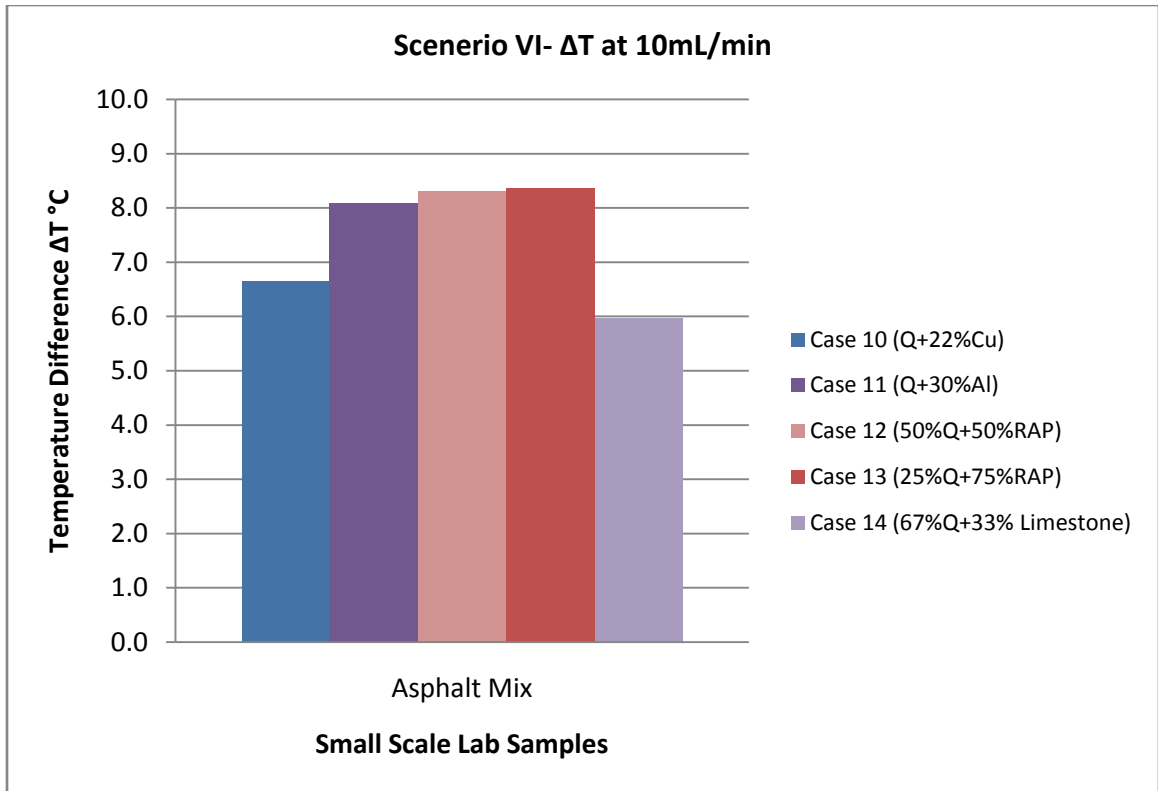


**Figure 5-11 Small scale testing (Scenario VI) temperature difference  $\Delta T$**

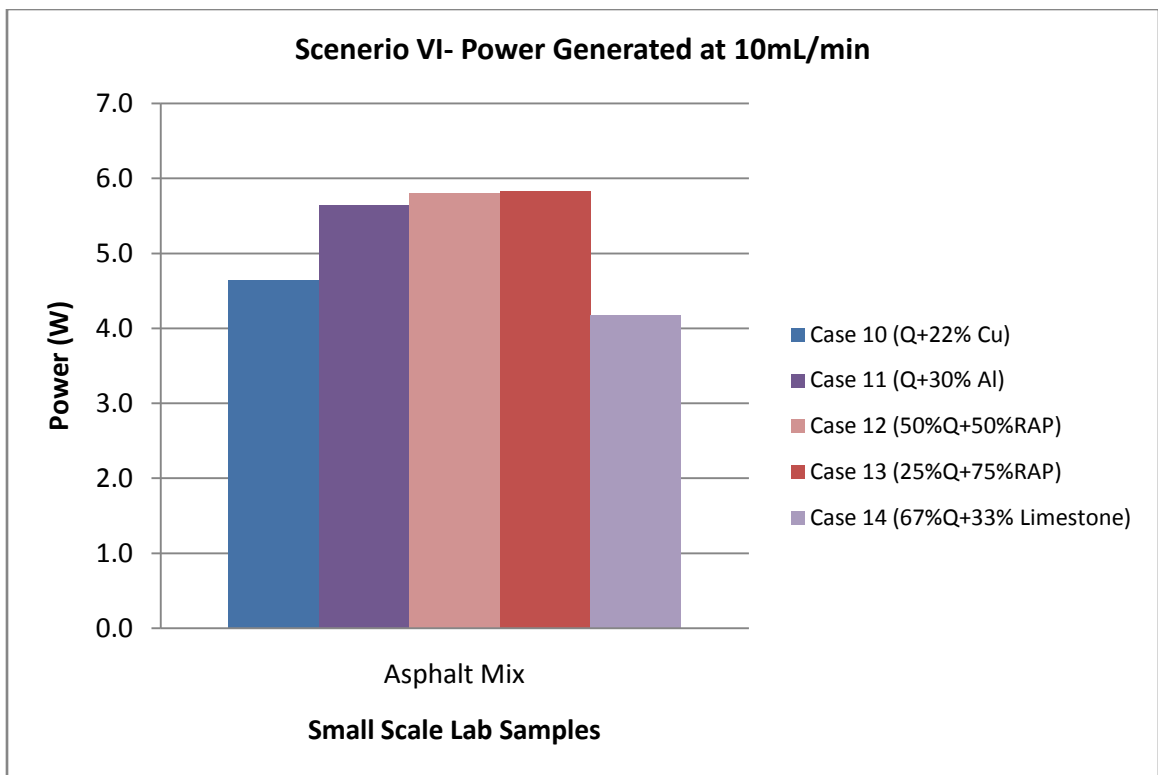


**Figure 5-12 Small scale testing (Scenario VI) power generated**

## Scenario V

The tinted glass disk was placed on the quartzite sample with 22% copper powder and 30% aluminum powder samples and observed the effect of modifying surface conditions. The quartzite sample with 22% copper powder was then covered with a layer of acrylic paint to observe any effect on delta T. As Figure 5-13, 5-14, and 5-15 showed, a significant increase in delta T was observed. This test with acrylic paint and tinted glass proved that there could be a significant rise in temperature due to a lowering of the reflective radiation losses and/or increase in the absorptivity on the surface. For certain flow rates the temperature rise is 40% more for the acrylic painted sample compared to the unpainted sample. (Figure 5-16)

While both aggregates of higher conductivity and absorptivity enhancing paint layer could improve the efficiency of heat capture, as mentioned earlier, the most important advantage of this system is the large surface area of available paved surfaces, and the ability to utilize it. Theoretically, one could argue that pipe system carrying water through a large surface area would be more efficient in terms of heat transfer.

**Table 5-14 Tinted glass on the surface of quartzite with 22% copper mix temperature difference**

Flow Rate (mL/min)	T <sub>initial</sub>	T <sub>final</sub>	ΔT
10	24.50	32.01	7.51
20	24.50	28.73	4.23
40	24.50	26.82	2.32
60	24.50	26.34	1.84
80	24.50	26.13	1.63
100	24.50	26.20	1.70

**Table 5-15 Acrylic paint on the surface of quartzite with 22% copper mix temperature difference**

Flow Rate (mL/min)	T <sub>initial</sub>	T <sub>final</sub>	ΔT
10	24.50	32.78	8.28
20	24.50	29.51	5.01
40	24.50	27.68	3.18
60	24.50	27.27	2.77
80	24.50	27.00	2.50
100	24.50	26.78	2.28

**Table 5-16 Tinted glass on the surface of quartzite with 30% aluminum mix temperature difference**

Flow Rate (mL/min)	T <sub>initial</sub>	T <sub>final</sub>	ΔT
10	24.50	32.63	8.13
20	24.50	29.46	4.96
40	24.50	27.45	2.95
60	24.50	26.81	2.31
80	24.50	26.81	2.31
100	24.50	26.41	1.91

**Table 5-17 Chipped glass with asphalt mix on the quartzite with 30% aluminum mix temperature difference**

Flow Rate (mL/min)	T <sub>initial</sub>	T <sub>final</sub>	ΔT
10	24.50	31.53	7.03
20	24.50	28.94	4.44
40	24.50	27.41	2.91
60	24.50	26.92	2.42
80	24.50	26.59	2.09
100	24.50	26.62	2.12

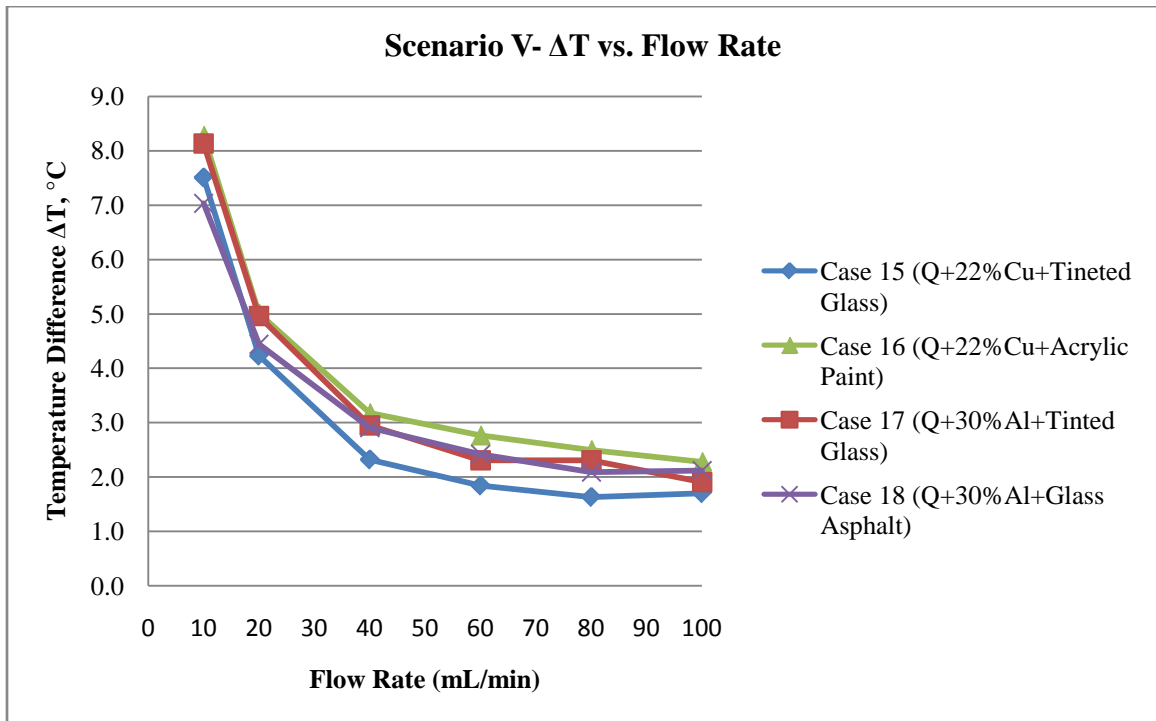


**Figure 5-13 Small scale testing (Scenario V) temperature vs. flow rate**

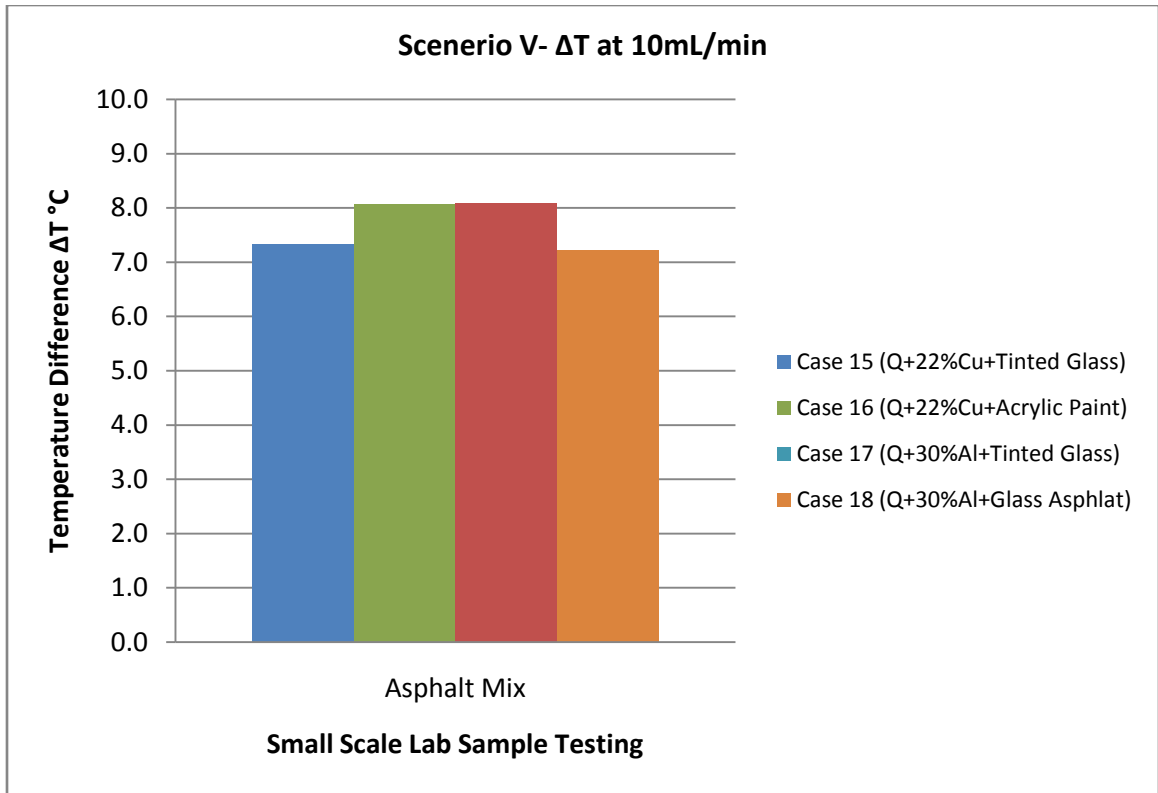


**Figure 5-14 Small scale testing (Scenario V) temperature difference  $\Delta T$**

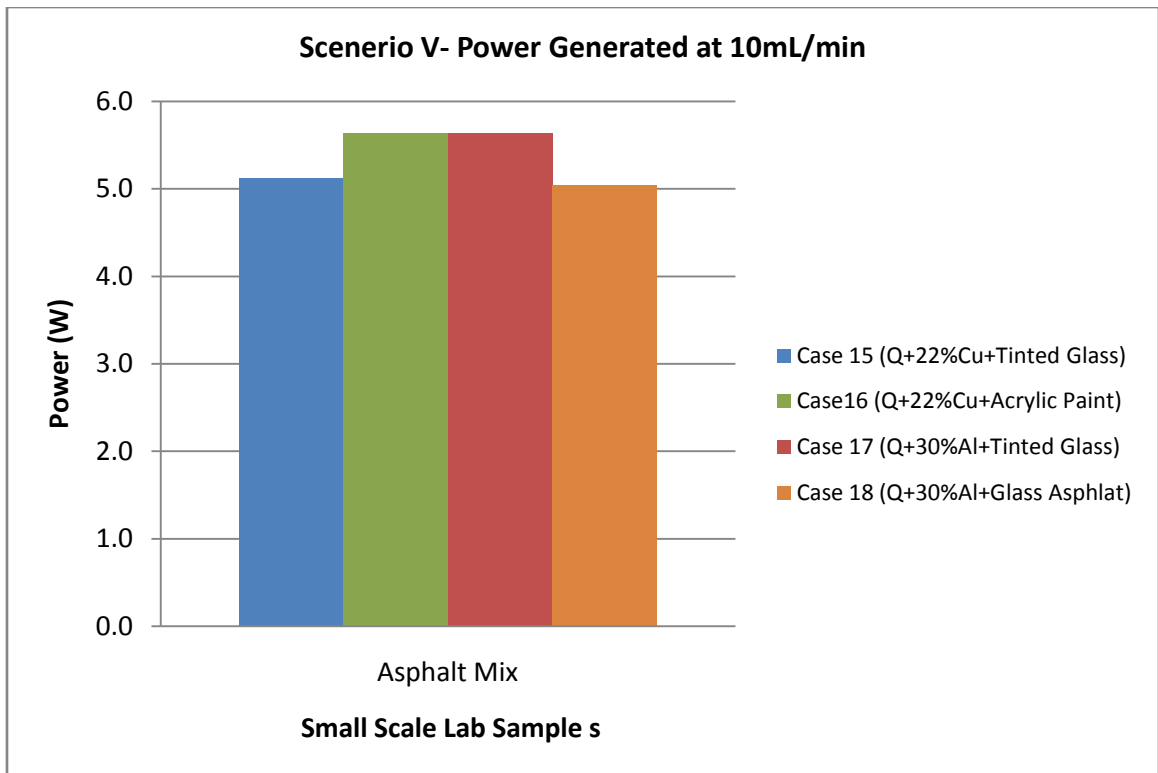


**Figure 5-15 Small scale testing (Scenario V) power generated**



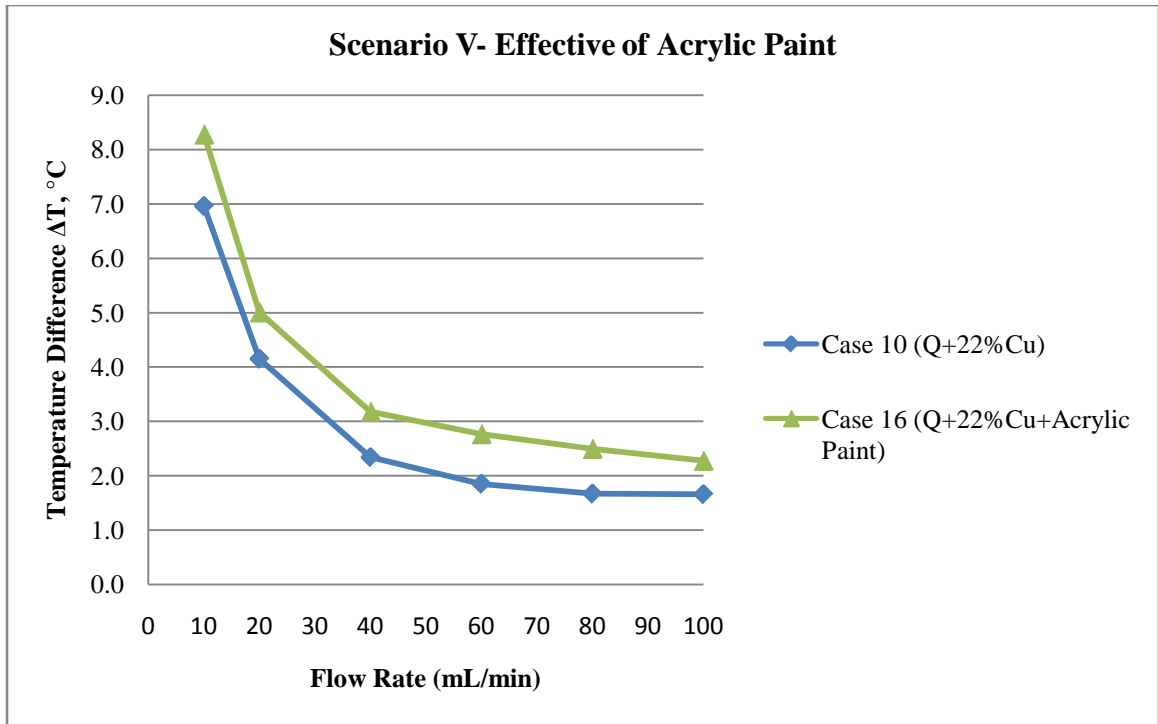


**Figure 5-16 Effective of Acrylic Paint**

The Figure 5-17 showed that the temperature difference (delta T) at 10mL/min for scenario II, III, IV, and V. The 100% quartzite sample yielded the highest temperature difference, and 100% RAP was the lowest compared to other samples. Therefore, the results could be concluded as that the introduced of the quartzite aggregates improved the overall heat transfer rate for the asphalt pavement.

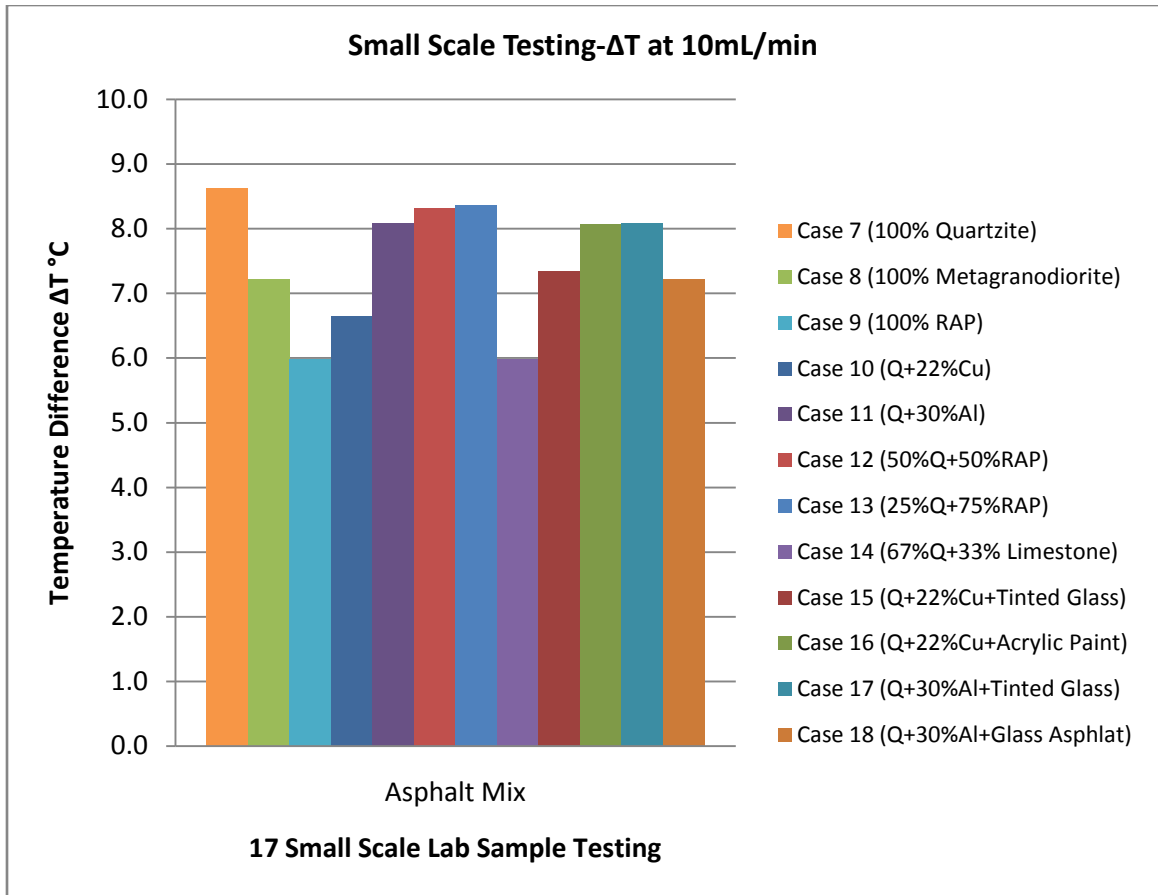


**Figure 5-17 Small scale testing temperature difference  $\Delta T$**

### 5.5 Robustness Test

The 67% quartzite with 33% limestone mix was selected to be tested its robustness on randomly testing time. The Figure 5-18 showed that the variability in delta T from a repeated set of experiments was found to be very low in -0.055 and 0.0916m location, and slightly higher variation close to the surface. The results indicated that the temperature distribution of asphalt mix was consistently over randomly heating period.

**Table 5-18 Repetitive test of 67% quartzite and 33% limestone mix**

	Apr. 3	Apr. 7	Apr. 9	Apr. 25	Apr. 28		
Depth (m)	T (°C)	T (°C)	T (°C)	T (°C)	T (°C)	Avg.	STDEV
0	76.54	82.52	81.67	78.49	78.66	79.58	2.46
-0.0254	69.33	73.48	72.08	68.95	68.55	70.48	2.18
-0.055	60.81	61.18	60.51	60.79	60.26	60.71	0.35
-0.0916	55.91	55.61	55.12	56.10	55.34	55.61	0.40

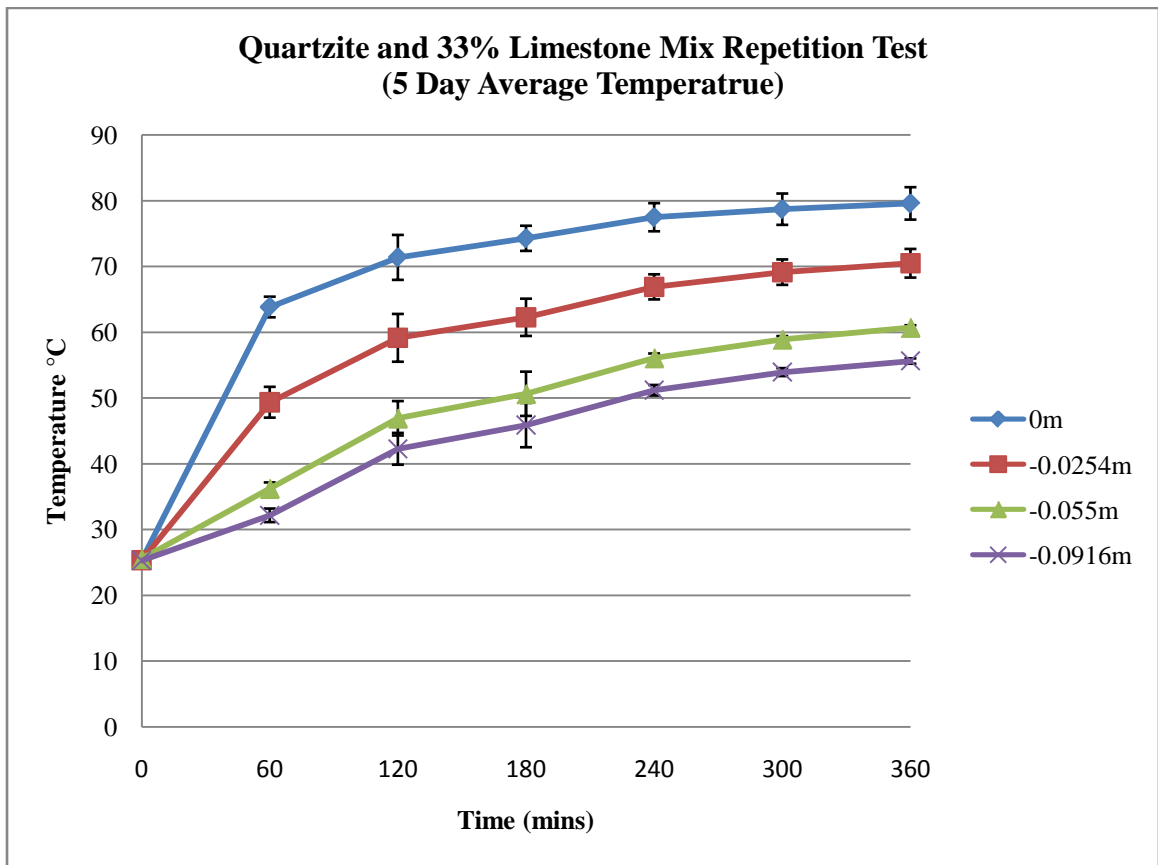


**Figure 5-18 5-days repetitive test of 67% quartzite and 33% limestone mix**

## 5.6 Finite Element Analysis/Modeling

The first set of finite element simulations was carried out to evaluate the effect of thermal conductivity of the aggregates on the heating process without water flow.

Assuming that the thermal conductivities ( $k$ ) of the mixtures are primarily influenced by the conductivity of the aggregates,  $k$  values of 5.38 and 2.15 W/m·K (28) were used to represent quartzite (consisting of mainly quartz) and limestone aggregates (representing approximately two extremes of thermal conductivity for aggregates) mixes, respectively.

The trial thermal conductivity and heat capacity values were used as seed values in finite element analysis and compared them with temperature distribution profile from laboratory data (Appendix D).

The finite element analysis results showed that the quartzite mix had higher thermal conductivity (Table 5-19) compared to limestone mix and confirmed the significant effect of thermal conductivity of the HMA on the change in temperature of the water bath (Figure 5-19) – a delta T of 10.13 and 5.02°C were noted for the quartzite and the limestone samples, respectively. The model was assumed to be thermally insulated at every boundary condition excepted for surface of sample. The boundary condition was assumed to have a heat flux of 1,000W/m<sup>2</sup> and convective heat transfer condition. The mesh size consisted of 32,838 elements and was solved for a time period of 360 minutes.

**Table 5-19 Thermal properties of quartzite and limestone sample mix (Appendix D)**

	Quartzite	Limestone
Thermal Conductivity ( $k$ )	1.8	1.4
Heat Capacity (C)	1050	950
Thermal Diffusivity ( $\alpha$ )	7.29e-7	7.61e-7
Lab $\Delta T$	10.13	5.02
FE $\Delta T$	22.77	18.55

The second set of finite element simulations (Figure 5-20) was to evaluate the effect of thermal conductivity of quartzite and metagranodiorite mixes with various water flow rates. The model was assumed to be thermally insulated at every boundary condition excepted for surface of sample, water inlet and water outlet. The boundary condition was assumed to have a heat flux of 1,000W/m<sup>2</sup> and convective heat transfer condition. The mesh size consisted of 19,165 and was solved for time equaled 60 minutes.

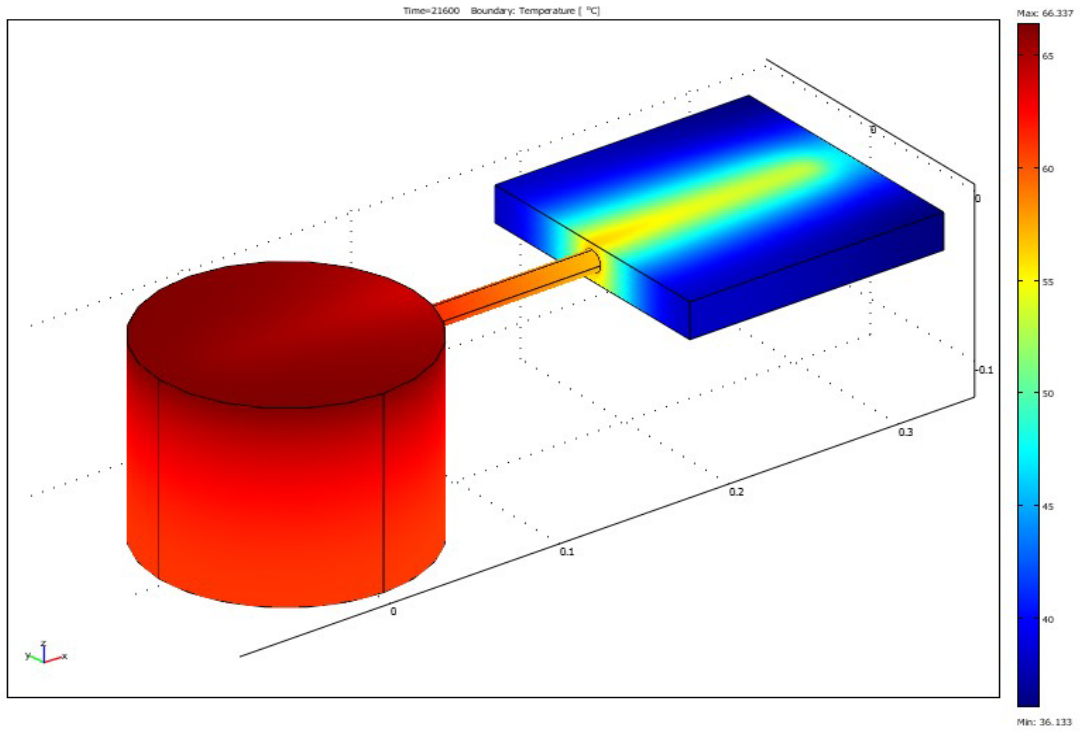


**Figure 5-19 Steady-state finite element model**

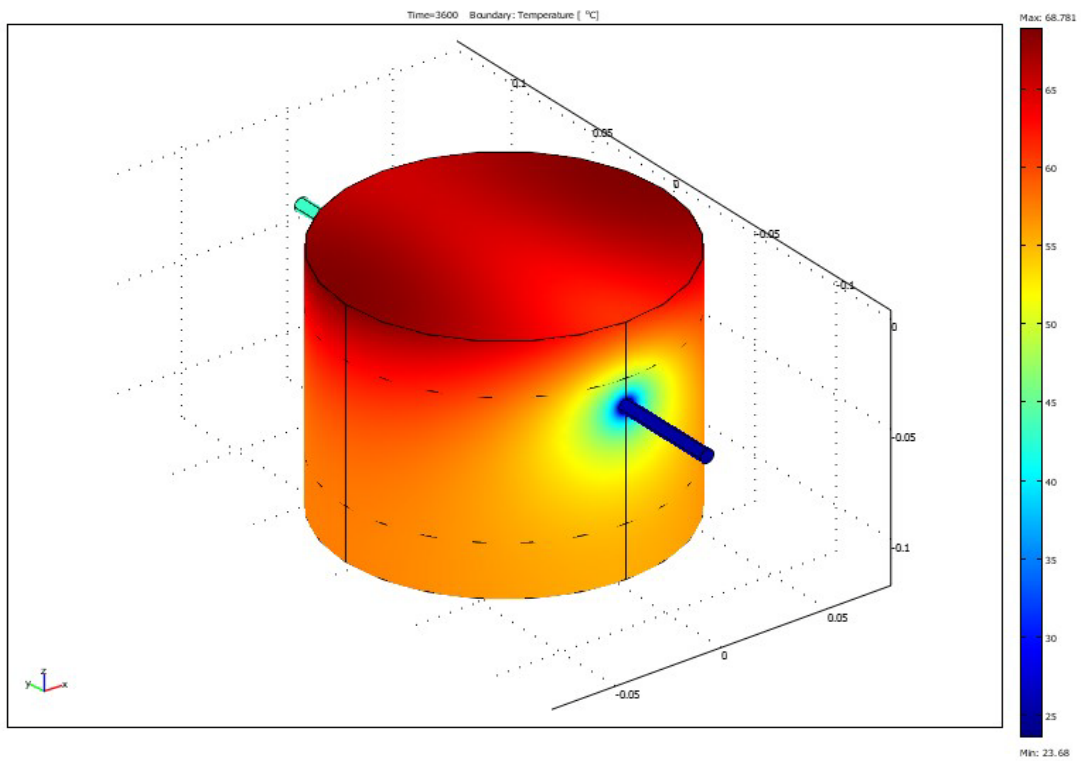


**Figure 5-20 Transient finite element model**

The value of the convection heat transfer coefficient for internal flow is dependent on the geometrical cross section of the pipe, the thermal boundary condition at the pipe wall, and the distance from pipe entrance.

The Nusselt number is defined as

$$Nu = \frac{hd_h}{k}$$

Where  $h$  is the heat transfer coefficient,  $d_h$  is the hydraulic diameter of the section and  $k$  is the thermal conductivity of the fluid.

The Reynolds number, the fluid flow can be characterized into two types of flow and the velocity profile of the fluid  $U$ , can be identified and calculated based on the Reynolds's number and Power Law of Velocity (22).

$$Re = \frac{\rho vd}{\nu}$$

Where  $\rho$  is the density of the fluid,  $v$  is the velocity of fluid,  $d$  is the diameter of pipe, and  $\nu$  is dynamic viscosity of the fluid.

Laminar flow  $Re \leq 2300$

$$U = V_{max} \left(1 - \left(\frac{r}{R}\right)^2\right)$$

Turbulent flow  $Re \geq 2300$

$$U = V_{max} \left(1 - \left(\frac{r}{R}\right)^7\right)$$

Where  $V_{max}$  is maximum velocity,  $r$  is any point at the diameter of pipe, and  $R$  is the radius of the pipe.

The fully developed laminar flow was assumed since water flow rate from 10 to 100 ml/min in 0.00675m (1/4") duct were all laminar flow ( $Re \leq 2300$ ). The Figure 5-21 and 5-22 showed the temperature distribution along the pipe length from entrance to exit (y-direction) of both samples, and quartzite mix had lower temperature variation at top and bottom boundary compared to Wrentham mix. The temperature profile from top to bottom boundary of pipe (z-direction) (Figure 5-23 and 5-24) indicated that the quartzite mix had higher heat transfer rate from asphalt to the water, resulting in higher temperature increased on the center line of the water profile.

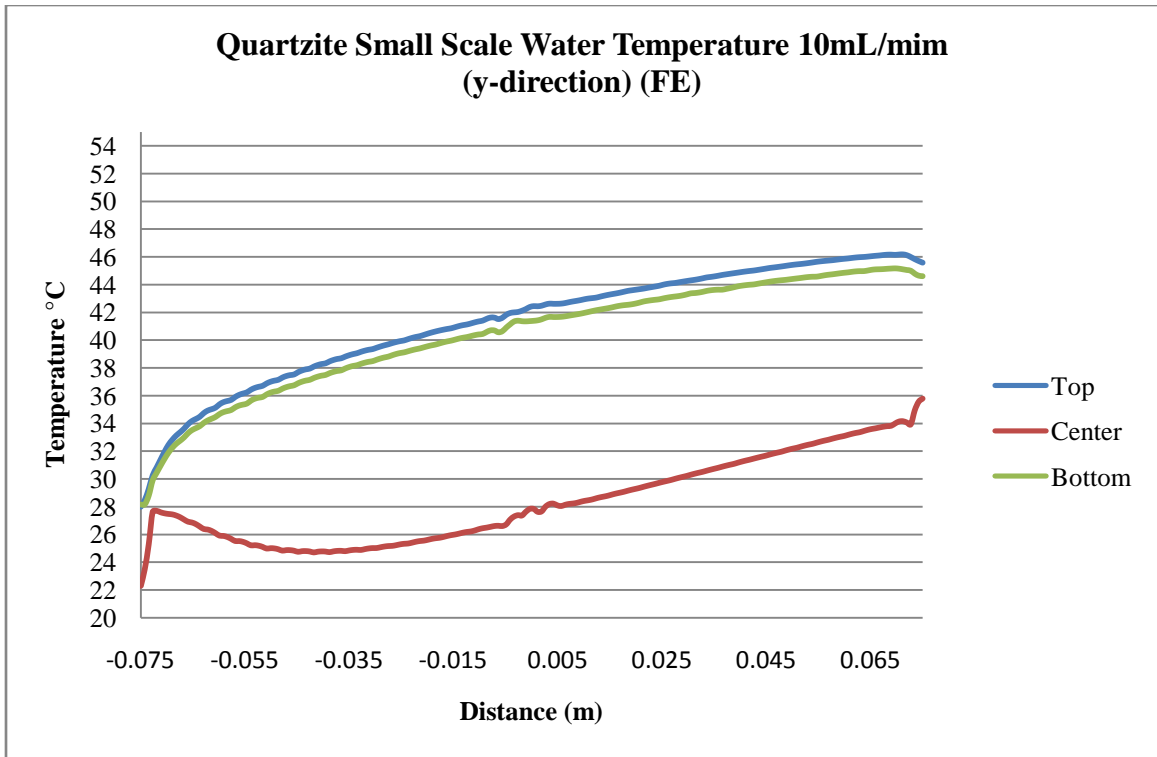


**Figure 5-21 Water temperature distribution along the length of copper pipe (Quartzite)**

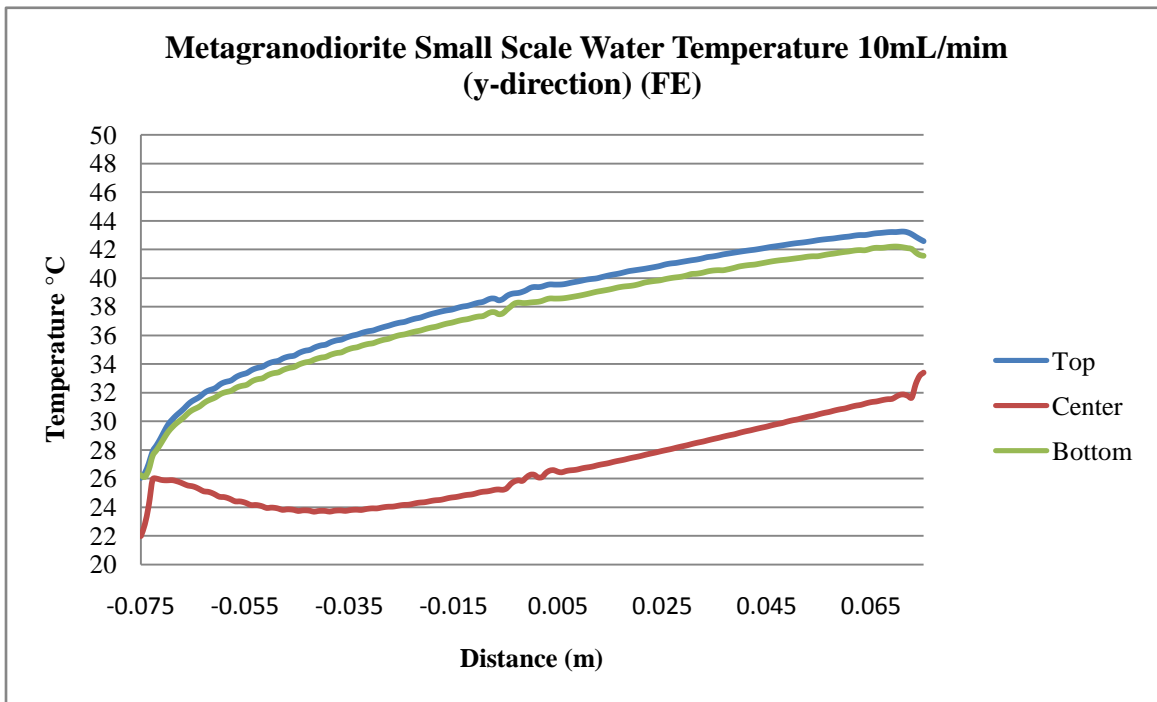


**Figure 5-22 Water temperature distribution along the length of copper pipe (Metagranodiorite)**

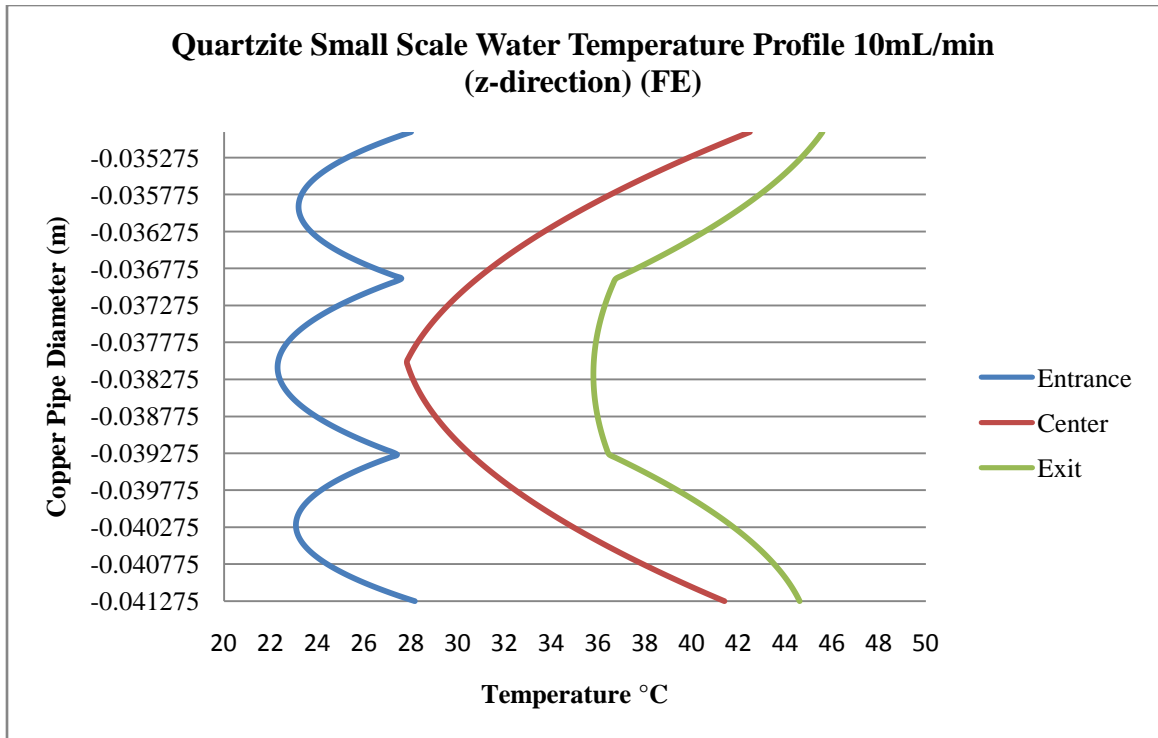


**Figure 5-23 Water temperature distribution along the depth of copper pipe (Quartzite)**

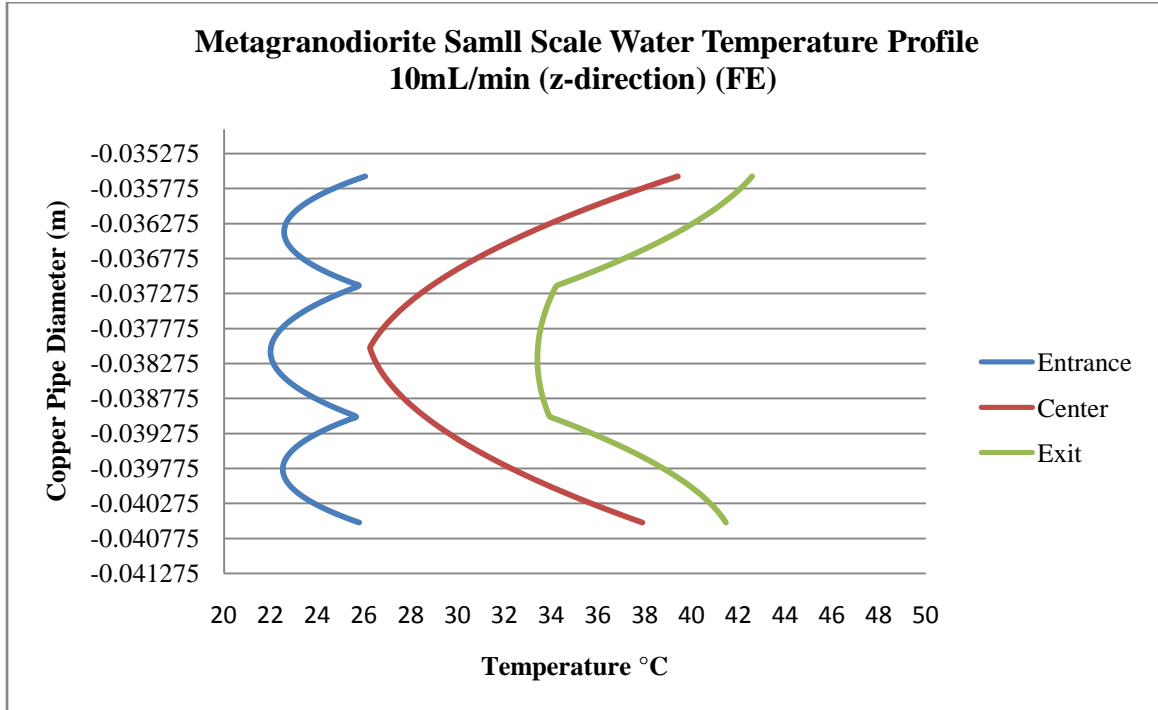


**Figure 5-24 Water temperature distribution along the depth of copper pipe (Metagranodiorite)**



The finite element analysis results (Table 5-20) showed that the quartzite mix had higher thermal conductivity compared to metagranodiorite mix and also confirmed the significant effect of thermal conductivity of the HMA on the change in temperature of the water outlet.

**Table 5-20 Thermal properties of quartzite and metagranodiorite mix (Appendix D)**

	Quartzite	Metagranodiorite
Thermal Conductivity (k)	1.8	1.2
Heat Capacity (C)	1050	800
Thermal Diffusivity ( $\alpha$ )	7.29e-7	6.38e-7
Lab $\Delta T$ (10mL)	8.64	7.52
FE $\Delta T$ (10mL)	15.20	13.63

The Figure 5-25 showed that there were 6°C temperature difference between laboratory and finite element simulations at depth of 0.0381m (1.5”) where was the location of copper pipe. The both laboratory data did not show the significant effect of water presented in this location, this can be the indication of that the contact between asphalt mix and copper pipe were compromised by the drilled hole where allowed copper pipe to be inserted.

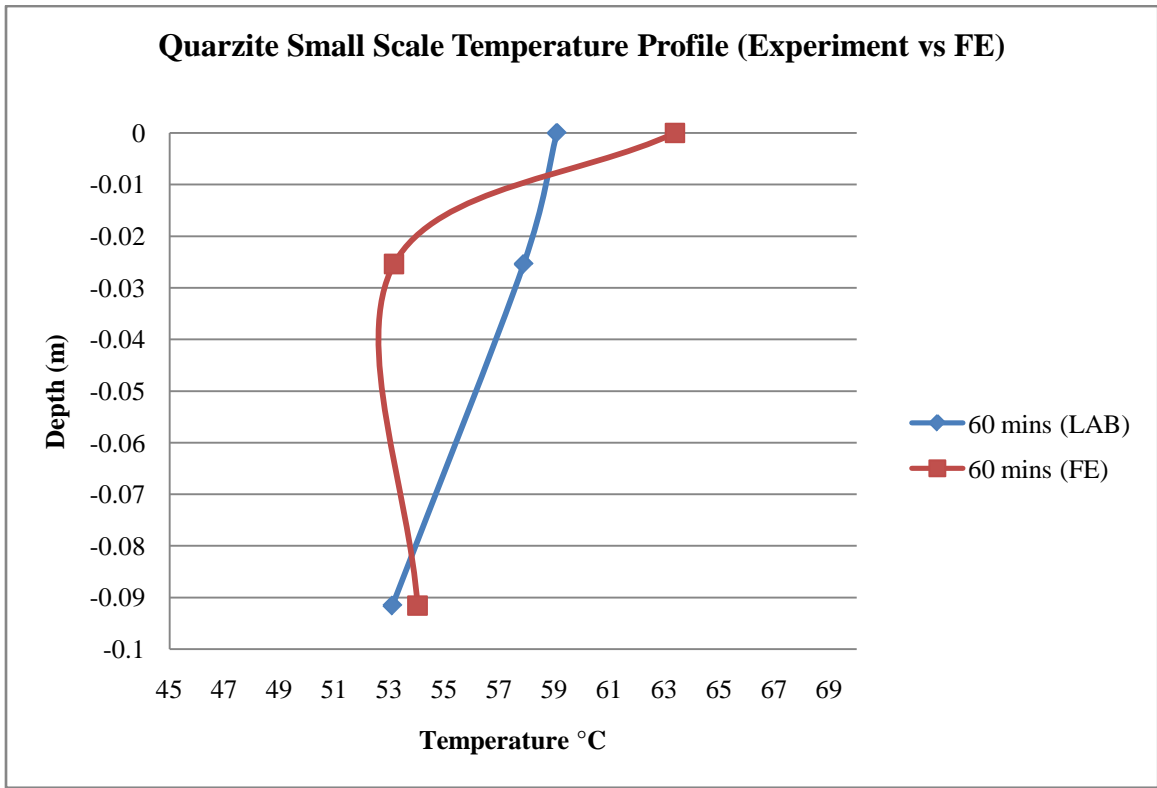


**Figure 5-25 Quartzite mix temperature profile**

## 5.7 Discussion

The experiment results showed the feasibilities of improving the overall thermal conductivity of asphalt pavement by

1. Replacing the conventional aggregate (metagranodiorite) by quartzite aggregate, which increased the overall thermal conductivity by nearly 50%.
2. Modifying the surface condition of asphalt pavement, such as using acrylic paint to increased the abosoptivity of pavement.

The asphalt mixes created by using different percentage of materials such as limestone and copper powder did not show the increased of water temperature in term of overall thermal conductivity. The higher conductive materials could be coated by the asphalt binder and resulted in lower thermal conductivity.

The water temperature profile in the copper pipe showed that the centerline of water temperature did not reach steady-state and not reach boundary layer temperature, which meant that the copper pipe length and surface area were needed to be increased in order to generate higher water outlet temperature.

The temperature distribution in the asphalt samples did not show the presence of water at the 1.5 inch location. The air gap could increase the thermal resistance between the asphalt mix and copper pipe and reduced the heat transfer efficiency.

## CHAPTER 6

### HAND-COMPACTED ASPHALT PAVEMENT TESTING

#### 6.1 Introduction

The results from chapter 5 showed that the major factors that would affect the heat transfer efficient in the asphalt pavement were surface area of copper pipe, thermal conductivity of aggregates, percentage of aggregates used in the mix, and contact between asphalt mix and copper pipe. It was hypothesized that air gap occurred between asphalt mix and copper pipes because the pipes were installed in the sample after drilling holes inside the sample which resulting in 6°C difference in sample temperature for experimental and finite element analysis results. Therefore, in this chapter, the seven hand-compacted samples were proposed to investigate the effectiveness of increasing surface area of copper pipe, using different thermal conductivity mix in layers, and improving contact between asphalt mix and copper pipe.

#### 6.2 Objective

The objectives of this chapter were to evaluate:

1. Contact between the asphalt mix and the pipe.
2. Different asphalt mix in layers.
3. Pipe layout configurations.

#### 6.3 Methodology

The set of samples (Table 6-1) were compacted and the pipe was placed at the depth of 0.0381m (Figure 6-1 and 6-2), the compaction procedures are:

1. Prepared one PVC molding (0.1016m (4") height and 0.1524 (6") in diameter) with one base plate.
2. Placed the first layer of asphalt mix, approximately 0.0127m (0.5") in depth, and compacted.
3. Positioned one thermocouple on the top center of the first layer.
4. Placed and compacted the second layer of asphalt mix, approximately 0.0381m (1.5") in depth.
5. Positioned one thermocouple on the top center of the second layer.
6. Place and compacted the third layer of asphalt mix, approximately 0.0127m (0.5") in depth.

7. Removed top half of PVC molding and placed 0.00635m (¼”) diameter cooper pipe on top of third layer. Placed back top half of molding in order to secure the copper pipe.
8. Placed and compacted the forth layer of asphalt mix, approximately 0.0127m (0.5”) in depth.
9. Positioned three thermocouples on the top center of forth layer with even spacing of 0.0381m (1.5”) from the edge.
10. Placed and compacted the fifth layer of asphalt mix, approximately 0.0254m (1”) in depth.

**Table 6-1 Description of compacted samples (Appendix E)**

Compacted Sample	Description
100% M*	100% Metagranodiorite mix
100% Q*	100% Quartzite mix
50% Q*+50% M*	50% Quartzite on the top and 50% Metagranodiorite on the bottom
35% W*+30% Q*+ 35%M*	35% Metagranodiorite on the top, 30% quartzite in the center layer, and 35% o Metagranodiorite on the bottom
100% M*+ Portland cement	100% Metagranodiorite mix with Portland cement placed around copper pipe
100% Q*+6 rings pipe	100% Quartzite mix with a copper pipe consists six rings
100% Q*+rough surface pipe	100% Quartzite mix with a rough surface copper pipe

M\*= Metagranodiorite mix, Q\*= Quartzite mix

Each sample was heated up for 6 hours before pumping water; the water flow rate was set to 10mL/min which showed highest temperature variation (the assumption was based on previous experiment). The water temperature was collected by thermocouple at the center of the water collector. The copper pipe with 6 rings was expected to created larger surface area to increase the heat transfer coefficient, and copper pipe with rough surface was intended to create a better contact with asphalt mix.

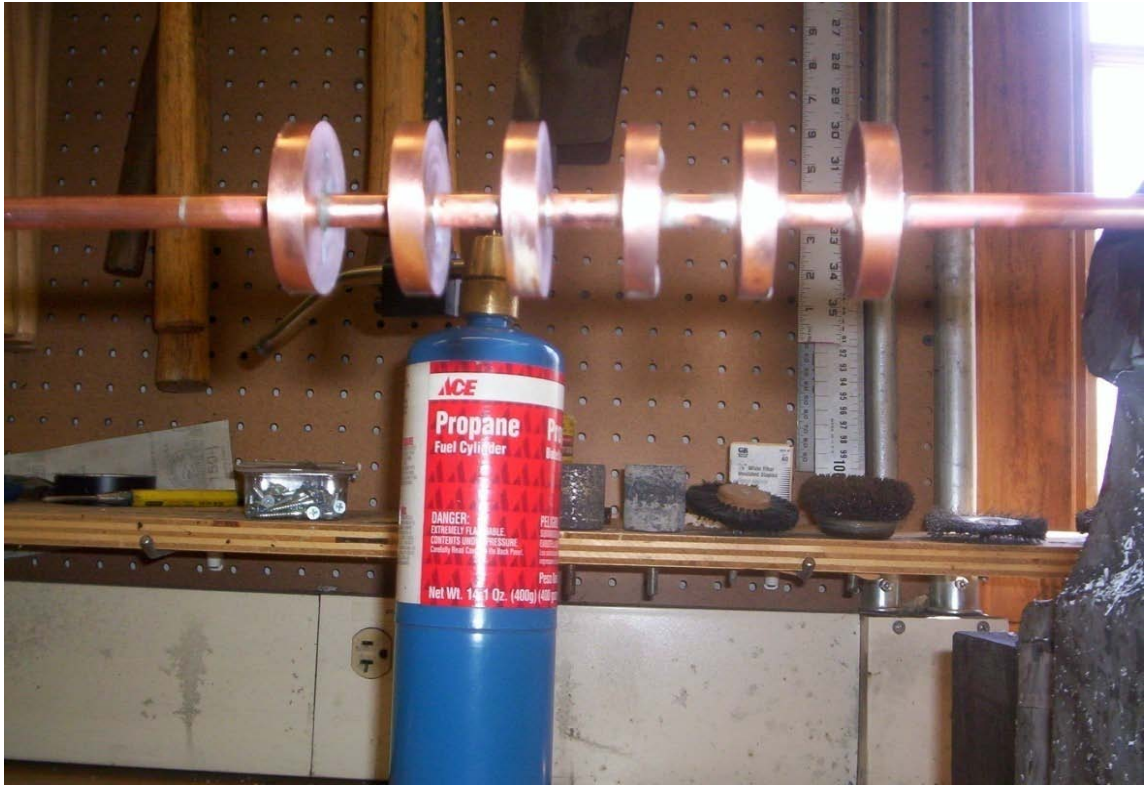


**Figure 6-1 Copper pipe with 6 rings**

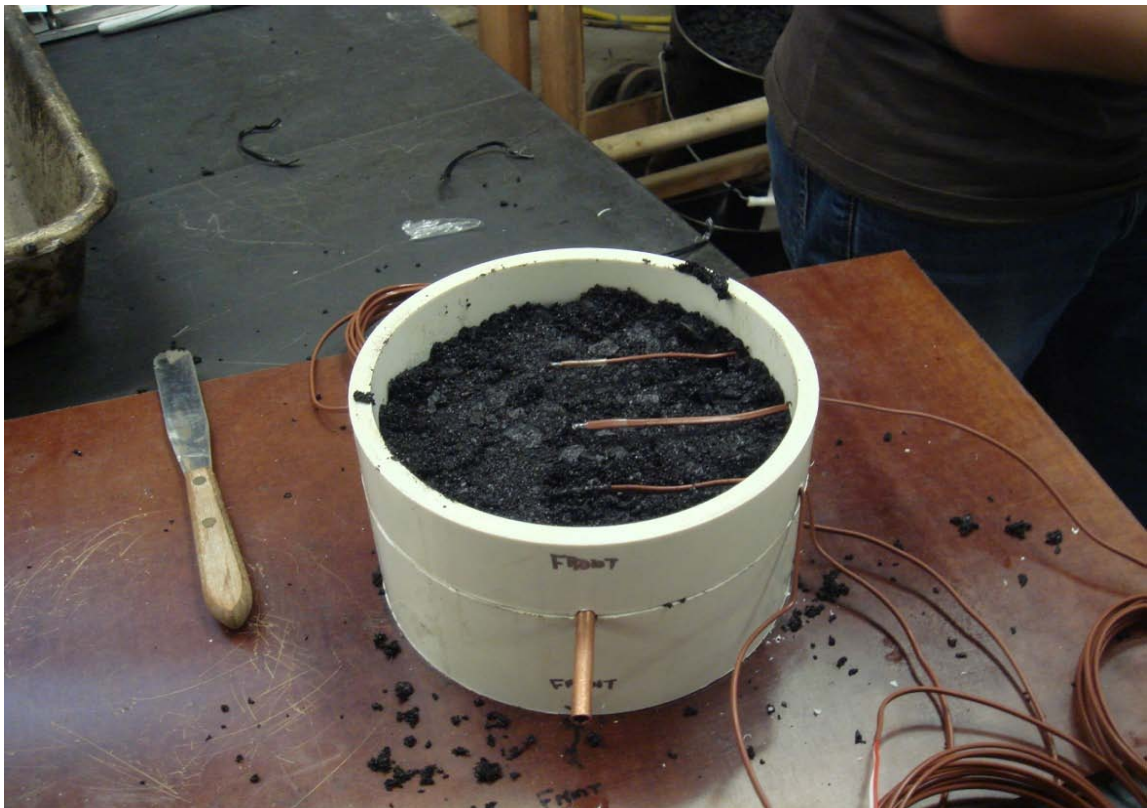


**Figure 6-2 Placement of thermocouples on top layer**

## 6.4 Experiment Results

The temperature distribution of metagranodiorite sample (Figure 6-3) showed lower temperature difference (approximately 4°C) at the pipe location (-0.0381m) compared to earlier drilled samples (approximately 6°C). In addition, the outlet water temperature was higher; this indicated an importance of the compaction process and the necessity to ensure maximum contact between the sample and the pipe.

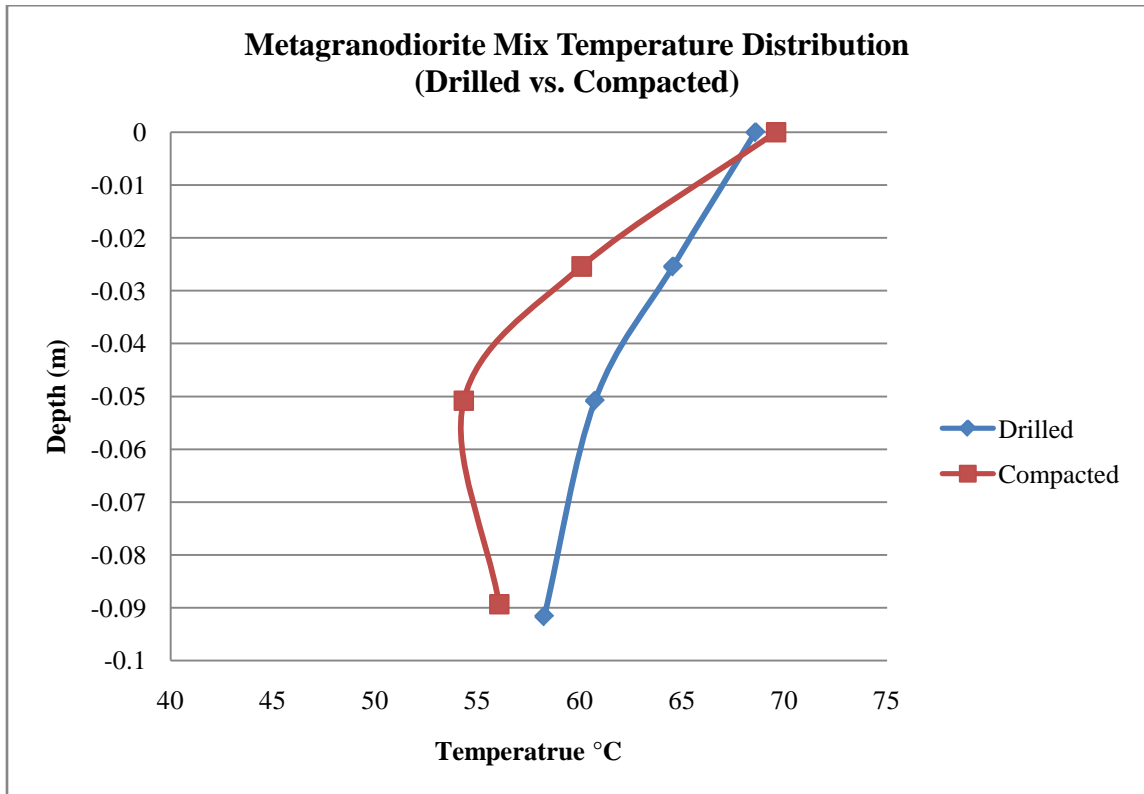


**Figure 6-3 Drilled vs. compacted sample temperature distribution**

The Table 6-2, 6-3, and Figure 6-4, 6-5 showed the water temperature after 60 minute and 180 minutes of heating, and results showed that the 100% quartzite mix had better ability to increased water temperature compared to metagranodiorite mix due to its higher thermal conductivity. In addition, the quartzite mix had higher thermal conductivity and heat capacity and improved the heat transfer when it was placed between metagranodiorite mixes.

The Portland cement that was placed surrounding the copper pipe and resulted in lowest water temperature generated; this was due to its low thermal conductivity and reduced heat transfer ability from asphalt mix to water.

The quartzite mix with 6 rings of copper pipe generated highest water temperature compared to other samples, this was due to its large surface area and the position of the rings were closer to the surface where experienced higher temperature. The quartzite mix with rough copper surface did not generated higher temperature as expected, which was due to the rough surface would be resulting in air trapped between uneven surface.

**Table 6-2 Temperature difference at time= 60 minutes (Lab Data); water flowing at 10 ml/minute**

Case	1st $\Delta T$	2nd $\Delta T$	3rd $\Delta T$	Average	STDEV
100% M*	9.44	10.05	10.12	9.87	0.37
100% Q*	10.73	12.79	10.12	11.21	1.40
50% Q*+50% M*	8.93	10.74	8.33	9.33	1.26
35%M*+30%Q*+ 35%M*	9.53	11.33	11.91	10.93	1.24
100% W*+ Portland cement	8.33	11.42	10.13	9.96	1.55
100% Q*+6 rings pipe	17.30	15.49	16.10	16.30	0.92
100% Q*+rough surface pipe	9.54	10.74	8.95	9.74	0.91

M\*= Metagranodiorite mix, Q\*= Quartzite mix

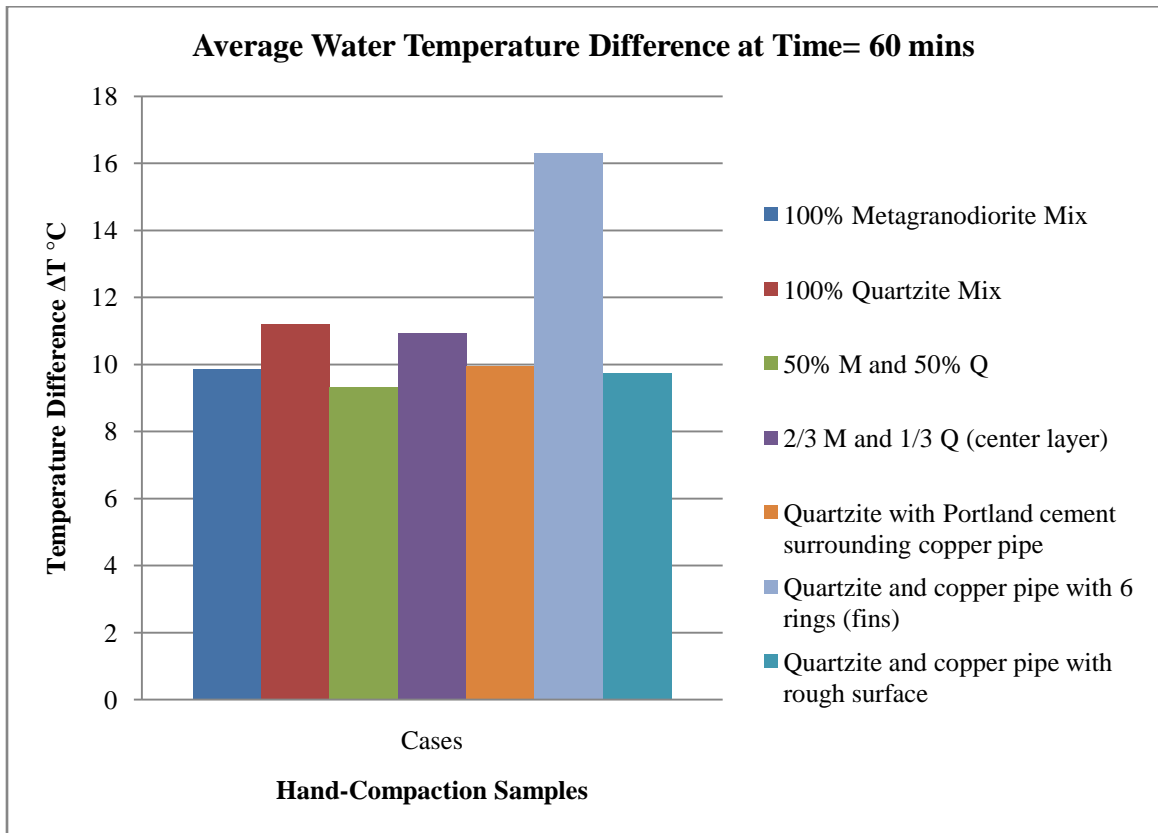


**Figure 6-4 Average water temperature difference at time = 60 minutes**

**Table 6-3 Temperature difference at time= 180 minutes (Lab Data)**

Case	1st $\Delta T$	2nd $\Delta T$	3rd $\Delta T$	Average	STDEV
100% M*	8.93	9.03	7.72	8.56	0.73
100% Q*	9.54	10.41	9.02	9.65	0.70
50% Q*+50% M*	8.33	9.54	8.24	8.70	0.73
35%M*+30%Q*+ 35%M*	8.33	10.13	9.52	9.33	0.92
100% W*+ Portland cement	7.13	9.53	8.93	8.53	1.25
100% Q*+6 rings pipe	13.72	13.70	12.52	13.32	0.69
100% Q*+rough surface pipe	8.34	8.34	7.75	8.14	0.34

M\*= Metagranodiorite mix, Q\*= Quartzite mix

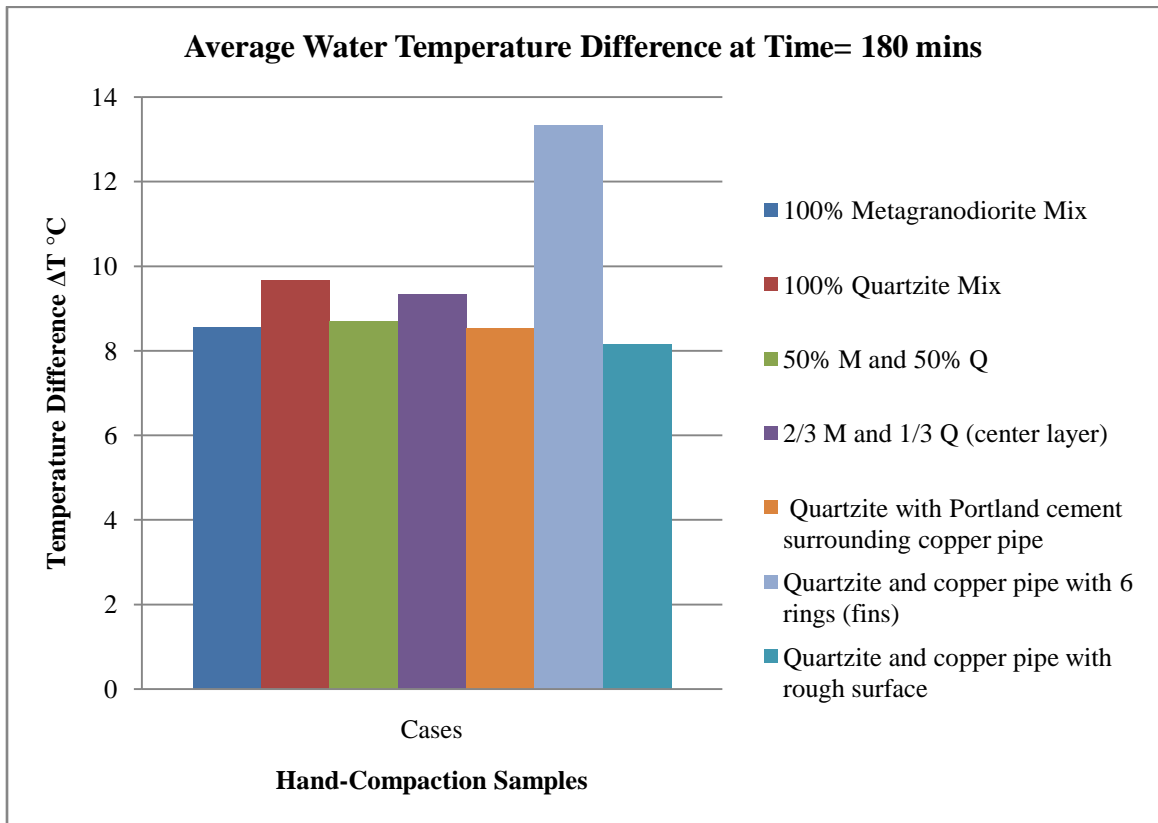


**Figure 6-5 Average water temperature difference at time = 180 minutes**

The water temperature at 60 and 180 minutes showed that the asphalt samples reached steady-state condition (equilibrium), the water temperature was stabilized and the standard deviation was decreased to within 1°C. The significant difference analysis was performed and found that there was no significant different when the confidence level was 95%



## 6.5 Finite Element Analysis/Modeling

The finite element analysis was used to validate the assumptions and laboratory data, with the initial temperatures of the three layers as designated by the three thermocouples after 6 hours as input. The thermal conductivity and heat capacity were back-calculated based on 6 hours heating period of metagranodiorite and quartzite to verify if there was difference between gyrator compaction and hand compaction (Appendix F).

Table 6-4 and 6-5 showed that the thermal properties were not affected significantly when two different compaction methods were used. The thermal diffusivity of hand-compacted quartzite mix was increased than gyrator compacted, and was decreased in metagranodiorite mix.

**Table 6-4 Quartzite mix back-calculated thermal properties**

	Gyrator Compacted	Hand-Compacted
Thermal Conductivity (k)	1.8	2.0
Heat Capacity (C)	1050	950
Thermal Diffusivity ( $\alpha$ )	7.29e-7	8.9e-7

**Table 6-5 Metagranodiorite mix back-calculated thermal properties**

	Gyrator Compacted	Hand-Compacted
Thermal Conductivity (k)	1.2	1.1
Heat Capacity (C)	800	900
Thermal Diffusivity ( $\alpha$ )	6.38e-7	5.2e-7

The results of finite element analysis (Table 6-6) showed that the water temperature of copper pipe with 6 rings generated highest temperature compared to the others.

**Table 6-6 Laboratory and finite element analysis temperature difference at time = 60 minutes comparison**

Case	Lab $\Delta T$ °C	FE $\Delta T$ °C
100% M*	9.87	13.91
100% Q*	11.21	15.91
50% Q*+50% M*	9.33	18.62
35%M*+30%Q*+ 35%M*	10.93	16.2
100% M*+ Portland cement	9.96	6.87
100% Q*+6 rings pipe	16.30	19.34
100% Q*+rough surface pipe	9.74	17.8

M\*= Metagranodiorite mix, Q\*= Quartzite mix

**Table 6-7 Laboratory and Finite Element temperature difference at time = 180 minutes comparison**

Case	Lab $\Delta T$ °C	FE $\Delta T$ °C
100% M*	8.56	12.89
100% Q*	9.65	14.91
50% Q*+50% M*	8.70	15.4
35%M*+30%Q*+ 35%M*	9.33	14.56
100% M*+ Portland cement	8.53	6.9
100% Q*+6 rings pipe	13.32	13.22
100% Q*+rough surface pipe	8.14	15.51

M\*= Metagranodiorite mix, Q\*= Quartzite mix

The finite element analysis results (Table 6-7) showed higher temperature compared to laboratory results because in finite element model, the asphalt sample was assumed to be homogenous material, and perfect contact with the copper pipe. However, the asphalt sample was mixed with different size of aggregate and asphalt binder, each of components has different thermal properties and affect heat transfer rate.

## **6.6 Discussion**

Improving the contact between the asphalt mix and copper pipe showed the evidence of increasing of water temperature (outlet) by 2.57°C for quartzite mix and 2.35 °C for metagranodiorite mix in 60 minute period when compared to small scale testing.

The 35% metagranodiorite on top layer, 30% quartzite in the center layer, and 35% metagranodiorite on the bottom layer showed the higher temperature difference in Finite Element results, which showed that the lower heat capacity (metagranodiorite) on the top layer was heated up faster to increase the heat transfer rate for the higher thermal conductivity (quartzite) in the center layer.

The water temperature never reached the asphalt sample temperature at 1.5 inch below the surface could be an indication of insufficient surface area of copper pipe. The experiment results showed that the increased of surface area and the location of pipe placement could greatly increase the outlet water temperature. Therefore, the analytical approach for effective pipe length, diameter, and water flow rate must be performed.

## CHAPTER 7

### DETERMINE EFFECTIVE PIPE LENGTH AND SPACING

#### 7.1 Introduction

The experimental results showed that the maximum average temperature below 0.0254m (1”) of the asphalt pavement surface was approximately 50 °C. The value was then used as uniform wall temperature to determine the effective copper pipe length, pipe diameter, and water flow rate by using analytical approach. The chart of the effective copper pipe length, diameter versus water flow rate was developed. The laboratory experimnts were performed to validated the effect of pipe legth and configuration in term of difference at water outlet temperature.

#### 7.2 Objective

The objectives of this chapter were to evaluate:

1. Effect of pipe length
2. Effect of pipe diameter
3. Effect of pipe spacing
4. Effect of water flow rate
5. Effect of pipe layout configuration

#### 7.3 Methodology

The value of the convection heat transfer coefficient for internal flow is dependent on the geometrical cross section of the duct, the thermal boundary condition at the pipe wall, and the distance from pipe entrance. The Nusselt number is defined as

$$Nu = \frac{hd_h}{k}$$

Where  $d_h$  is the hydraulic diameter of the section and  $k$  is the thermal conductivity of the fluid,  $h$  is the heat transfer coefficient.

There are two types of boundary conditions used in convection heat transfer, uniform wall flux and uniform wall temperature.

Uniform wall flux  $\dot{q}_w$  is when the heat flux at the wall of the duct is uniform,

$$T_b = \frac{\dot{q}_w'' A}{\dot{m} C_p} + T_i$$

$$\dot{q}_w'' = h_x (T_w - T_b)$$

Where  $T_b$  is the exit temperature,  $A$  is the surface area of the duct,  $\dot{m}$  is the mass flow rate,  $C_p$  is heat capacity,  $T_i$  is the initial temperature at the entrance,  $h_x$  is the local heat transfer coefficient, and  $T_w$  is the wall temperature.

Uniform wall temperature is when the temperature at the wall is uniform; the local heat flux is replaced by  $h_x(T_w - T_b)$ , the equation can be rearranged as (21)

$$\frac{T_w - T_b}{T_w - T_i} = \exp \left[ -\frac{\bar{h}A}{\dot{m}C_p} \right]$$

Where  $\bar{h}$  is the average heat transfer coefficient.

**Table 7-1 The typical Nusselt number for fully developed flow**

	Uniform Heat Flux	Uniform Wall Temperature
Circular Duct	4.36	3.66

**Table 7-2 Calculated required pipe length at wall temperature= 50 °C**

Pipe Diameter (m)	Water Flow Rate (mL/min)										
	100	200	400	600	800	1000	2000	4000	6000	8000	10000
0.005	7.5	15	30	45	60	75	150	300	450	600	750
0.01	7.5	15	30	45	60	75	150	300	450	600	750
0.02	7.5	15	30	45	60	75	150	300	450	600	750
0.03	7.5	15	30	45	60	75	150	300	450	600	750
0.04	7.5	15	30	45	60	75	150	300	450	600	750
0.05	7.5	15	30	45	60	75	150	300	450	600	750
0.06	7.5	15	30	45	60	75	150	300	450	600	750
0.07	7.5	15	30	45	60	75	150	300	450	600	750
0.08	7.5	15	30	45	60	75	150	300	450	600	750
0.09	7.5	15	30	45	60	75	150	300	450	600	750
0.1	7.5	15	30	45	60	75	150	300	450	600	750
Pipe length (m)											

\*highlight is where turbulent flow occurs

The heat transfer coefficient was inversely proportional to the hydraulic diameter (wet perimeter of pipe diameter), therefore, the smaller diameter of pipe resulted in highest heat transfer coefficient and required shorter length to achieve the 50°C wall temperature. In contrast, the larger diameter of copper pipe required longer length (Figure 7-1).

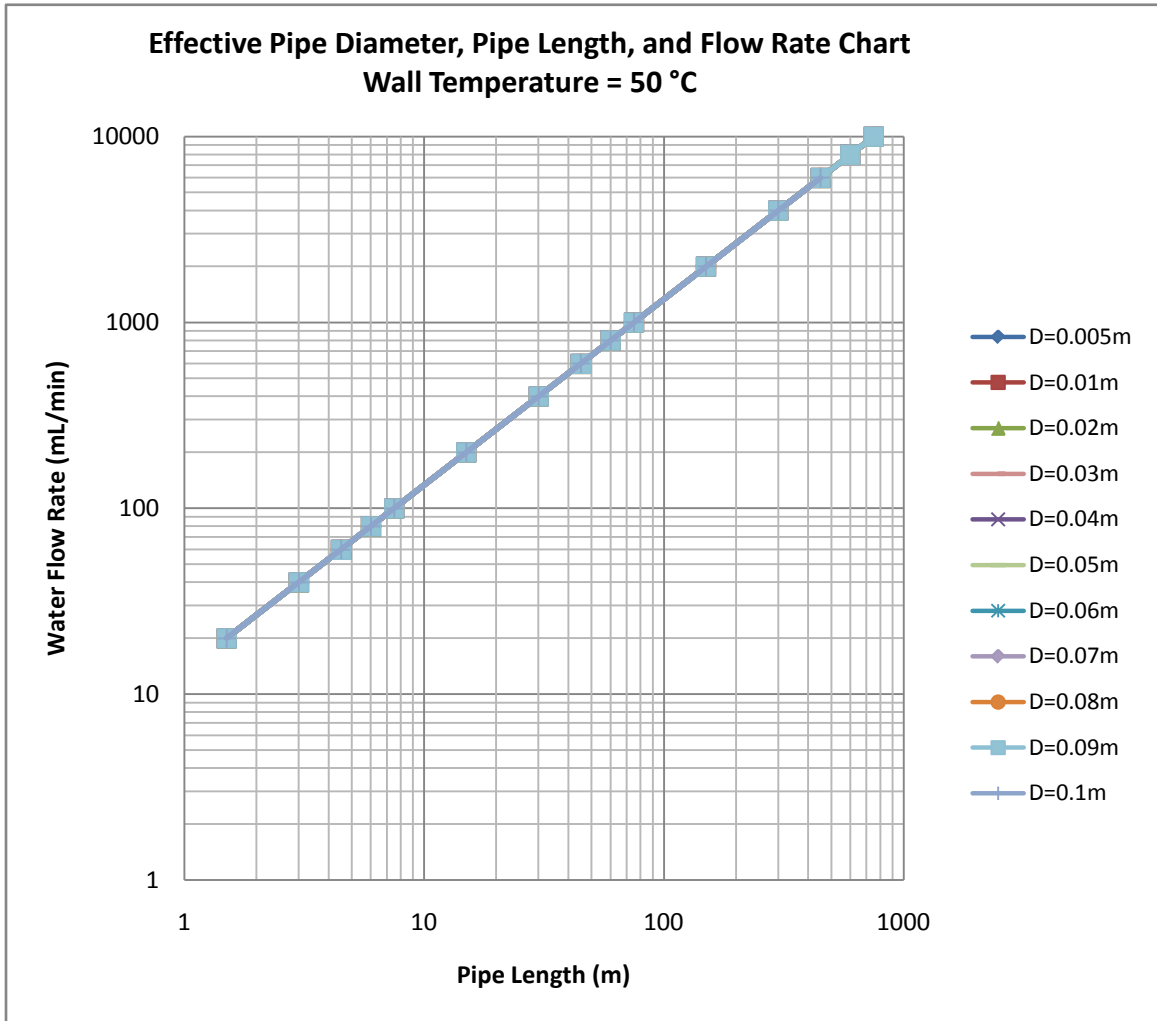


Figure 7-1 Effective pipe diameter, length, and flow rate chart

## 7.4 Experiment Results

Since the actual length of pipe is limited, and it cannot be provided as a straight section, therefore, 3 different pipe layouts (1) 0.1524m (6") straight pipe, (2) 0.3556m (14") serpentine style pipe, and (3) 0.7112 (28") serpentine style pipe (Figure 7-2) were proposed to validate the theoretical approach. The same compaction procedures were used as Charter 6. Each sample was heated up for 6 hours before pumping water; the water flow rate was set to 10mL/min which showed highest temperature variation (the assumption was based on previous experiment). The water temperature was collected by thermocouple at the center of the water collector.



**Figure 7-2 Serpentine pipe being placed and compacted**

**Table 7-3 Average water temperature difference at time= 60 minutes**

Case	1st $\Delta T$	2nd $\Delta T$	3rd $\Delta T$	Average	STDEV
6" Straight Pipe	10.73	12.79	10.12	11.21	1.40
14" Serpentine Pipe	21.75	18.79	19.76	20.10	1.51
28" Serpentine Pipe	25.13	20.85	22.89	22.89	2.15

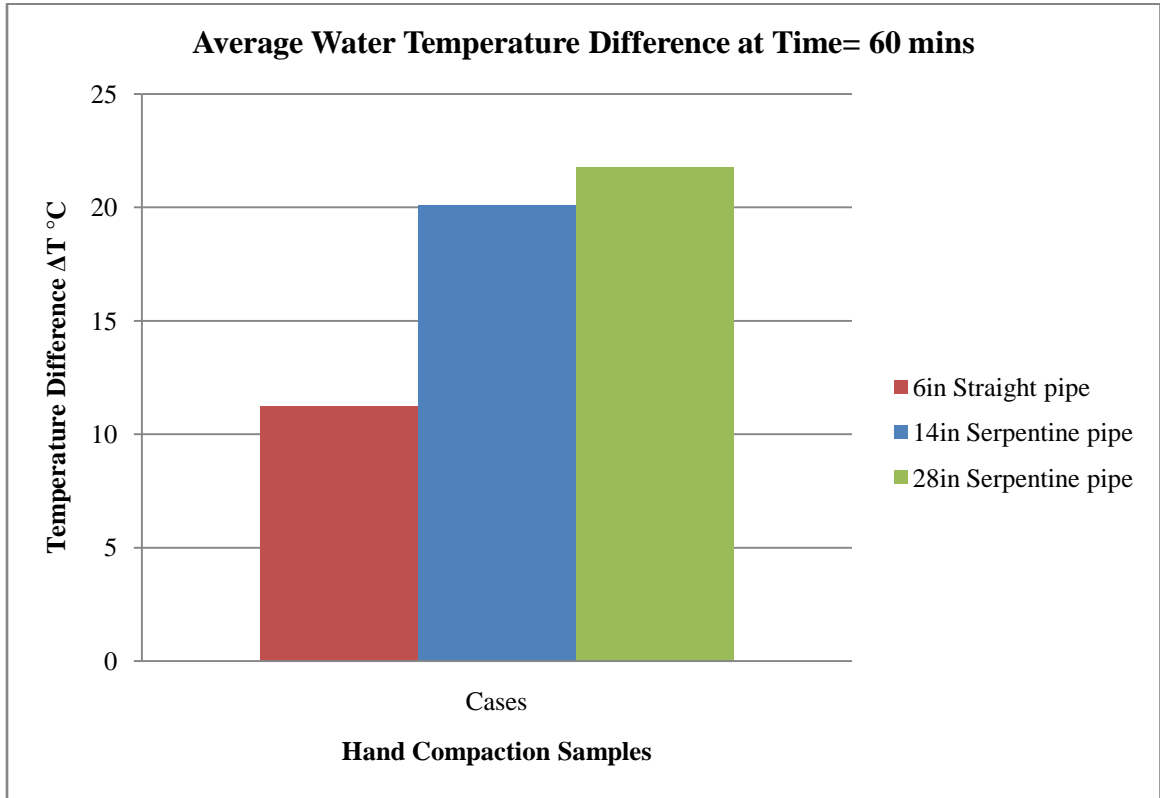


**Figure 7-3 Average water temperature difference at time = 60 minutes**



**Table 7-4 Average water temperature difference at time= 180 minutes**

Case	1st $\Delta T$	2nd $\Delta T$	3rd $\Delta T$	Average	STDEV
6" Straight Pipe	9.54	10.41	9.02	9.65	0.70
14" Serpentine Pipe	17.49	15.07	16.15	16.24	1.21
28" Serpentine Pipe	21.22	17.81	18.05	19.03	1.90

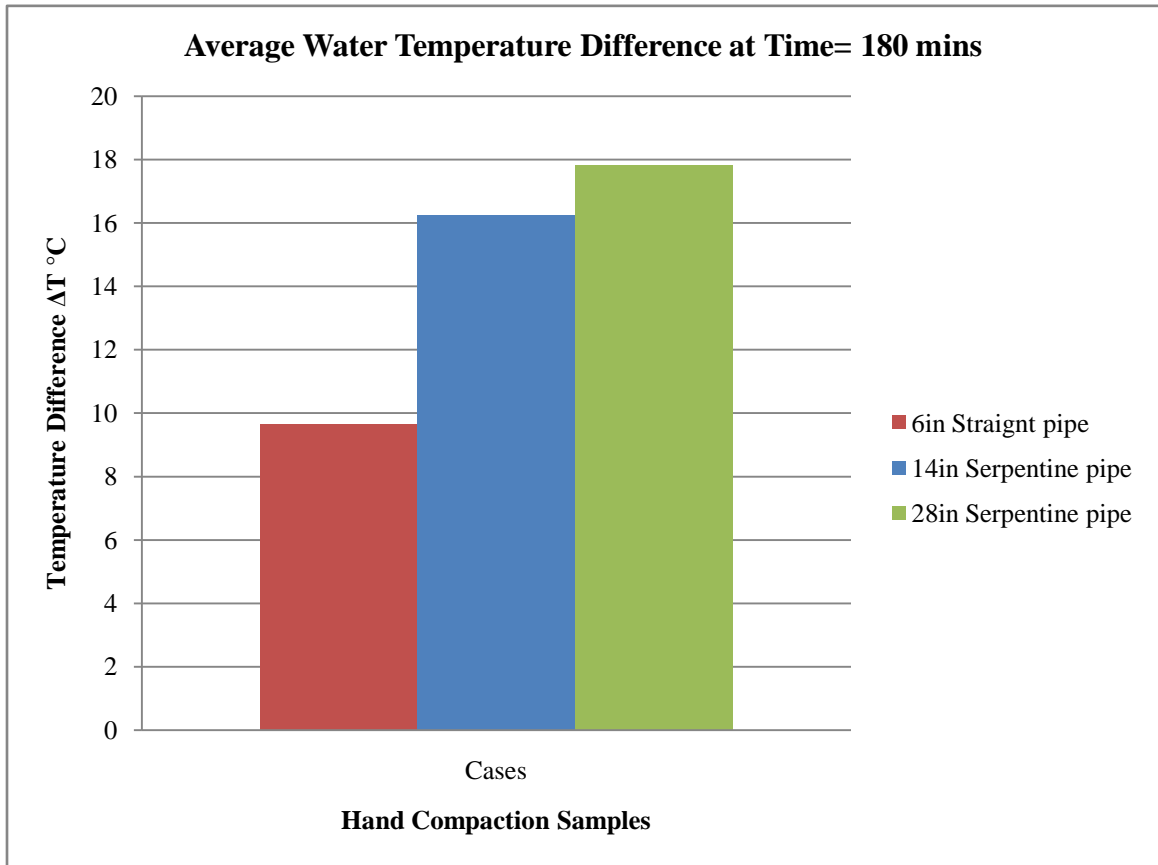


**Figure 7-4 Average water temperature difference at time = 180 minutes**

The experiment results showed that the pipe with larger surface area yielded higher temperature at the water exit. When the pipe length increased from 0.1524m (6") to 0.3556m (14"), the temperature resulted in approximately 8.55°C difference, when the pipe length increased from 0.3556m (14") to 0.7112m (28"), the temperature only increased approximately 7.37°C, which meant that the large surface area of pipe yielded higher temperature.

## 7.5 Finite Element Analysis/Modeling

Based on the analytical results, the copper length and diameter ratio was very large ( $>5000$ ), and finite element analysis approach was unable to model in 3D simulation, therefore, the finite element was used to determine the effective pipe spacing and investigated where the lowest temperature zone occurred between different pipe spacing because finite element analysis simulated the heat transfer interaction between asphalt pavement and water, and the lowest temperature zone meant that the asphalt pavement temperature would be very close to water temperature, and the convective heat transfer of water would not be affected by another water domain. The asphalt pavement temperature was assumed to be constant temperature  $50^{\circ}\text{C}$ , water temperature was constant  $25^{\circ}\text{C}$ , and the various pipe diameters were analyzed by using the pipe spacing from  $0.0254\text{m}$  (2") to  $0.6096\text{m}$  (24").

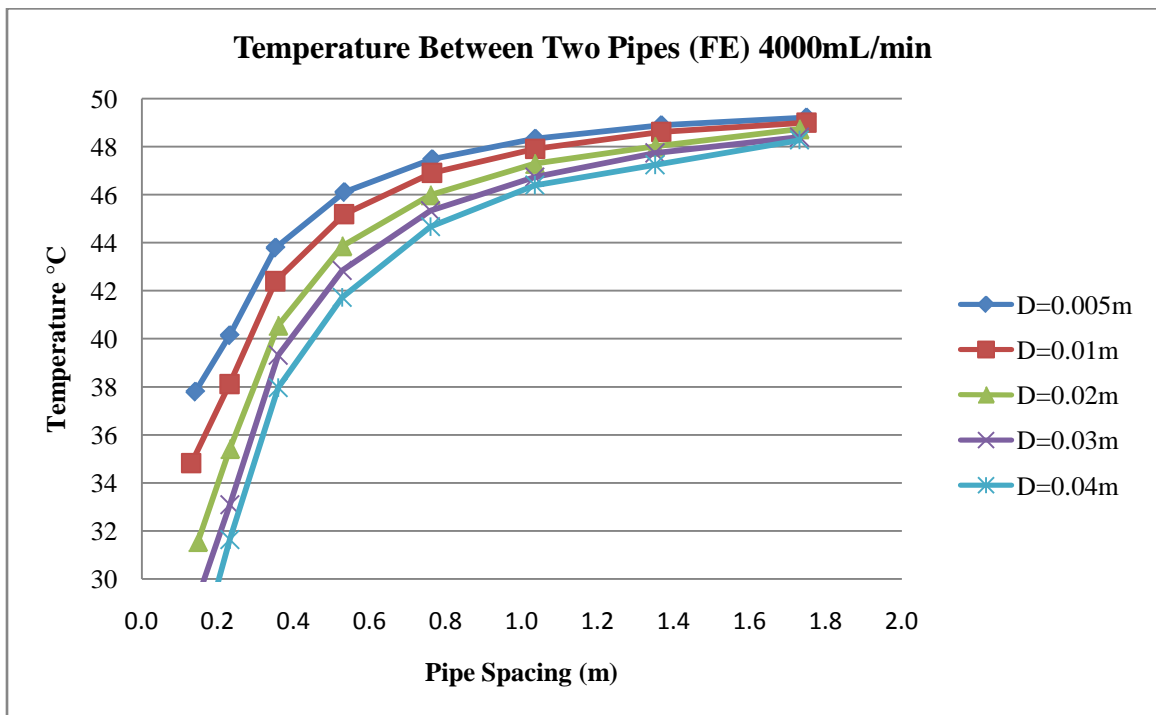


**Figure 7-5 Temperature variation between two pipes**

Note that the smaller hydraulic diameter resulted in lower temperature variation between the pipes, when the pipe spacing were equal to  $0.3556\text{m}$  (14") and  $0.4064\text{m}$  (16"), - the temperature variation was minimal because the convective heat transfer coefficient was greater and the temperature drop between pipes was increased (as asphalt

pavement temperature = 50°C). On the other hand, the convective heat transfer coefficient was decreased when the flow rates increased and this resulted in lower temperature drop between two pipes.

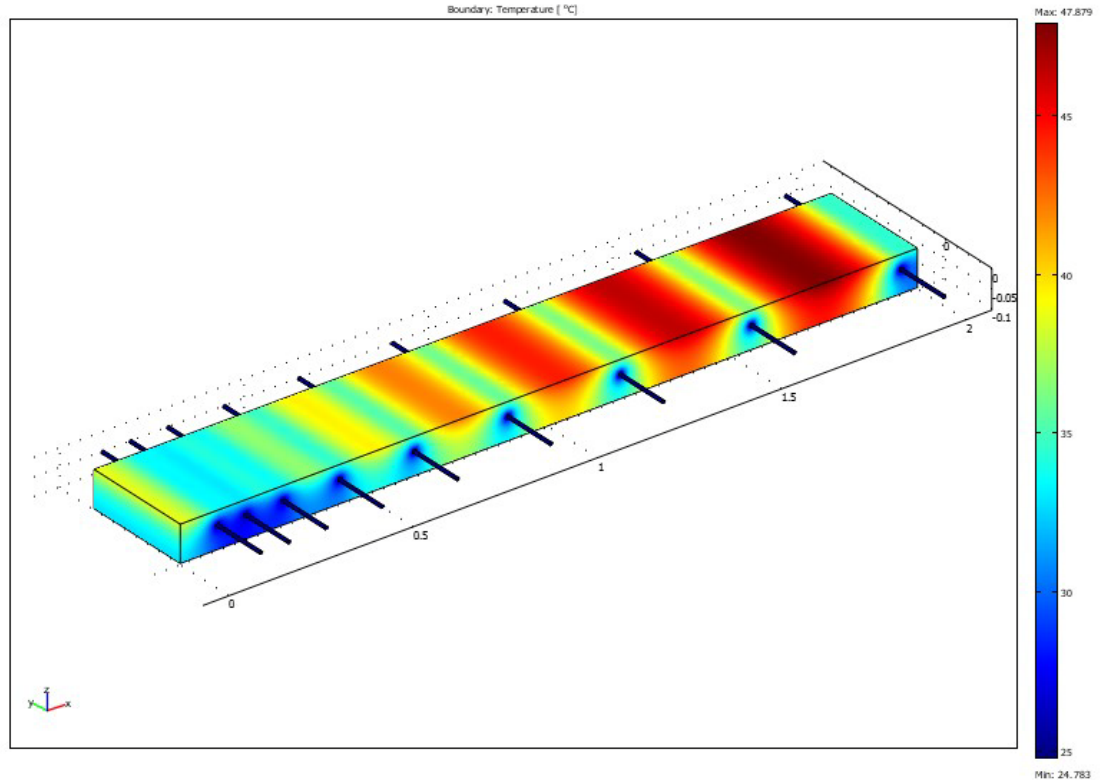


**Figure 7-6 Finite element model for temperature variation between various pipe spacing**

Three serpentine pipe layouts were analyzed by assuming the boundary conditions to a constant temperature (based on lab data) along the interface with asphalt sample and others are thermally insulated, and 10mL/min water flow rate (fully developed laminar flow) was used as water velocity; in actual experiment the temperature of the pipe will not be constant along the diameter of the sample, since because of the cold water entering, the pipe part near the inlet will be at a lower temperature than the remaining part; this could at least partially explain the difference between finite element analysis (higher) and the lab delta Ts.

The results of the finite element analysis (Figure 7-7 to 7-9) clearly showed the higher temperature of the water for the serpentine pipes as compared to the straight pipe.

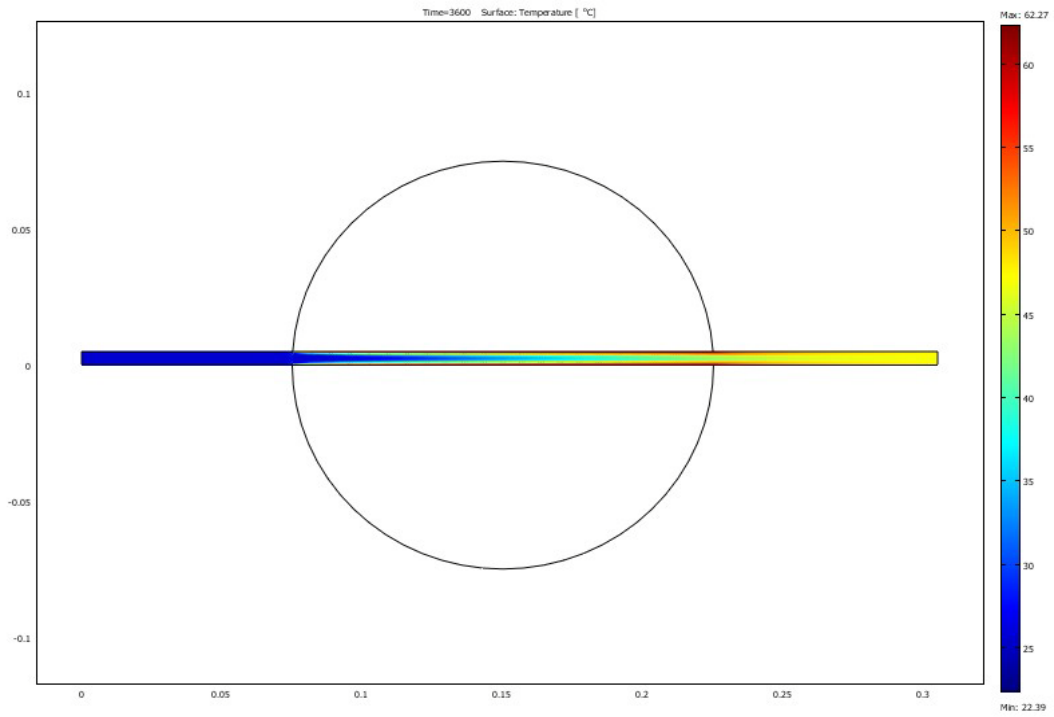


**Figure 7-7 Straight pipe 0.1524m (6'') (temperature distribution)**

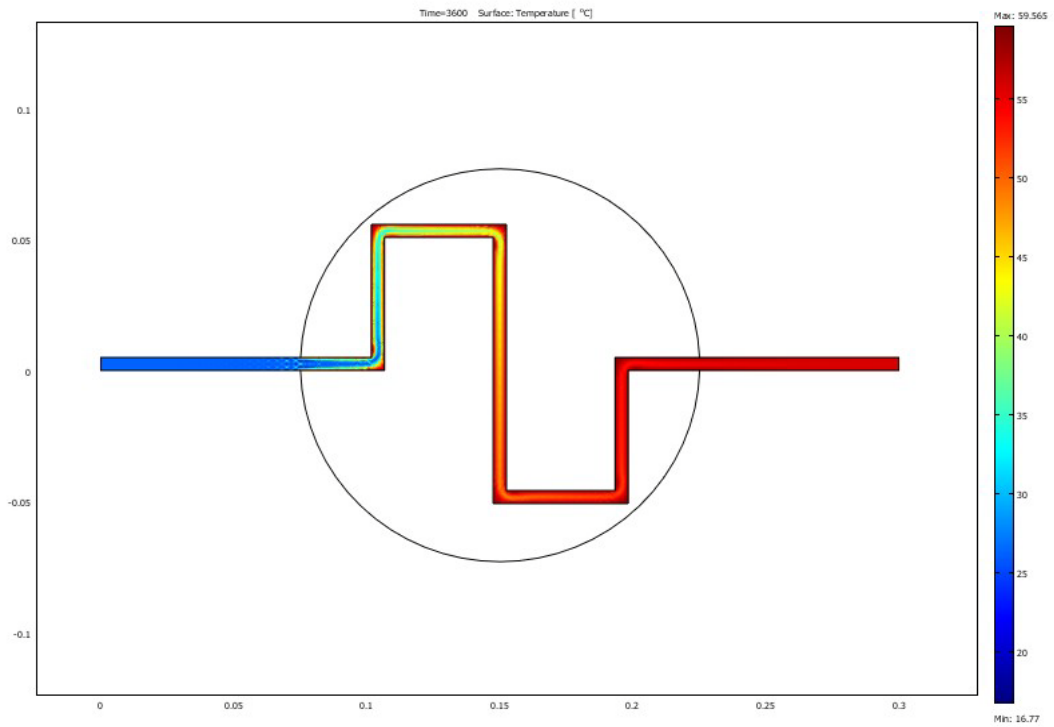


**Figure 7-8 Serpentine pipe 0.3556m (14'') (temperature distribution)**

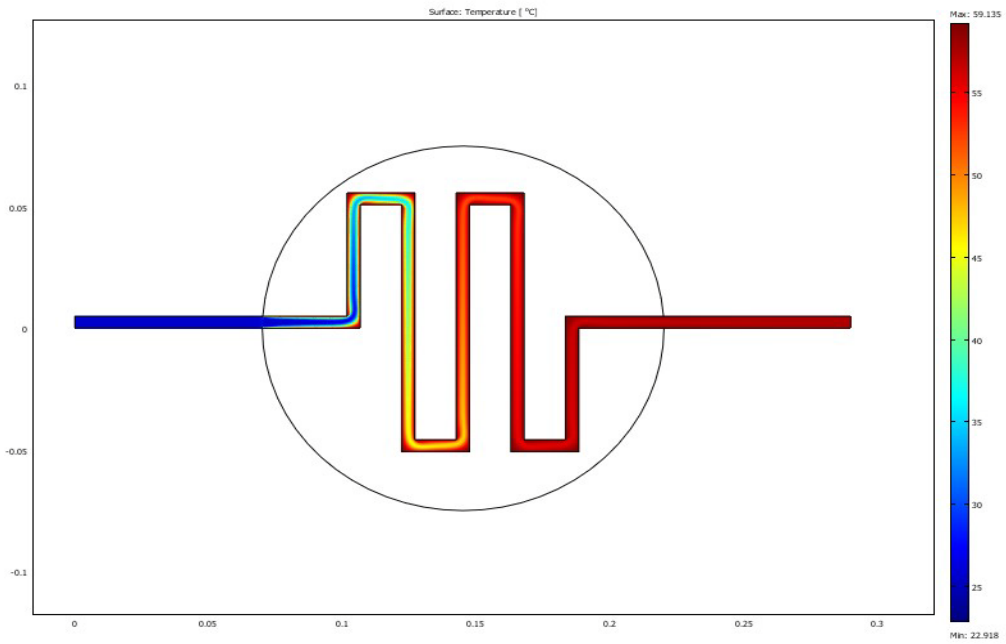


**Figure 7-9 Serpentine pipe 0.7112m (28") (temperature distribution)**

## 7.6 Discussion

The experiment results showed the evidence of increasing surface area of copper pipe yielded higher temperature difference at water outlet by 8.55 °C and 15.92 °C for 14 and 28 inch pipe respectively

The finite element analysis was carried with serpentine pipes to validate experiments. The results from both experiments and finite element analysis (in terms of delta T, the difference between outlet and inlet water temperature) are shown in Table 7-5. The effective pipe length was relative to pipe diameter, water flow rate, and wall temperature; these factors were needed to be taken into consideration when designing the pipe layout.

**Table 7-5: Water temperature comparison**

	Quartzite Mix 10mL/min at 60mins	
	LAB $\Delta T$	FE $\Delta T$ (2D Analysis)
6" Straight Pipe	11.21	20.65
14" Serpentine Pipe	19.76	28.35
28" Serpentine Pipe	27.13	33.25

## **CHAPTER 8**

### **REDUCE URBAN HEAT-ISLAND EFFECT**

#### **8.1 Introduction**

Asphalt pavements get heated up by solar radiation, and numerous studies have been conducted on evaluation of temperature profiles inside asphalt pavements, and the effect of different parameters on such temperature. Because surface radiation follows the Stefan-Boltzmann equation, which involves the fourth power of temperature, a slight increase in the surface temperature results in a significant increase in the emitted heat. This leads to significant increase in energy consumption in order to maintain comfort level. Additionally, studies have shown that air quality also deteriorates under increased temperature due to the Urban Heat-Island Effect.

The hypothesis of this chapter is that the surface temperature of the asphalt pavement will be reduced due to the convective heat transfer of water flowing underneath it, which will decrease the back radiated energy emitted from asphalt pavement to the air.

#### **8.2 Objective**

The objectives of this chapter were to evaluate

1. The effect of the surface temperature of asphalt pavement based on different thermal conductivity of mix.
2. The effect of the surface temperature of asphalt pavement based on different surface area of copper pipe.

#### **8.3 Methodology**

The transfer of energy by electromagnetic waves is called radiation heat transfer. All matter at temperature greater than absolute zero will radiate energy. Energy can be transferred by thermal radiation between a gas and solid surface or between two or more surface. The rate of energy emitted by an ideal surface (black body) with emissivity equal to 1 is given by the Stefan-Boltzmann law (20):

$$E_b = \varepsilon\sigma T_s^4$$

Where  $E_b$  is the rate of black body radiation energy,  $\varepsilon$  is the emissivity of the material, and  $\sigma =$  Stefan-Boltzmann constant  $= 5.68 \times 10^{-8} \text{ W}/(\text{m}^2 \cdot \text{K}^4)$ , and  $T_s$  is surface temperature, K.

The emitted radiation intensity from the pavement surface to its surroundings is calculated as:

$$q_r = \varepsilon\sigma(T_s^4 - T_{air}^4)$$

Where  $q_r =$  emitted radiation,  $h$  is heat transfer coefficient,  $\varepsilon$  is the emissivity of the material,  $\sigma =$  Stefan-Boltzmann constant  $= 5.68 \times 10^{-8} \text{ W}/(\text{m}^2 \cdot \text{K}^4)$ ,  $T_s$  is surface temperature in Kelvin,  $T_{air}$  is air temperature Kelvin.

The emissivity of a material  $\varepsilon$  is the ratio of energy radiated by the material to energy radiated by a black body at the same temperature. It is a measure of a material's ability to absorb and radiate energy. A true black body would have the value of  $\varepsilon = 1$  while any real object would have  $\varepsilon < 1$ . Emissivity depends on factors such as temperature, emission angle, and wavelength. Based on Stefan- Boltzmann law, the variable that would reduce the back-radiated energy is the temperature difference between the asphalt pavement surface and ambient temperature (air).



## 8.4 Experiment Results

In the first step, three thermocouples were used for the temperature data collection from the surface one directly at the center, and other two 0.0254m (1") from the sample edge (Figure 8-1). This arrangement was made for four samples – two for quartzite mix and two for metagranodiorite mix. The samples were compacted in similar manner, using the same amount of asphalt binder. (Bulk specific gravity for Q mix= 2.208 and M mix= 2.265). Of the two samples made for each mix, one was fitted with a copper pipe approximately 1.5 inch below the surface to flow water through it.

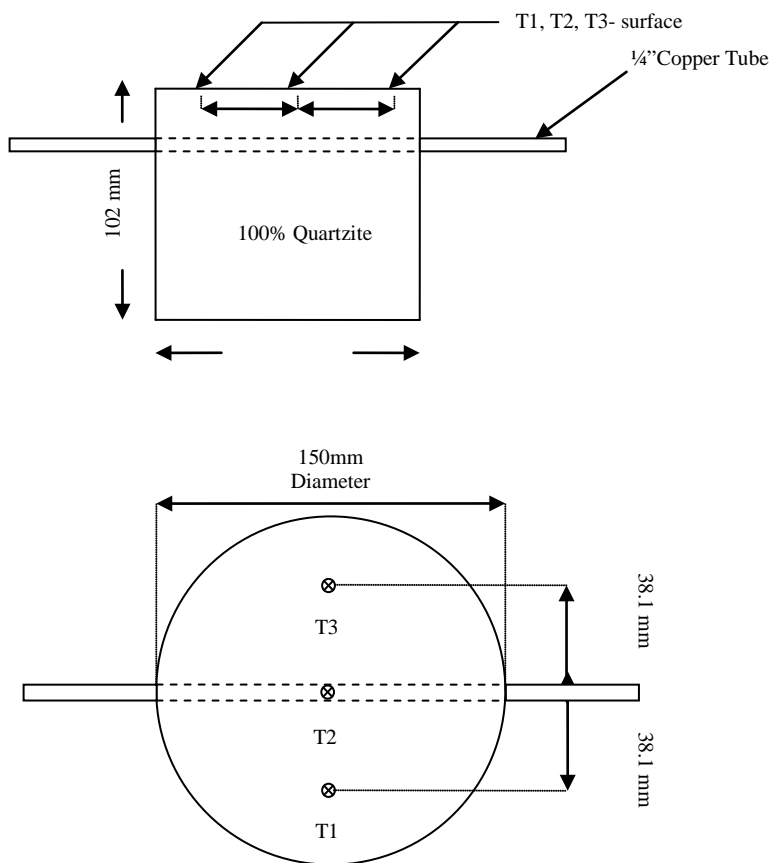


**Figure 8-1 Samples with three thermocouples**

For the samples without pipe, the lamp was left on for eight hours, and then switched off, and data were collected for the next eight hours; this procedure was repeated three times for each sample with 24 hours interval between two successive heating cycles.

For the sample with pipe, the lamp was left on for four hours, without flowing water, and water was flowed for four hours after which the lamp was switched off and the water was kept flowing for another four hours. This procedure was repeated three times for each sample with 24 hours interval between two successive heating cycles.

Plots of surface temperature versus time are shown in Figures 8-2 and 8-3. Figure 8-2 showed that the maximum temperature of the metagranodiorite mix is higher than the maximum temperature of the quartzite mix. This is due to the higher thermal conductivity of the quartzite mix. Figure 8-3, in comparison to Figure 8-2, showed clearly that the maximum temperatures reached in the two samples with water flow were significantly lower compared to those without any water flow.

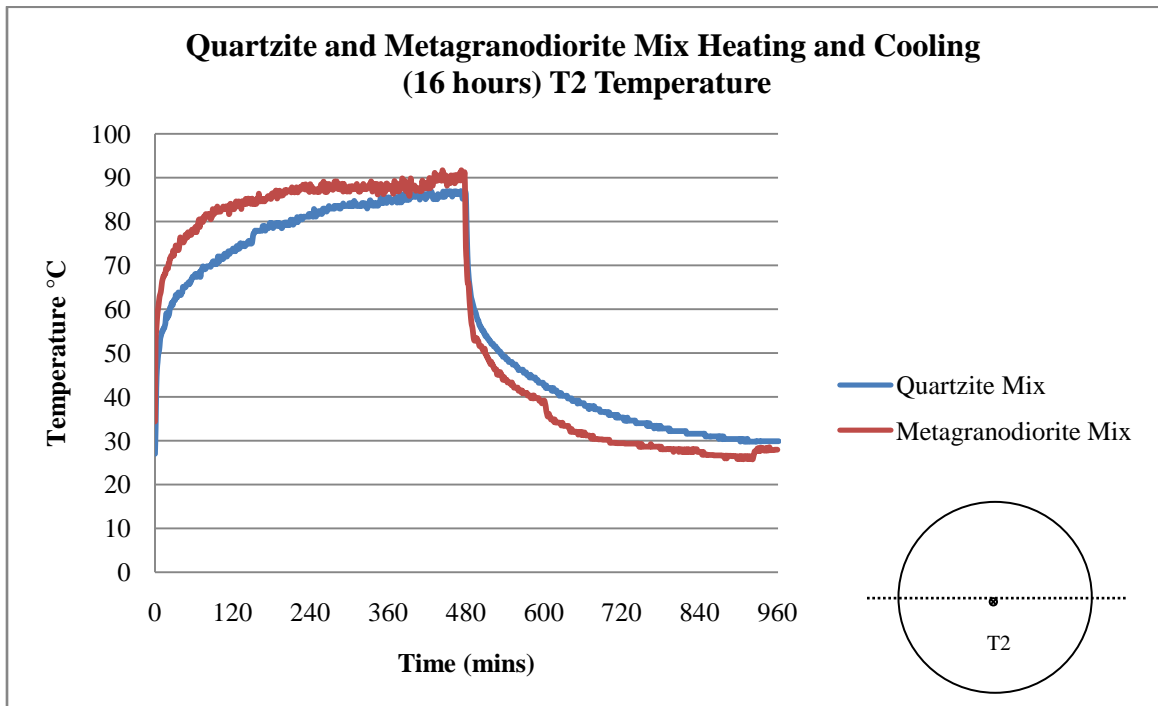


**Figure 8-2 Quartzite and metagranodiorite mixes for 8 hour heating and 8 hour no heating data for surface temperature (T2 thermocouple)**

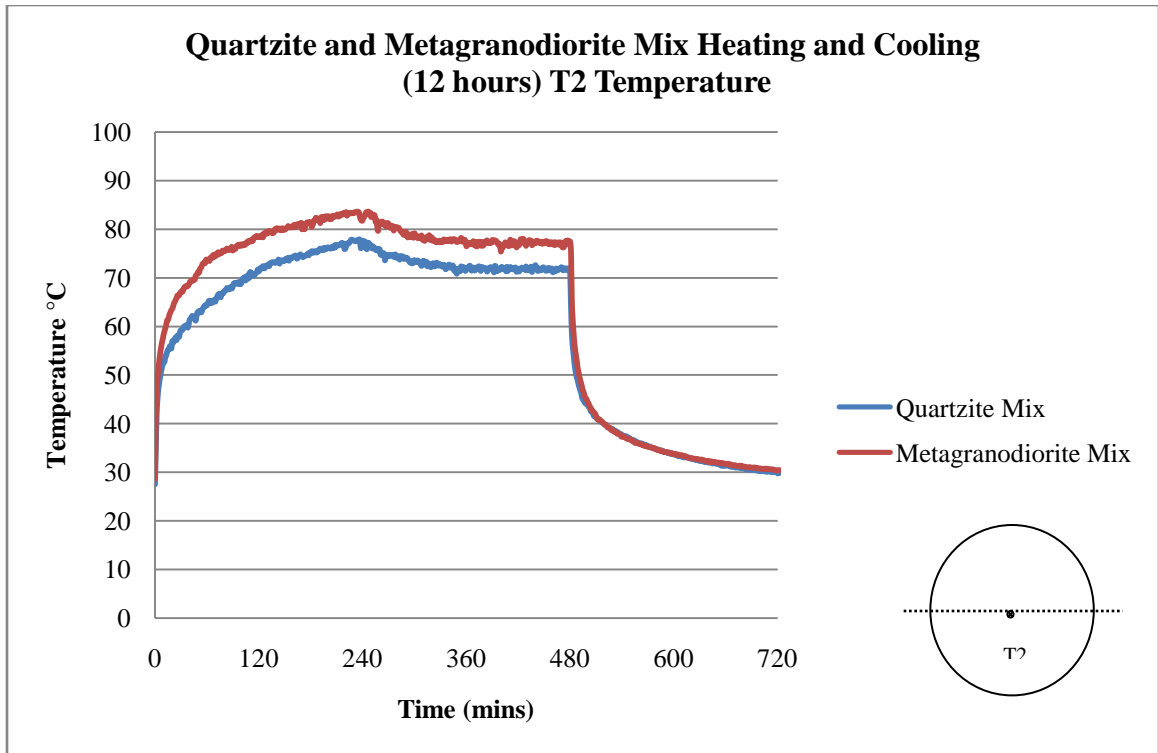


**Figure 8-3 Heating with water flow data for surface temperature (T2 thermocouple) for quartzite and metagranodiorite Mixes.**

In the next step, a detailed investigation of the quartzite samples only was conducted, using seven thermocouples for each sample, as shown in Figure 7-4 and 7-5.

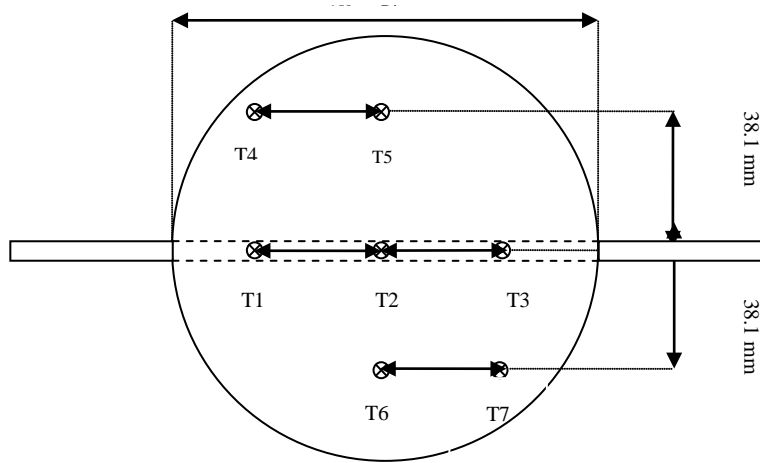


**Figure 8-4 Schematic of thermocouple locations on the surface of asphalt sample**

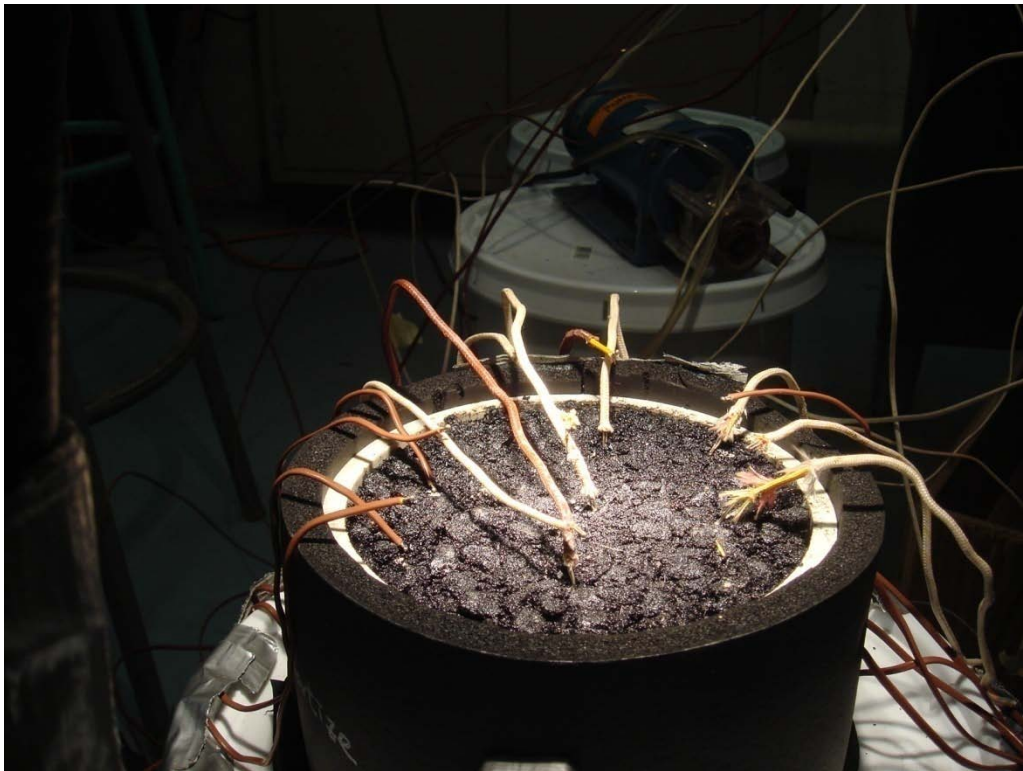


**Figure 8-5 Thermocouple locations on the surface of asphalt sample**

The following plots (Figure 8-6 to 8-12) showed the temperature versus time data for each of the seven thermocouples (T1 through T7) on the surface, for the case where the sample was heated for 8 hours and then not heated for the next 8 hours (designated as 8/8 hrs), and the case for which the sample was heated for 8 hours, where water was flowed after the first 4 hours of heating and then not heated for 4 hours (designated as 4/4/4 hrs).

All of the plots, except the one for the T7 thermocouple, showed that there was a significant reduction in surface temperature of the sample as a result of flowing water. They also showed that at the end of the heating period, the cooling rate was higher for the samples that have water flowing through them.

The results were more prominent for the T1, T2 and T3 thermocouples, which were at the center line of the sample and fell immediately above the copper pipe carrying water inside the sample.

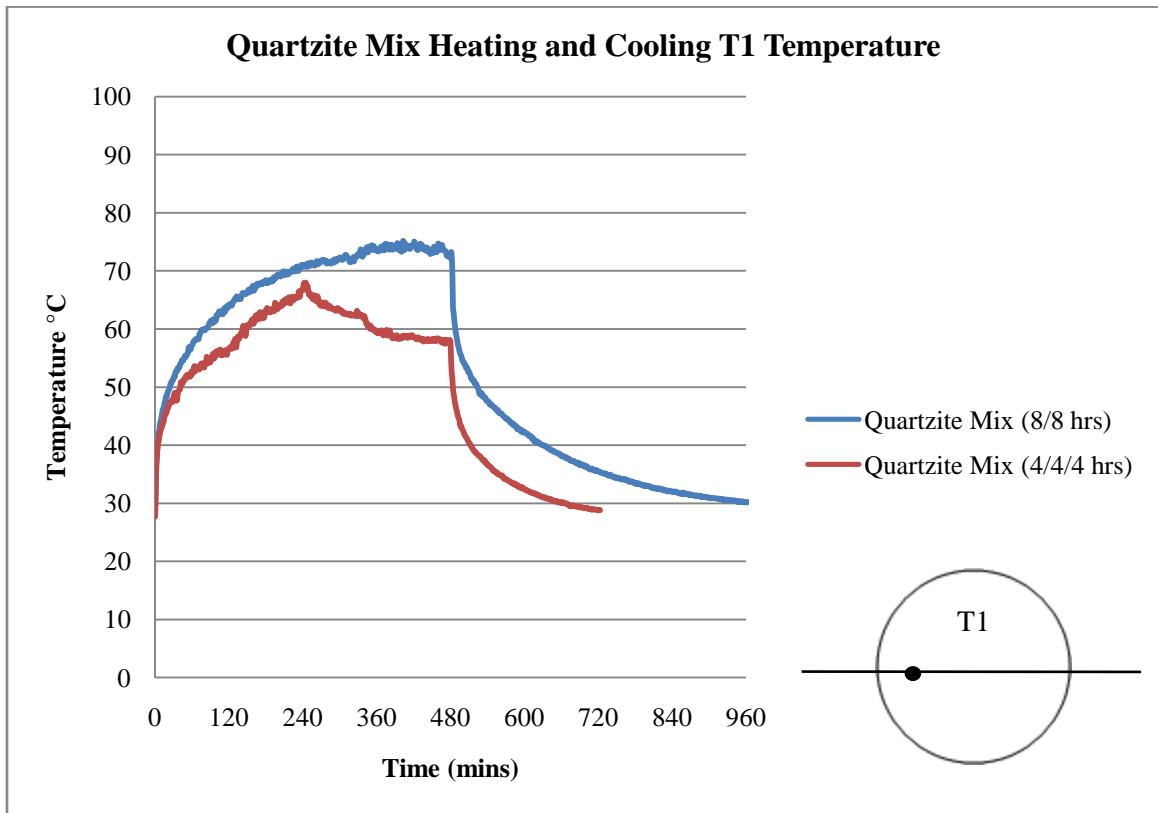


**Figure 8-6 Plots of time versus temperature (T1)**

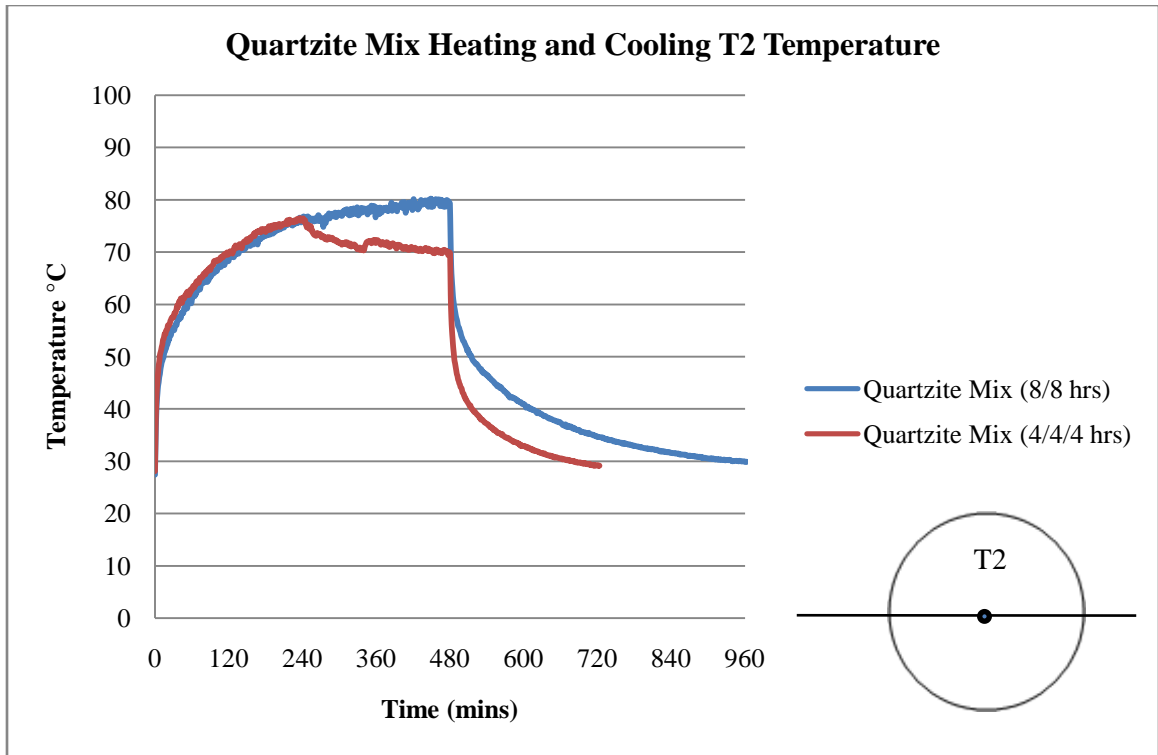


**Figure 8-7** Plots of time versus temperature (T2)

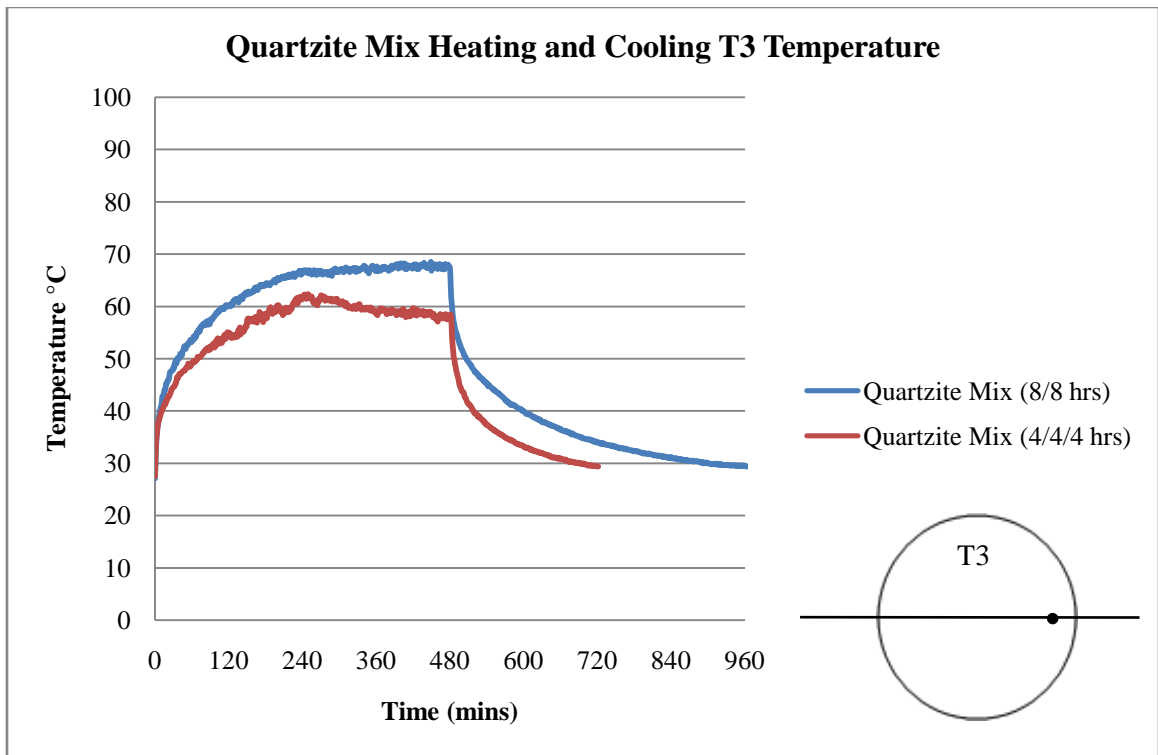


**Figure 8-8** Plots of time versus temperature (T3)

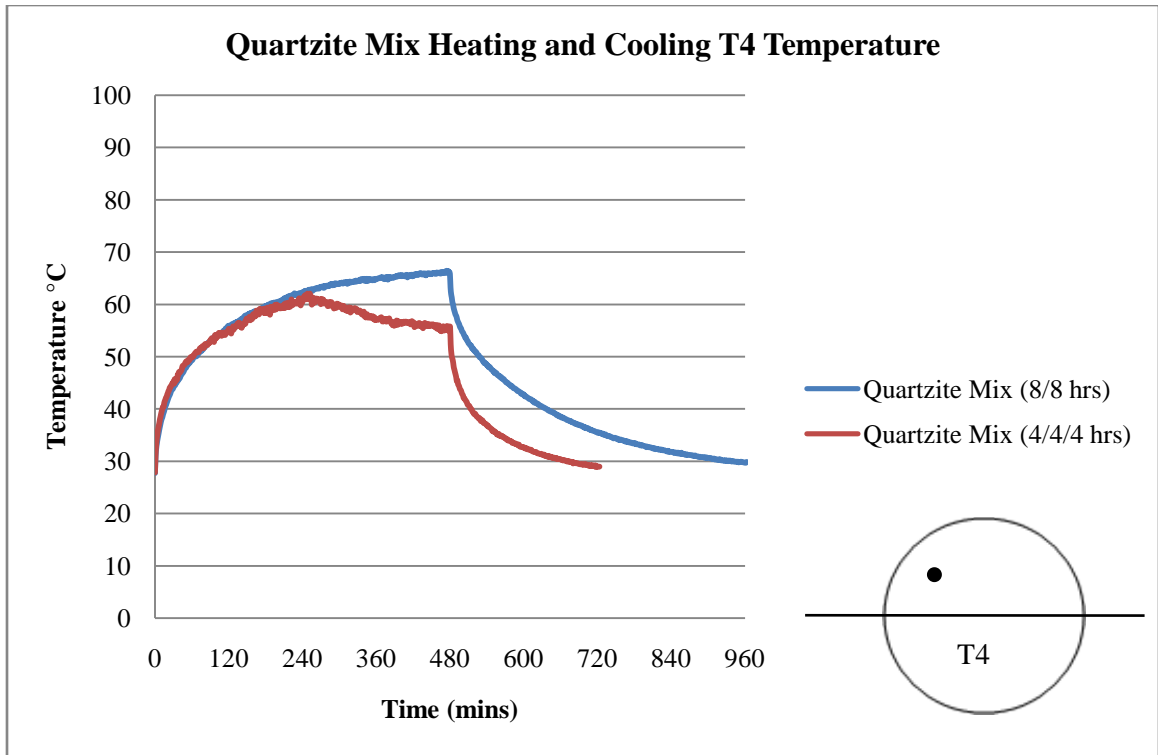


**Figure 8-9 Plots of time versus temperature (T4)**

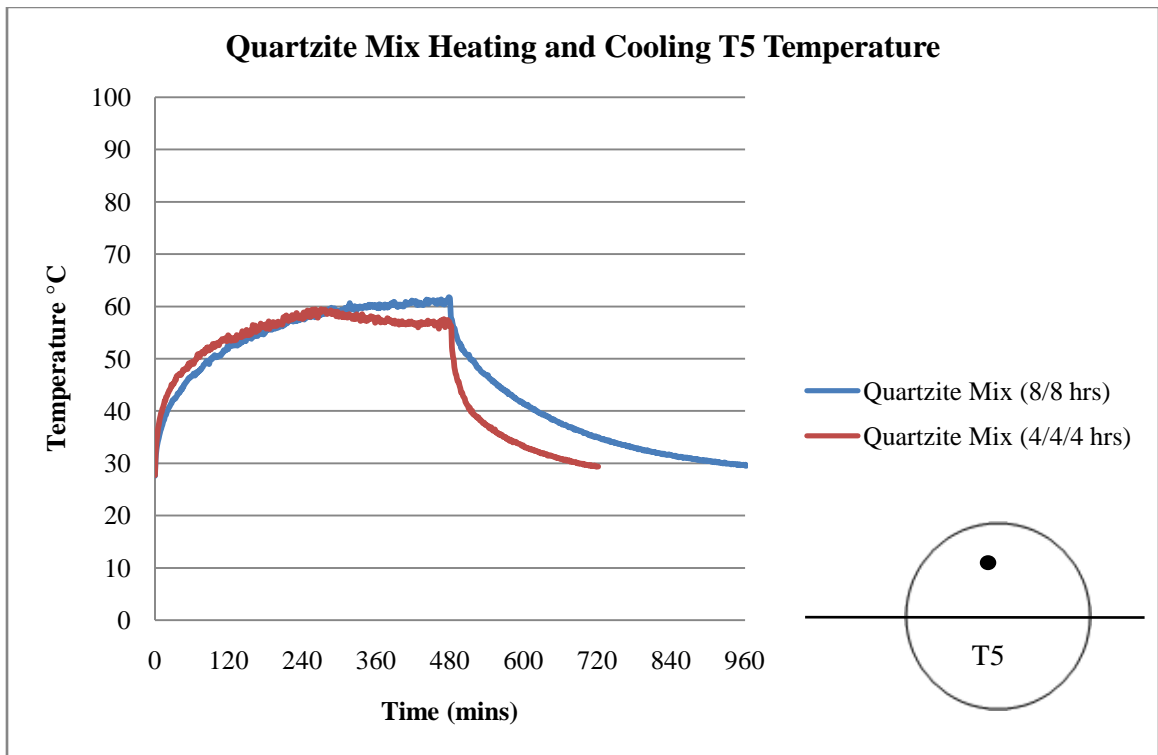


**Figure 8-10 Plots of time versus temperature (T5)**

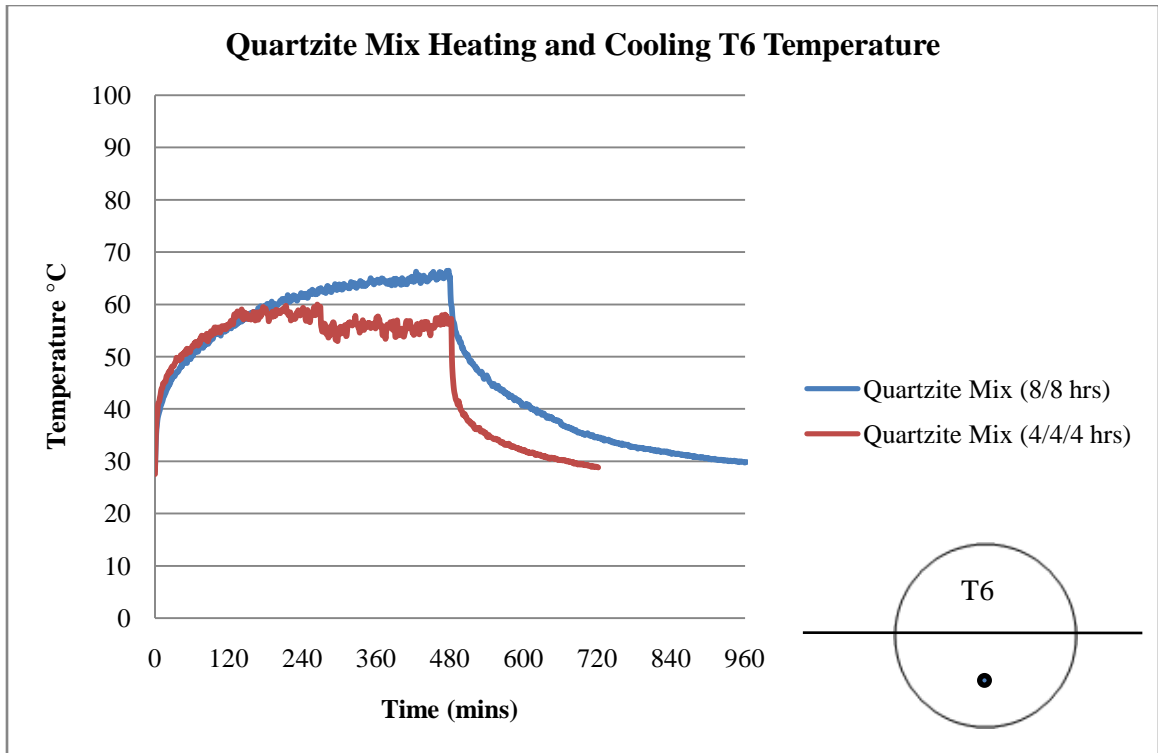


**Figure 8-11 Plots of time versus temperature (T6)**

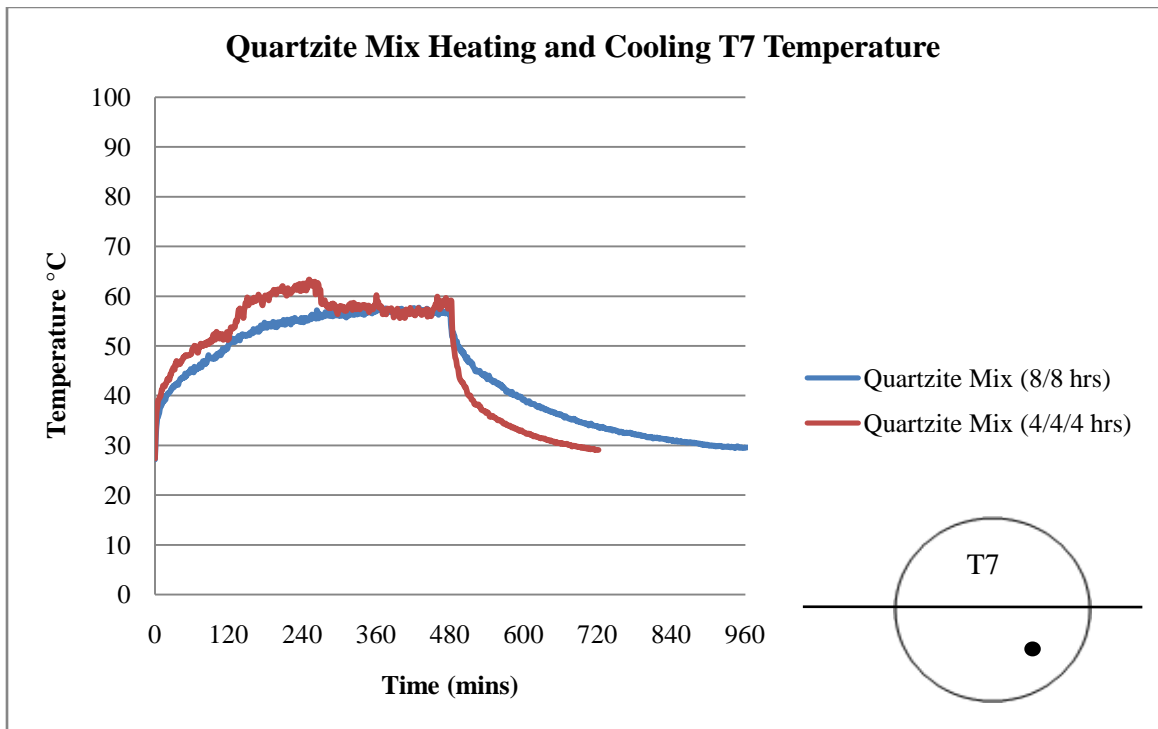


**Figure 8-12 Plots of time versus temperature (T7)**



The filament of the halogen lamp operated at very high temperature and delivers a “cone” heat flux onto sample surface. The thermocouples on the sample surface were very sensitive to the position of the halogen lamp; this caused slightly different temperature measurement (as shown for T7). Table 8-1 showed the average reduction of temperature for the different locations on the sample.

**Table 8-1 Average reduction in surface temperature due to flowing water**

Thermocouple	T1	T2	T3	T4	T5	T6	T7
Max	70.83	76.77	61.30	66.98	64.31	61.71	57.12
Min	57.40	72.09	56.33	57.32	58.94	55.69	55.10
$\Delta T$ (°C)	13.43	4.68	4.96	9.65	5.37	6.02	2.02

Note: The position of T2 is right underneath the halogen filament and the measured temperature is always slightly higher

From the various plots in Figure 8-14 to 8-20, it can be seen that for the first 4 hours all thermocouples showed similar rise in temperature; however when water was turned on thermocouples T1-T6 show lower temperature over the next four hours. The mean drop on temperature ( $\Delta T$ ) was 13.43°C for T1 because its location is near the pipe (water) entrance region which had the coldest water (25.5°C) that led to the largest drop in temp. The effect seems to taper off in the midsection by T2 and also in the tail-end section (T3).

The other prominent effect was the significant lowering of temperature at T4 which is placed 38.1mm from the centerline of the pipe. The temperature at this location fell by almost 10°C. The numbers steadied to between 5 and 6°C in the midsection at these far locations (38.1mm). Results indicate that the cooling potential of water flowing through a pipe can radially extend for almost 40mm.

To evaluate the effect of increased surface area of pipe on the drop in temperature, experiments were conducted with pipes of serpentine (S) shape (Figure 8-13), so as to cover more area of the HMA sample. The plots for the experimentally obtained data for the 28 inch serpentine pipe for T1-T7 are shown in Figure 8-14 to 8-20.

The results clearly show the higher reduction of surface temperature for the serpentine pipes compared to the straight pipe.

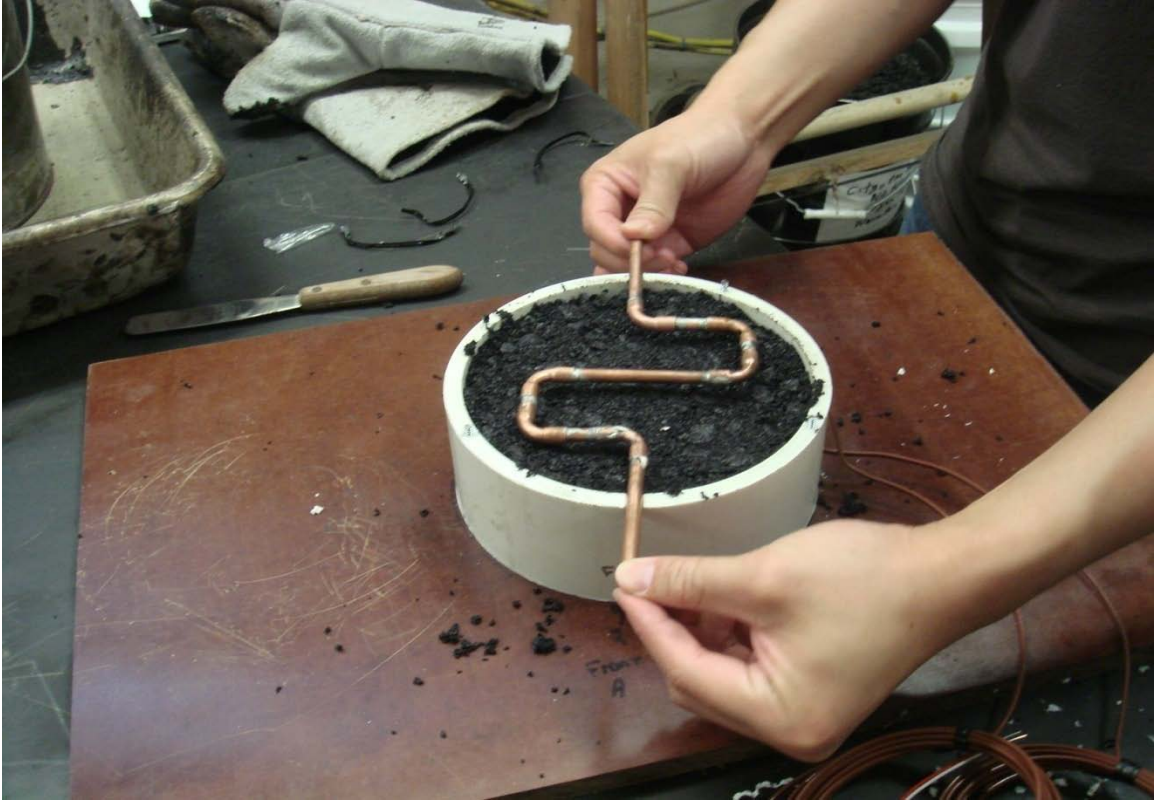


**Figure 8-13 Serpentine pipe in a sample (during compaction)**

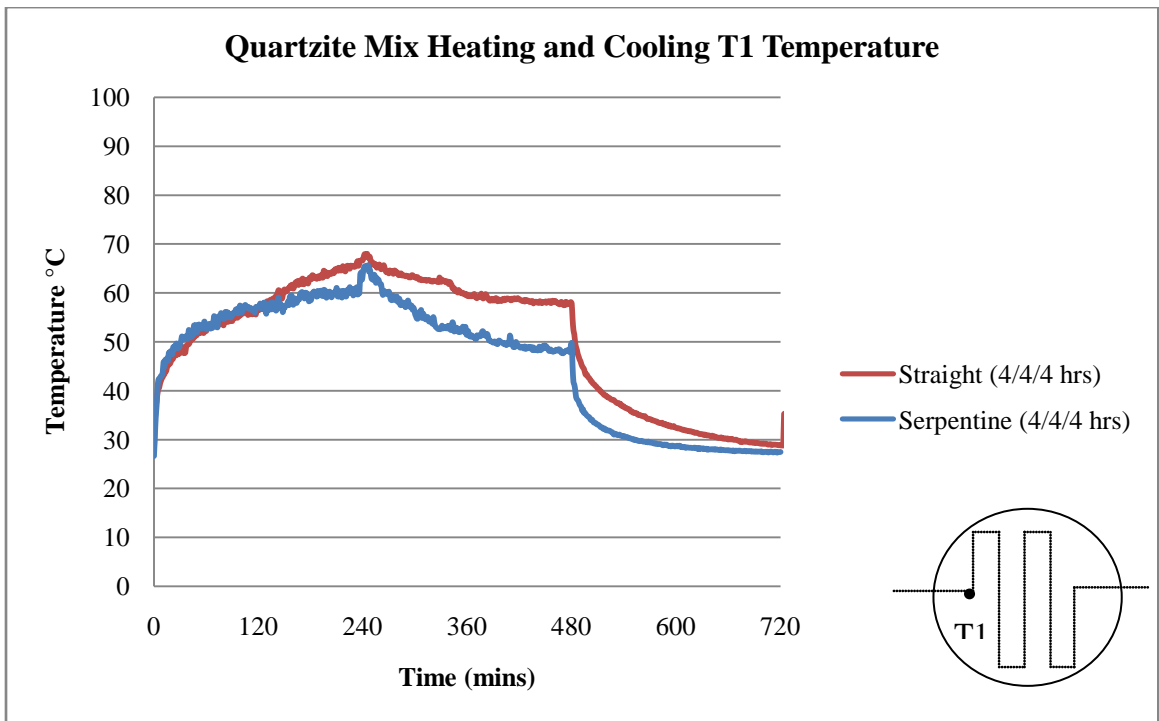


**Figure 8-14 Plots of time versus temperature (T1)**

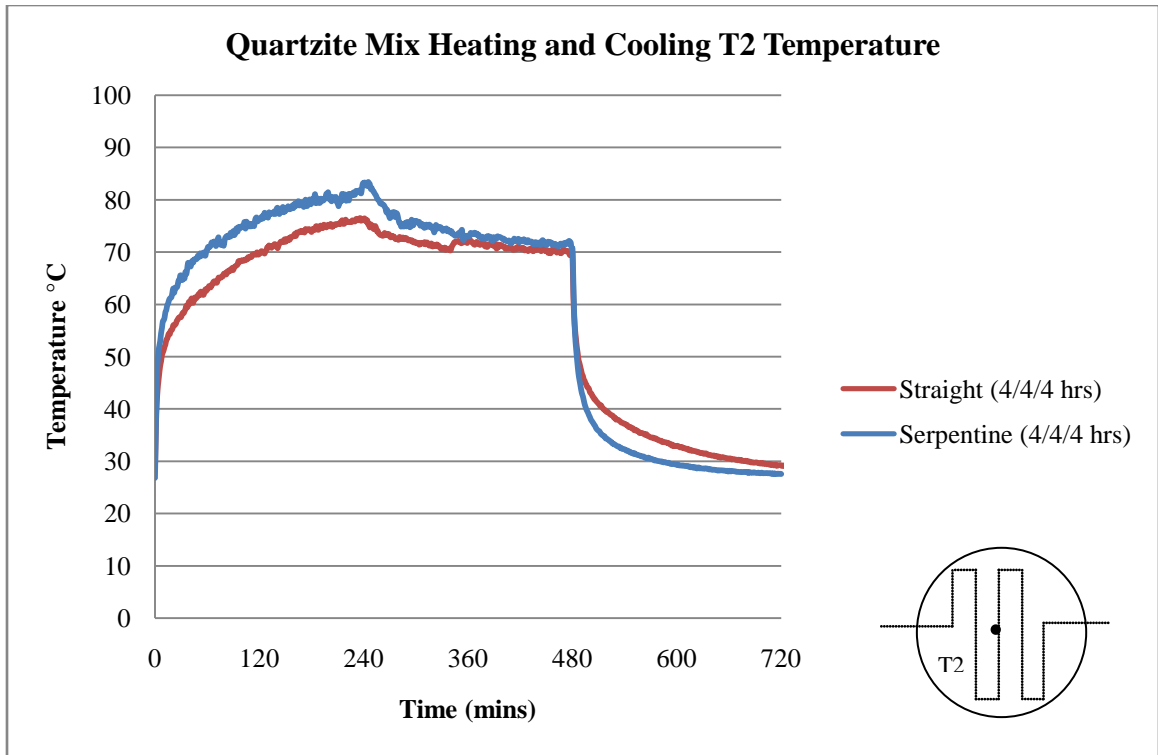


**Figure 8-15 Plots of time versus temperature (T2)**

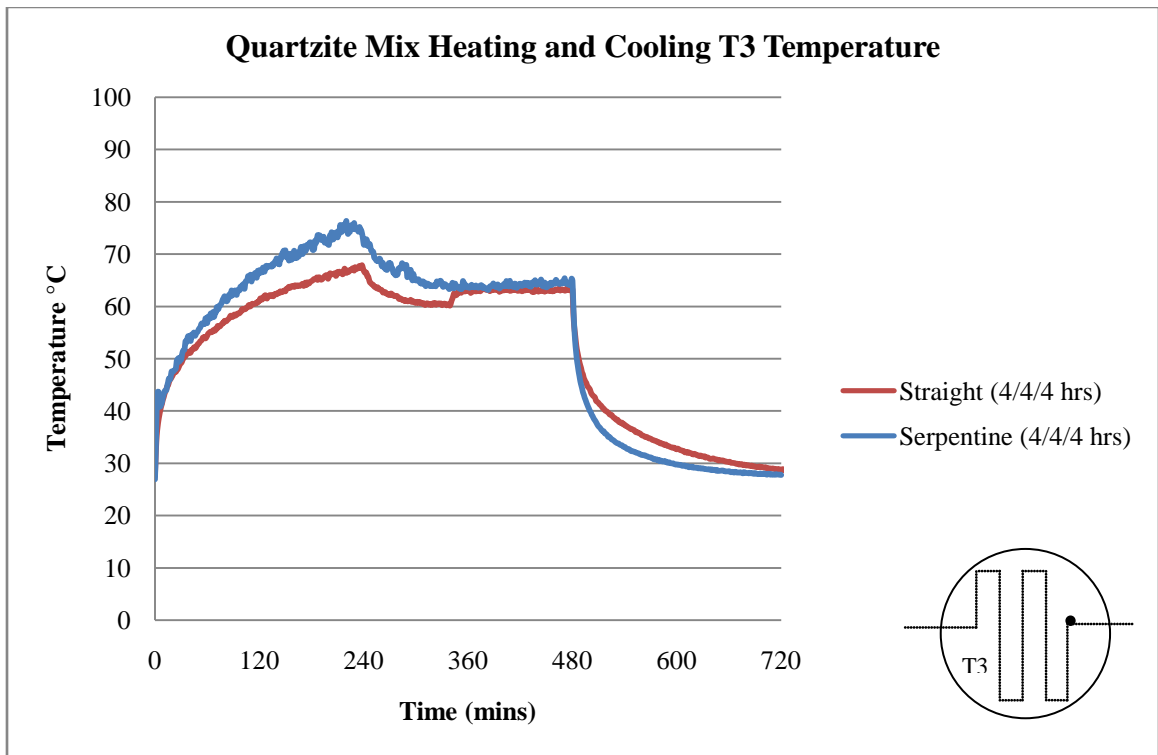


**Figure 8-16 Plots of time versus temperature (T3)**

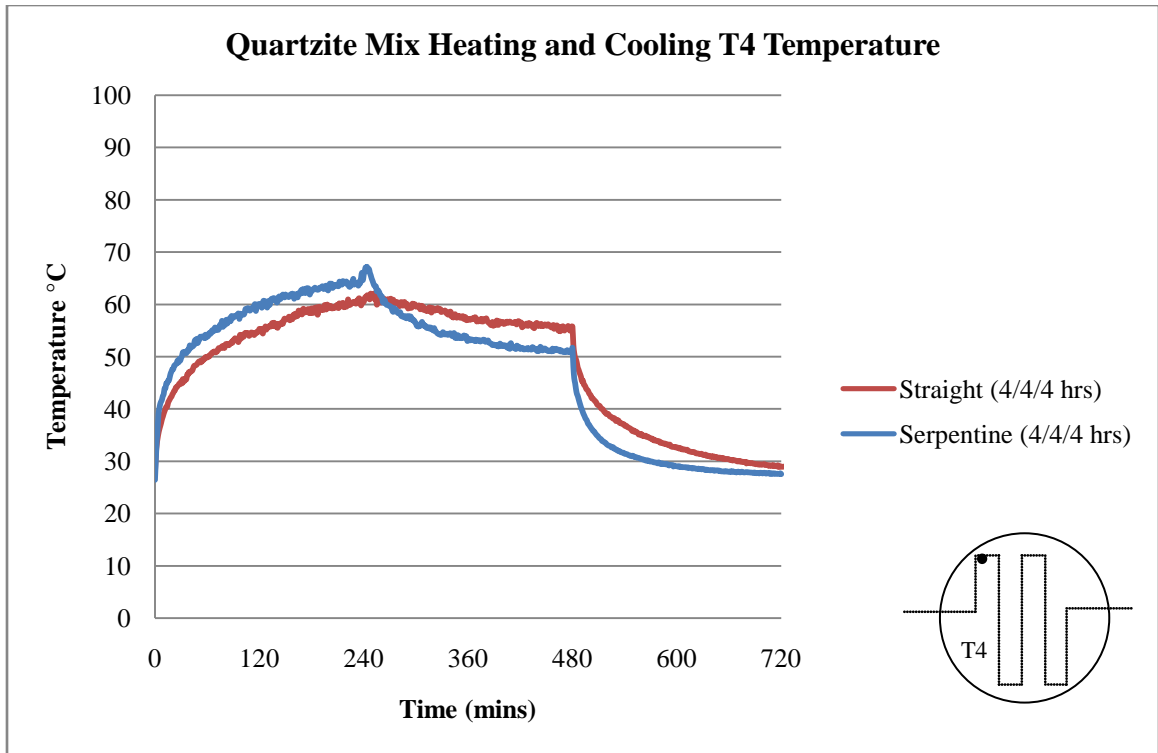


**Figure 8-17 Plots of time versus temperature (T4)**

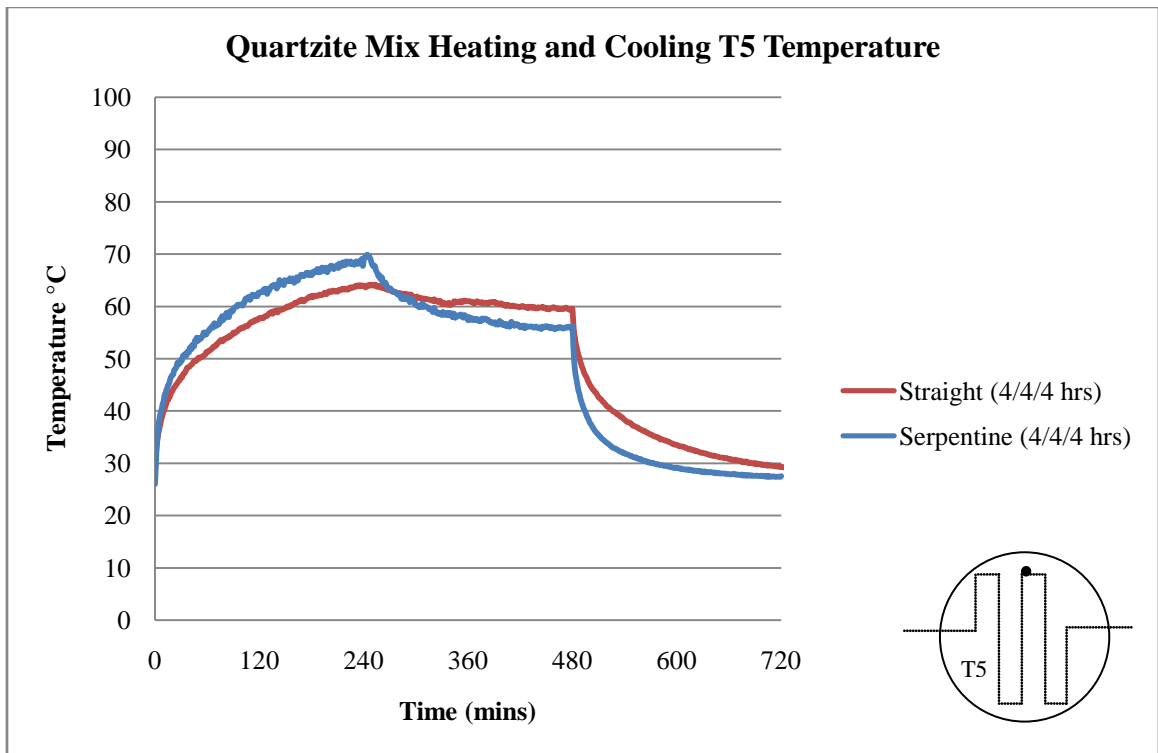


**Figure 8-18 Plots of time versus temperature (T5)**

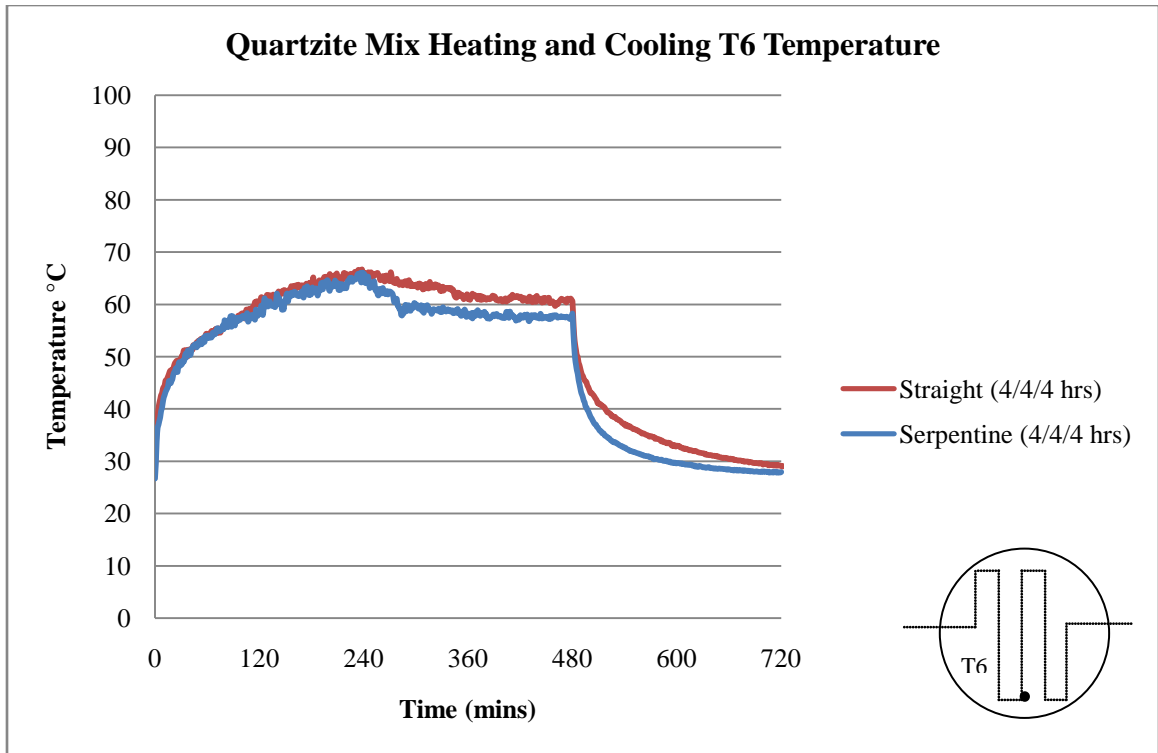


**Figure 8-19 Plots of time versus temperature (T6)**

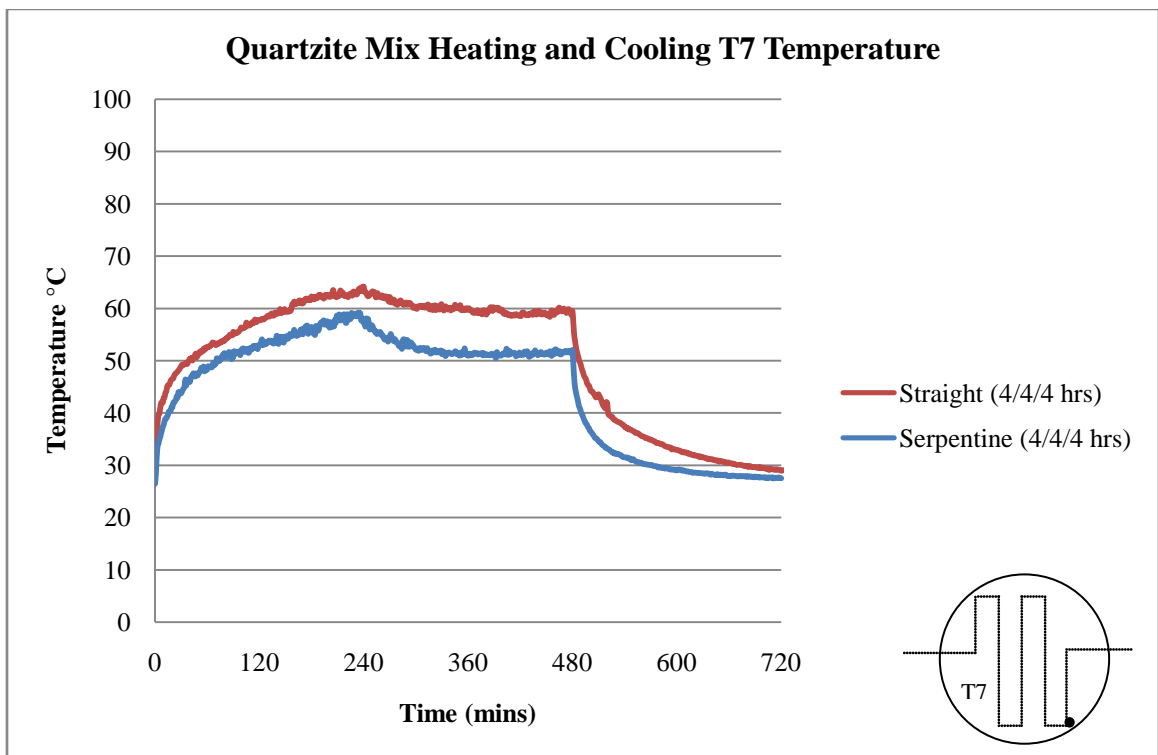


**Figure 8-20 Plots of time versus temperature (T7)**

## 7.5 Discussion

The experiment results of 8 hours heating and 8 hours cooling of quartzite and metagranodiorite mixes showed that the surface temperature of higher thermal conductivity of quartzite mix was lower than the metagranodiorite by approximately 4°C.

The experiment results of heating and cooling with water flowing showed that the surface temperature of quartzite mix was not heated up rapidly and was 7°C lower than metagranodiorite mix.

The results of seven thermocouples on quartzite mix measurement showed that the T1 (water inlet) yielded highest surface temperature difference, approximately 13.5°C, which was due to the greater heat transfer coefficient of water flow at water inlet.

Quartzite mix (higher thermal conductivity) with greater surface area of copper pipe showed the evidence of reducing Heat Island Effect by decreasing the surface temperature and reduced back-radiated energy emitted to air.

## CHAPTER 9

### LARGE SCALE ASPHALT PAVEMENT TESTING

#### 9.1 Introduction

In this chapter, tests were carried out with large scale slabs. Two slabs were prepared – each with approximately 125 mm thick HMA layer, with a frame of copper pipes (Appendix E) embedded inside. The copper pipes were provided for pumping water (heat exchanger) through the slab. Thermocouples were inserted along the depth and at various points in the slabs, including points in line with the copper pipe locations, and inlet and outlet points of the water flowing through the copper pipes.

Two types of materials were used for preparing mixes for the two slabs. The entire 125mm thickness of the first slab was prepared with a metagranodiorite mix obtained from a local HMA plant (using aggregates identified as greywacke, with quartz and feldspar), whereas the second slab was prepared with the local mix for the bottom 64mm, and quartzite aggregate mix (prepared in the laboratory) in the middle and the top layers. Mixes with both aggregates were made with the same gradation and asphalt content. Copper pipe frames with multiple pipes along the width and one pipe along the length were placed approximately 38mm below the surface in both slabs, during placement and compaction inside wood carts.

The schematics of the two slabs, with copper pipe frame as well as thermocouple locations are shown in Figure 9-1 to 9-4.

#### 9.2 Objective

The objectives of this chapter were to evaluate

1. Temperature distribution of asphalt pavement based on partial replacement of granite aggregate with quartzite, and performing different water flow rate and pipe opening combinations.
2. The effect of heat exchanger system to pavement temperature and validate the previous laboratory experiments.

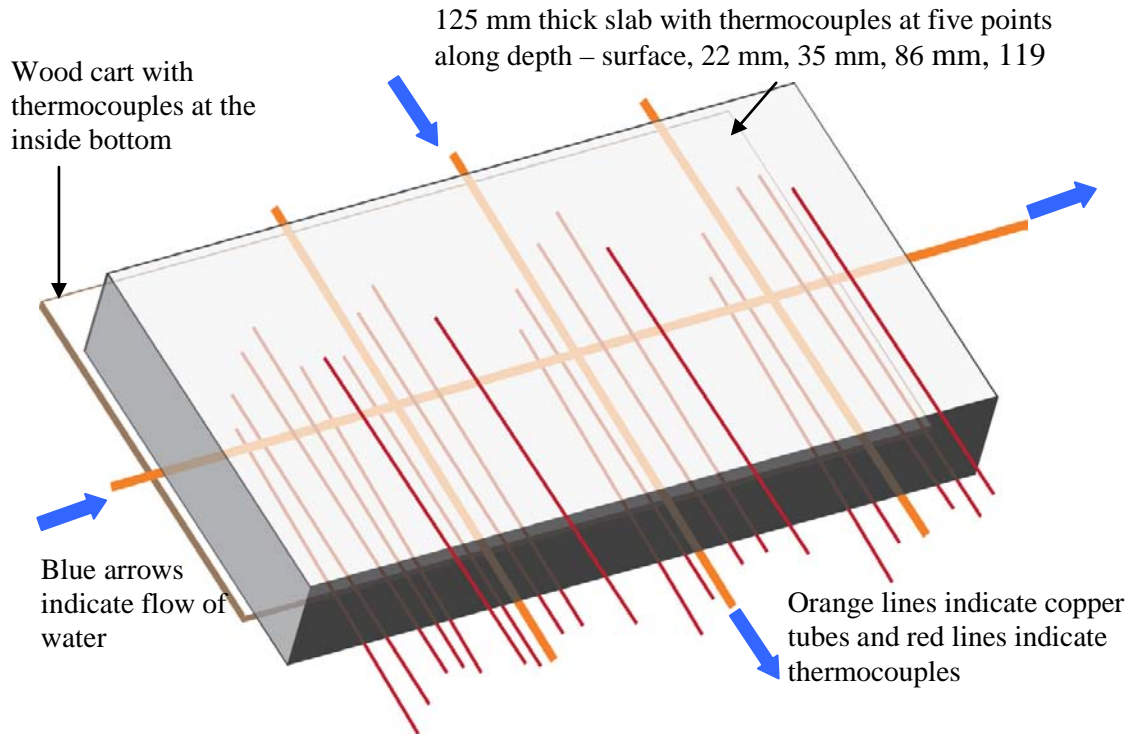


**Figure 9-1 Schematics of slab with thermocouple, copper pipes, and water flow direction**

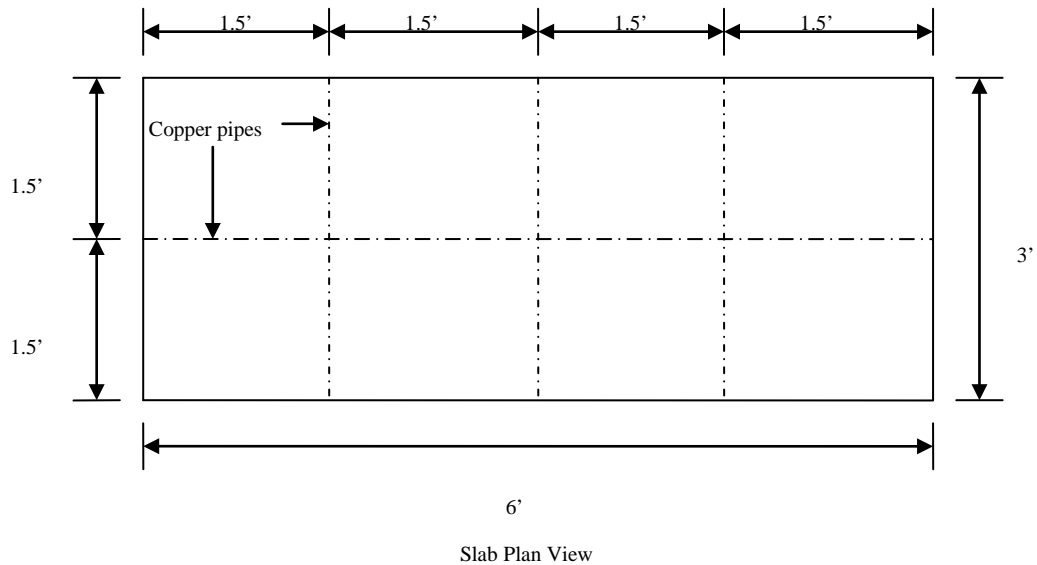


**Figure 9-2 Dimension of slab and copper frame**



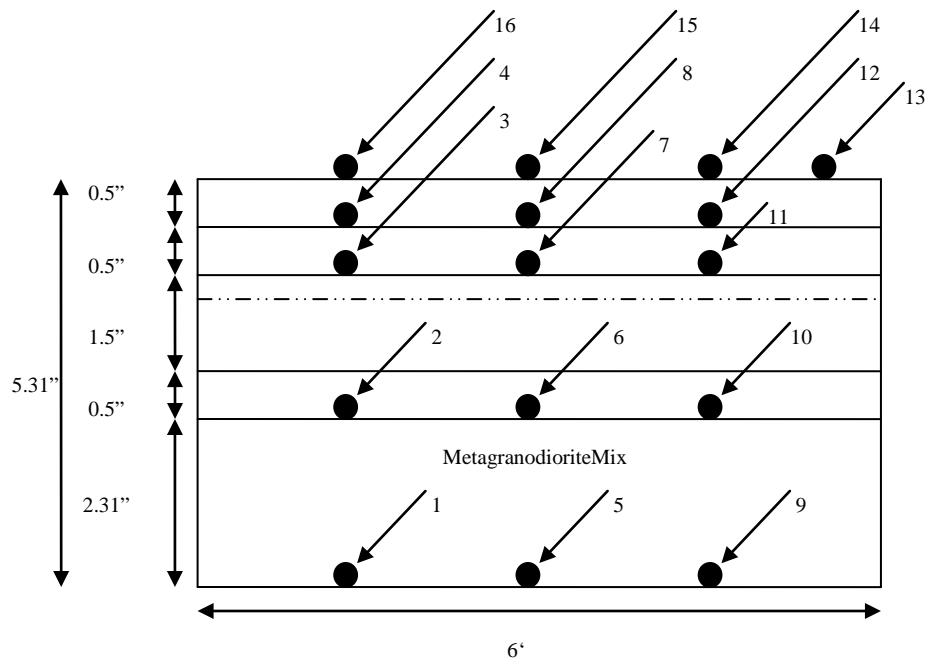


**Figure 9-3 Metagranodiorite mix slab thermocouple location**

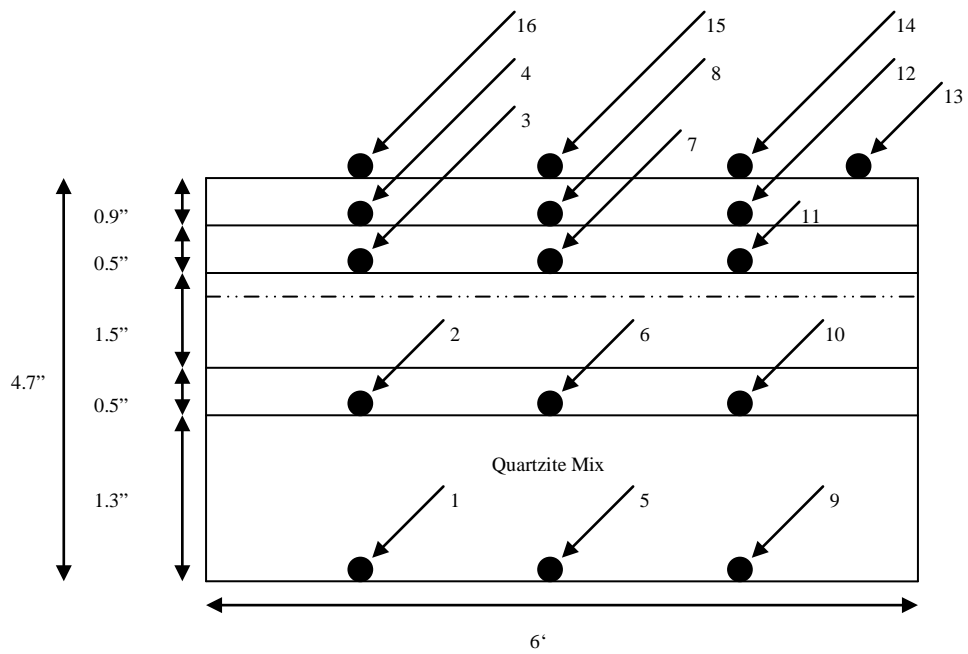


**Figure 9-4 Quartzite mix slab thermocouple location**

## **9.2 Objective**

The objectives of this chapter were to evaluate

1. Effect of temperature distribution of asphalt pavement based on partial replacement of metagranodiorite aggregate with quartzite.
2. Effect of temperature distribution of asphalt pavement by performing different water flow rate and pipe opening combinations.
3. Effect of convective heat transfer at surface of asphalt pavement.
4. Feasibility of reduce Urban Heat-Island Effect by inserting heat exchanger system underneath of asphalt pavement.

## **9.3 Methodology**

Temperature data was first collected for both slabs without flow any water. The data received from the thermocouples (Figure 9-3 and 9-4) inserted at various points were used to determine the temperature profile within the slabs.

Next, a hose was connected from the same water supply to pump water through the copper tubes in both slabs at the same rate. First, before flowing any water, the slabs were kept under the sun for approximately two hours, and temperatures at the various depths at the center of the slabs were recorded. Next, water was pumped at 1, 2, 3 and 4L/min through both slabs with different pipe opening combinations, and temperature of the slab at the middle copper pipe location as well as incoming and outgoing water were measured (Figure 9-5).



**Figure 9-5 Two slabs tests under the field conditions**

## 9.4 Experiment Results

Figure 9-6 and 9-7 illustrated both slabs temperature profiles over time at different depths over a period of 5 hours and under an average of  $716\text{W/m}^2$  solar radiation. As clearly indicated by the temperature profiles of thermocouples placed with increasing depth, temperature was a function of depth, with thermocouples placed closer to the surface recording higher temperature at any instant of time. This process was consistent through all the reading and progressive depths. However, an important observation from these sets of graphs was that the time at which steady state was reached at different depths vary.

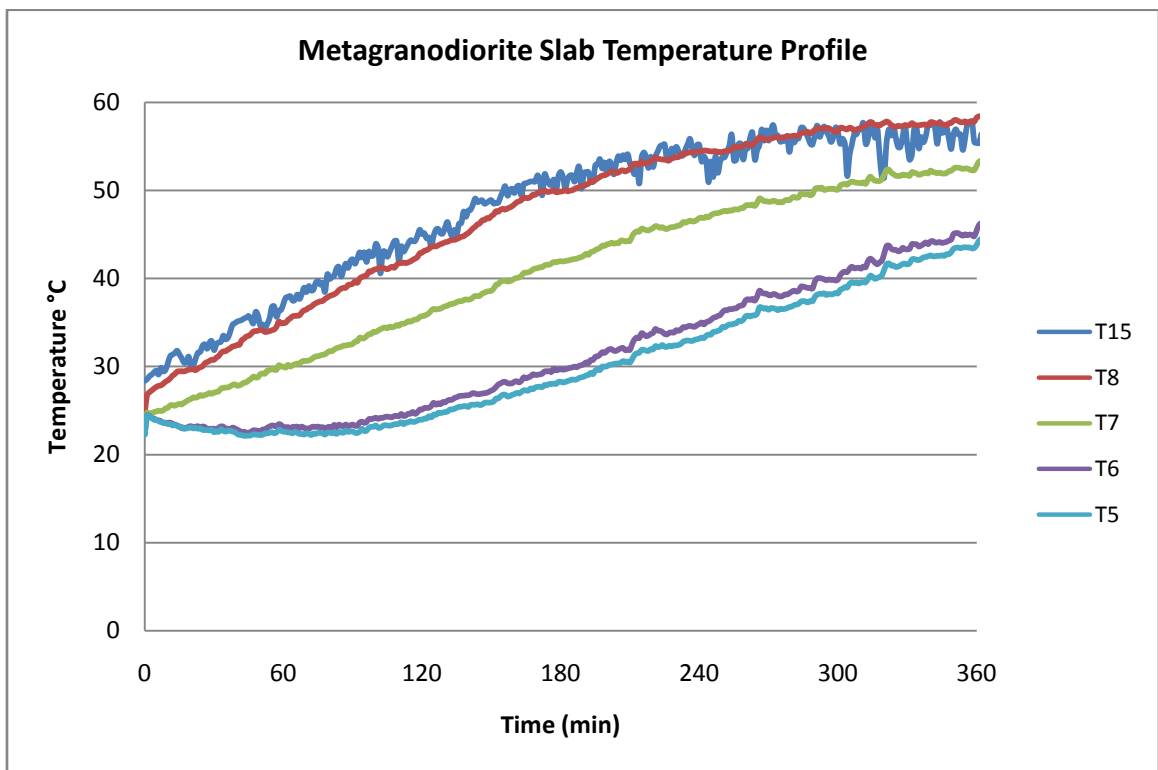
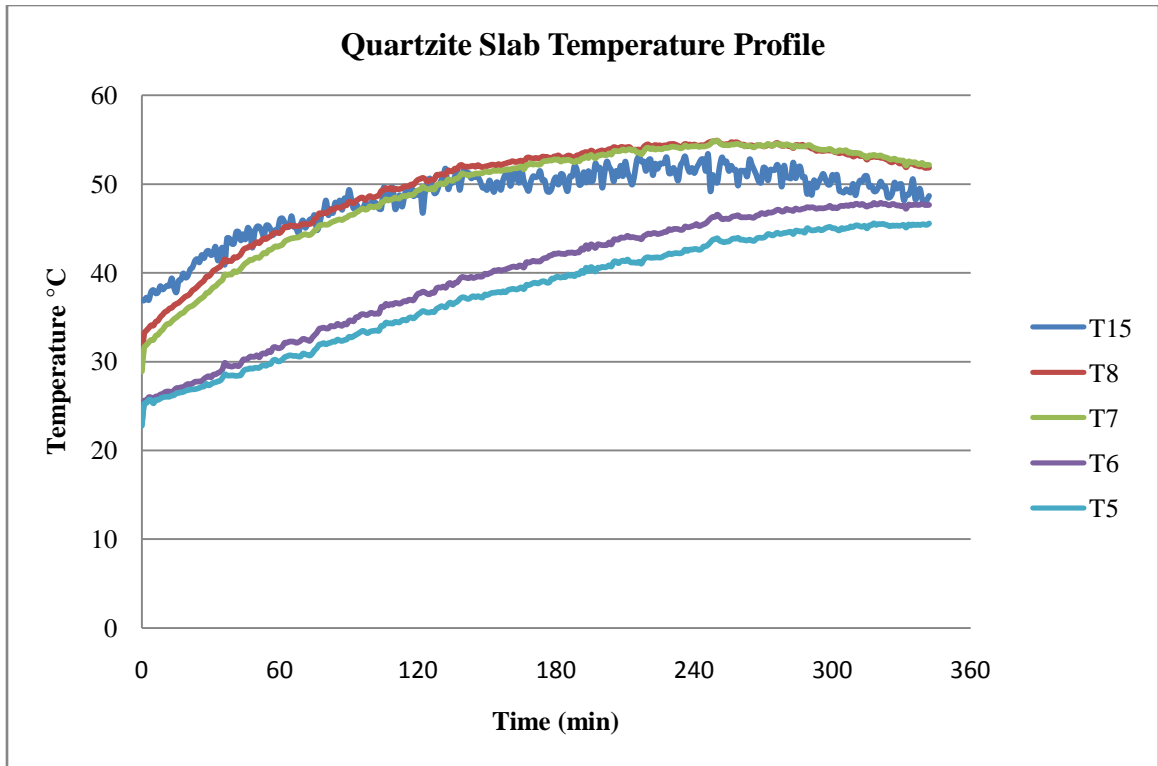


Figure 9-6 Metagranodiorite mix slab temperature profile



**Figure 9-7 Quartzite mix slab temperature profile**

At 0.0127m (T8) depth of metagranodiorite slab, steady state was reached quickly (the scatter in the data induced by solar radiation fluctuation and wind velocities made the exact prediction impossible). At 0.0254m of metagranodiorite slab, the steady state was reached in 300 minutes, and quartzite slab showed much faster heating rate when it reached steady state at 60 to 120 minutes. The lowest 2 thermocouples (T5 and T6) of metagranodiorite slab reached steady state at the end of the 360 hours period, and quartzite slab reached at 300 minutes. The temperature profile of two slab showed that the quartzite slab had higher heating rate compared to metagranodiorite, this was also the indication of the higher thermal conductivity of quartzite slab opposed to metagranodiorite slab.

The results indicated that the depth (0.0381m) at which the pipes were placed was clearly important for a temperature profile like this as seen from the graphs. At a hypothetical depth of 0.0254m, the steady state temperature of approximately 50°C can be obtained for heating pipes whereas at 0.0254m the temperature was 50°C and transient for a longer period.

The both slabs were tested with 4 difference flow rates (1, 2, 3, 4L/min) and all copper pipes running water. The water temperature was taken at 3 and 6ft of copper pipe. The Figure 8-8 showed the typical thermocouple locations for collecting temperature data.

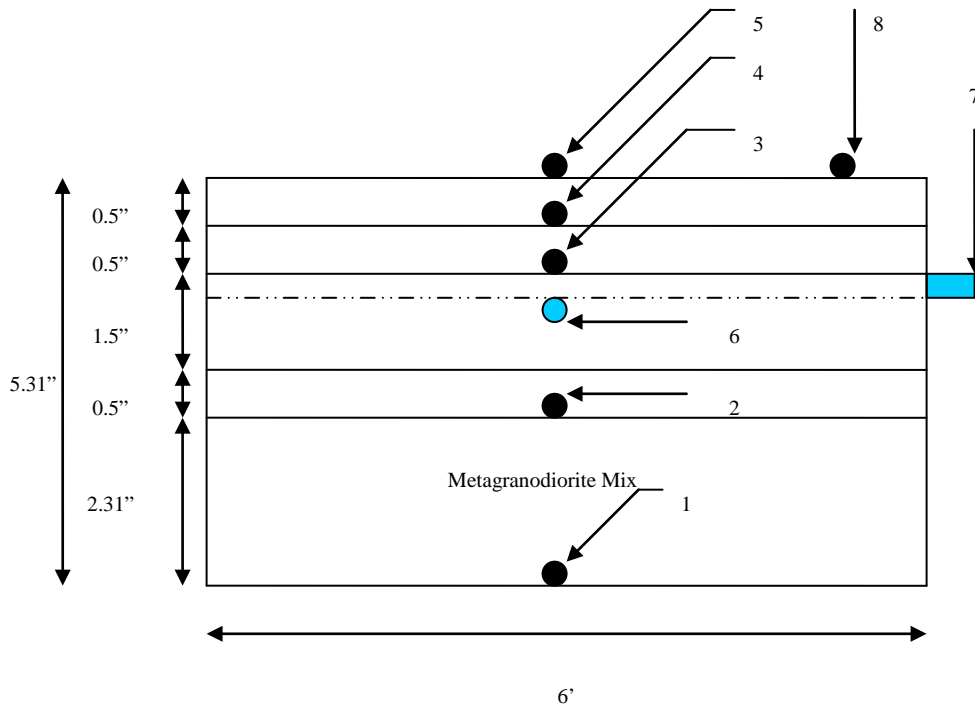


**Figure 9-8 Metagranodiorite slab thermocouple locations**

Table 9-1 and Figure 9-9 showed that, with increasing flow rate the temperature raised of water flowing through a pipe are reduced. The temperature rise was generally more for the longer tube because of the higher area of heat transfer available due to the longer length. This translated into more power being extracted by flowing the water through a longer pipe. The results also showed that the quartzite slab which had higher thermal conductivity can yield higher temperature at the water outlet.

**Table 9-1 Metagranodiorite slab water temperature (all pipe open)**

	T <sub>initial</sub> (°C)	T <sub>final</sub> (°C)	ΔT (°C)
1L/min (3')	22.98	24.52	1.54
2L/min (3')	22.72	23.71	0.99
3L/min (3')	22.73	23.22	0.49
4L/min (3')	22.74	23.59	0.85
1L/min (6')	22.98	24.61	1.63
2L/min (6')	22.72	24.56	1.84
3L/min (6')	22.73	24.03	1.30
4L/min (6')	22.74	23.87	1.13

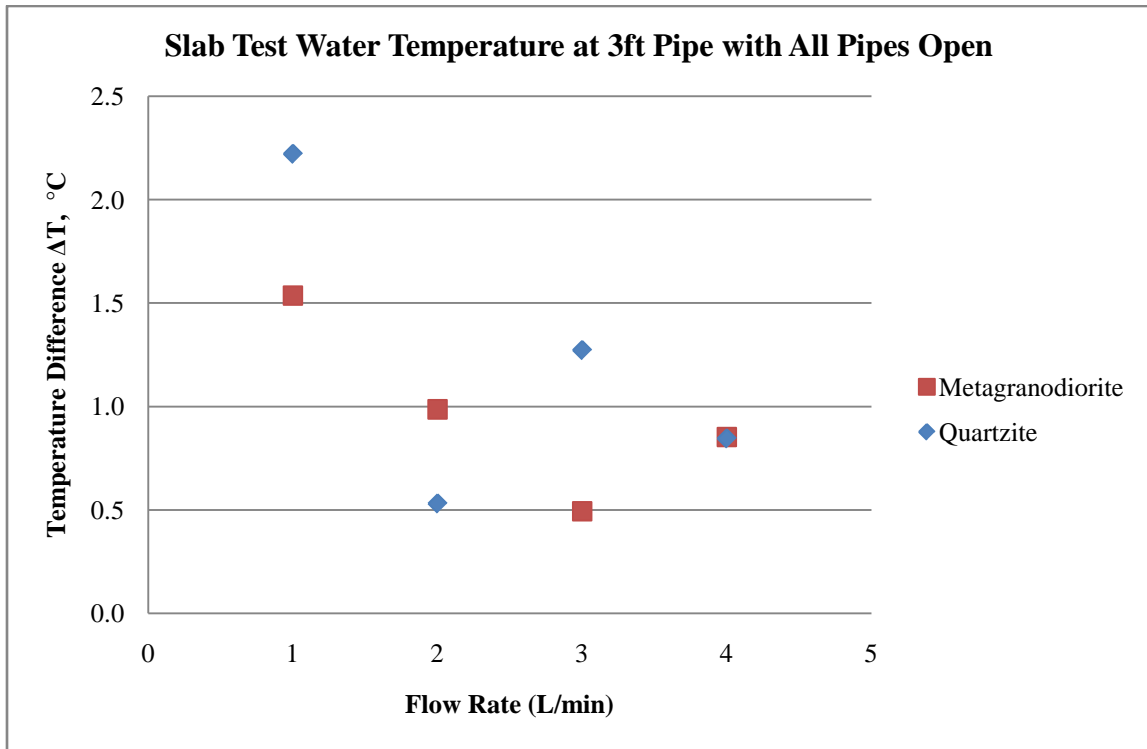


**Figure 9-9 Water temperature measured at 3ft pipe outlet for both slabs**

**Table 9-2 Quartzite slab water temperature (all pipe open)**

	T <sub>initial</sub> (°C)	T <sub>final</sub> (°C)	ΔT (°C)
1L/min (3')	22.98	25.20	2.22
2L/min (3')	22.72	23.25	0.53
3L/min (3')	22.73	24.00	1.27
4L/min (3')	22.74	23.59	0.85
1L/min (6')	22.98	25.47	2.49
2L/min (6')	22.72	23.37	0.65
3L/min (6')	22.73	24.16	1.43
4L/min (6')	22.74	23.62	0.88

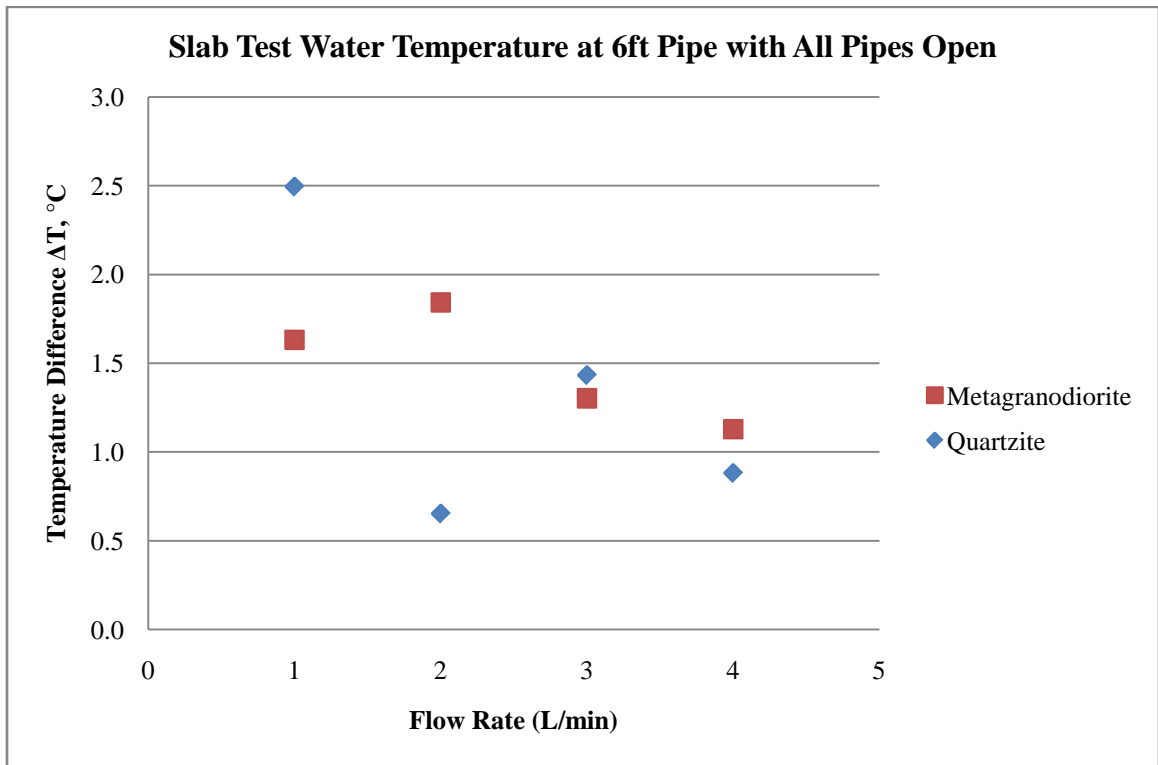


**Figure 9-10 Water temperature measured at 6ft pipe outlet for both slabs**

The results (Table 9-2 and Figure 9-10) indicated the beneficial effect of having heat exchangers with a large surface area exposed to the pavement for extraction of heat. A comparison between quartzite and metagranodiorite mix slabs showed that the temperature difference from the quartzite pavement was higher for flow rate of 1 and 3L/min, whereas the metagranodiorite slab showed higher temperature for the long pipe at 4 L/min.

The quartzite slab was then tested with four water flow rates with only one 3ft long copper pipe, and 1L/min for two 3ft long copper pipes to obtain the temperature



profile as well as effect of flow rate and copper pipe spacing (Table 9-3 to 9- 6, and Figure 9-11 to 9- 14).

**Table 9-3 Quartzite slab temperature profile with 1L/min (1 pipe)**

Time (min)	-0.11938m	-0.08636m	-0.03556m	-0.02286m	0m
0	37.23	40.38	50.15	50.95	50.64
10	37.46	37.11	46.85	49.47	49.69
20	36.76	36.88	48.56	49.24	48.27
30	36.30	36.06	47.64	47.87	48.52
35	37.50	37.48	48.68	48.79	47.73

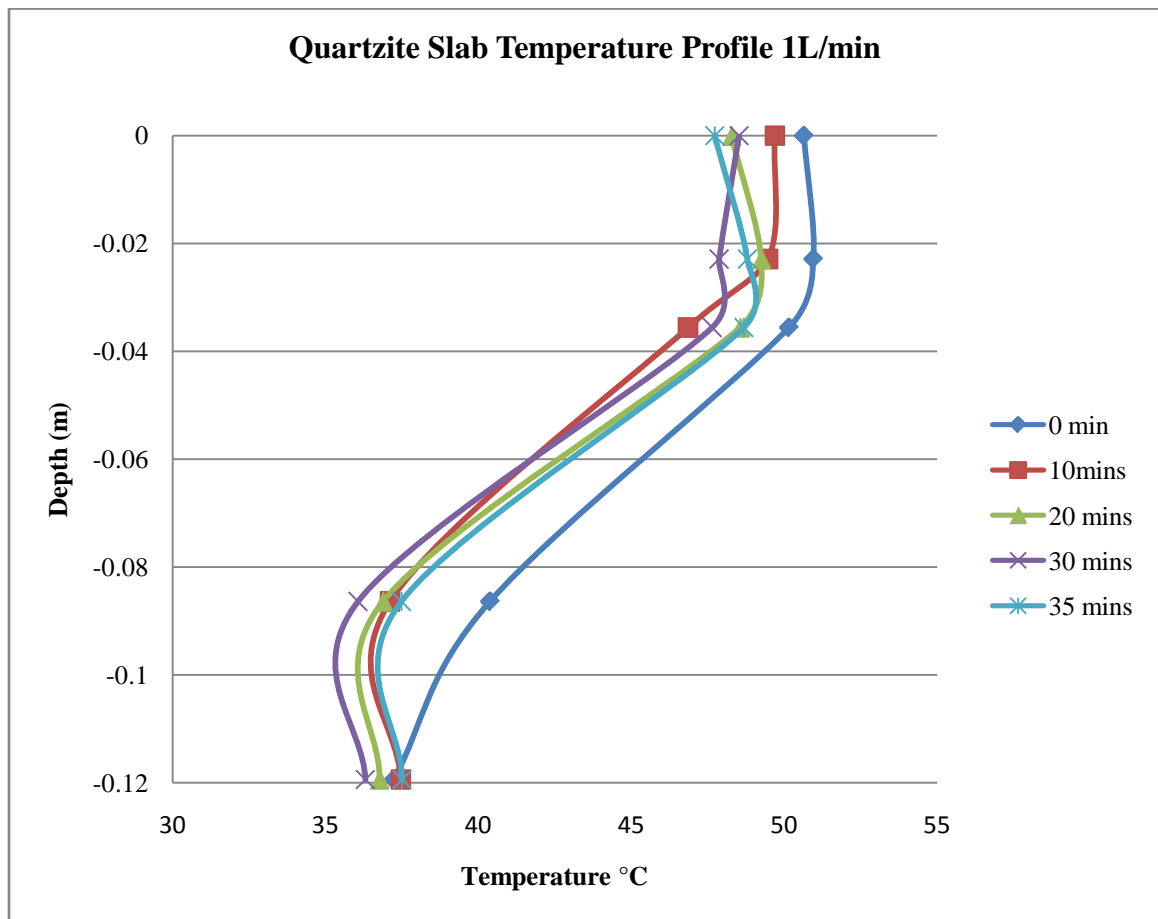


**Figure 8-11 Quartzite mix slab temperature profile (1L/min)**

**Table 9-4 Quartzite slab temperature profile with 2L/min (1 pipe)**

Time (min)	-0.11938m	-0.08636m	-0.03556m	-0.02286m	0m
0	37.50	37.48	48.68	48.79	47.73
10	36.22	35.86	46.41	47.20	47.39
20	36.31	35.25	46.39	46.50	47.25
30	35.86	34.91	45.94	46.17	47.39
35	36.36	35.05	46.19	46.30	46.46

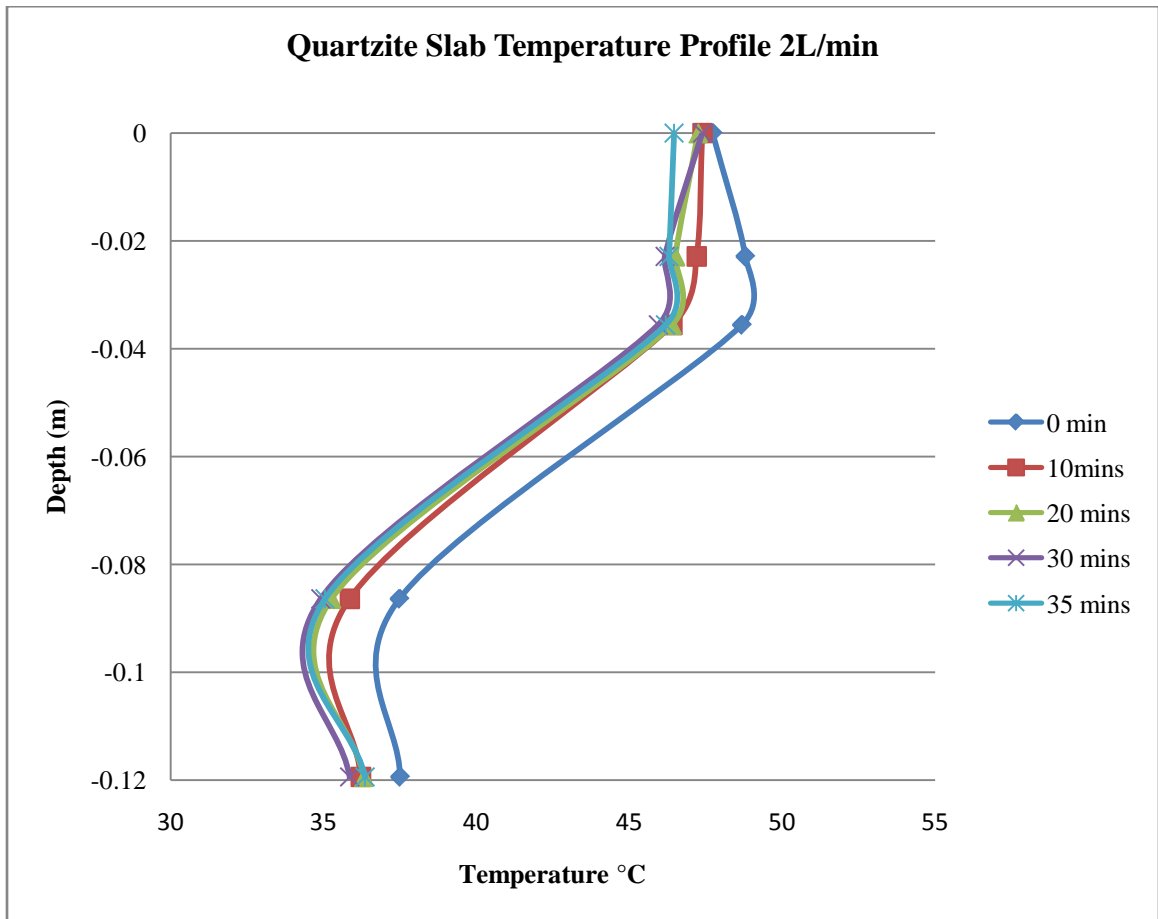


**Figure 9-12 Quartzite mix slab temperature profile (2L/min)**

**Table 9-5 Quartzite slab temperature profile with 3L/min (1 pipe)**

Time (min)	-0.11938m	-0.08636m	-0.03556m	-0.02286m	0m
0	36.36	35.05	46.19	46.30	46.46
10	36.17	34.85	45.53	45.64	45.09
20	35.95	34.41	44.41	45.20	45.36
30	35.84	33.71	44.30	43.94	44.06
36	35.99	33.97	43.98	44.09	44.82

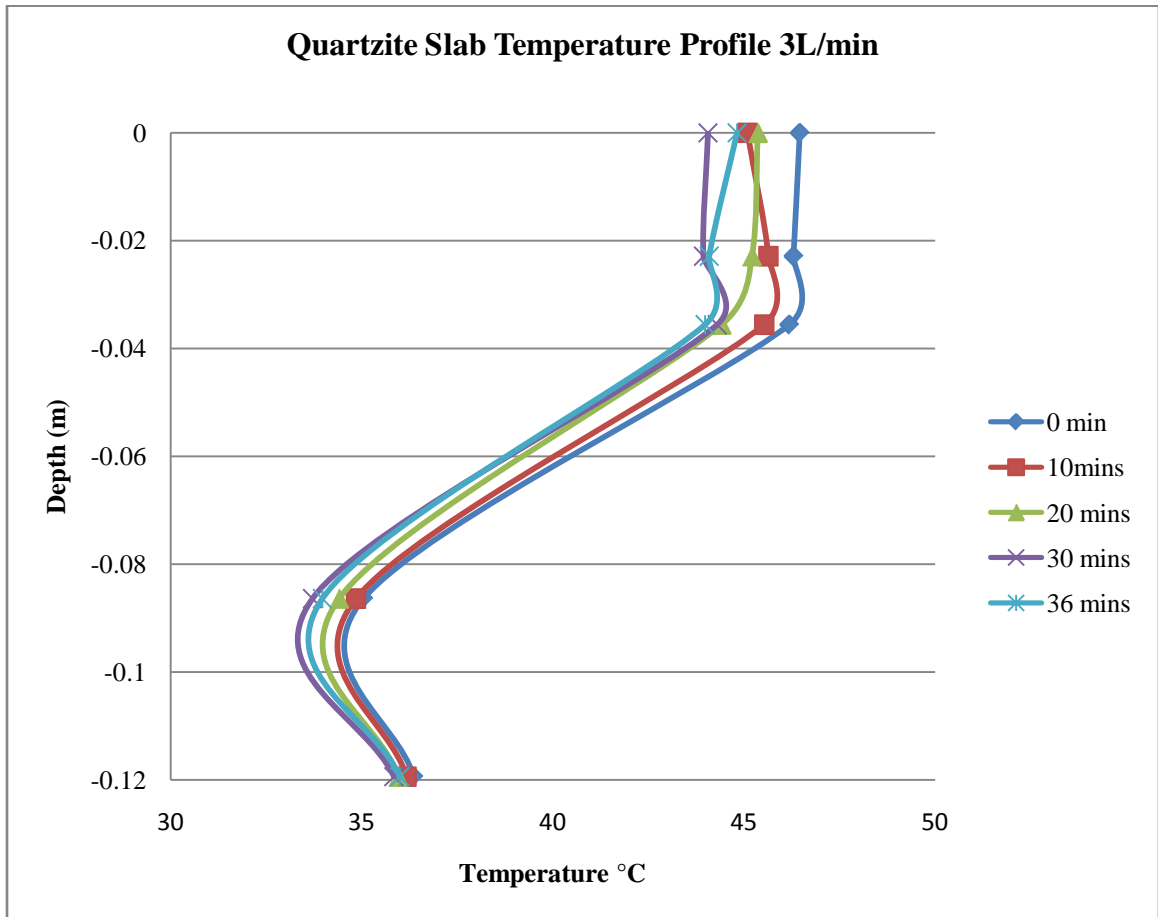


**Figure 9-13 Quartzite mix slab temperature profile (3L/min)**

**Table 9-6 Quartzite slab temperature profile with 4L/min (1 pipe)**

Time (min)	-0.11938m	-0.08636m	-0.03556m	-0.02286m	0m
0	35.30	33.86	43.87	43.98	44.82
5	35.46	33.54	42.98	43.77	44.49
10	35.24	33.21	42.76	42.867	43.08
15	34.93	32.99	42.44	42.66	42.17

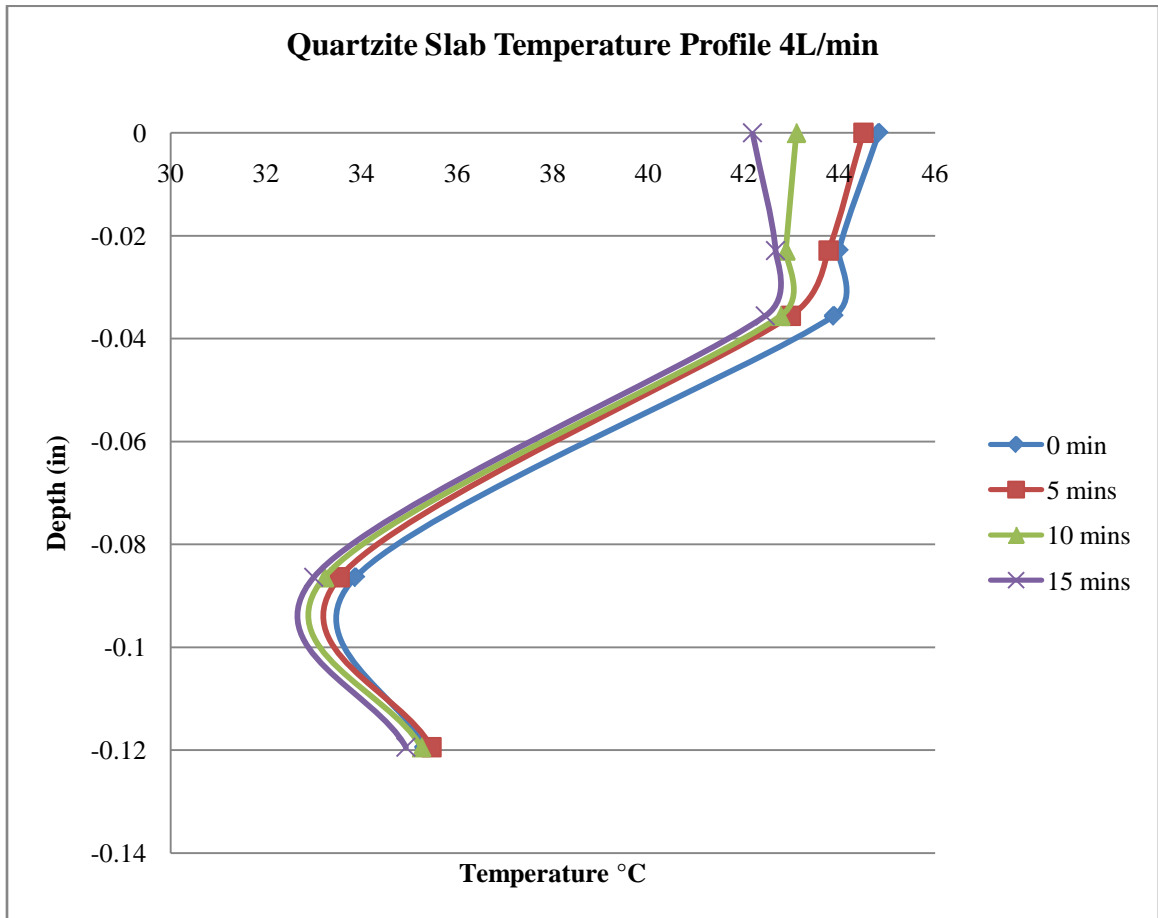


**Figure 9-14 Quartzite mix slab temperature profile (4L/min)**

The results showed that the temperature at each thermocouple location was not noticeably reduced when the water flow rate increased. However, the higher temperature variation occurred when the water flow rate decreased. This indicated that the overall heat transfer coefficient of the water was increased when the flow rate decreased, and heat transfer coefficient was decreased when the flow rate increased.

**Table 9-7 Quartzite slab temperature profile with 1L/min (2 pipes open)**

Time (min)	-0.11938m	-0.08636m	-0.03556m	-0.02286m	0m
0	35.30	32.97	40.20	39.62	37.30
10	34.66	33.40	38.28	37.70	35.87
20	34.37	32.89	36.52	35.93	34.78
30	34.37	32.80	35.83	35.25	33.99
38	34.28	32.81	35.26	34.67	33.41

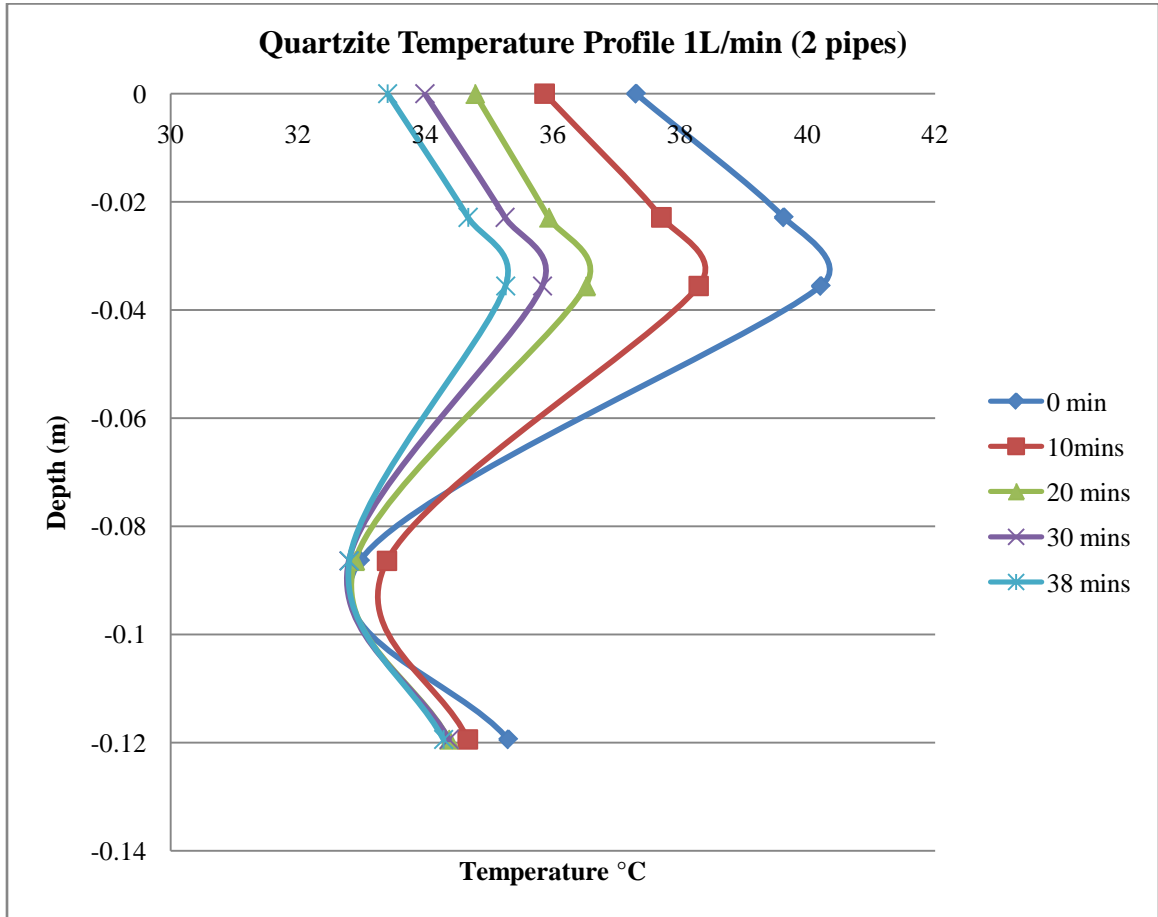


**Figure 9-15 Quartzite mix slab temperature profile (1L/min at 2 3ft pipes)**

The Table 9-7 and Figure 9-15 showed that the temperature was 5°C lower when another copper pipe (1.5ft apart) was also flowing the water. The two copper pipes with 1L/min water flow rate significantly reduced the overall temperature of the quartzite slab. The Figure 9-16 and 9-17 indicated that the temperature gradient along length (6ft) while two copper pipe were running 1L/min water. The temperature was 10°C lower between two open copper pipes compared to one without opening.

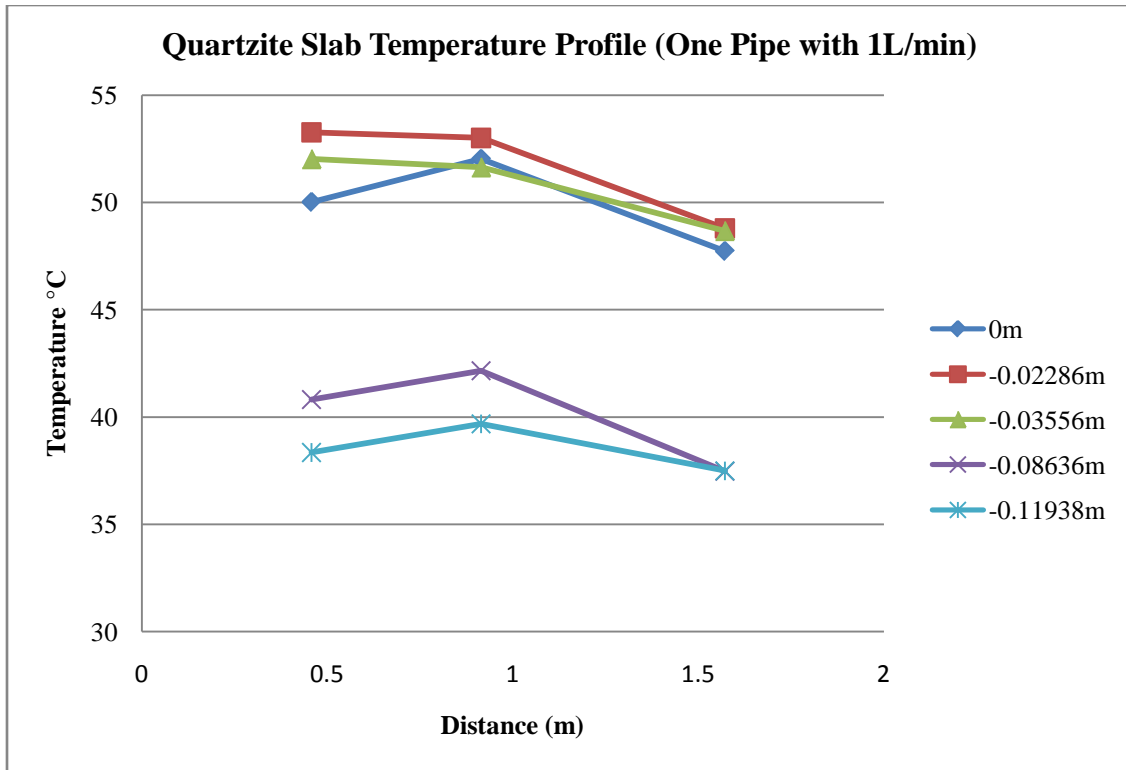


**Figure 9-16 Quartzite slab temperature profile (1 pipe with 1L/min)**

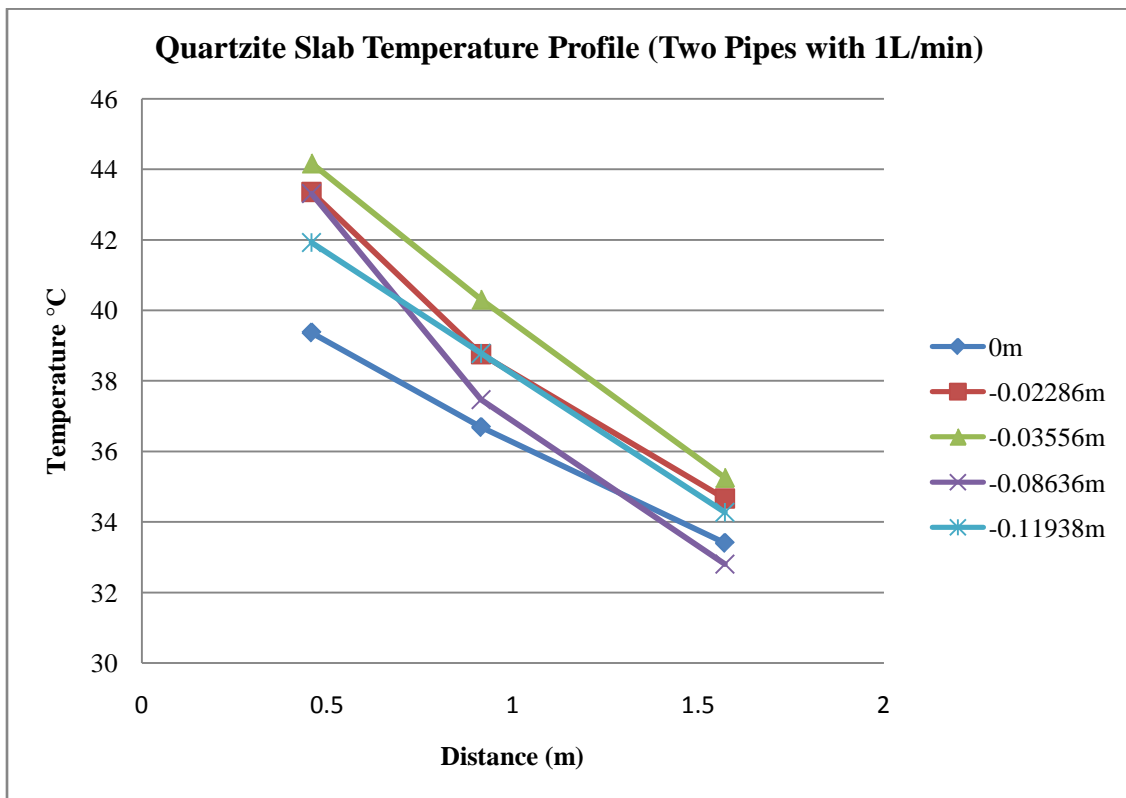


**Figure 9-17 Quartzite slab temperature profile (2 pipes with 1L/min)**

## 8.5 Finite Element Analysis/Modeling

The first set of finite element model was to determine the thermal conductivity and heat capacity based on the actual environmental conditions such as solar radiation and wind speed. The initial conditions were used as same as field testing of quartzite and metagranodiorite (Wrentham) slab. The solar radiation can be expressed as polynomial equation (Figure 9-18) and the average wind speed was 2.27m/s. The mesh size of the both models was 50,768 elements (Figure 9-19) and each slab was sectioned into 12 initial temperature zones to represent the initial thermocouple readings (Figure 9-20).

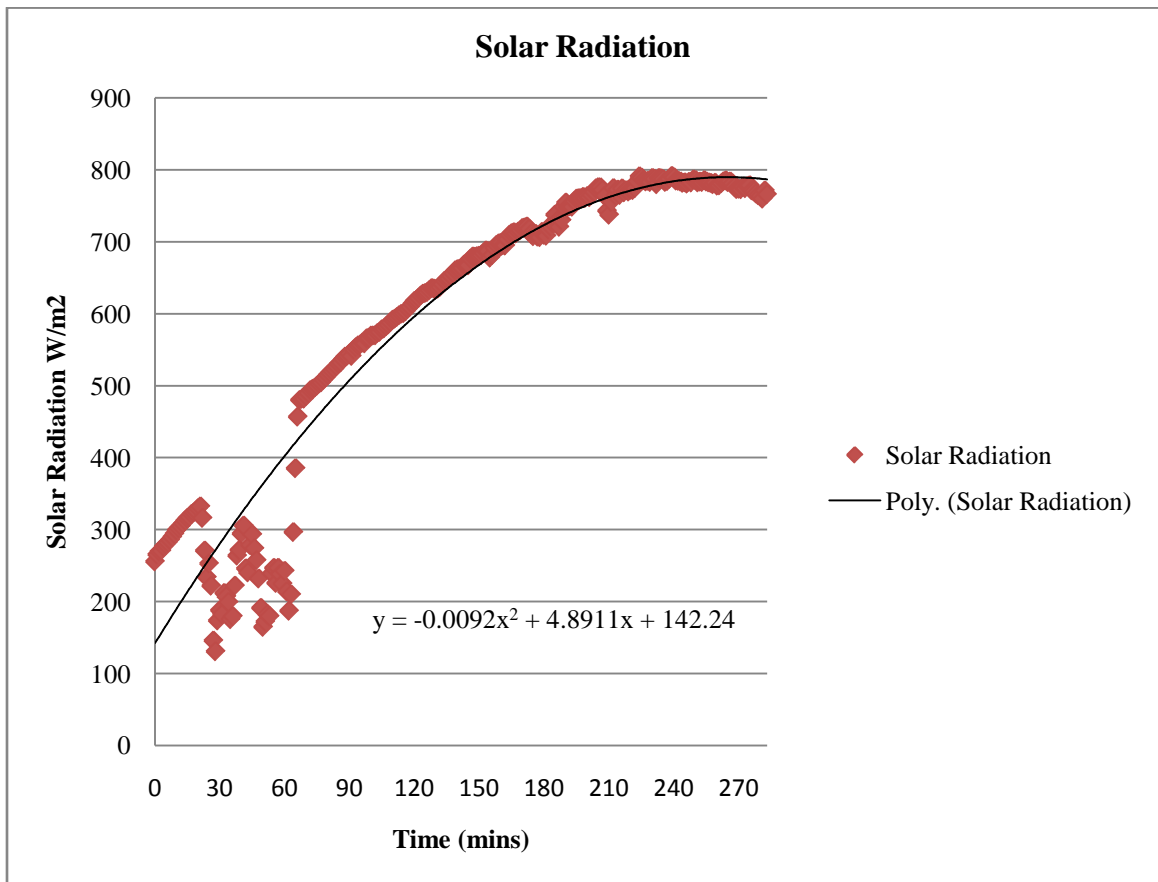
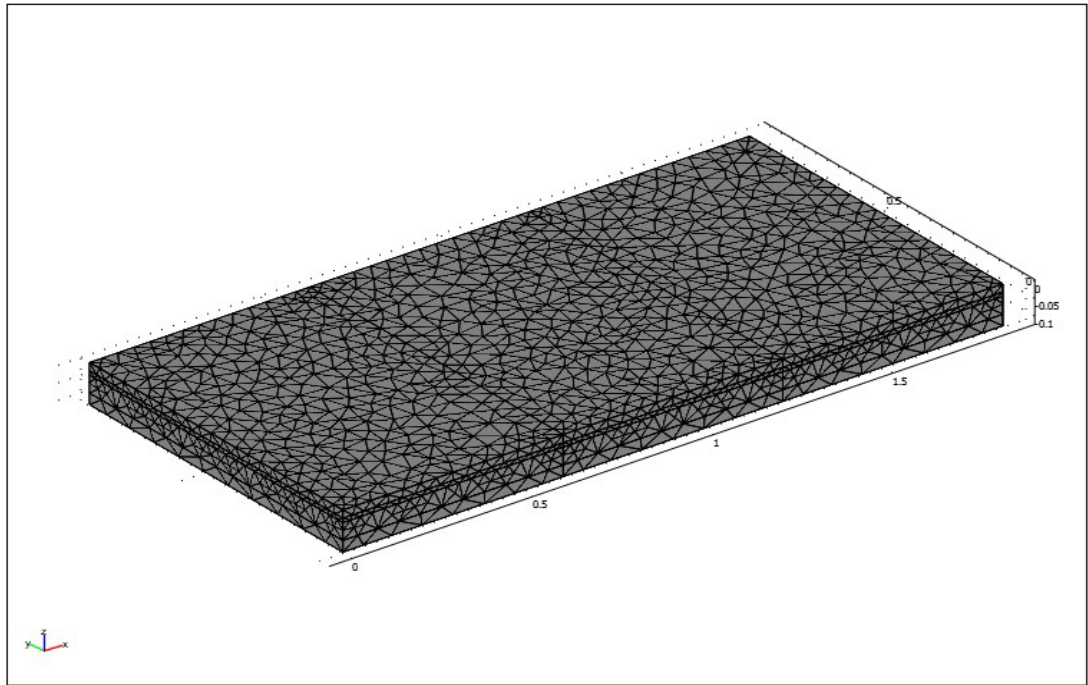
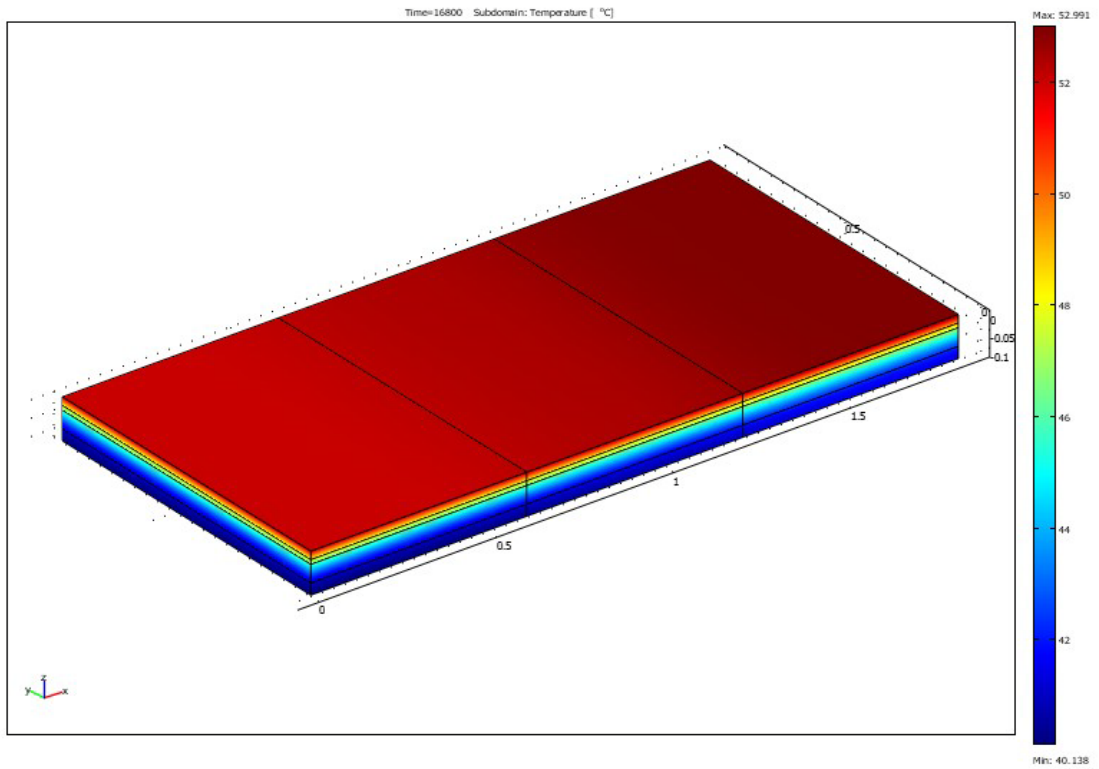


Figure 8-18 Solar Radiation



**Figure 9-19 Finite element mesh model**



**Figure 9-20 Finite element model of heating period**



**Table 9-8 Thermal conductivity and heat capacity of two slab mixes**

	Metagranodiorite	Quartzite
Thermal Conductivity (k)	1.2	1.8
Heat Capacity (Q)	800	1050

The Figure 9-21 showed the experiment data and finite element model final temperature at one section of the quartzite slab. The thermal properties of metagranodiorite (Wrentham) and quartzite mix were back-calculated as shown in Table 9-8.

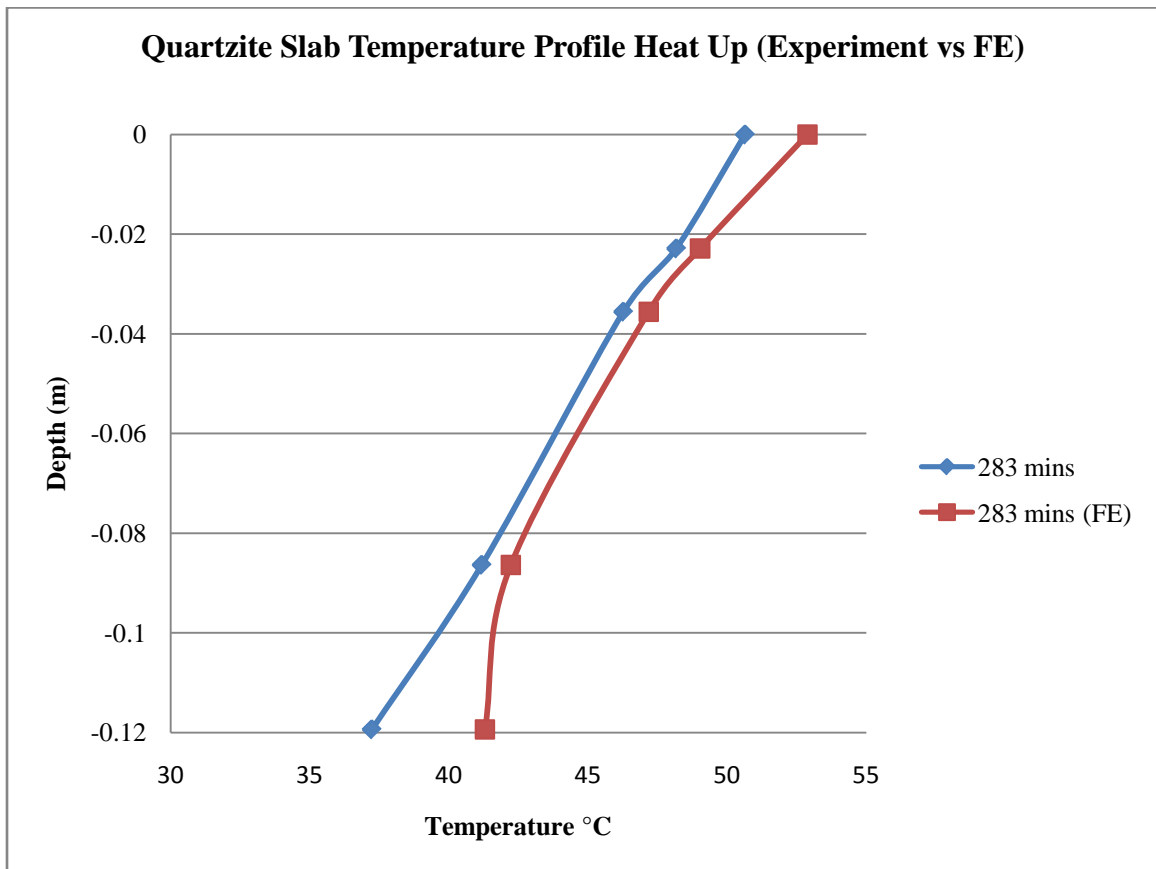


**Figure 9-21 Quartzite slab temperature profile of heat-up period**

The second set of finite element model was to determine the temperature distribution of quartzite slab and water inside the copper pipe. The temperature of experiment data at 283 minutes was used as initial temperature for simulating water flow conduction (Figure 9-22) and the mesh size consisted of 58,937 elements (Figure 9-23).

The Figure 9-24 and 9-25 showed temperature distribution of 1L/min water flow

rate and also showed that the temperature was fluctuated due to the uniform wall temperature and heat flux.

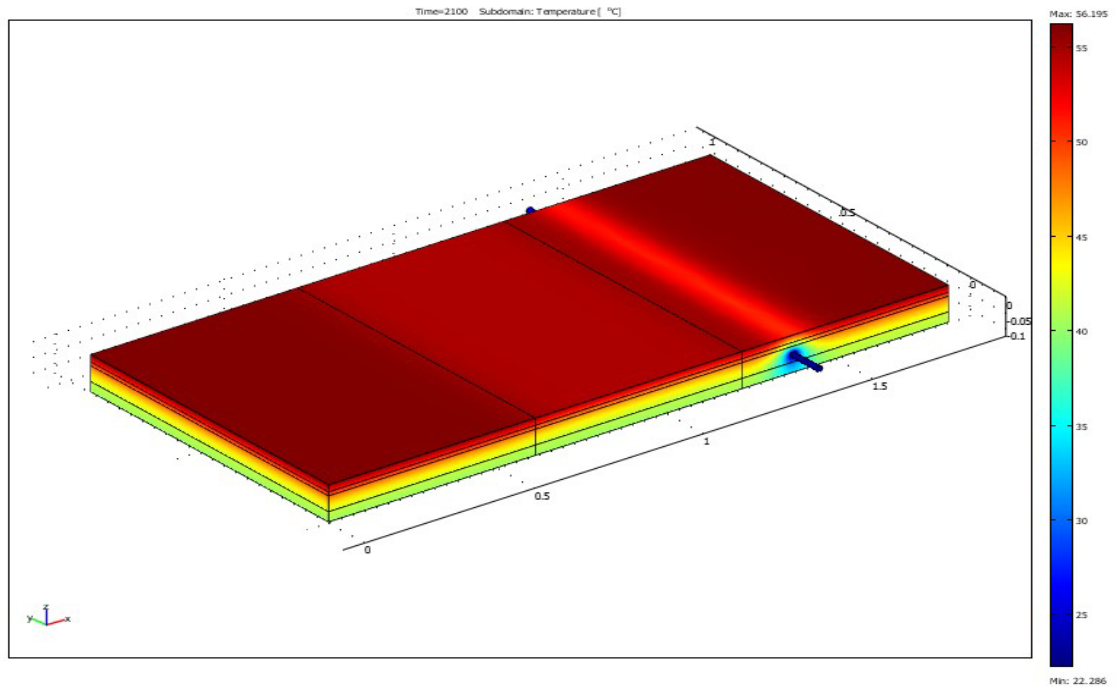


**Figure 9-22 Finite element model with various water flow rates**

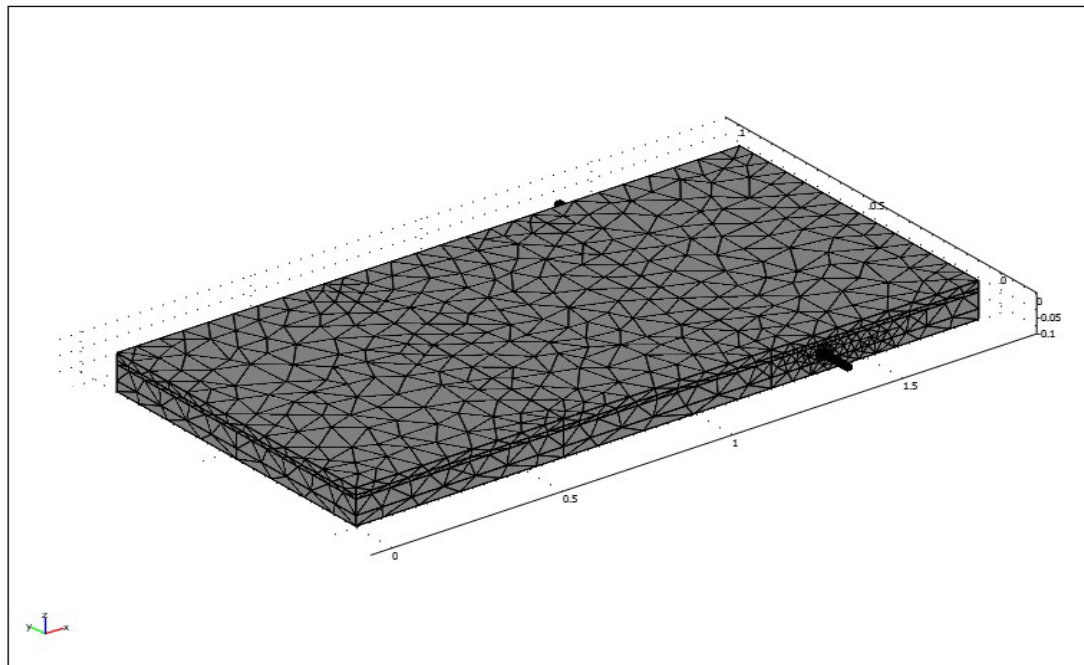


**Figure 9-23 Finite element mesh model**

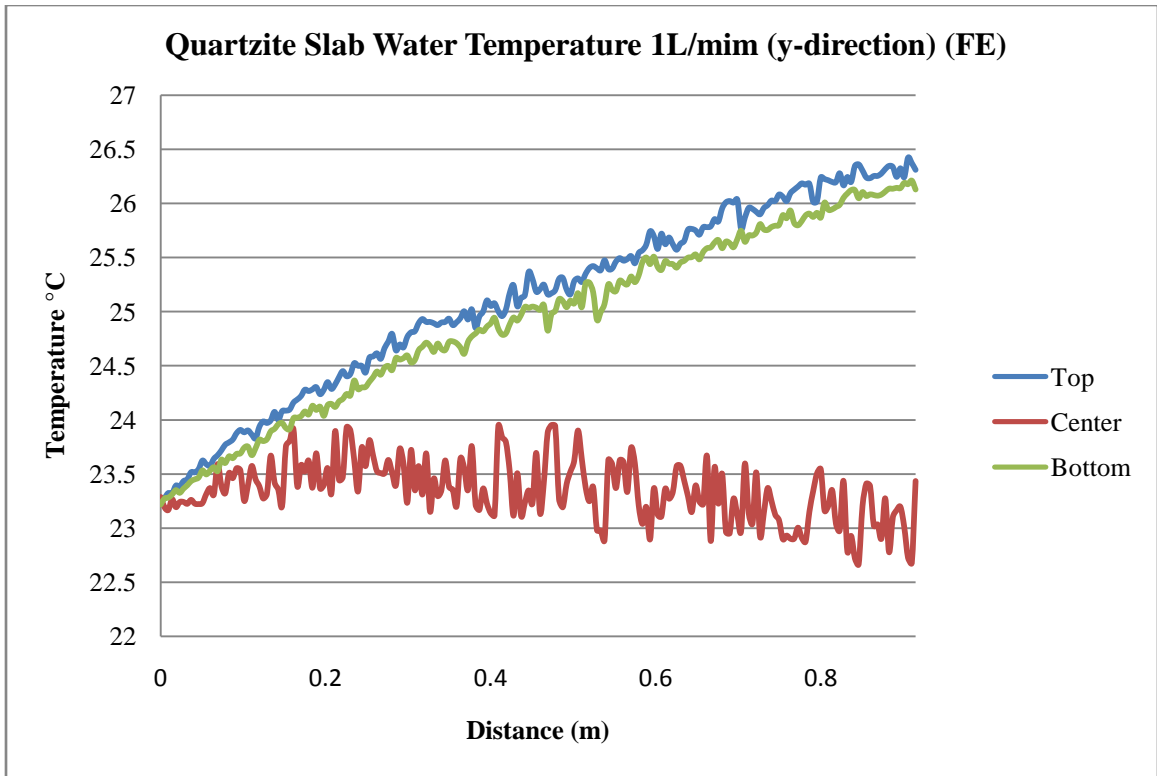


**Figure 9-24 Water temperature distribution along the length of copper pipe**

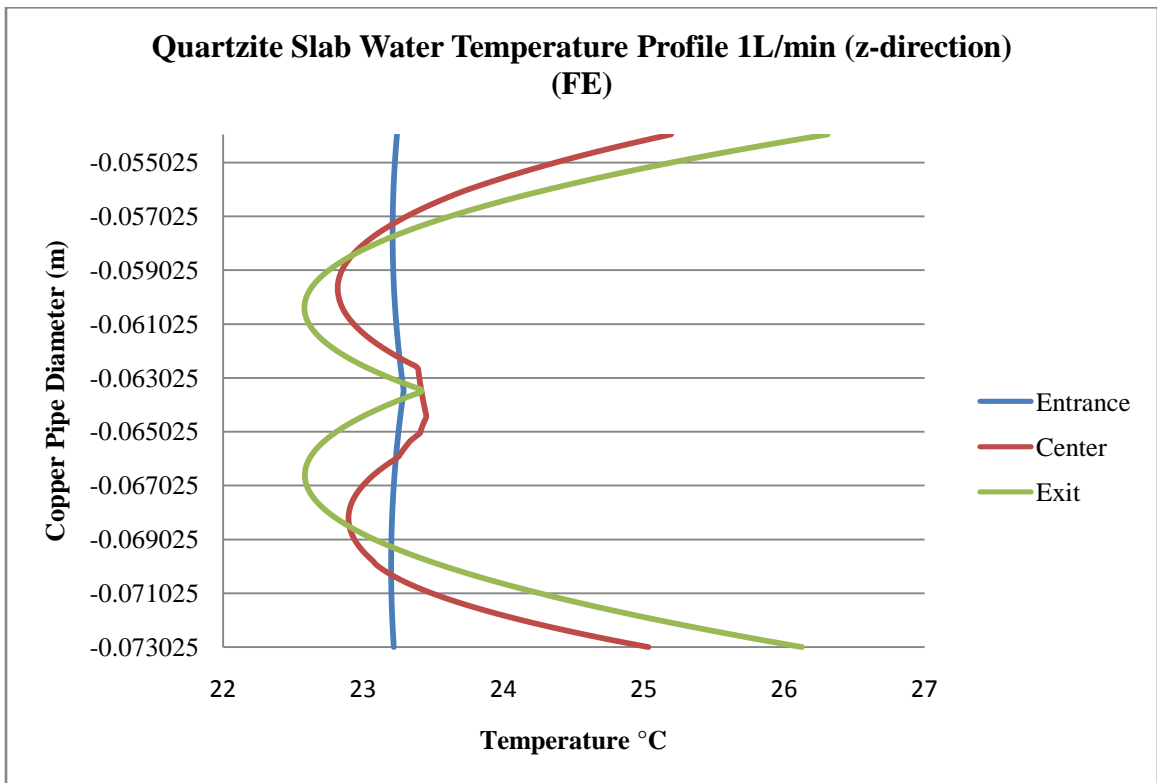


**Figure 9-25 Water temperature distribution along the depth of copper pipe**

The thermal conductivity and heat capacity of quartzite slab were used for modeling water flowing through one copper pipe at rate of 1, 2, 3, and 4L/min, and to determine the water outlet temperature and temperature profile. The Table 9-9 to 9-13, and, Figure 9-26 to 29 showed the temperature profile at the mid-section of the slab.

**Table 9-9 Quartzite slab 1L/min (35mins)**

	Quartzite Slab 1L/min (35mins)		
	T <sub>initial</sub> (°C)	T <sub>final</sub> (°C)	ΔT (°C)
LAB	23.2	30.17	6.97
FE	23.2	25.29	2.09

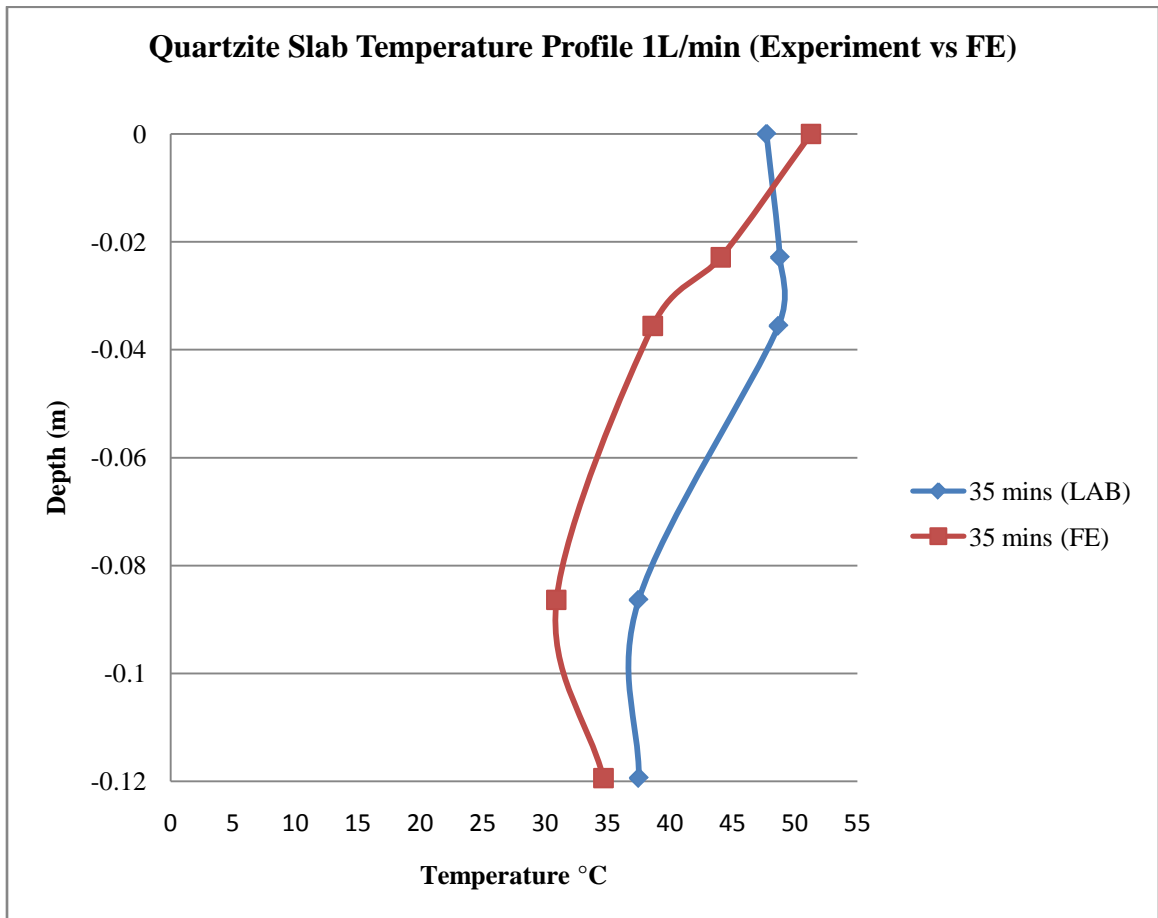


**Figure 9-26 Quartzite slab temperature profile 1L/min (laboratory vs. finite element analysis)**

**Table 9-10 Quartzite slab 2L/min (35mins)**

Quartzite Slab 2L/min (35mins)			
	T <sub>initial</sub> (°C)	T <sub>final</sub> (°C)	ΔT (°C)
LAB	24.2	28.54	4.34
FE	24.2	26	1.80

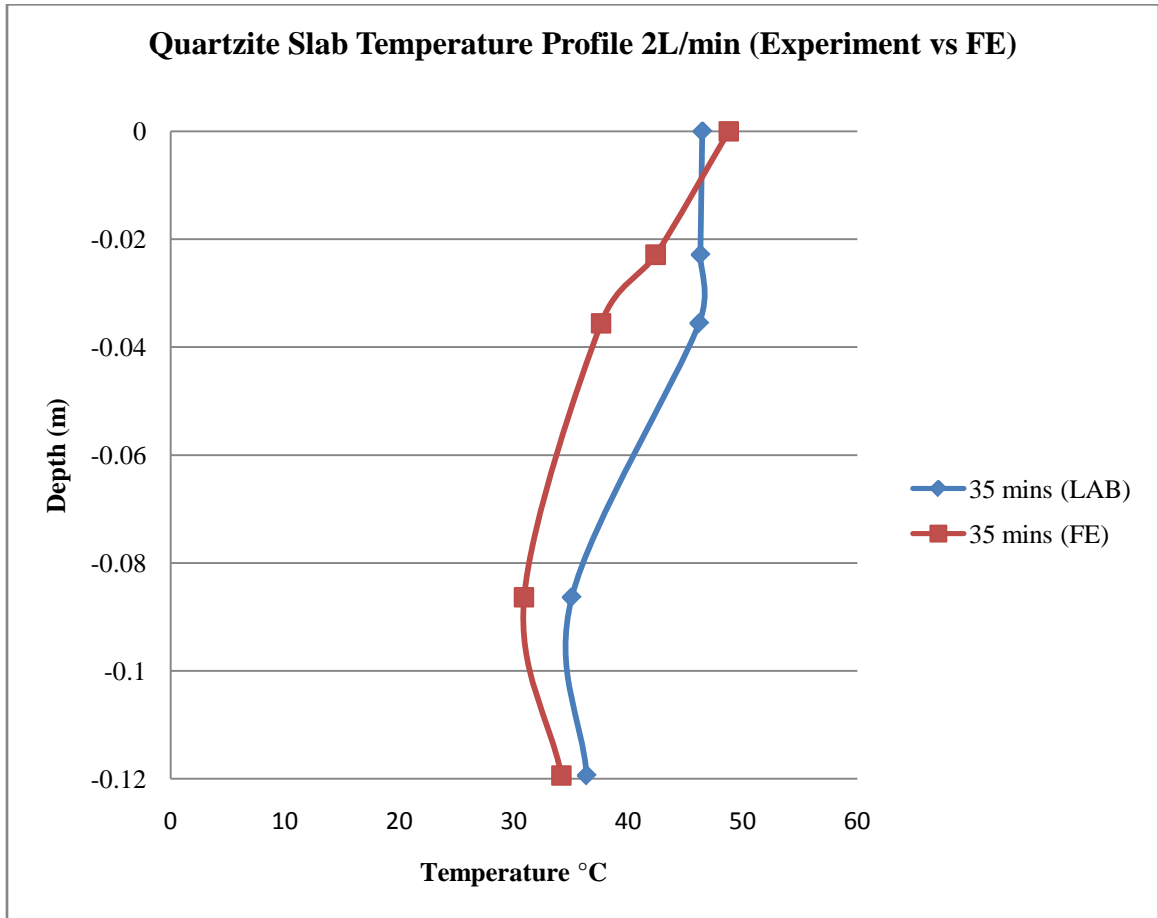


**Figure 9-27 Quartzite slab temperature profile 2L/min (laboratory vs. finite element analysis)**

**Table 9-11 Quartzite slab 3L/min (36mins)**

Quartzite Slab 3L/min (36mins)			
	T <sub>initial</sub> (°C)	T <sub>final</sub> (°C)	ΔT (°C)
LAB	23.2	25.32	2.12
FE	23.2	24.84	1.64

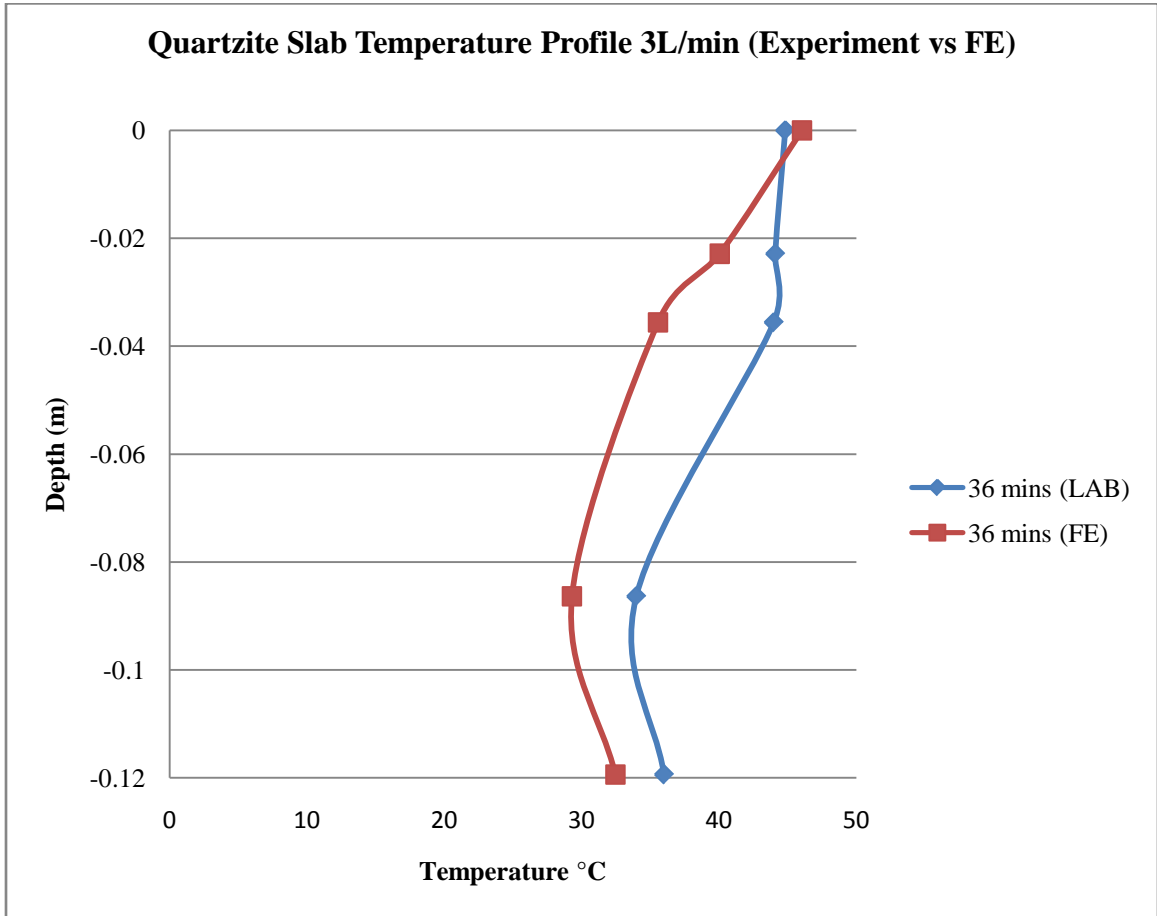


**Figure 99-28 Quartzite slab temperature profile 3 L/min (laboratory vs. finite element analysis)**

**Table 9-12 Quartzite slab 4L/min (15mins)**

	Quartzite Slab 4L/min (15mins)		
	T <sub>initial</sub> (°C)	T <sub>final</sub> (°C)	ΔT (°C)
LAB	22.10	23.23	1.13
FE	22.1	23.52	1.42

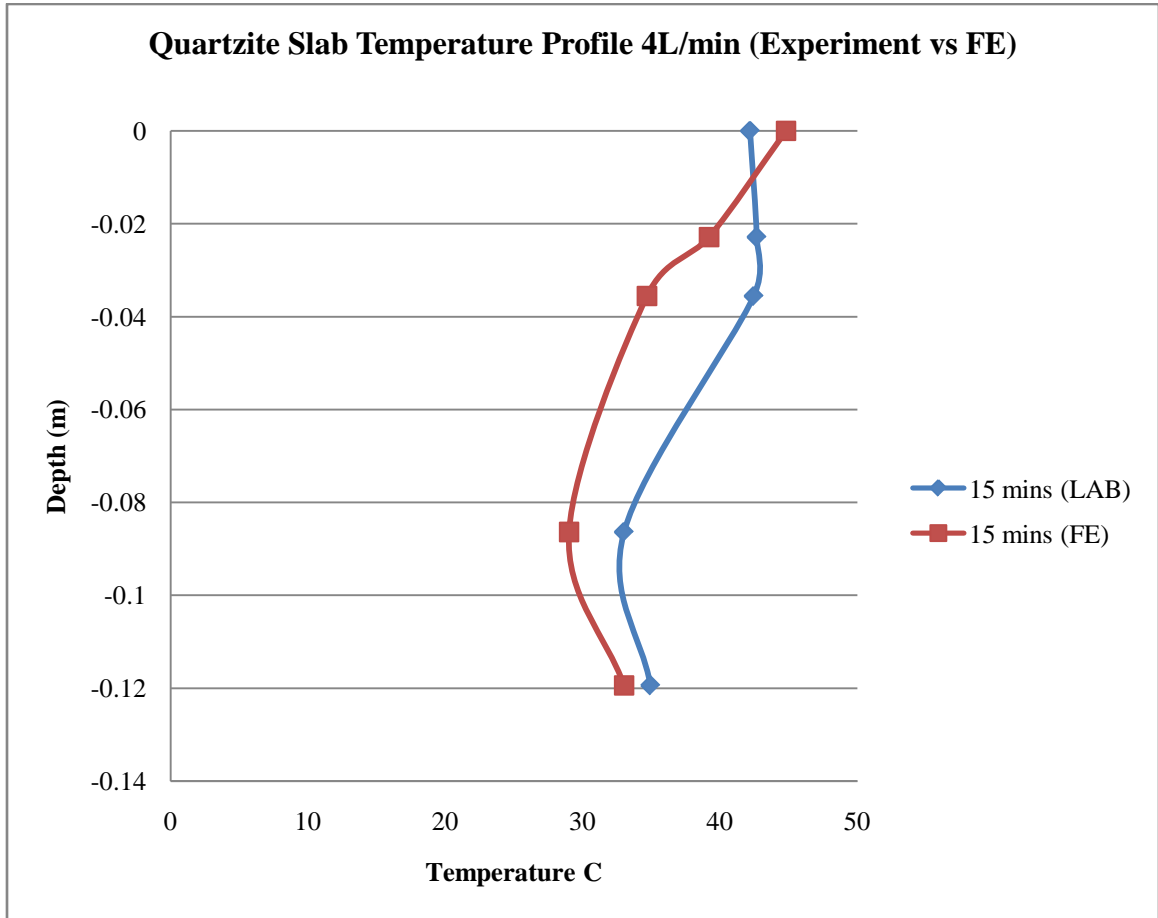


**Figure 9-29 Quartzite slab temperature profile 4L/min (laboratory vs. finite element analysis)**

The temperature profile was not varied significantly at copper pipe location (0.0381m) when the water flow rate increased for both field experiment and finite element analysis. The water temperature of field experiment at 1 and 2L/min flow rates were much higher than finite element analysis (Figure 9-30). This were due to different location of water temperature measurement, for example, the field experiment measured water temperature at one location (outlet) inside of copper pipe, and finite element analysis integrated temperature at water outlet (exit boundary).

In addition, the quartzite slab was assumed as homogenous material to have same thermal conductivity and heat capacity in finite element analysis. However, the quartzite slab was consisted of aggregate and asphalt binder, which had different thermal properties, would affect the overall heat transfer rate between the asphalt mix and water.

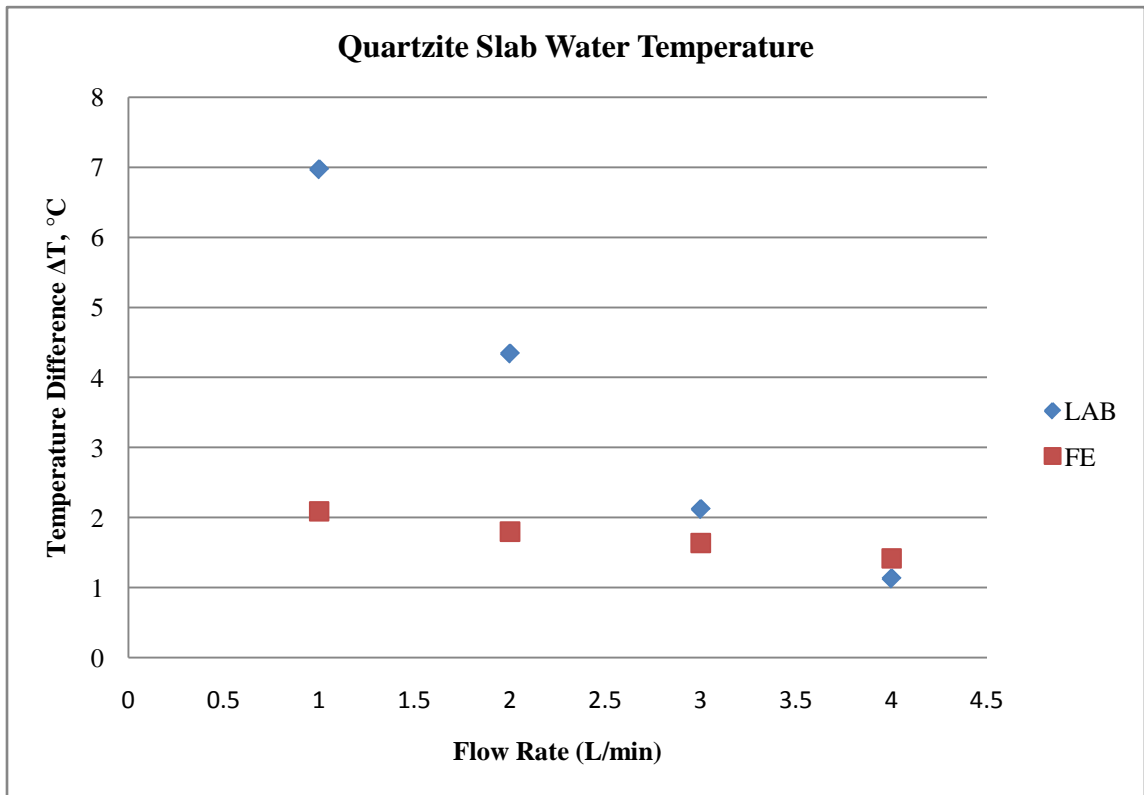


**Figure 9-30 Quartzite slab water temperature at various water flow rate (labortory vs. finite element analysis)**



## 9.6 Discussion

The experiment results of all pipes open for 3ft and 6ft directions showed that the quartzite slab yielded higher water temperature at lower water flow rate. However, metagranodiorite was higher at higher flow rate, this could be due to the sensitivity of thermocouple measurement.

The experimnt results showed that the surface temperature of quartzite slabs could be reduced as much as 5°C for one pipe flowing water, and 10°C for two pipes flowing water. This was the evidence that showed the effect of flowing water underneath of higher conductive asphalt pavement to decrease pavement temperature and reduce Heat-Island Effect.

The water outlet temperature of quartzite slab with one pipe open was greater than metagranodiotite at flow rate 1L/min. The temperature differences for two slabs were not stable for the flow rate 2L, 3L, and 4L/min. This could be due to insufficient thermal isolation around the copper pipes and resulting in external heating during the experimnt.

Another reason could be the inaccurately measuring the water flow rates because the measurement were taken by using measuing cup at the water outlet, which could be resulting in inconsistent water flow rates.

The water temperature distribution from finite element analysis showed that the water temperature at the centerline was not reach to the bounday (wall) temperature, this was the indication of insufficient pipe length.

## CHAPTER 10

### CONCLUSION

Based on the results of this study, the following conclusions and recommendations can be made:

1. Temperature profiles along the depth of pavements with different structures/subsurface layers are different.
2. Predictive equations for both maximum subsurface and base temperature for pavements with different base layers have significantly different coefficients.
3. Back-calculated thermal conductivity and heat capacity values for similar materials but placed with different densities and gradations and with different base layers are different.
4. Thermal conductivity values of surface+binder HMA range from 1.0 to 1.8 W/m·K, whereas the heat capacity range from 1,100 to 1,800 J/kg·K. For the base materials, for the HMA materials, thermal conductivity ranges from 1.1 to 1.8 W/m·K, whereas those for the other materials range from 1.3 to 1.5 W/m·K. For heat capacity, the values range from 1,200 to 1,400 J/kg·K for the HMA materials, and from 1,200 to 1,800 J/kg·K for the other materials.
5. As needed one can either use ASTM E1952 or determine thermal properties of different layers from in-place data. An alternative option is to test full depth pavement samples under controlled conditions in the laboratory and use finite element analysis to back-calculate the thermal properties of the different layer.
6. Validation of temperature predicted through the use of laboratory obtained thermal properties should be made with the help of in-place data.
7. The use of a higher conductivity aggregate, such as quartzite (1.8W/m·K), can enhance the heat transfer efficiency to a significantly higher degree.
8. To increase heat transfer, the use of a higher conductive aggregate is most likely a much better alternative to using commercial high conductivity additives (e.g. copper powder) because of practical concerns.
9. The use of a reflectivity decreasing/absorptivity increasing paint on the surface of the pavement can enhance the heat transfer efficiency.

10. The depth of heat exchanger is critical and an effective heat exchanger design will be the key in extracting maximum heat from the pavement. Better contact between the pipe and the pavement mix would lead to improved efficiency of heat transfer.
11. The amount of heat that can be extracted depends on the surface area of the pipes carrying the fluid.
12. Serpentine pipes can be used to improve the efficiency of heat transfer by providing larger surface area.
13. It is possible to lower the maximum of 13.5° C of the asphalt pavements surface temperature by flowing water underneath the pavement.
14. The reduction in temperature is affected by the type of conductivity of the mix – higher the conductivity, higher is the reduction temperature.
15. The process of reduction in temperature can be optimized by the maximum extraction of heat from the pavement through a fluid.

## CHAPTER 11

### FUTURE STUDY RECOMMENDATION

In the future, the study of this research should carry out both analytical and experimental investigate on: 1.What is the effect of the outlet water temperature by using different piping materials and working fluids? 2. How to increase the water temperature to meet the minimum efficient requirement of turbine for it to generate electricity? 3. How much pavement life can be extended by using asphalt pavement as solar collector?

#### **11.1 What is the effect of the outlet water temperature by using different piping materials and working fluids?**

The material of the heat exchanger system (which consists of pipes) should have a high conductivity and the layout should be such as to allow the exposure of the pipes to the pavement for sufficient length to allow the fluid to reach the maximum temperature achievable in the system. Copper material has higher thermal conductivity but it usually more costly, therefore, the study should selecte other alternative piping materials, for example, graphite, iron, and PVC pipe to see the effect of replacing copper materials.

The working fluid inside the pipe should be such that it can be pumped easily and can absorb the energy quickly (low heat capacity) such as Butane (gaseous fluid). In applications where vaporization of the fluid is required, the fluid should ideally have a low boiling point.

#### **11.2 How to increase the water temperature to meet the minimum temperature requirement of turbine to generate electricity?**

The pavement temperature depends on the location of the pavement, the pavement temperature in Worcester MA area normally is 50°C during the summer time and it will be approximately 70°C in Houston area. The Rankin-Cycle turbine engine, for example, requires the minimum of 70°C water temperature in order to operate at minimum efficiency. Therefore, it is always possible to use a secondary non-energy consuming technology, such as a solar concentrator or a water heating reservoir to increase the temperature from the maximum temperature in the pavement to the minimum temperature required for the end use.

### **11.3 How much pavement life can be extended by using asphalt pavement as solar collector?**

The NCHRP 1-37A Mechanistic Empirical Pavement Design (MEPDS, commonly referred to as the Design Guide 2002, or DG2002) software is a Windows-based application for the simulation of pavement structures. It can be used to simulate pavement structures under different traffic and climatic conditions. The software has the ability to predict the amount of damage that a structure will display at the end of its simulated design life. In addition to using laboratory test results, predicting properties for pavement mixes can be done by using correlations. Values (either default or entered by the user) that represent structural, climatic, or traffic properties are used in calculating distresses.

The software can be used for predicting the rutting damage over different years, considering the usual pavement temperature, and then a range of temperatures that are lower than the usual temperature. To do this, the weather database in the MEPDS can be utilized. For this example, Houston was selected to consider a range of maximum pavement temperatures, from 70 to 52°C. A pavement located in Houston was simulated, using the climatic information to determine the rutting damage over the years, and the years to failure, for the range of temperatures (70 to 52°C).

The results are shown in Figure 11-1. It can be seen, that for the same traffic and the same materials, the life of the pavement can be extended by 5 years for a drop of temperature of 5°C. The drop in temperature is more effective in extending the life of the pavement at higher temperatures.

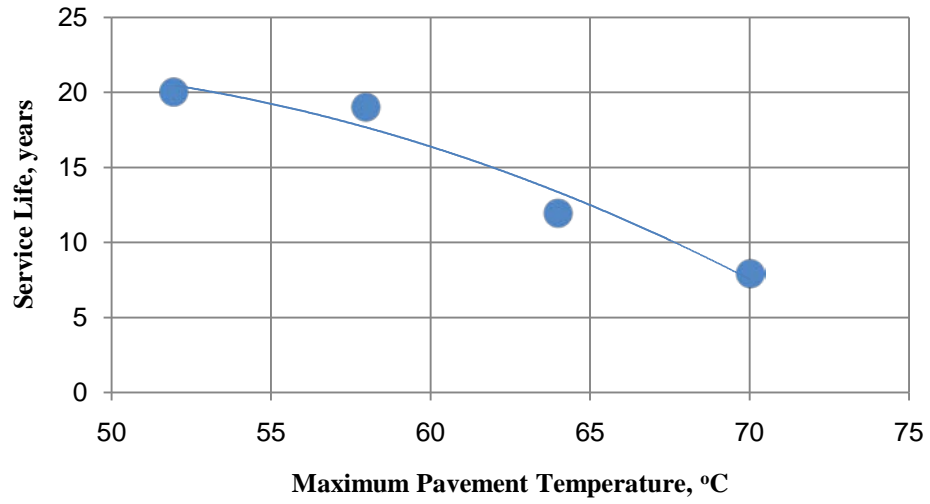


**Figure 11-1 Extended service life of pavement by reducing pavement temperature**

## **CHAPTER 12**

### **REFERENCES**

1. Southgate, H.F. and Deen, R.C. “Temperature Distribution within Asphalt Pavements and its Relationship to Pavement Deflection.” Transportation Research Record 291, Transportation Research Board, National Research Council, Washington, DC, 1969.
2. Hermansson, Ake. “Simulation Model for Calculating Pavement Temperatures Including Maximum Temperature.” Transportation Research Record, No. 1699, Transportation Research Board, National Research Council, Washington, DC, 2000.
3. Park, Donh-Yeob, Buch, Neeraj, Chatti Karim. “Effective Layer Temperature Prediction Model and Temperature Correction via Falling Weight Deflectometer Deflections.” Transportation Research Record, No. 1764, Transportation Research Board, National Research Council, Washington, DC, 2001.
4. Yavuzturk, C. K., Ksaibati, Chiasson, A.D., “Assessment of Temperature Fluctuations in Asphalt Pavements Due to thermal Environment Conditions Using a Two Dimensional, Transient Finite-Difference Approach.” Journal of Materials in Civil Engineering, ASCE Volume 17, Issue 4, July/August 2005.
5. Solaimanian, M. and Kennedy, T.W. “Predicting Maximum Pavement Surface Temperature Using Maximum Air Temperature and Hourly Solar Radiation.” Transportation Research Record, No. 1417, Transportation Research Board, National Research Council, Washington, DC, 1993.
6. Huber, G. A “Strategic Highway Research Program Report SHRP 648A: Weather Database for the Superpave Mix Design System.” Transportation Research Board, National Research Council, Washington, DC, 1994.
7. Solaimanian, M. and Bolzan, P. “Strategic Highway Research Program Report SHRP –A-637: Analysis of the Integrated Model of Climate Effects on Pavements.” Transportation Research Board, National Research Council, Washington, DC, 1993.

8. Donald E. Watson, Jingna Zhang, and Powell Buzz, "Analysis of Temperature Data for the NCAT Test Track." Transportation Research Record, No. 1891, Transportation Research Board, National Research Council, Washington, DC, 2004.
9. Diefenderfer, K. Brian, Al-Qadi, Imad L. and Stacey, D. "Model to Predict Pavement Temperature Profile." The Journal of Transportation Engineering, ASCE, Vol. 132, No. 2, February 1, 2006.
10. Mrawira, Donath and Luca, Joseph, "Thermal Properties and Transient Temperature Response of Full-Depth Asphalt Pavements." Transportation Research Record, No. 1809, Transportation Research Board, National Research Council, Washington, DC, 2002.
11. Luca, Joseph and Mrawira, Donath "Solar-Convection Simulator for Laboratory Investigation of Transient Temperature Fluctuations in HMAC Pavements." 83<sup>rd</sup> Annual Meeting of the Transportation Research Board, Washington, DC, 2004.
12. Luca, Joseph and Mrawira, Donath "New Measurement of thermal Properties of Superpave Asphalt Concrete." Journal of Materials in Civil Engineering ASCE Volume 17, Issue 1, (January/February 2005).
13. Bijsterveld, W. T. van, Houben, Scarpas, A. and Molenaar, A. A. A. „Effect of Using Pavement as Solar Collector on Pavement Temperature and Structural Response." Journal of The Transportation Research Record, No No. 1778, Transportation Research Board, National Research Council, Washington, DC 2001
14. Hasebel M., Kamikawa Y. and Meiarashi S. "Thermoelectric Generators using Solar Thermal Energy in Heated Road Pavement." 2006 International Conference on Thermoelectrics, IEEE.
15. The United States Environmental Protection Agency, "Heat Island Effect", <http://www.epa.gov/hiri/>
16. Martina Soderlund, Stephen T. Muench, Kim A. Willoughby, Jeffrey S. Uhlmeyer, Jim Weston, "Green Roads: A Sustainability Rating System for Roadways" Transportation Research Board 87th Annual Meeting, 2008



17. Mark Belshe, Kamil E. Kaloush, Jay S. Golden, Michael S. Mamlouk, Patrick Phelan, "Asphalt-Rubber Asphalt Concrete Friction Course Overlays as Pavement Preservation Strategy for Portland Cement Concrete Pavement" Transportation Research Board 86th Annual Meeting, 2007
18. Gui, Jooseng Gavin, Phelan, Patrick E., Kaloush, Kamil E. and Golden, Jay S. "Impact of Pavement Thermophysical Properties on Surface Temperatures." Journal of Materials in Civil Engineering, Vol. 19, No. 8, August 1, 2007
19. Kanok Boriboonsomsin, Farhad Reza, "Mix Design and Benefit Evaluation of High Solar Reflectance Concrete for Pavements" Transportation Research Record: Journal of the Transportation Research Board No. 2011. 2007.
20. Frank W. Schmidt, Robert E. Henderson, Carl H. Wolgemuth "Introduction to Thermal Sciences: Thermodynamics, Fluid Dynamics, Heat Transfer." John Wiley & Sons, 1993.
21. J. E. Vehrencamp, "Experimental Investigation of Heat Transfer at an Air-Earth Interface." Transportation, American Geophysical Union, Vol. 34, No. 1, 1953.
22. Bruce R. Munson, Donald F. Young, and Theodore H. Okishi, "Fundamentals of Fluid Mechanics." 5th edition, John Wiley & Sons (Asia) Pte Ltd. 2005.
23. Daryl L. Logan, "A First Course in the Finite Element Method", 2nd Edition, PWS Publish Company, 1993
24. Nazarian, Soheil and Alvarado Gisel, "Impact of Temperature Gradient on Modulus of Asphaltic Concrete Layers, Journal of Materials in Civil Engineering." Vol. 18, No. 4, July/August 2006.
25. National Cooperative Highway Research Program (NCHRP). "Guide for Mechanistic-Empirical Design." Transportation Research Board, Washington, DC, Design Inputs, March 2004.
26. COMSOL. "Heat Transfer Module User's Guide." COMSOL Multiphysics 3.2, 2005
27. Côté Jean and Konrad Jean-Marie, "Estimating Thermal Conductivity of Pavement Granular Materials and Subgrade Soils." Transportation Research

Record, 1967, Transportation Research Board, National Research Council, Washington, DC, 2006.

28. Christoph Clauser, Ernst Huenges, "Thermal Conductivity of Rocks and Minerals." American Geophysical Union, 1995.

## APPENDIX A

### SIX EXISTING PAVEMENT THERMOCOUPLE LOCATIONS

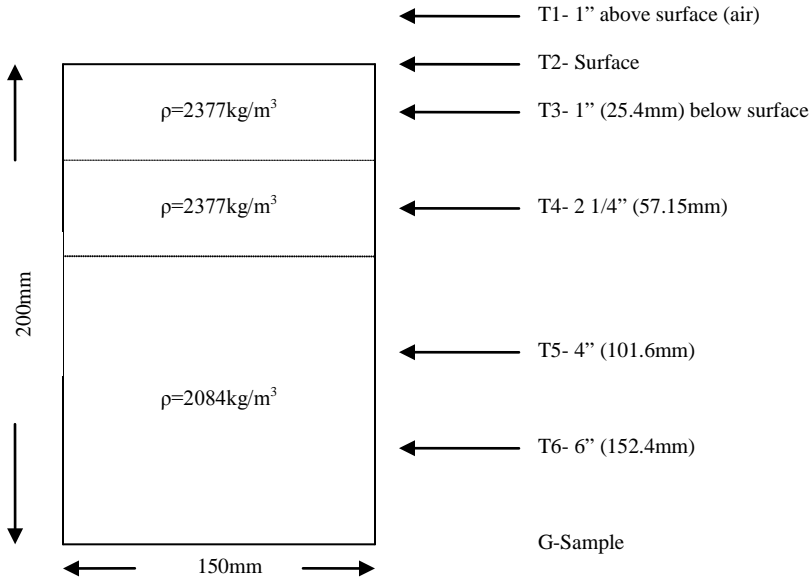


**Figure A-1 G Sample - Highway-HMA layers over HMA base with different NMAS**

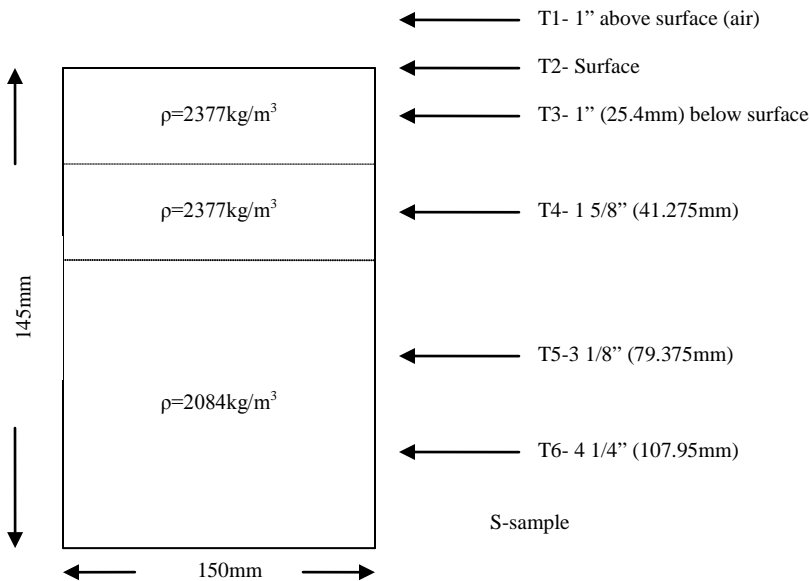


**Figure A-2 S Sample -HMA layers over PMRAP base**

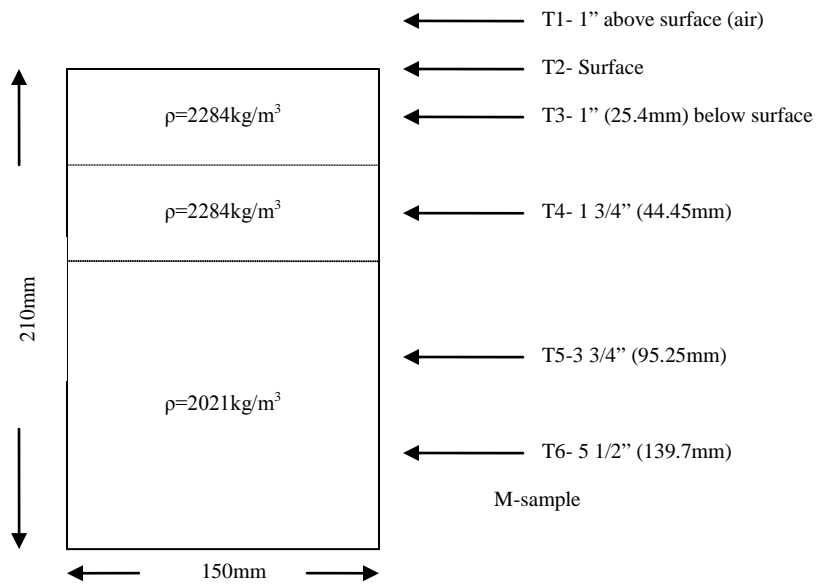


**Figure A-3 M Sample- HMA layers over Foamed Asphalt base**

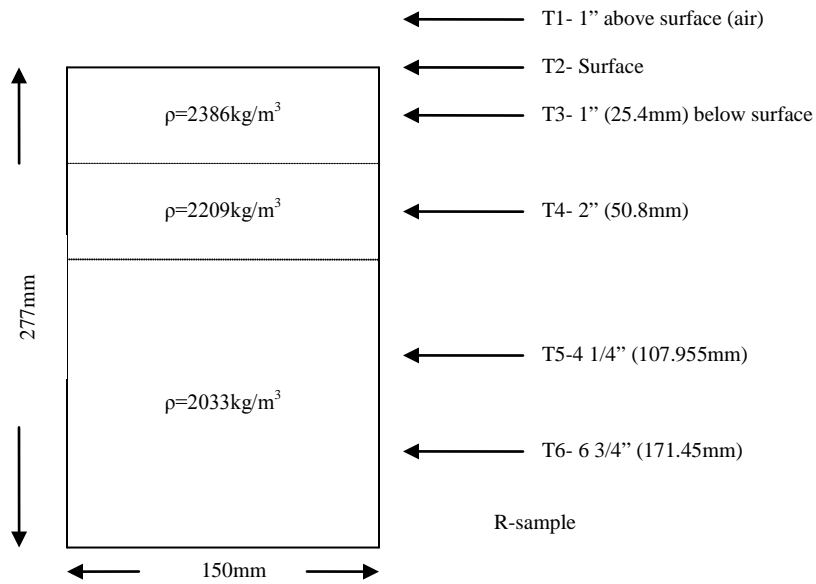


**Figure A-4 R Sample- HMA layers over cement treated base**

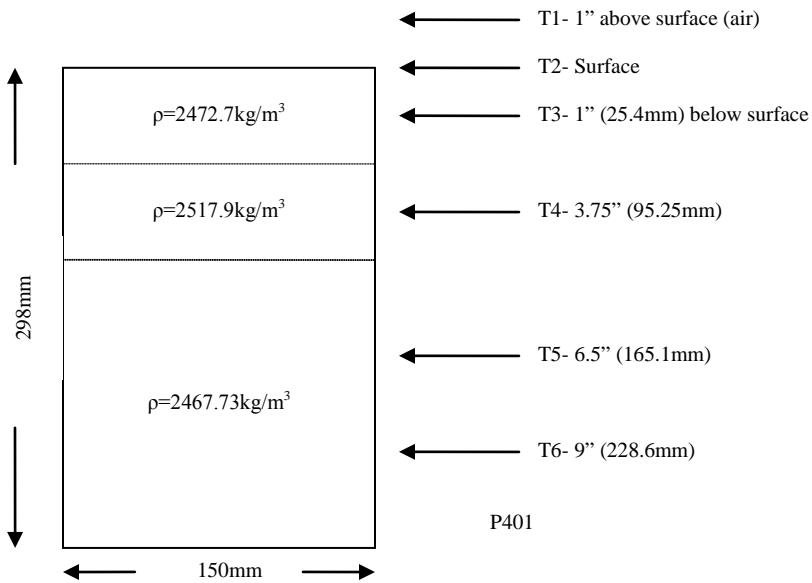


**Figure A-5 P401 Sample- HMA layers of same NMAS**

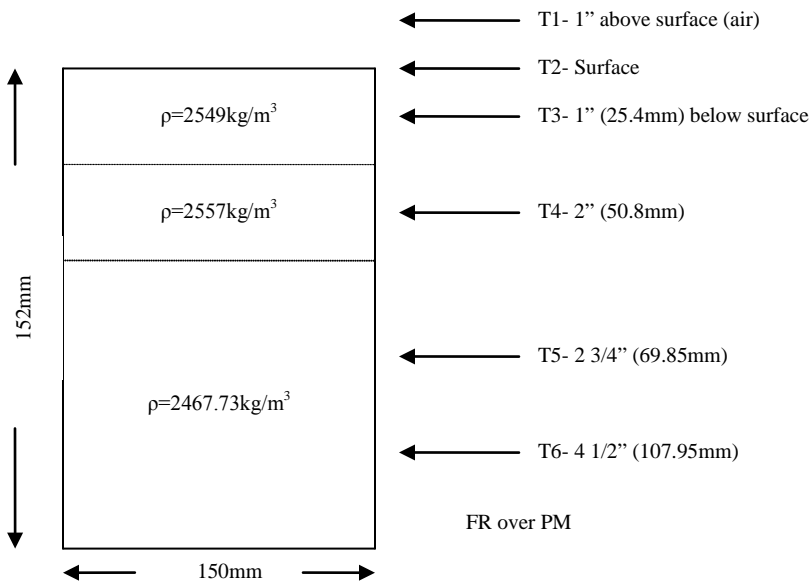


**Figure A-6 FR Sample- HMA layers of different types two lifts**

## APPENDIX B

### DETERMINE THERMAL PROPERTIES OF R, P401, M, AND FR SAMPLES

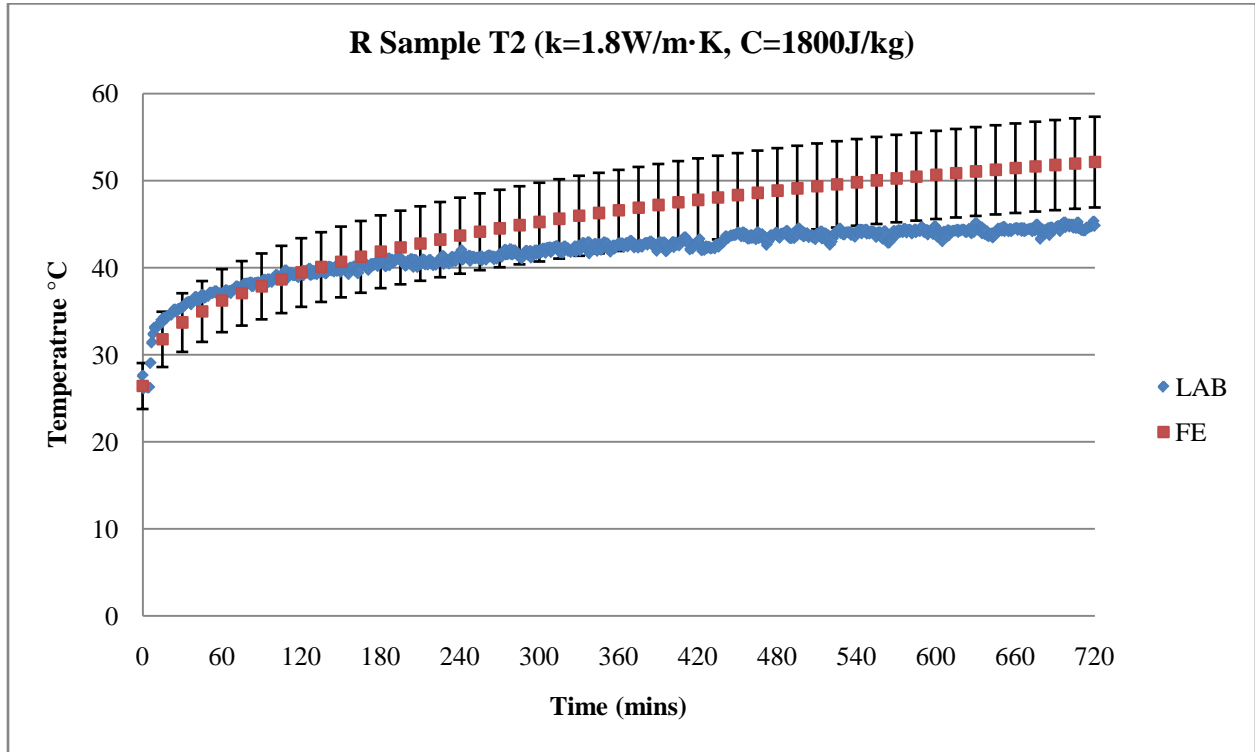


Figure B-1 R sample temperature at T2 (finite element predicted vs. laboratory results)

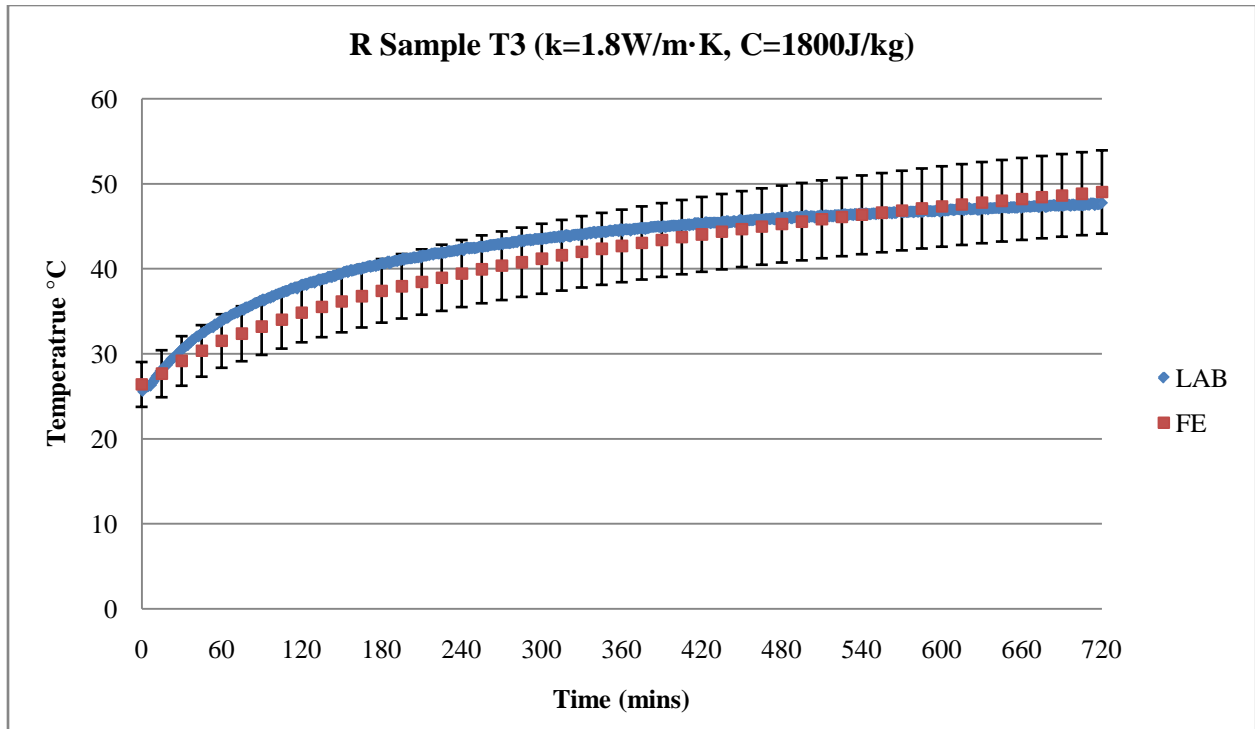
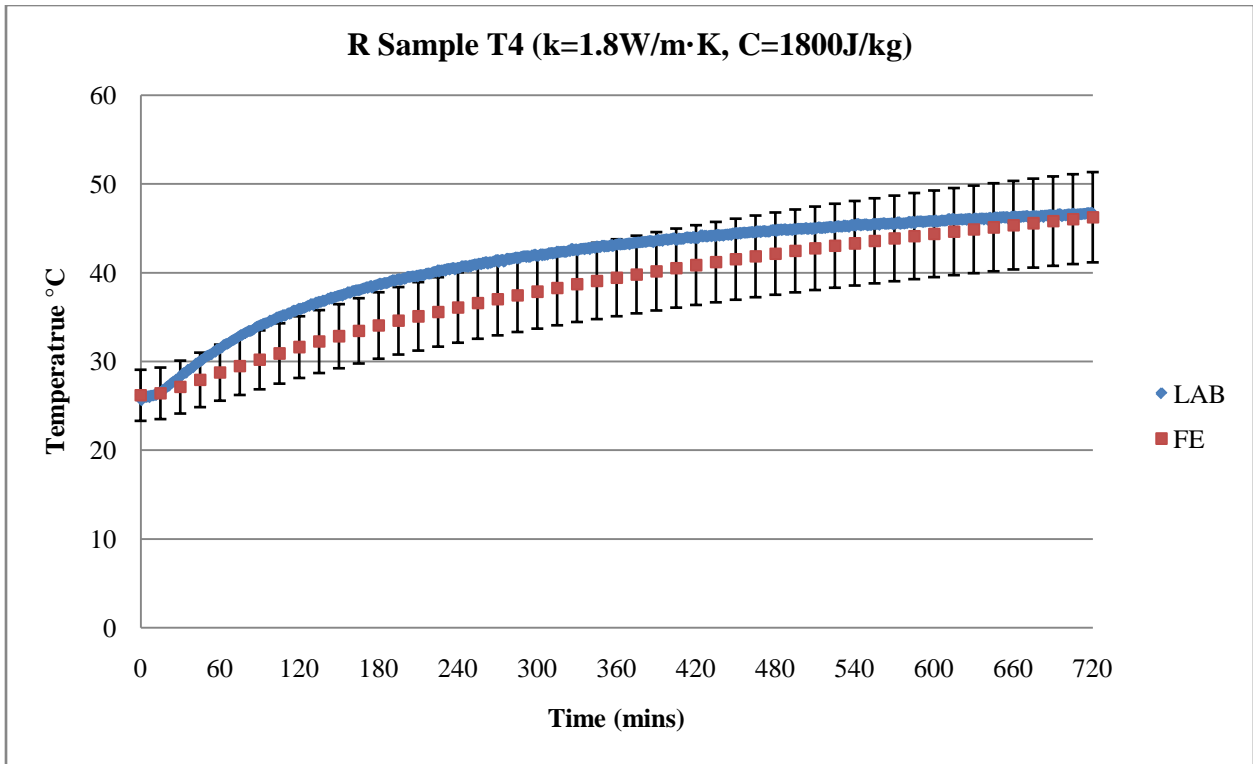
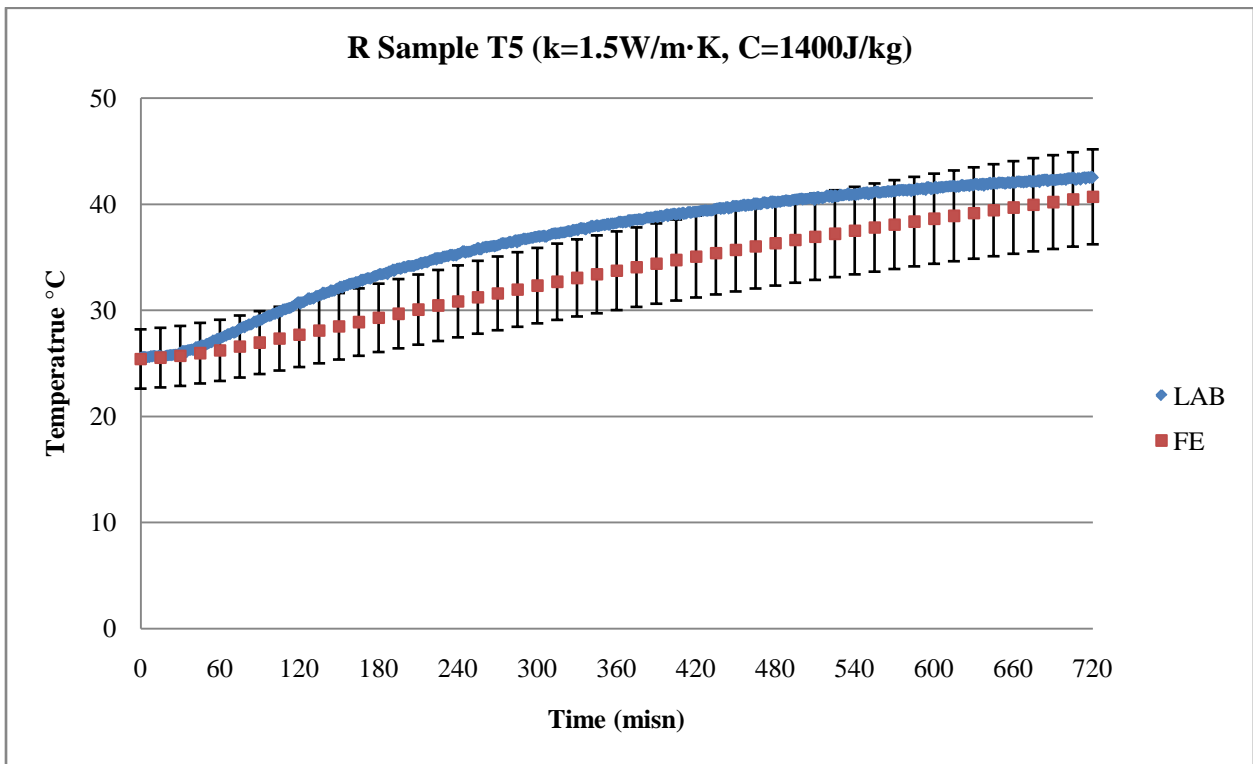


Figure B-2 R sample temperature at T3 (finite element predicted vs. laboratory results)



**Figure B-3 R sample temperature at T4 (finite element predicted vs. laboratory results)**



**Figure B-4 R sample temperature at T5 (finite element predicted vs. laboratory results)**

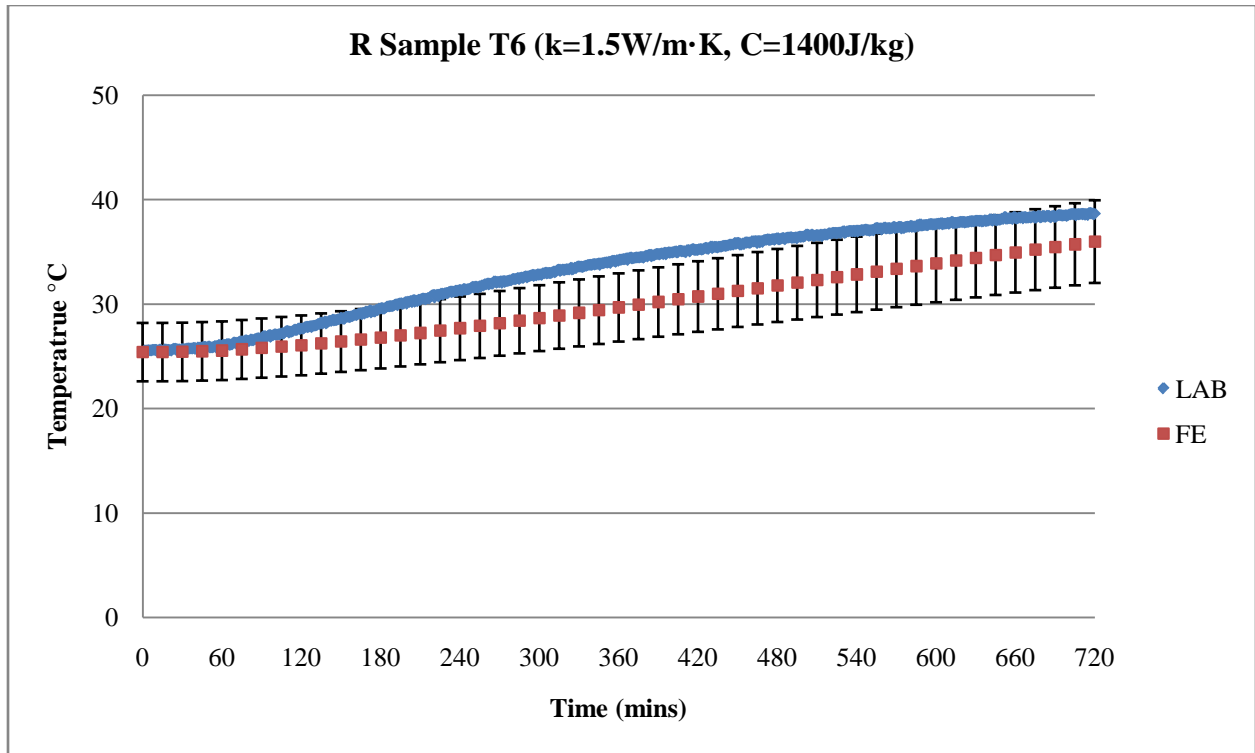


**Figure B-5 R sample temperature at T6 (finite element predicted vs. laboratory results)**

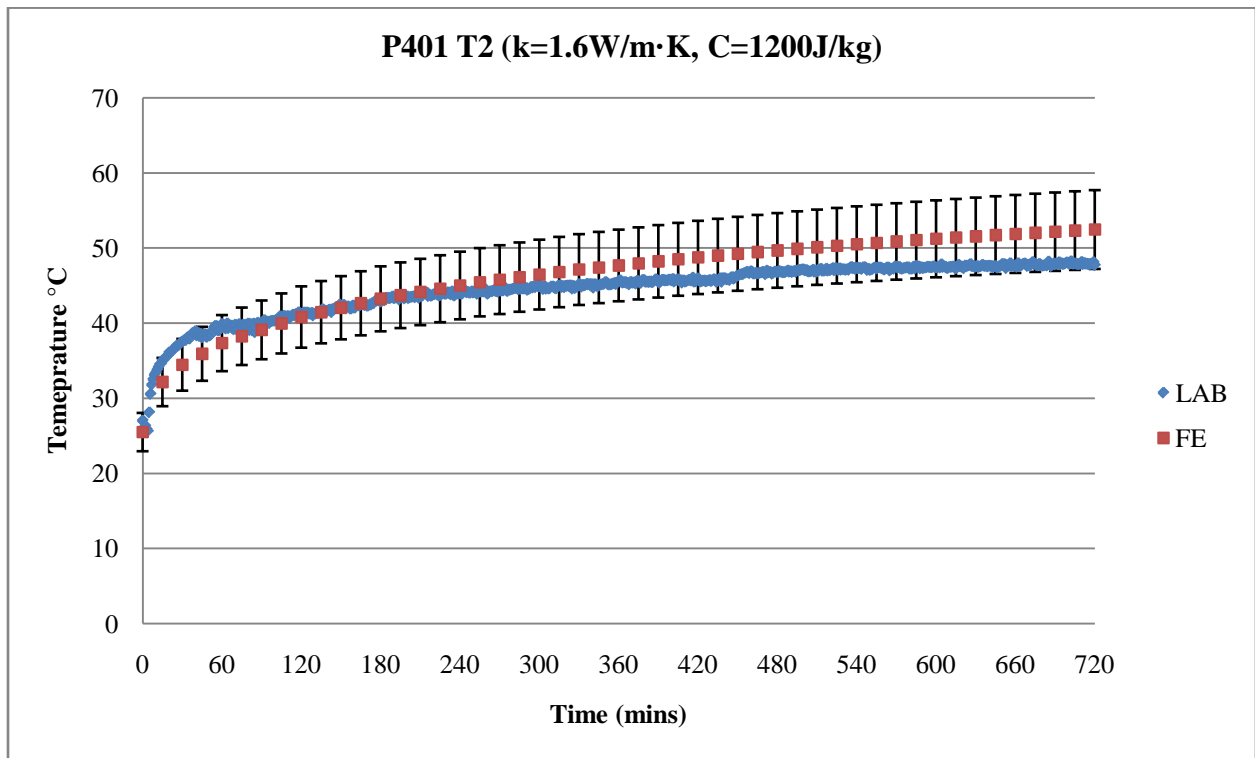


**Figure B-6 P401 sample temperature at T2 (finite element predicted vs. laboratory results)**



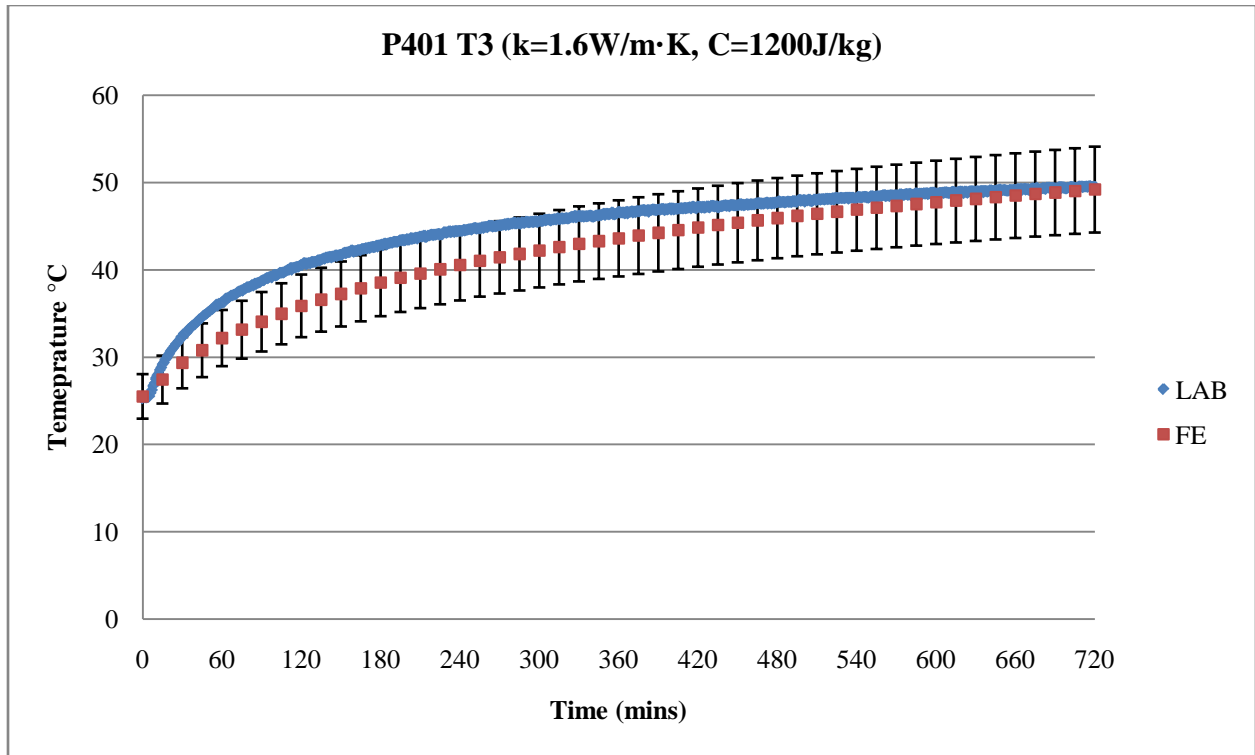


**Figure B-7 P401 sample temperature at T3 (finite element predicted vs. laboratory results)**

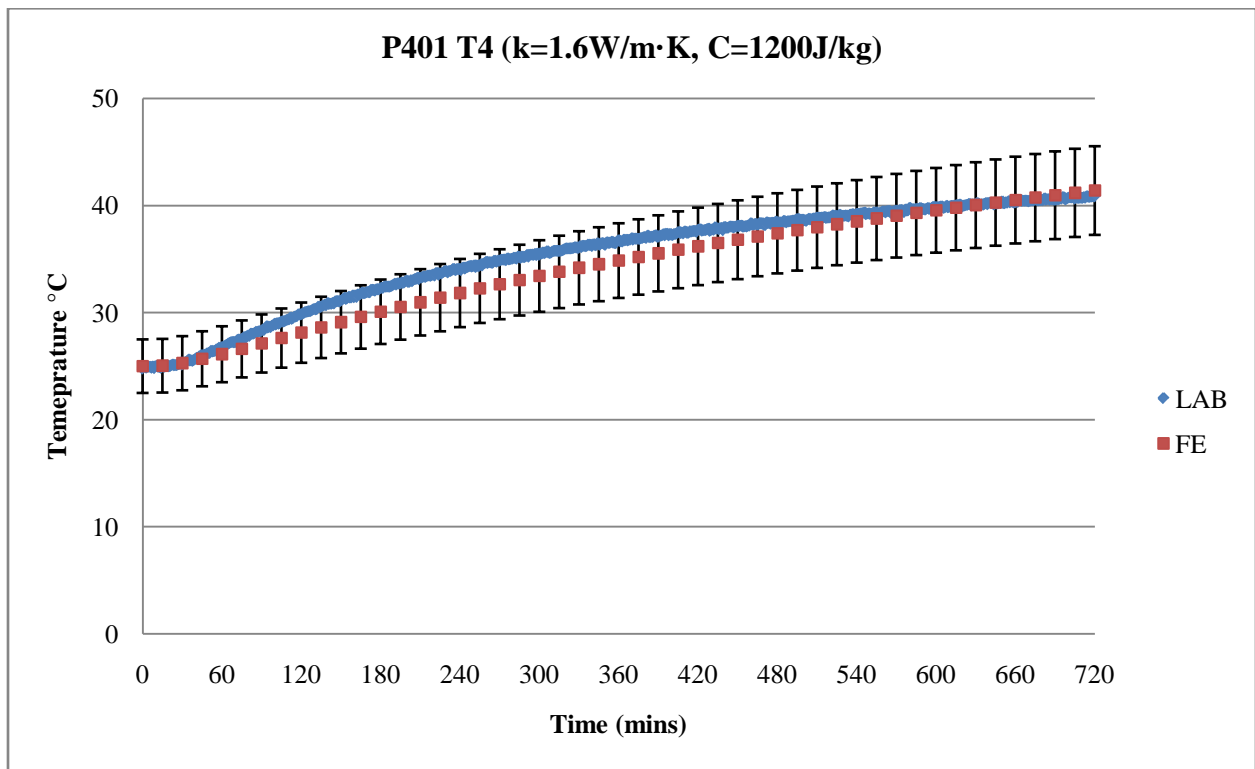


**Figure B-8 P401 sample temperature at T4 (finite element predicted vs. laboratory results)**

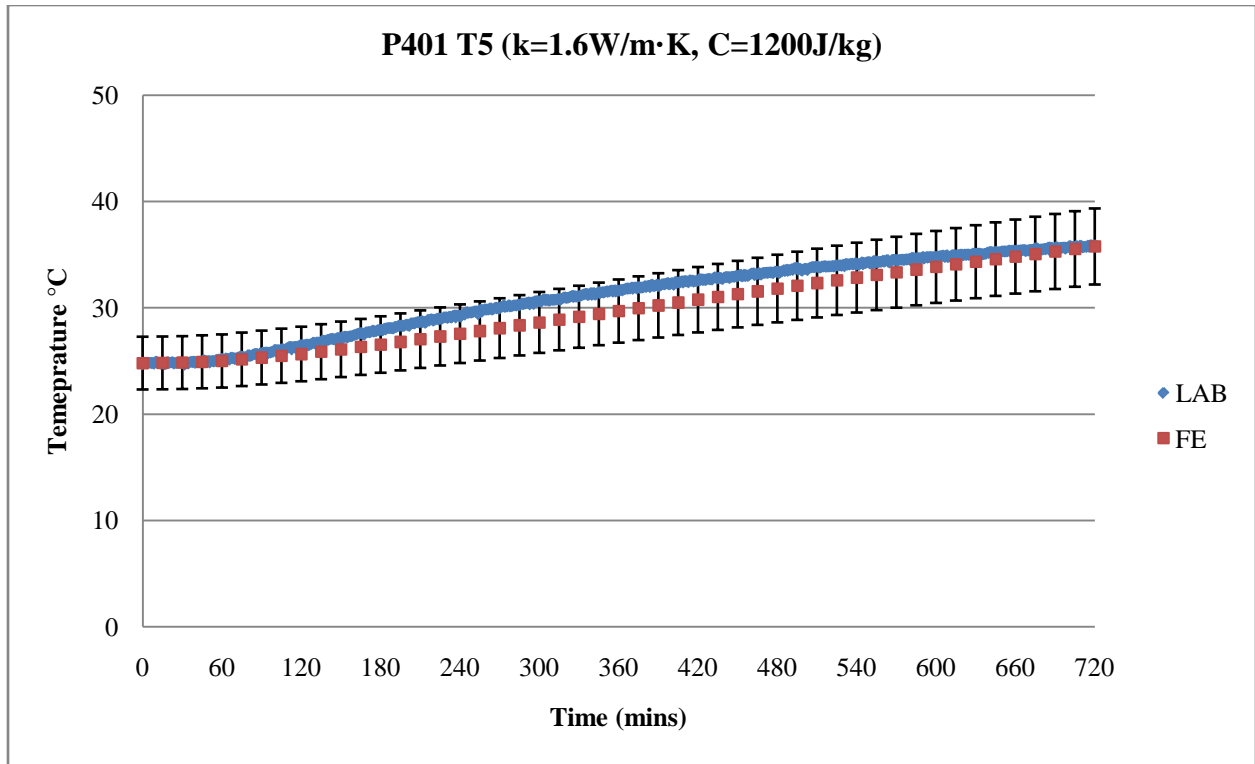


**Figure B-9 P401 sample temperature at T5 (finite element predicted vs. laboratory results)**

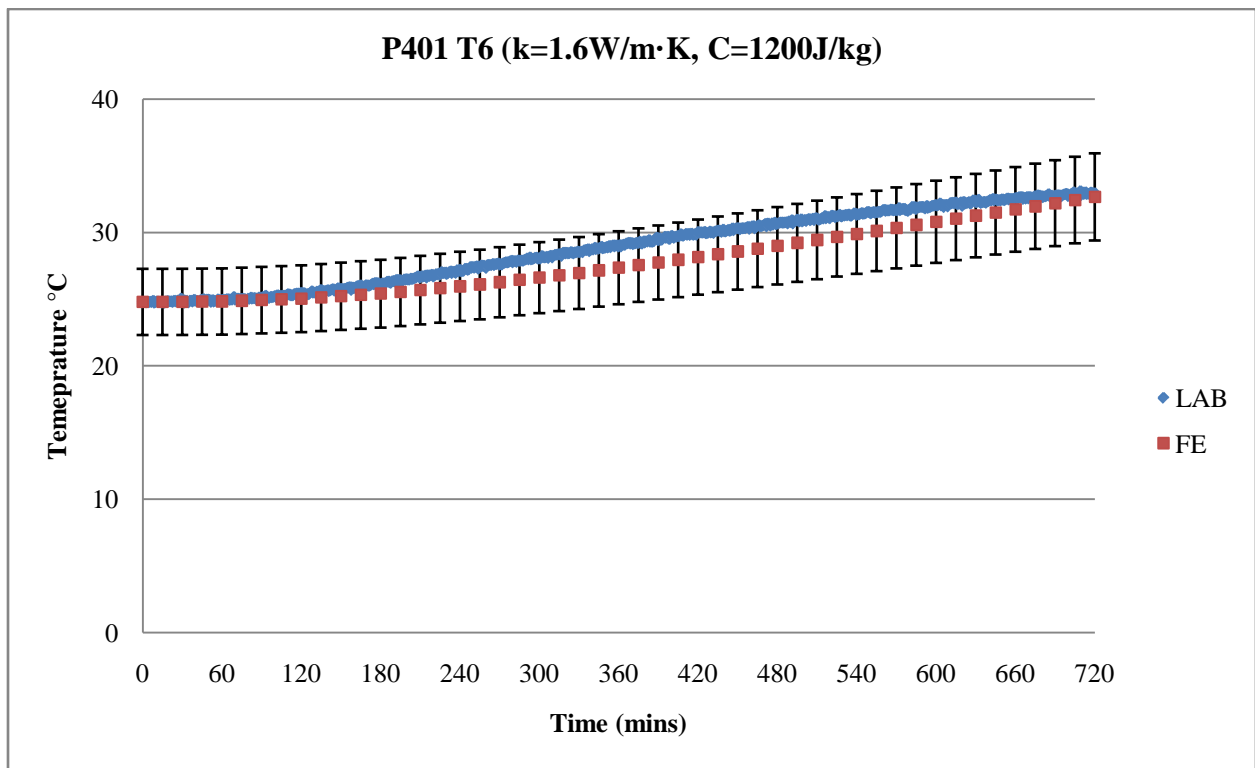


**Figure B-10 P401 sample temperature at T6 (finite element predicted vs. laboratory results)**

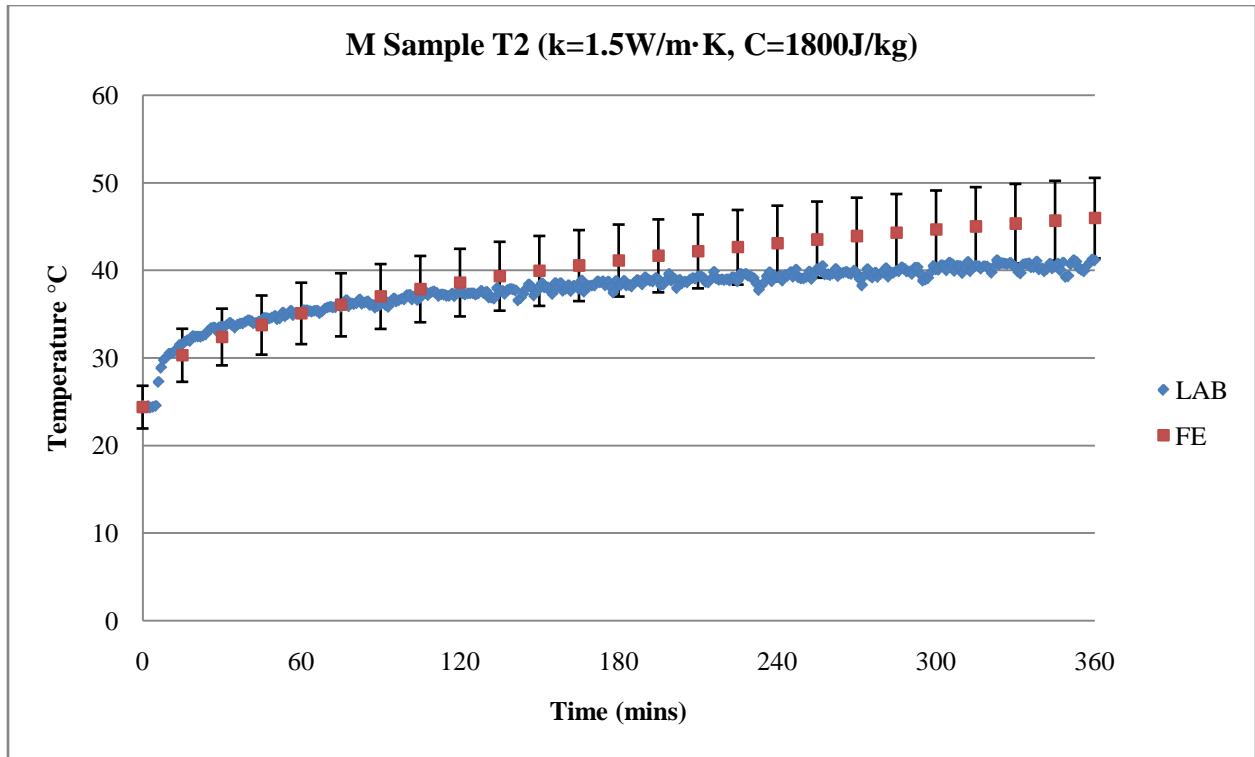


**Figure B-11 M sample temperature at T2 (finite element predicted vs. laboratory results)**

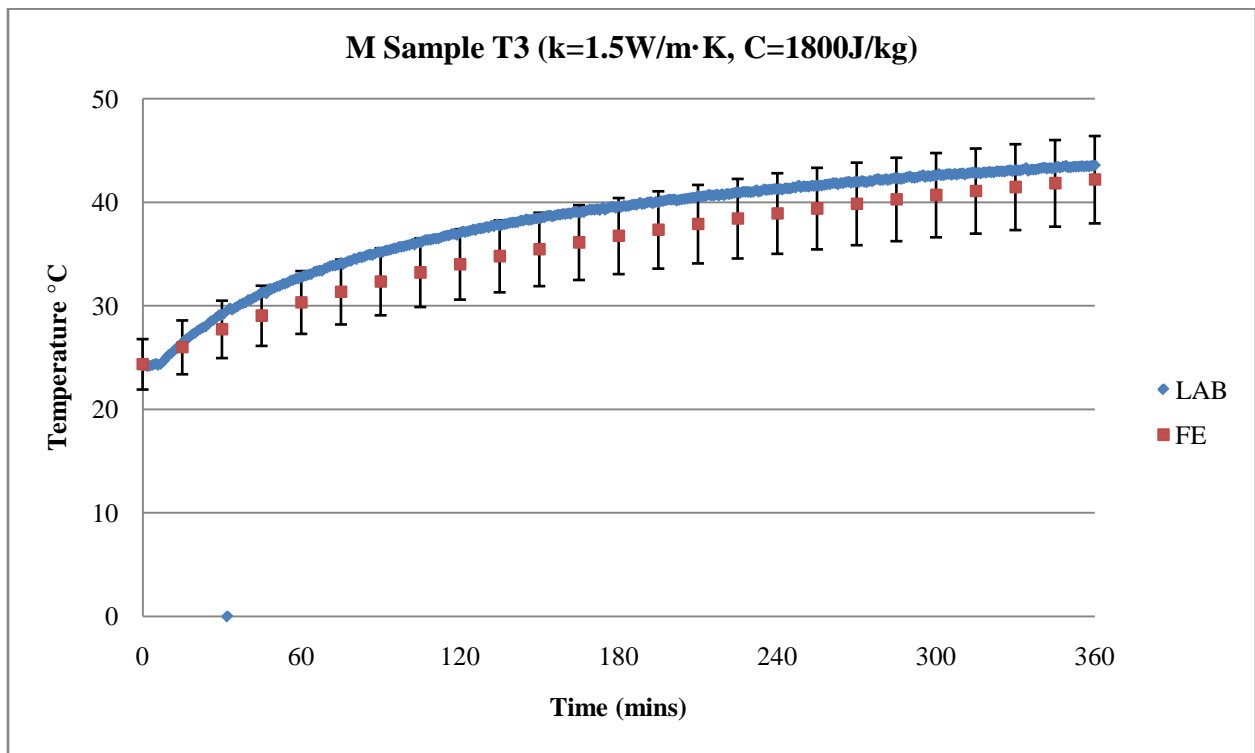


**Figure B-12 M sample temperature at T3 (finite element predicted vs. laboratory results)**

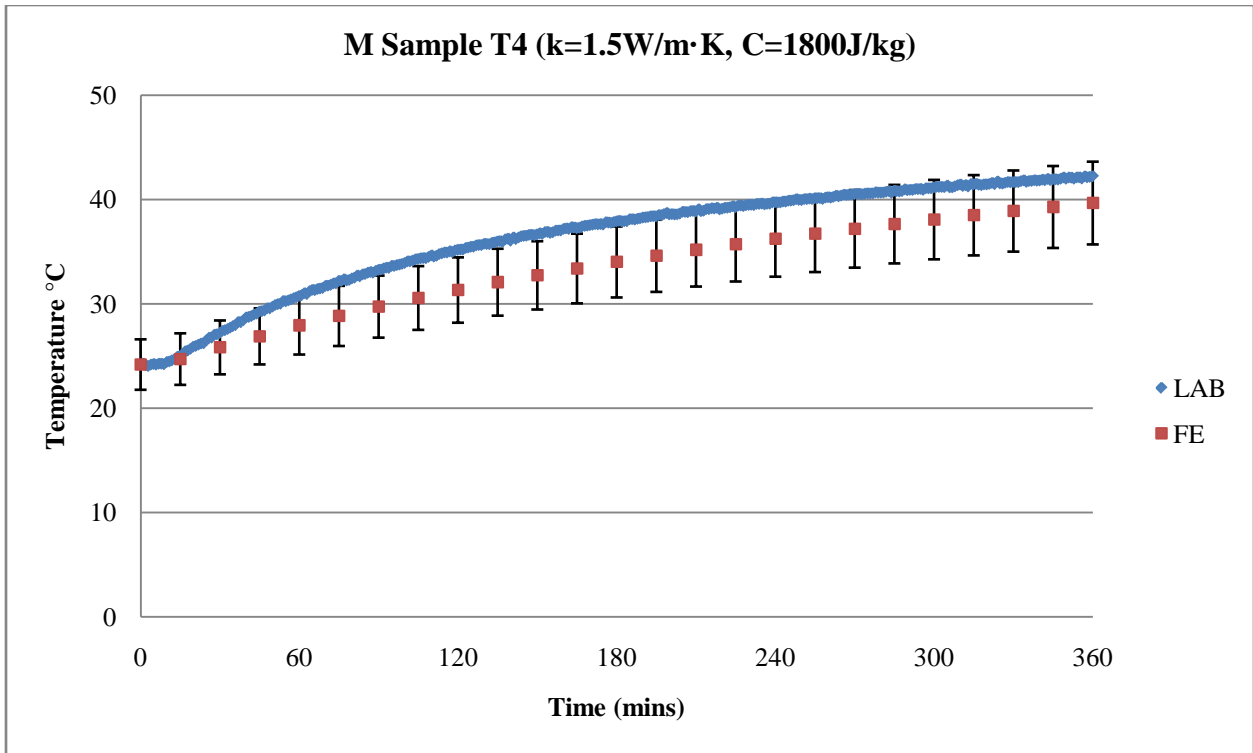


**Figure B-13 M sample temperature at T4 (finite element predicted vs. laboratory results)**

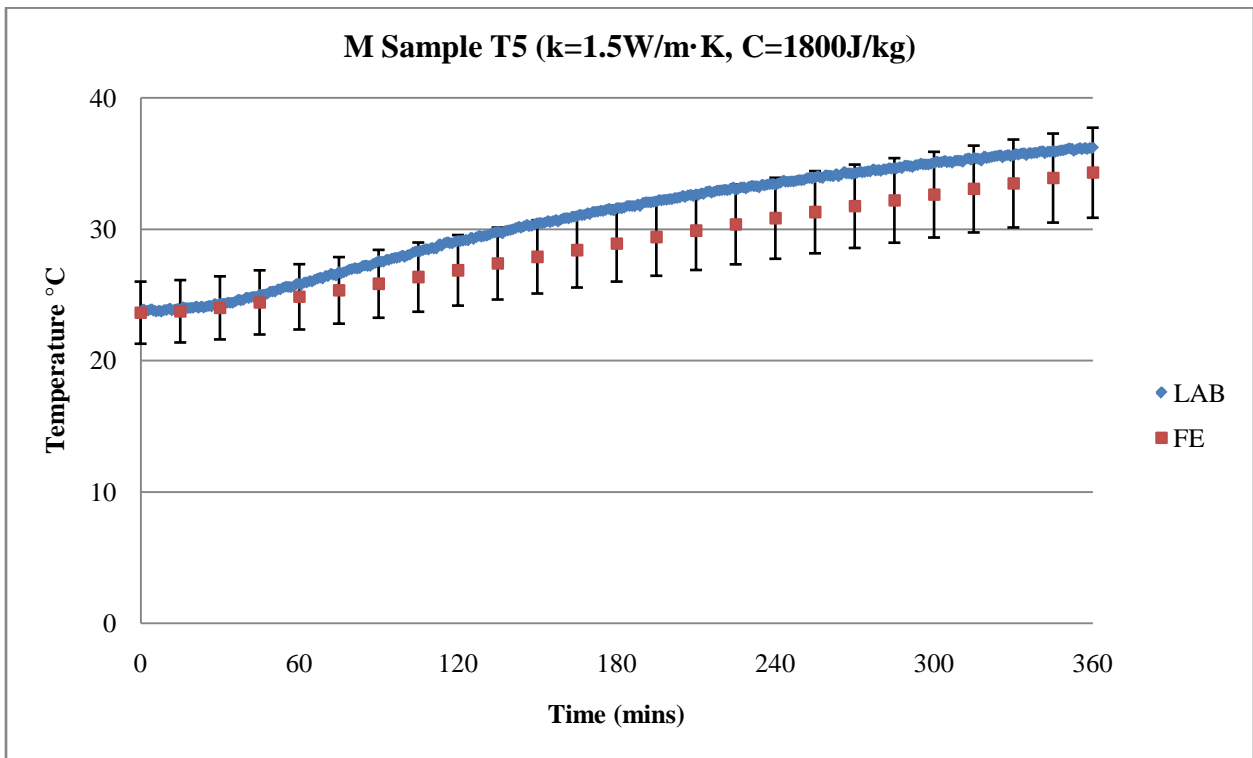


**Figure B-14 M sample temperature at T5 (finite element predicted vs. laboratory results)**

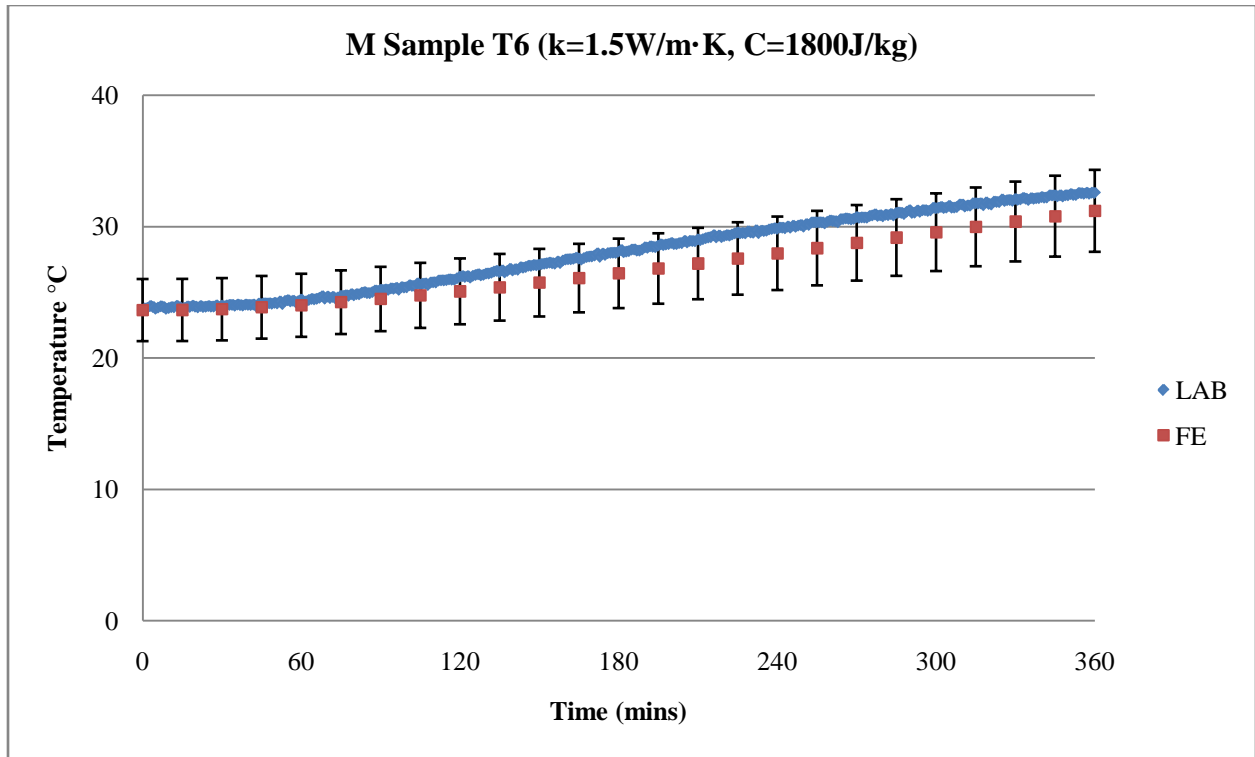


**Figure B-15 M sample temperature at T6 (finite element predicted vs. laboratory results)**

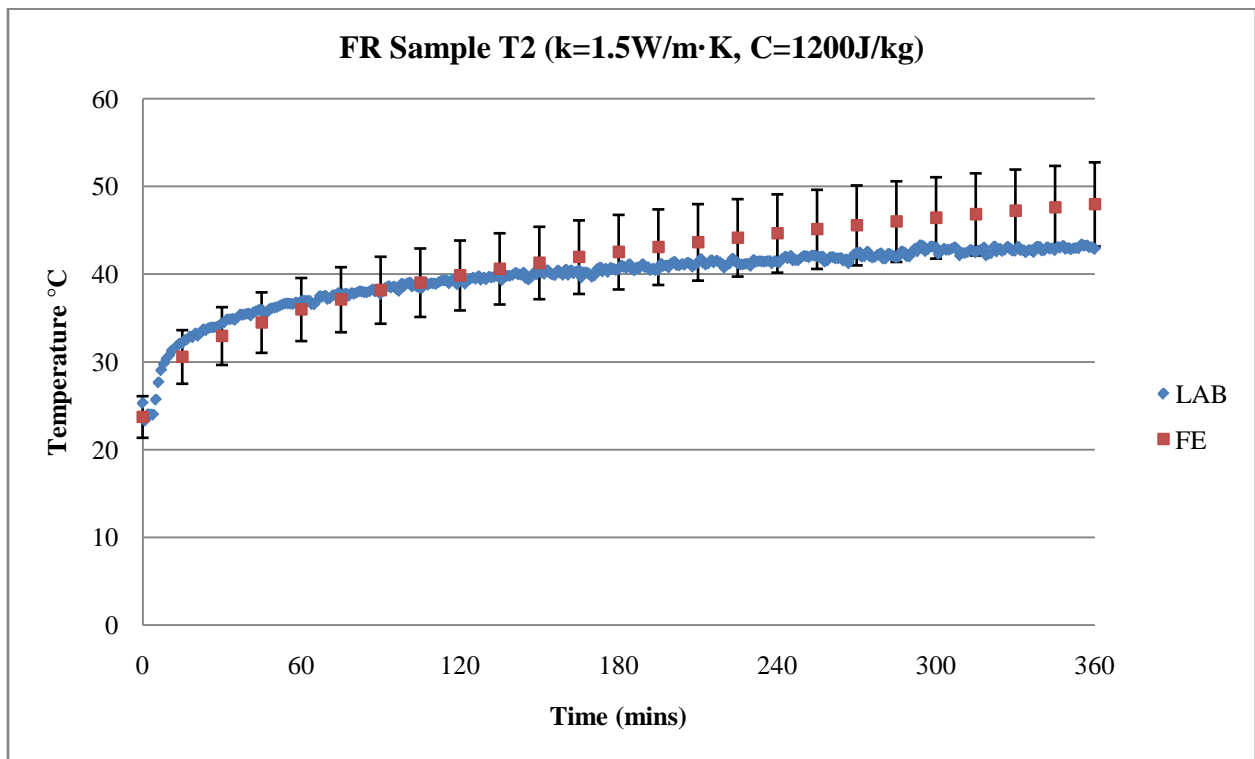


**Figure B-16 FR sample temperature at T2 (finite element predicted vs. laboratory results)**

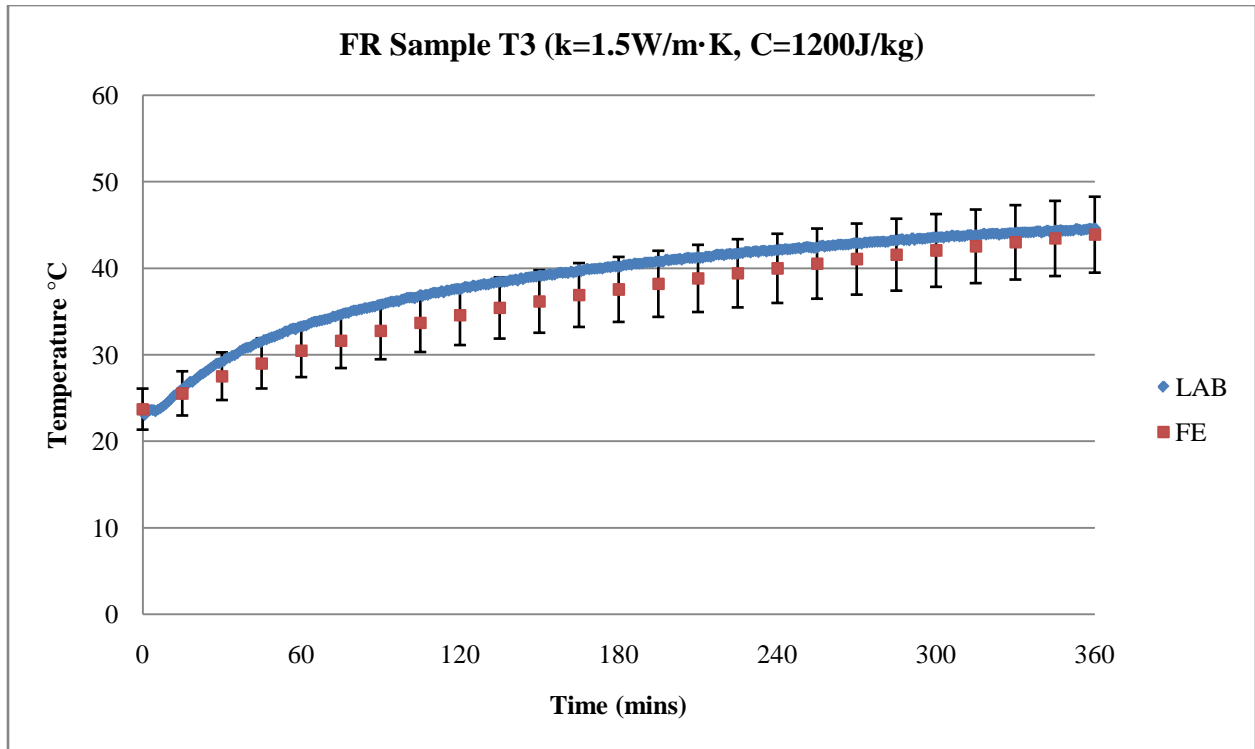


**Figure B-17 FR sample temperature at T3 (finite element predicted vs. laboratory results)**

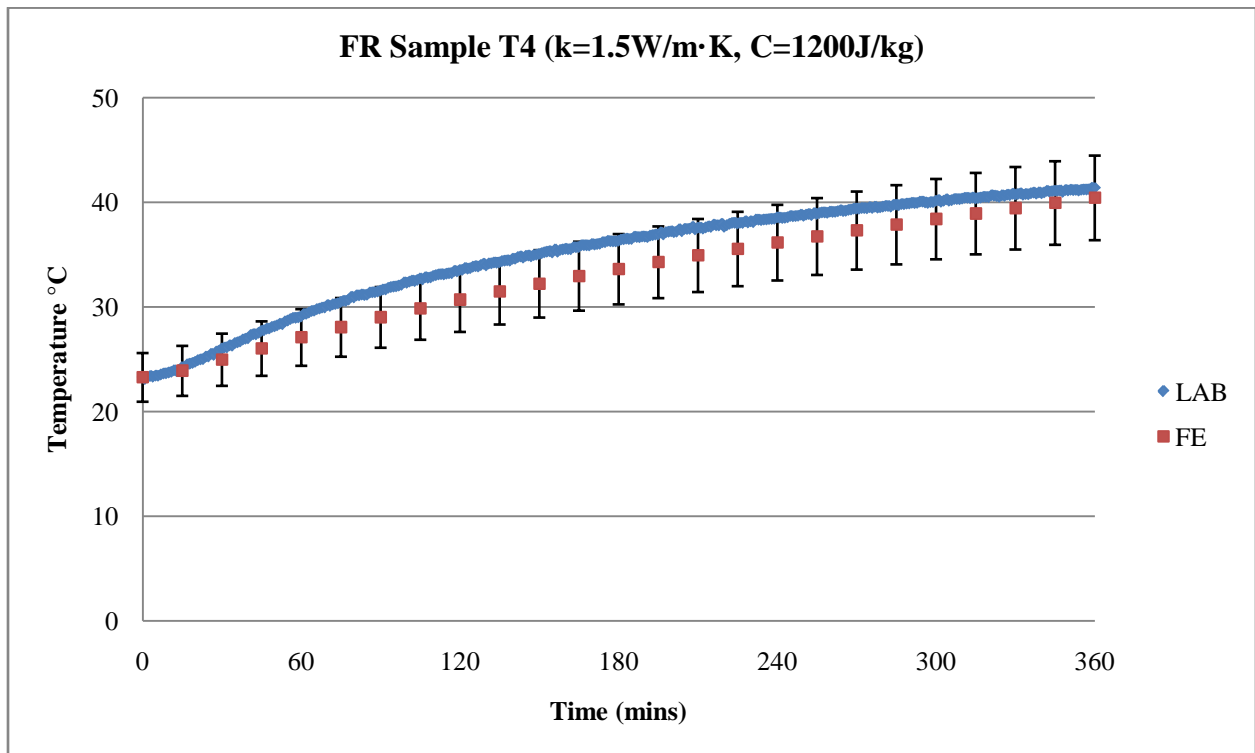


**Figure B-18 FR sample temperature at T4 (finite element predicted vs. laboratory results)**

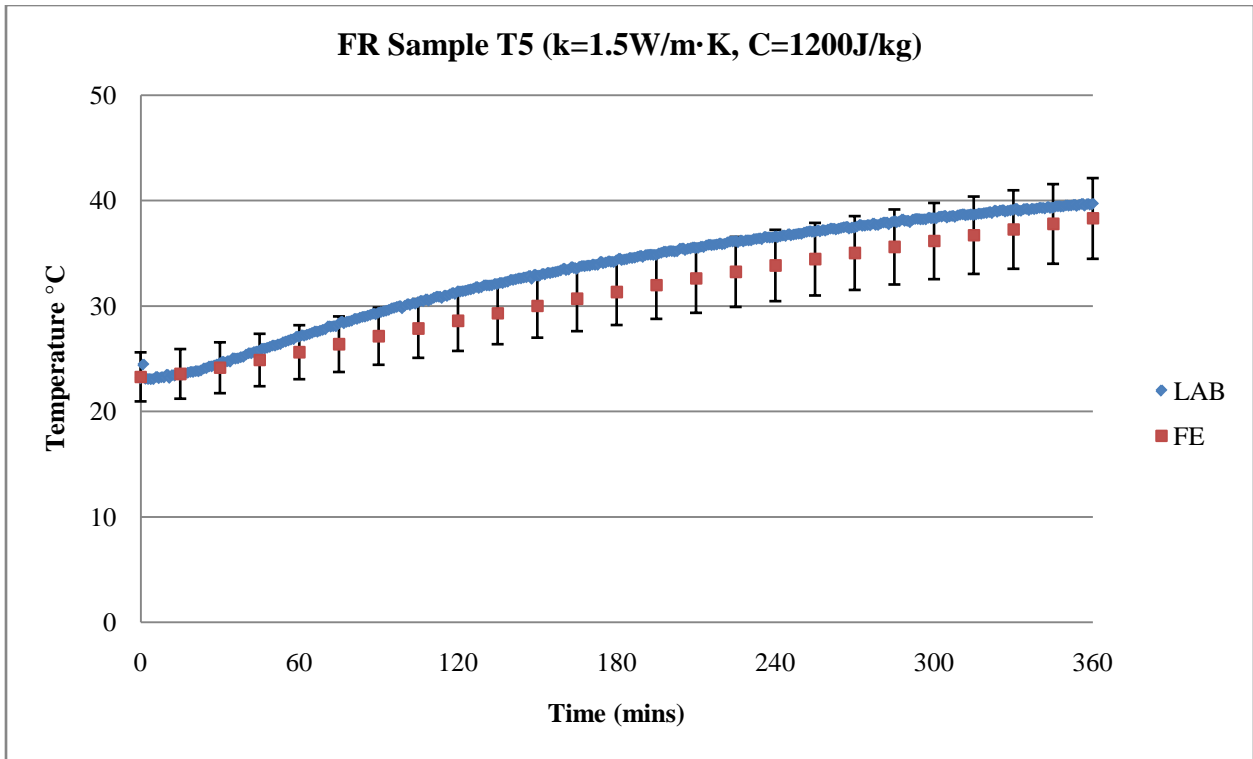


**Figure B-19 FR sample temperature at T5 (finite element predicted vs. laboratory results)**

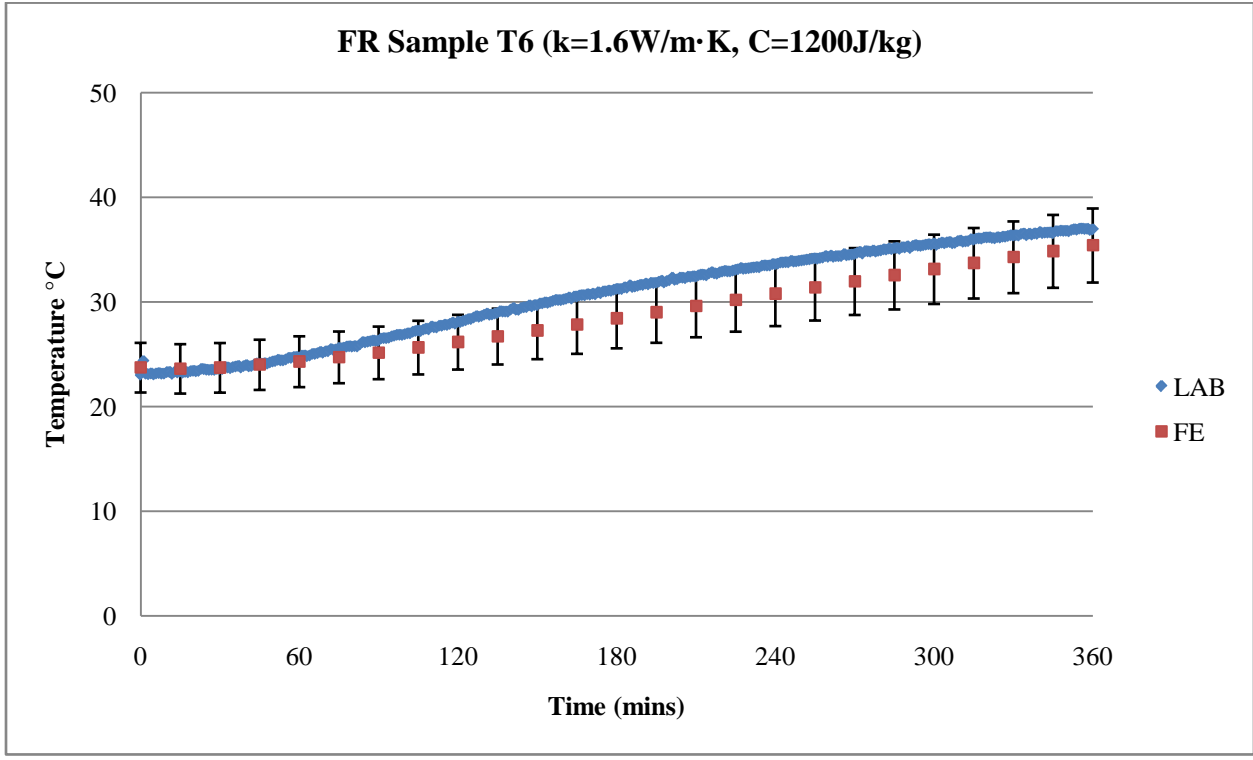


**Figure B-20 FR sample temperature at T6 (finite element predicted vs. laboratory results)**

**APPENDIX C**  
**EXPERIMENT SETUP FOR FIVE SCENARIOS**

**Scenario I**



**Figure C-1 Steady-state setup**

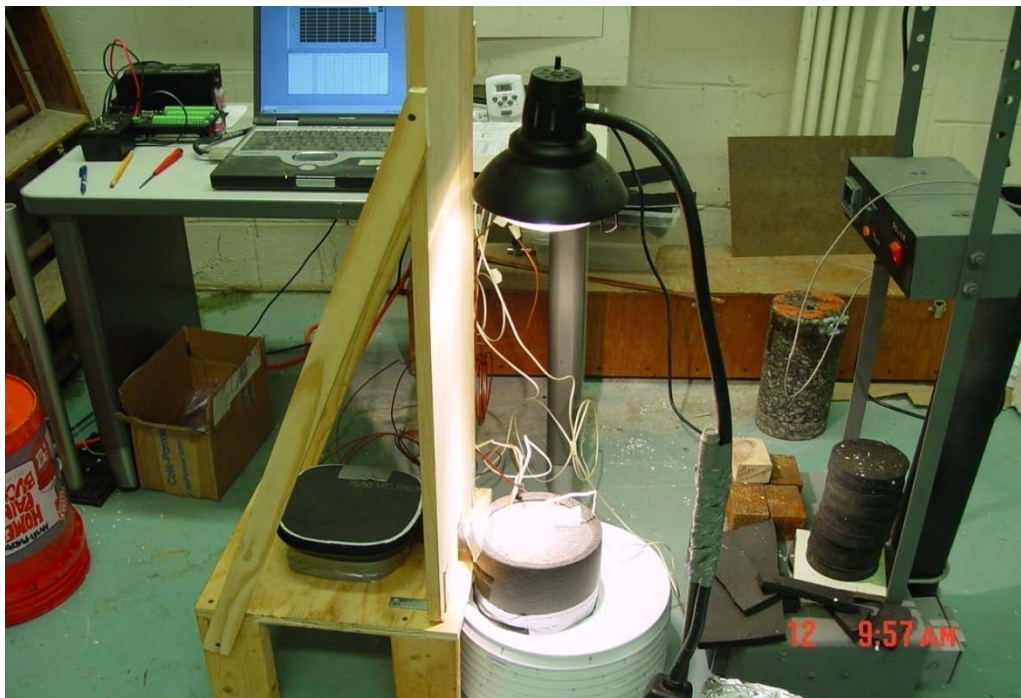


**Figure C-2 Steady-state setup with halogen lamp on**



**Scenario II**



**Figure C-3 Complied 5 asphalt pavement testing**



**Figure C-4 Complied 5 asphalt pavements testing without halogen lamp on**

**Scenario III and VI**



**Figure C-5 Transient testing setup**

**Scenario V**

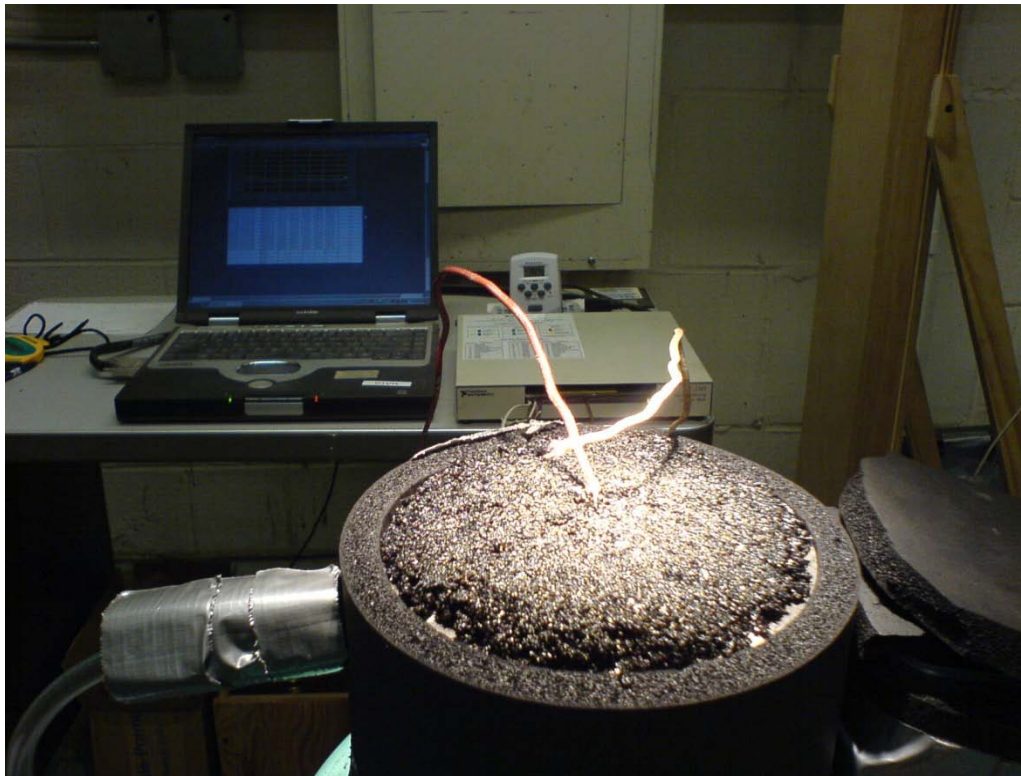


**Figure C-6 Glass chips-Asphalt mix placed on top of asphalt sample**





**Figure C-7 Tinted glass placed on top of asphalt sample**

## APPENDIX D

### DETERMINE THERMAL PROPERTIES OF QUARTZITE, LIMESTONE, AND METAGRANODIORITE (SMALL SCALE)

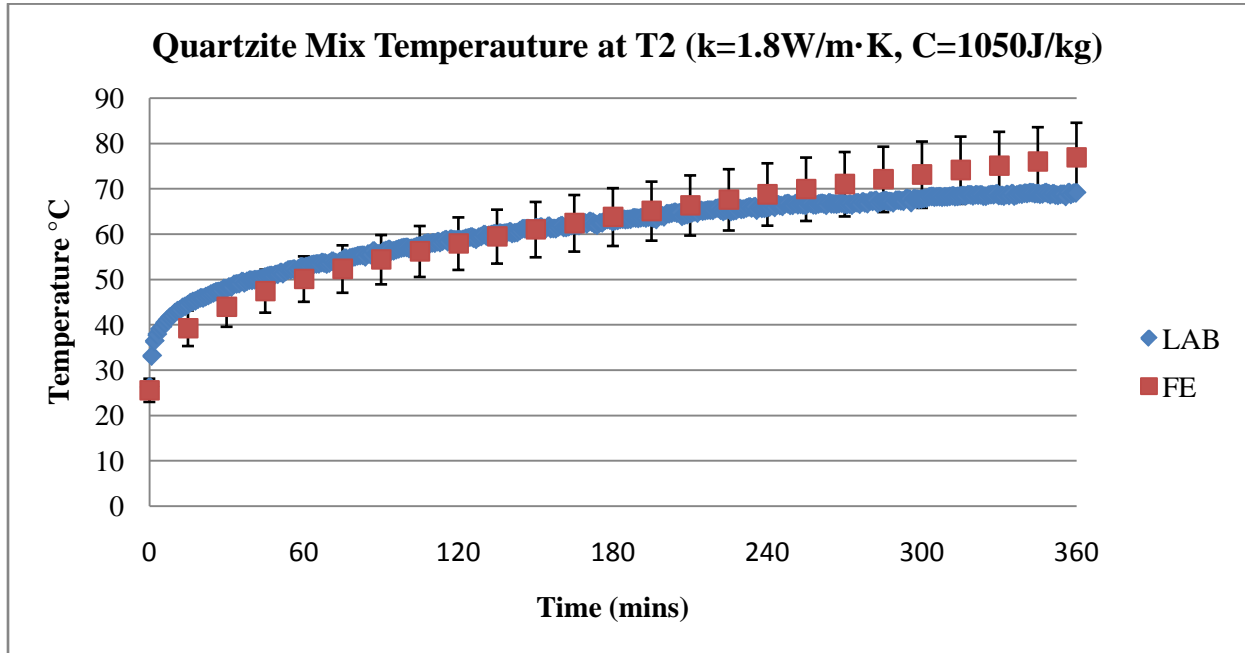


Figure D-1 Quartzite sample temperature at T2 (finite element predicted vs. laboratory results)

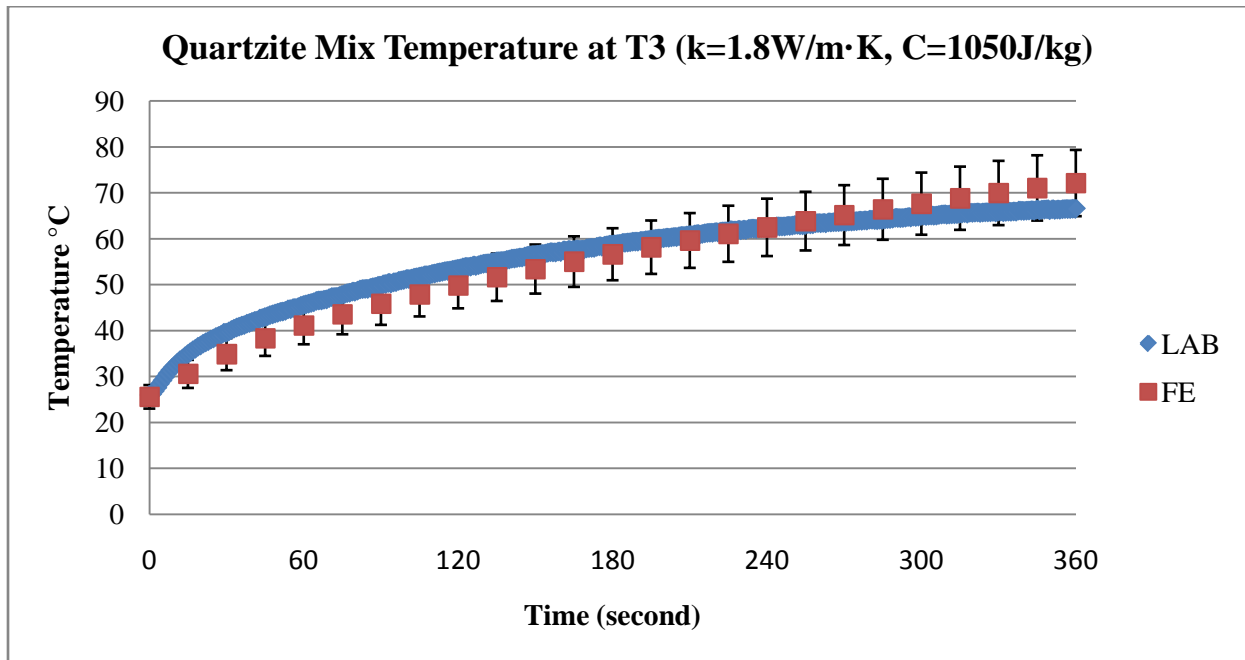
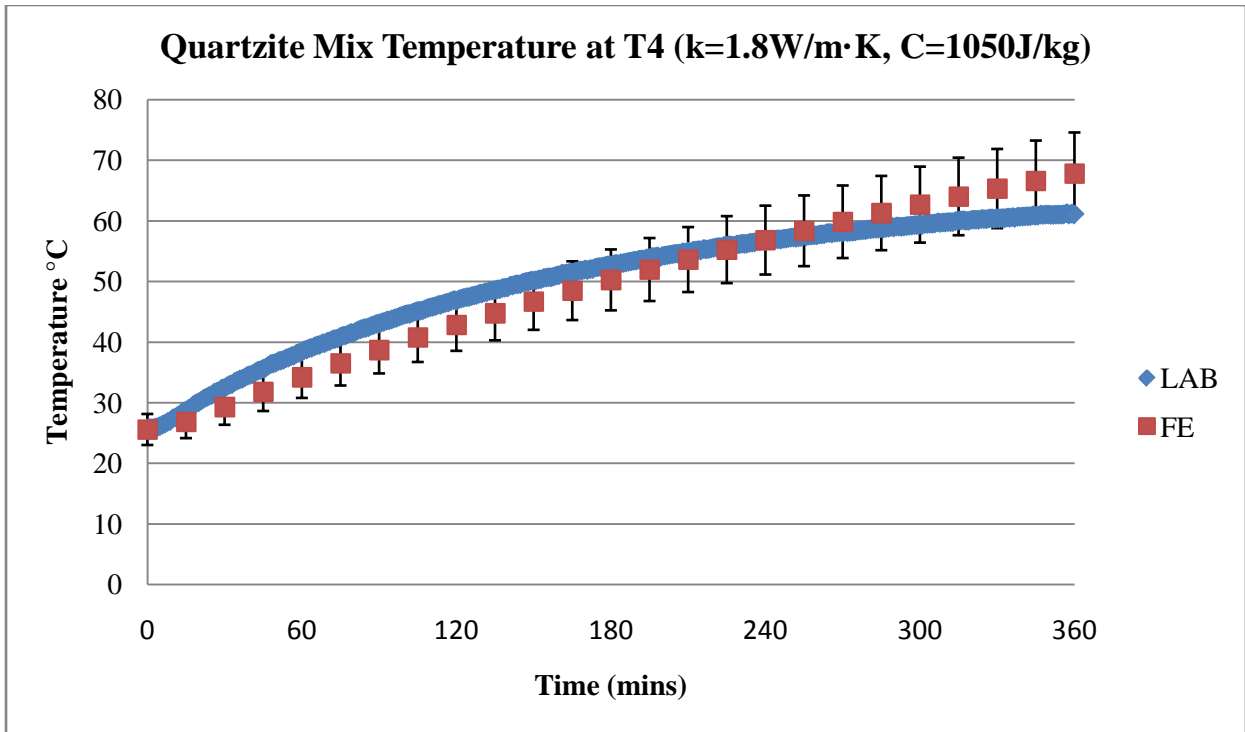
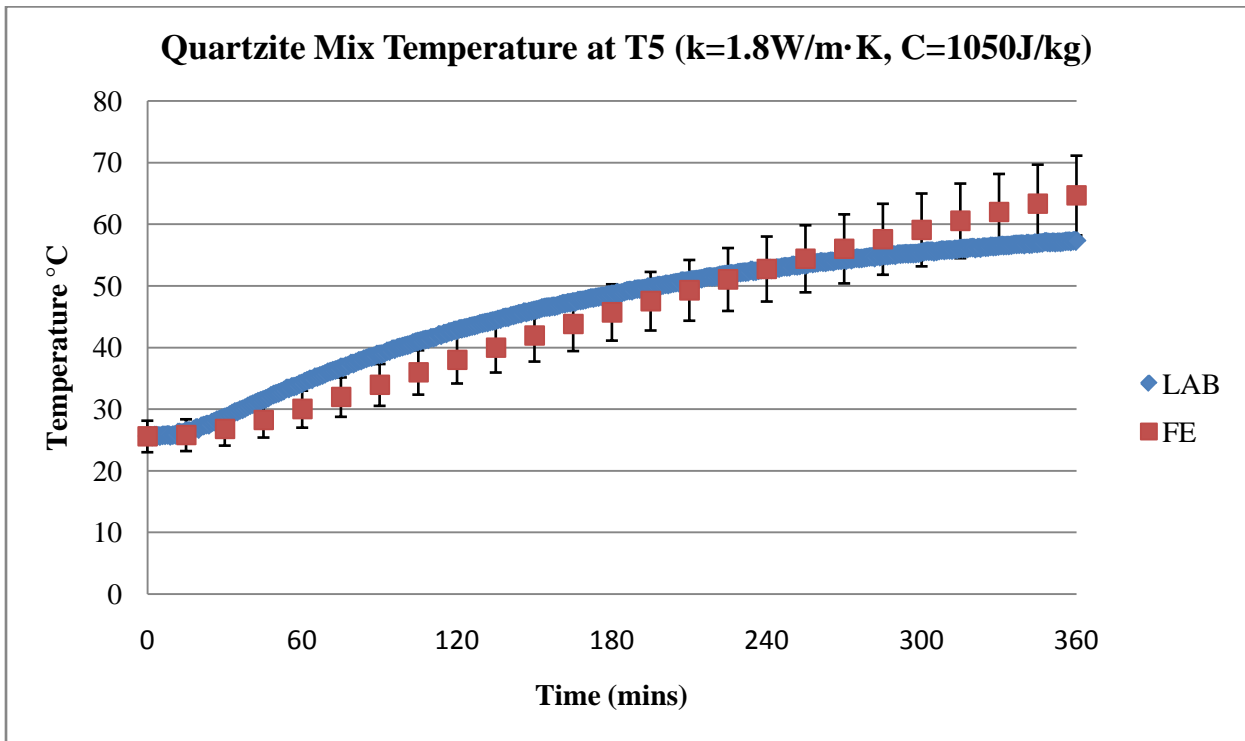


Figure D-2 Quartzite sample temperature at T3 (finite element predicted vs. laboratory results)



**Figure D-3 Quartzite sample temperature at T4 (finite element predicted vs. laboratory results)**



**Figure D-4 Quartzite sample temperature at T5 (finite element predicted vs. laboratory results)**

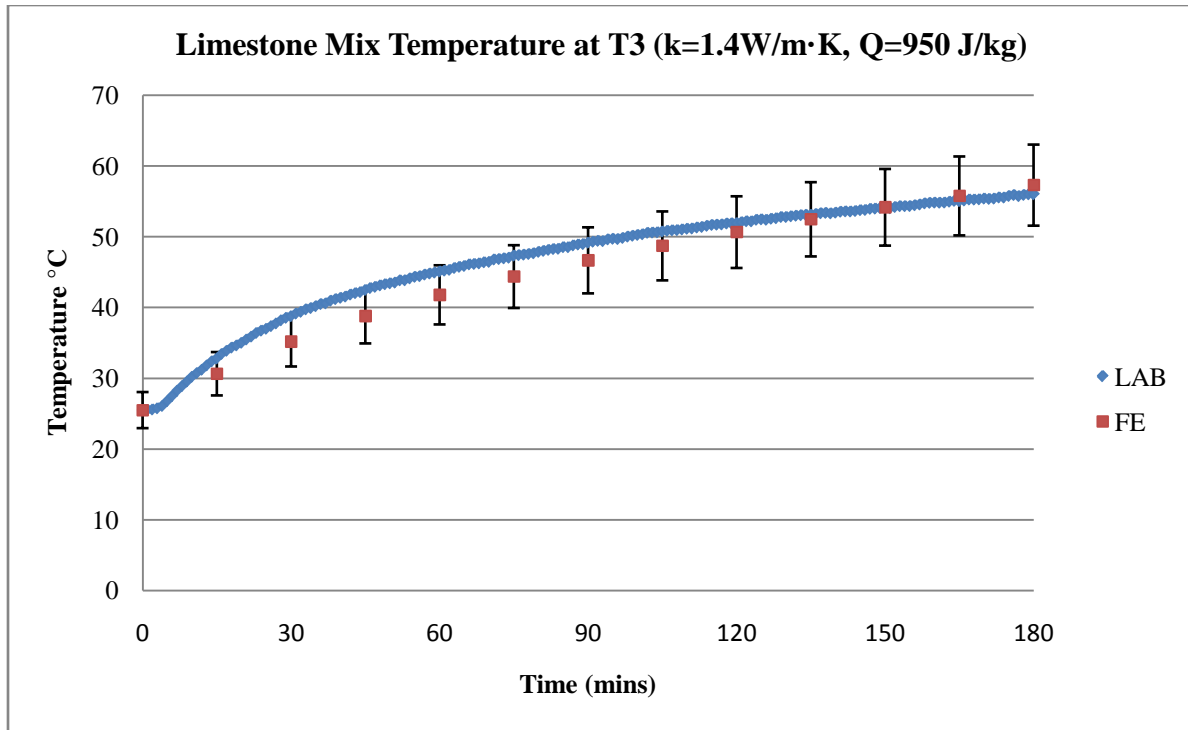


**Figure D-5 Limestone sample temperature at T3 (finite element predicted vs. laboratory results)**

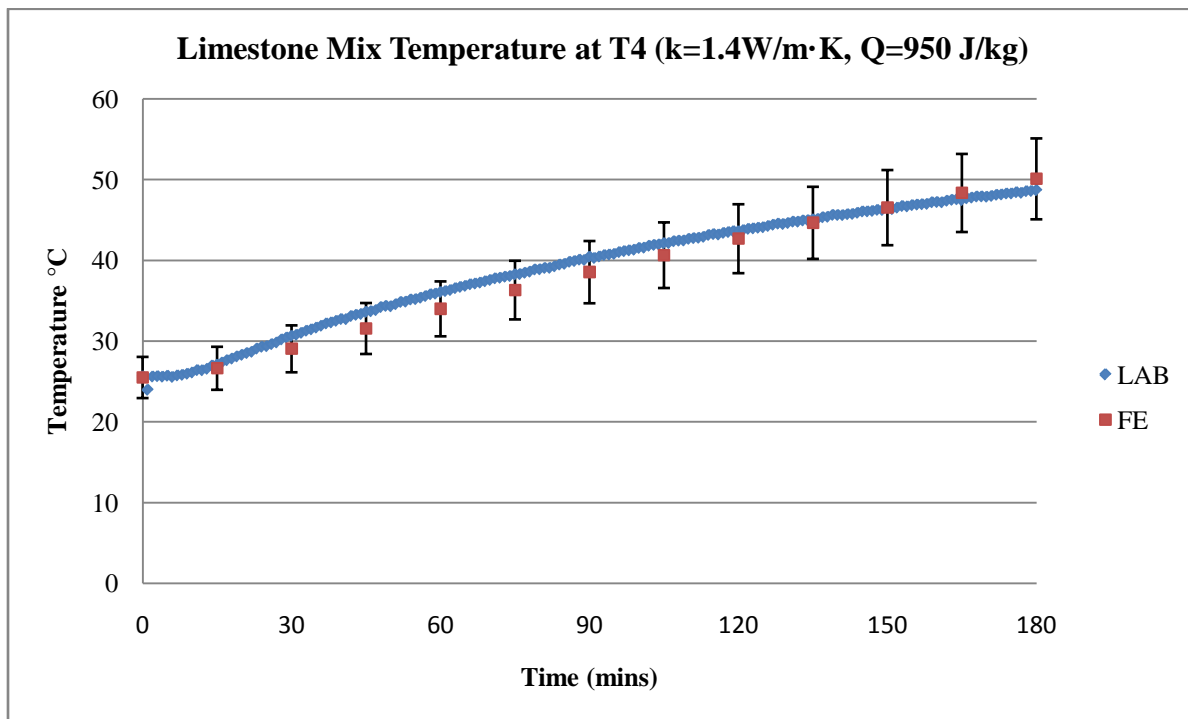


**Figure D-6 Limestone sample temperature at T4 (finite element predicted vs. laboratory results)**

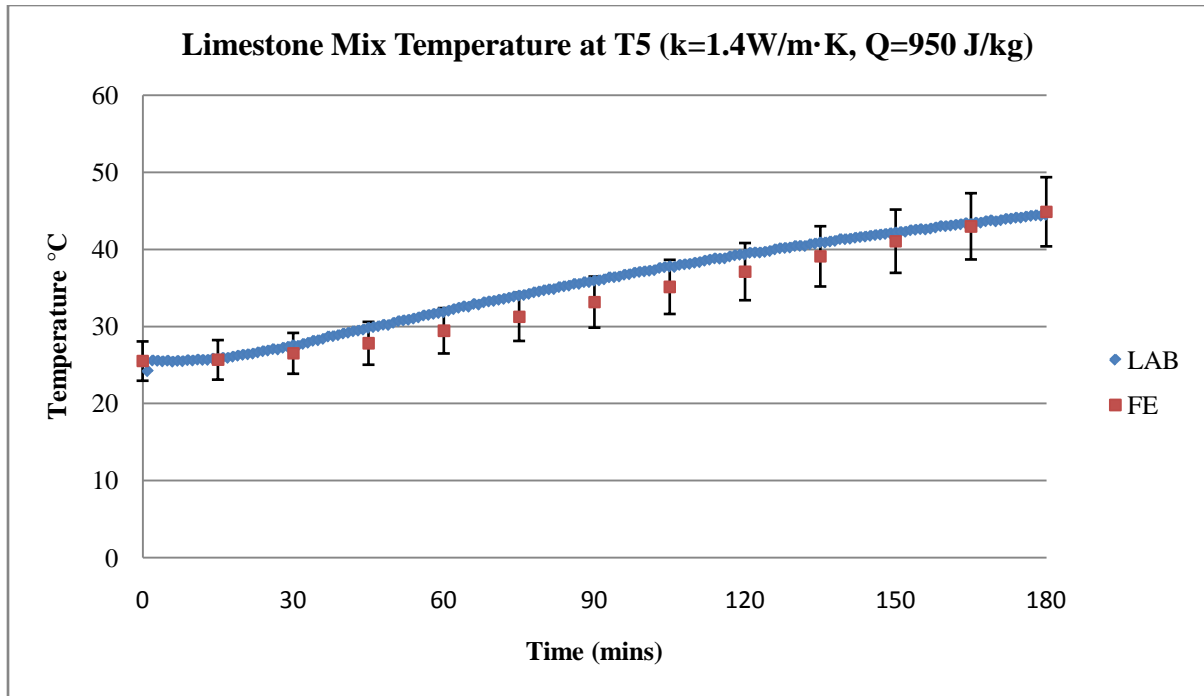


**Figure D-7 Limestone sample temperature at T5 (finite element predicted vs. laboratory results)**

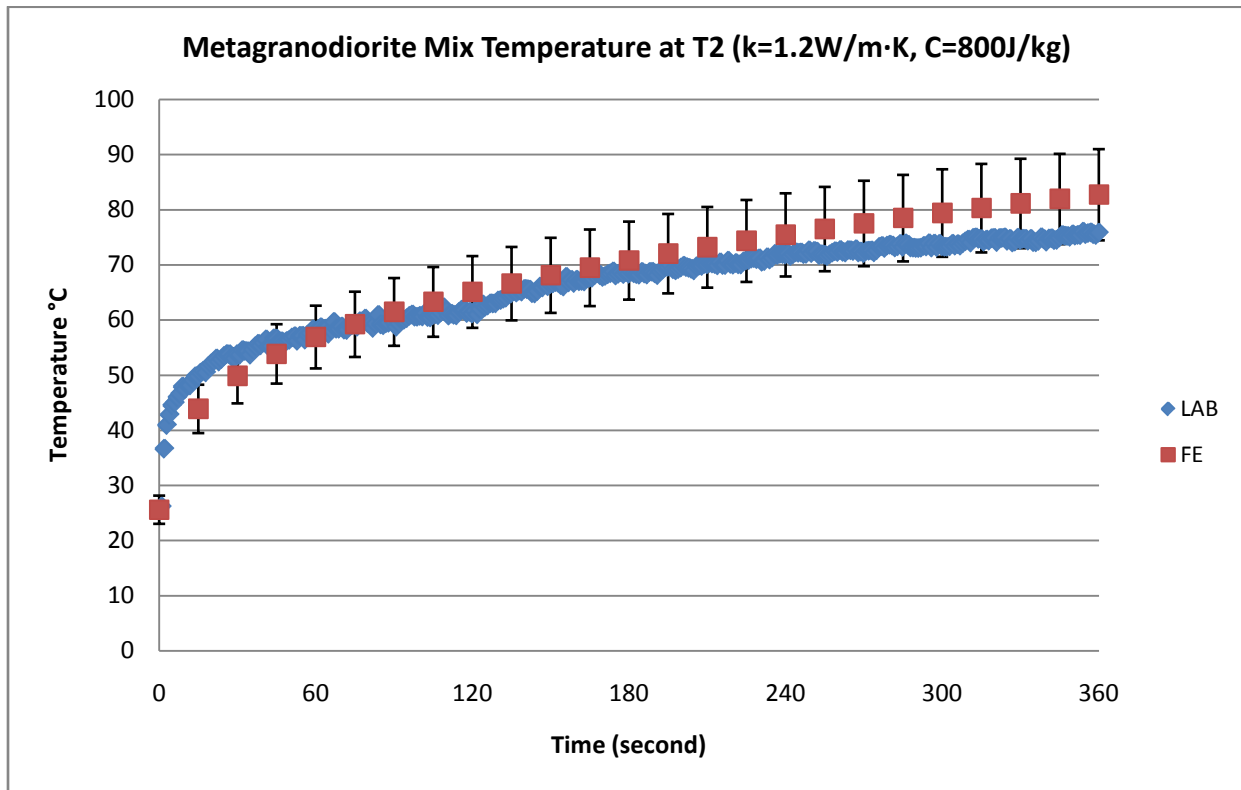


**Figure D-8 Metagranodiorite sample temperature at T2 (finite element predicted vs. laboratory results)**

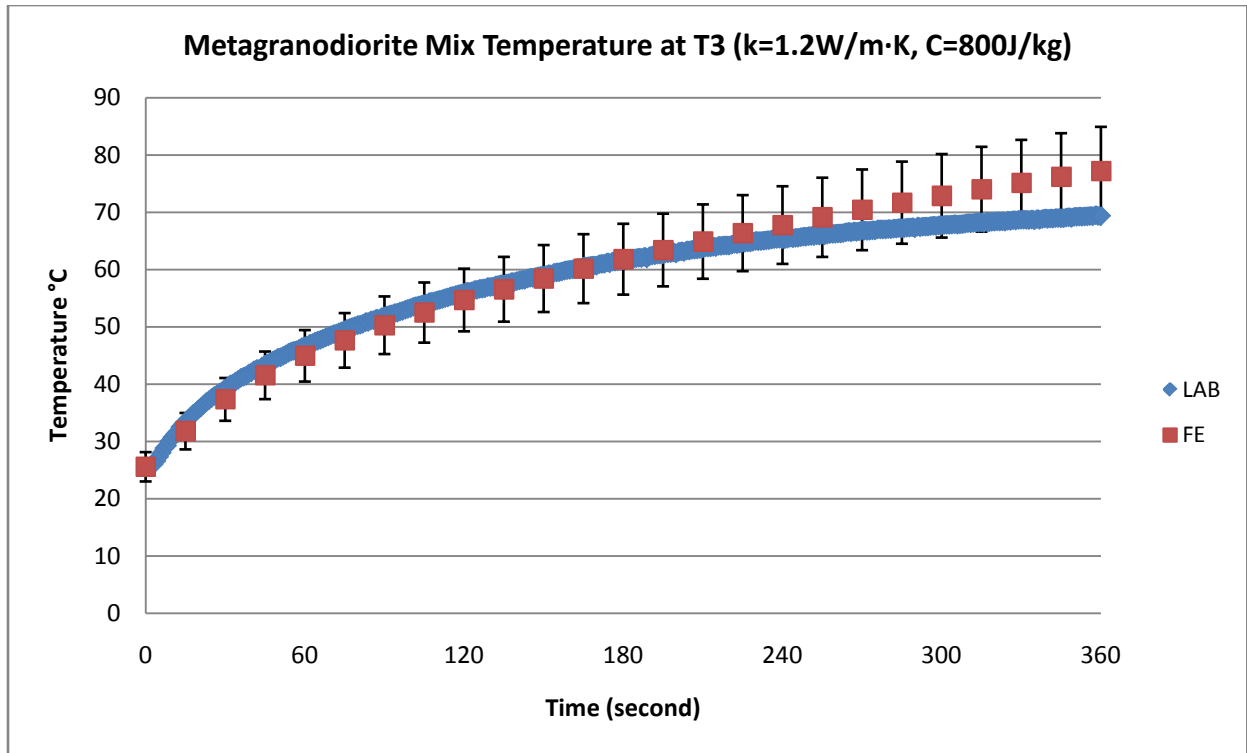


**Figure D-9 Metagranodiorite sample temperature at T3 (finite element predicted vs. laboratory results)**

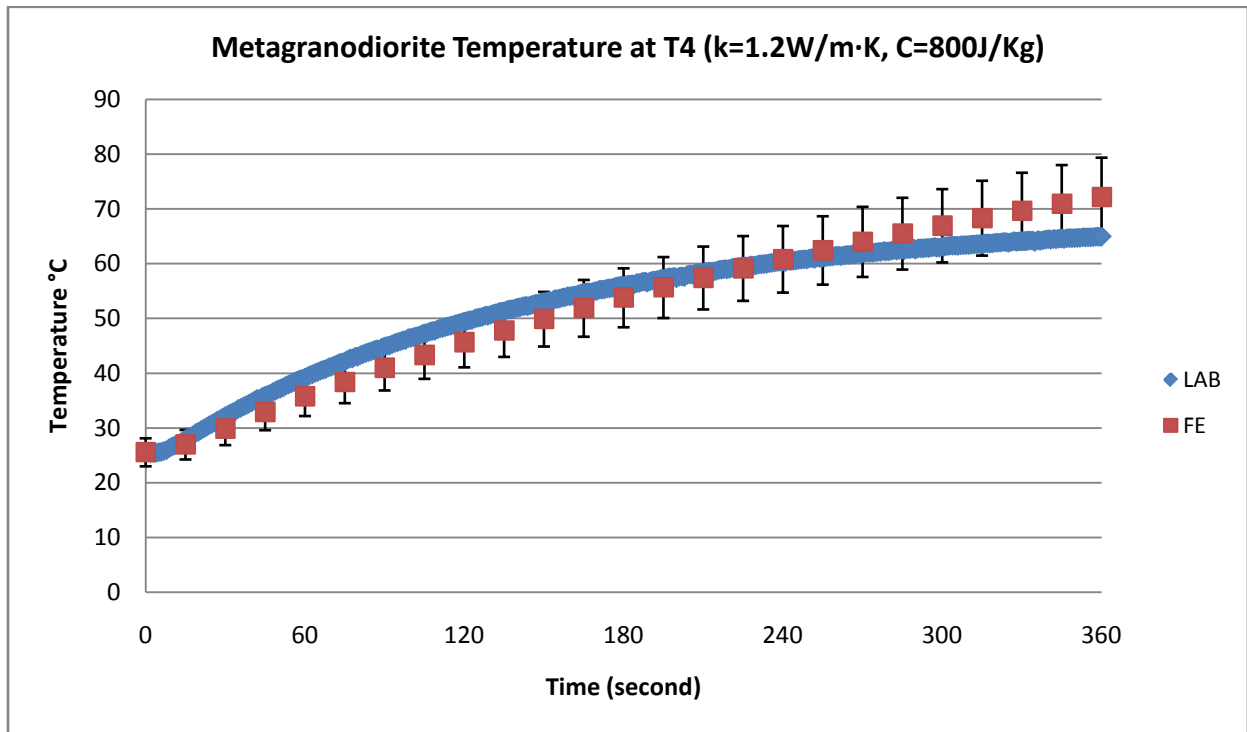


**Figure D-10 Metagranodiorite sample temperature at T4 (finite element predicted vs. laboratory results)**



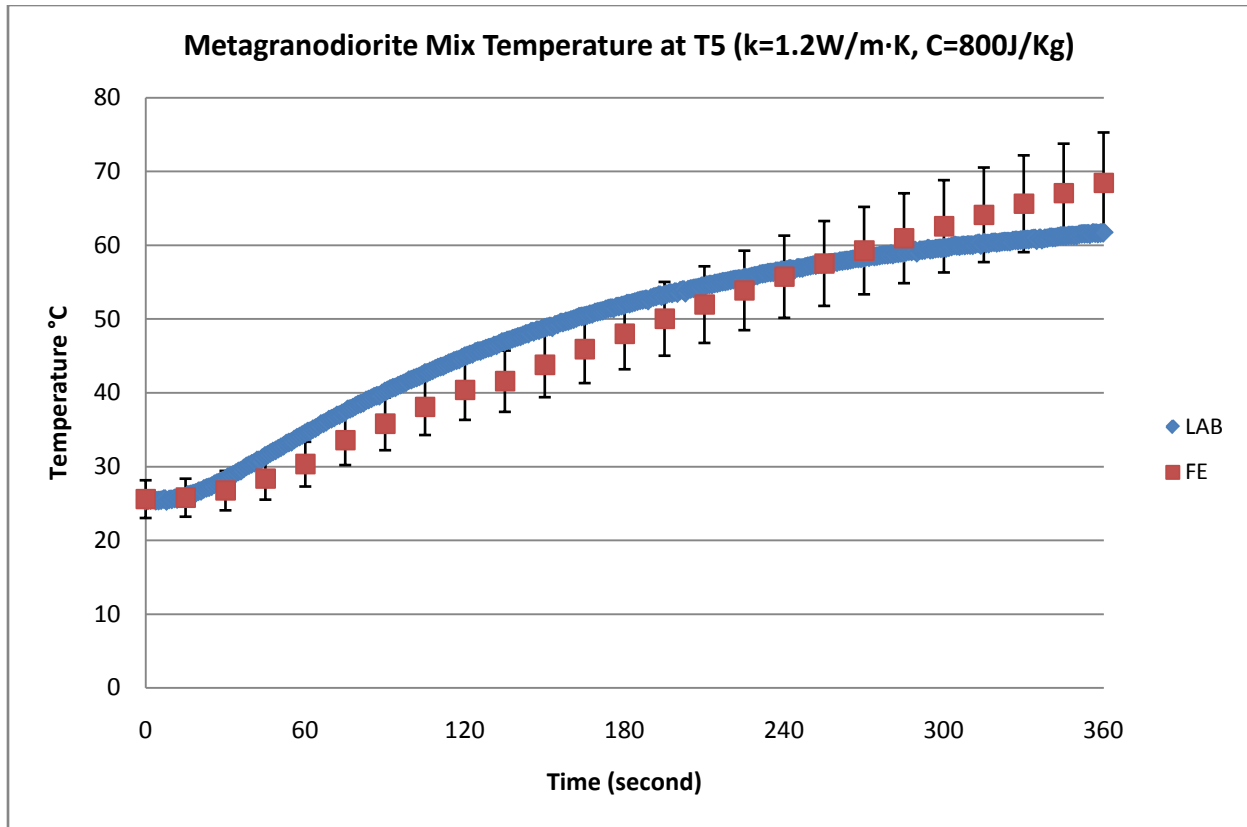


**Figure D-11 Metagranodiorite sample temperature at T5 (finite element predicted vs. laboratory results)**

## APPENDIX E

### SKETCH AND DIMENSION OF HAND-COMPACTED SAMPELS

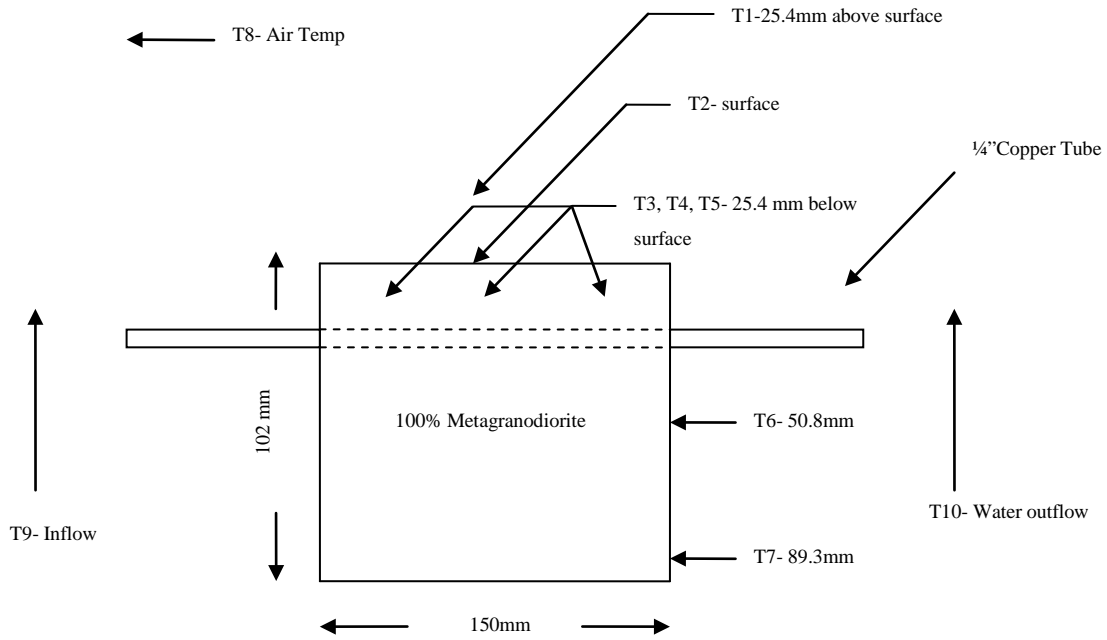


**Figure F-1 100% Metagranodiorite mix**

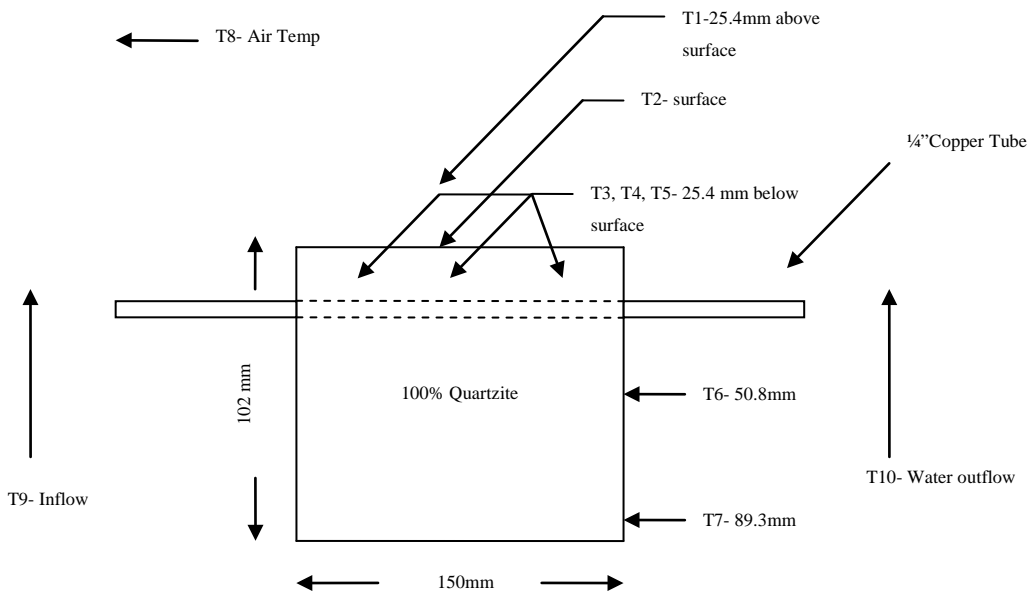


**Figure F-2 100% Quartzite mix**

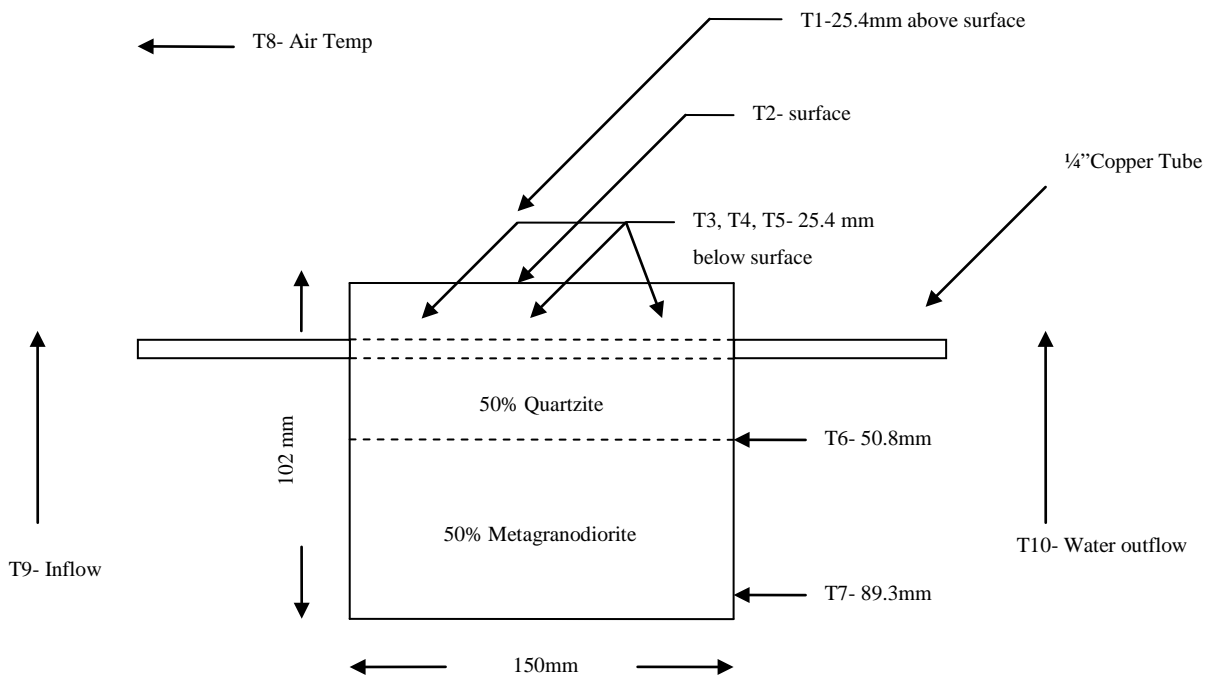


**Figure F-3 50% Quartzite on the top and 50% Metagranodiorite on the bottom**

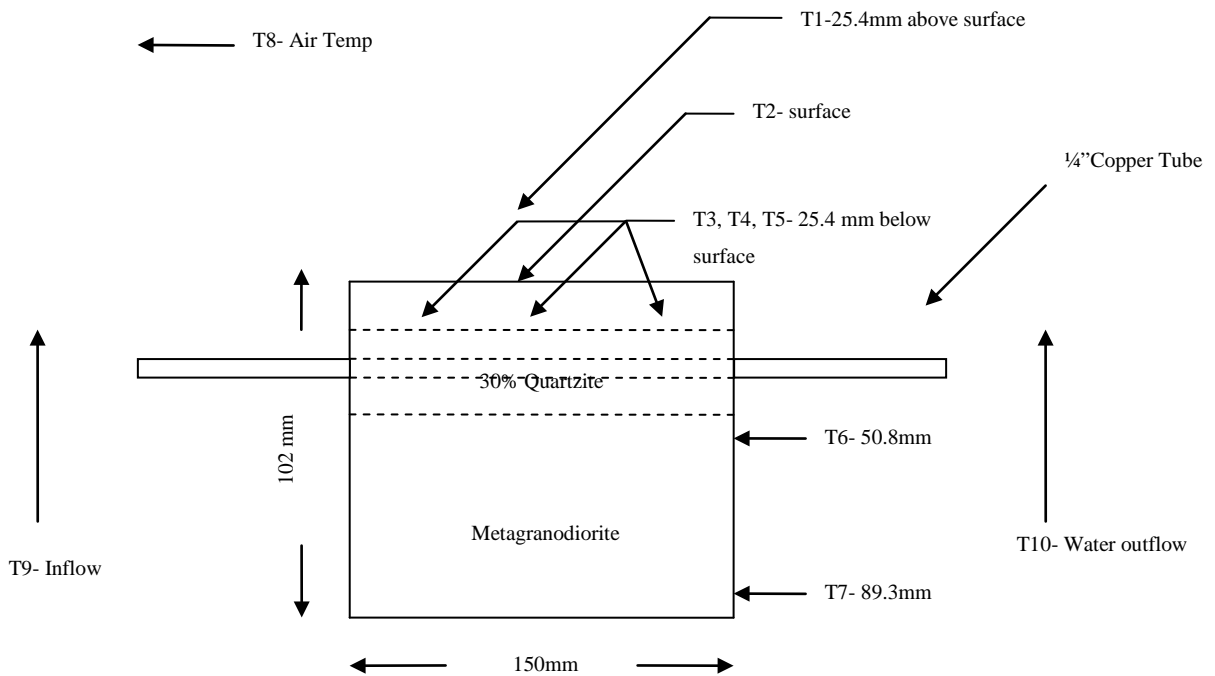


**Figure F-4 35% Metagranodiorite on the top, 30% quartzite in the center layer, and 35% Metagranodiorite on the bottom**

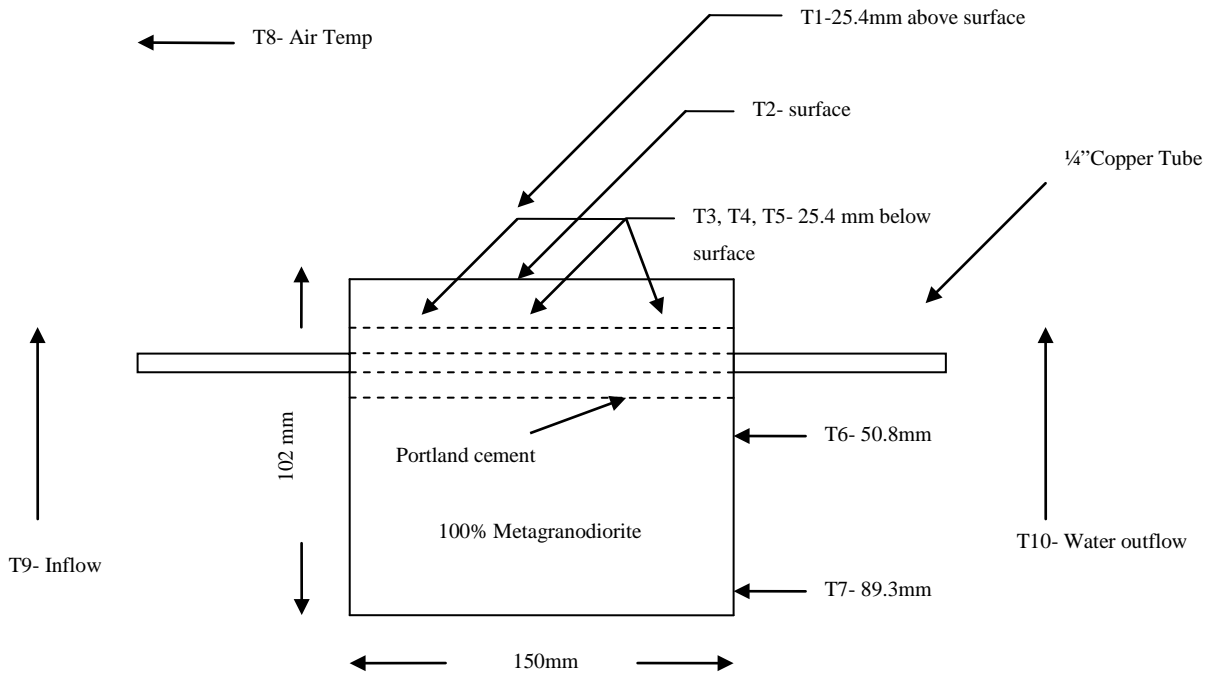


**Figure F-5 100% Metagranodiorite mix with Portland cement placed around copper pipe**

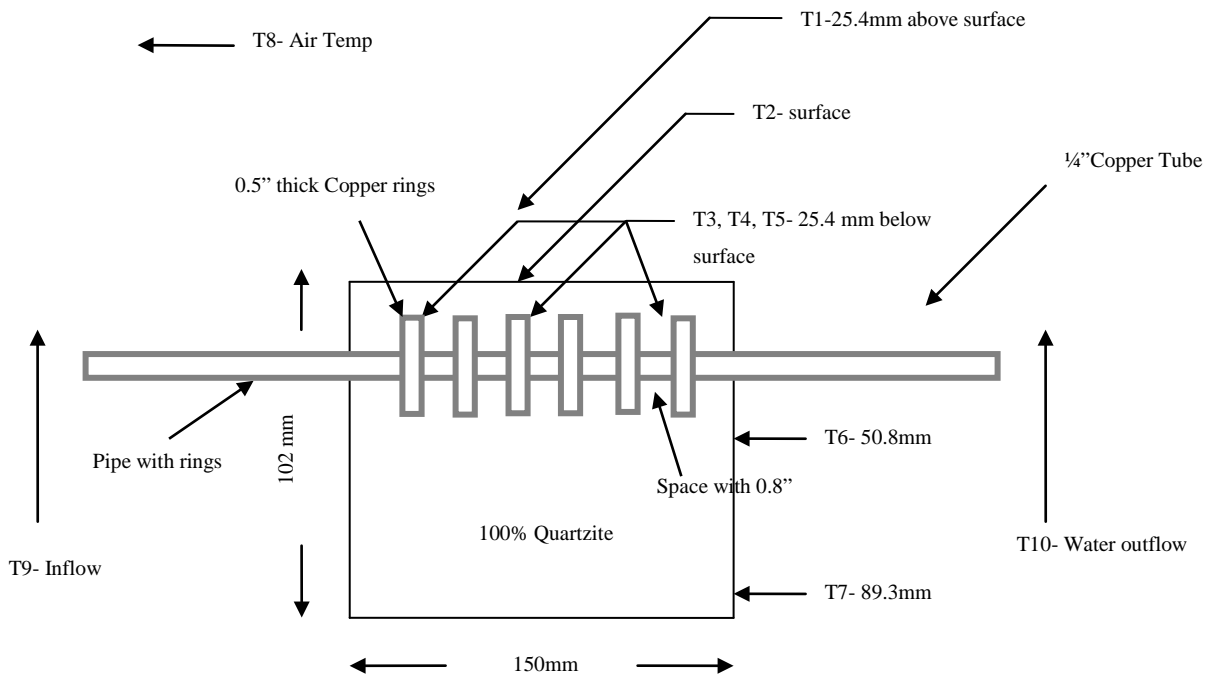


**Figure F-6 100% Quartzite mix with a copper pipe consists 6 rings**

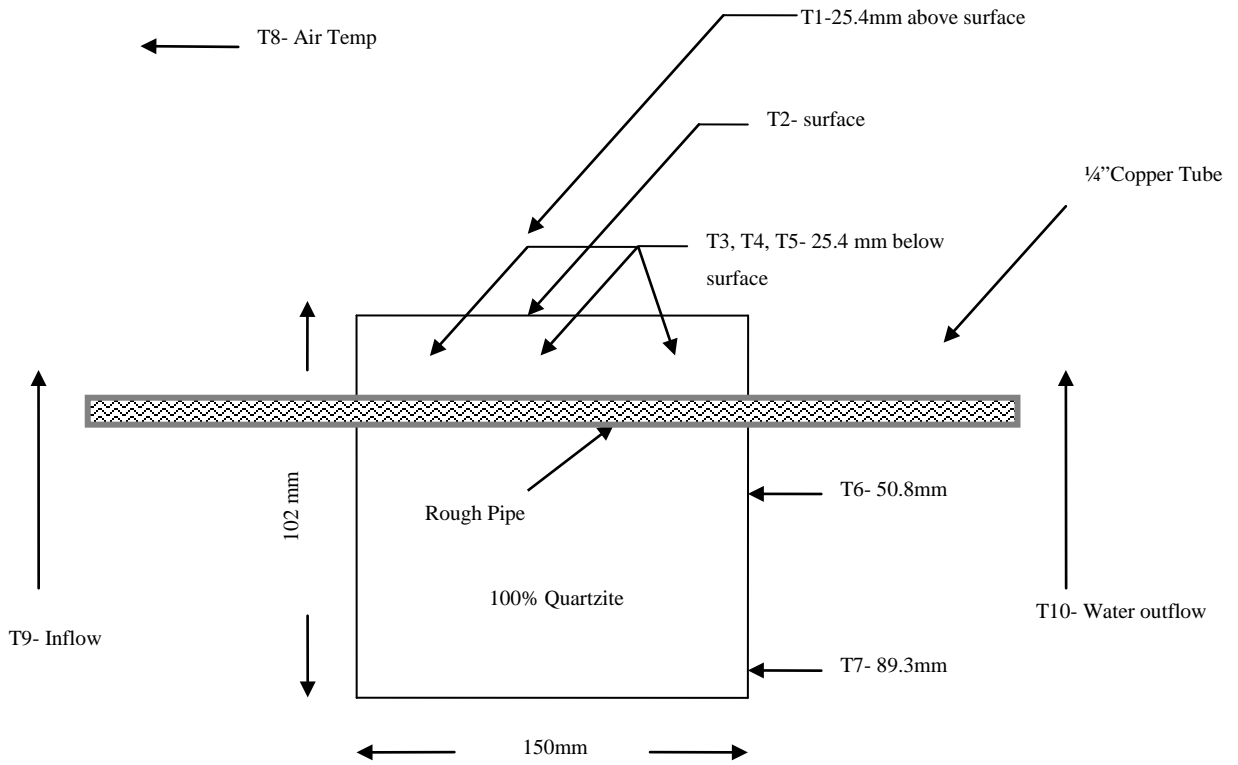


**Figure F-7 100% Quartzite mix with a rough surface copper pipe**

## APPENDIX F

### DETERMINE THERMAL PORPerties OF METAGRANODIORITE AND QUARTZITE (HAND-COMPACTED SAMPLES)

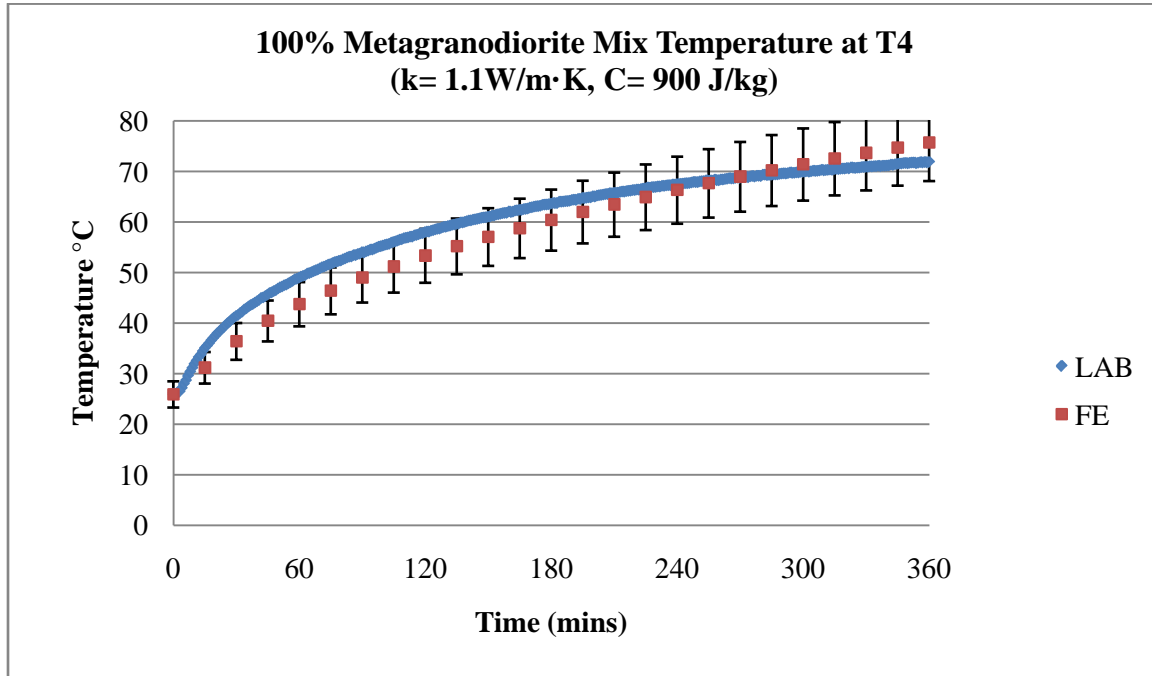


Figure E-1 Metagranodiorite sample temperature at T2 (finite element predicted vs. laboratory results)

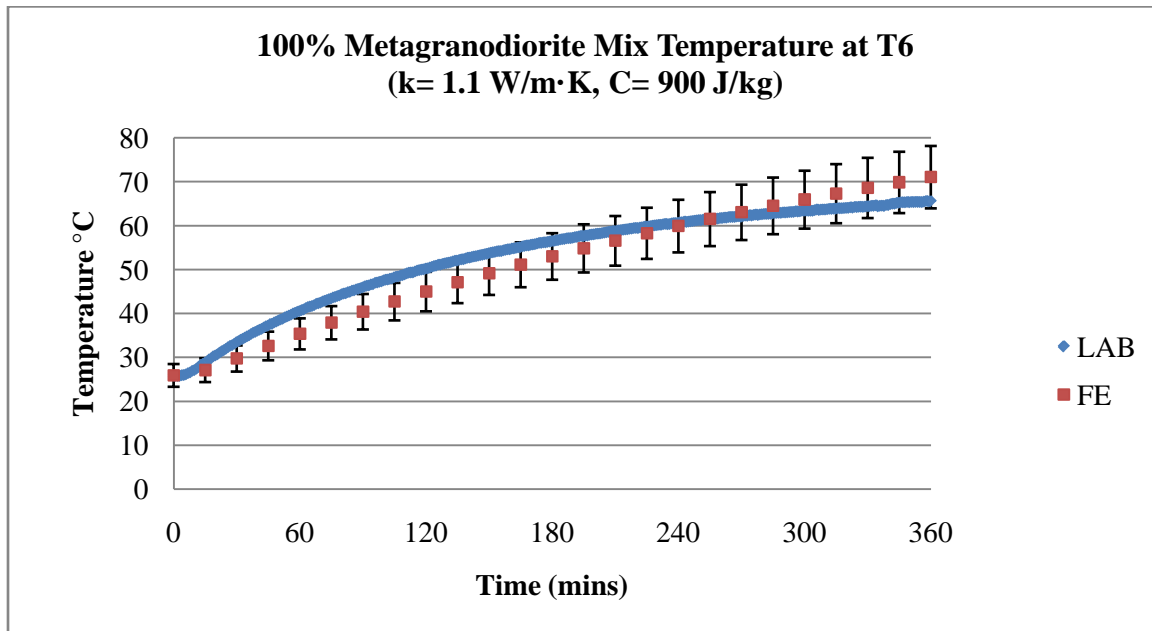
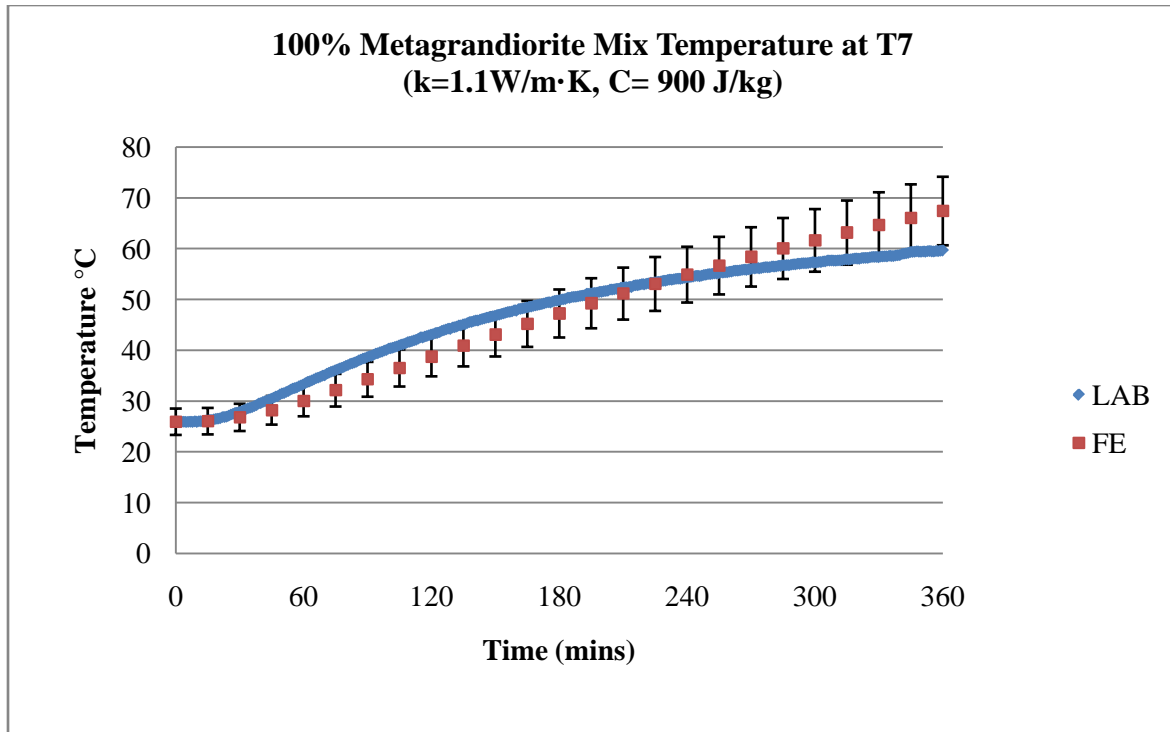
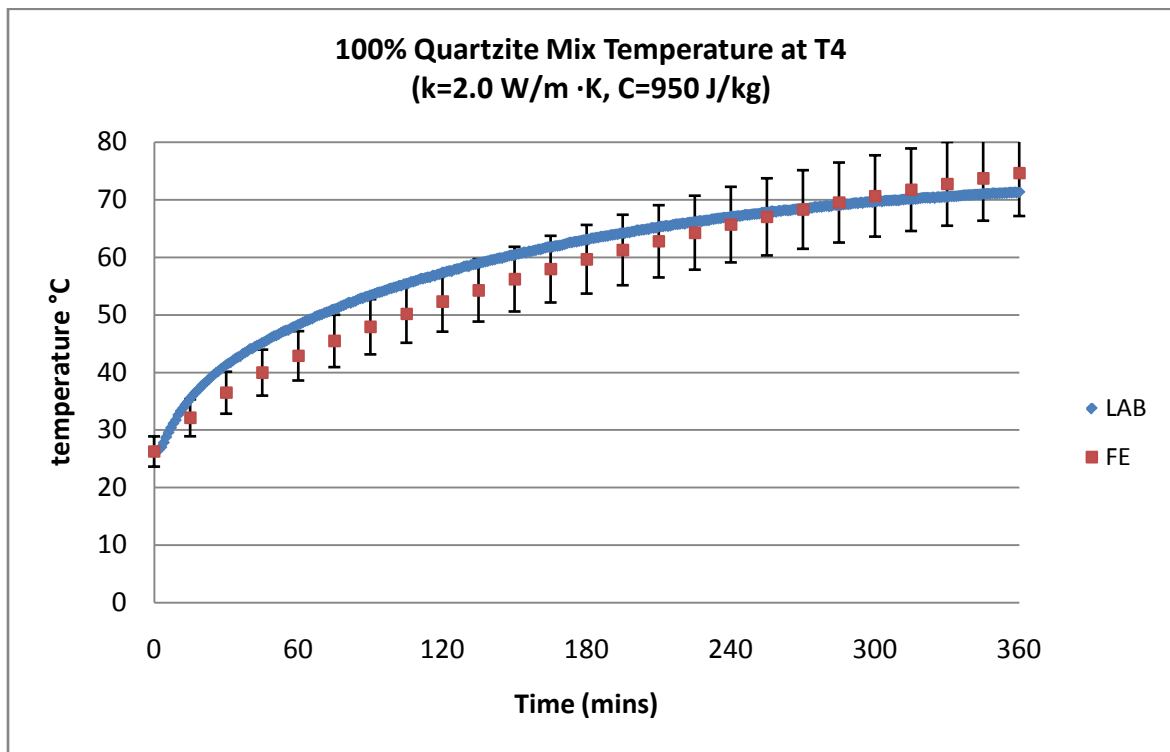


Figure E-2 Metagranodiorite sample temperature at T6 (finite element predicted vs. laboratory results)



**Figure E-3 Metagrandiorite sample temperature at T7 (finite element predicted vs. laboratory results)**



**Figure E-4 Quartzite sample temperature at T4 (finite element predicted vs. laboratory results)**

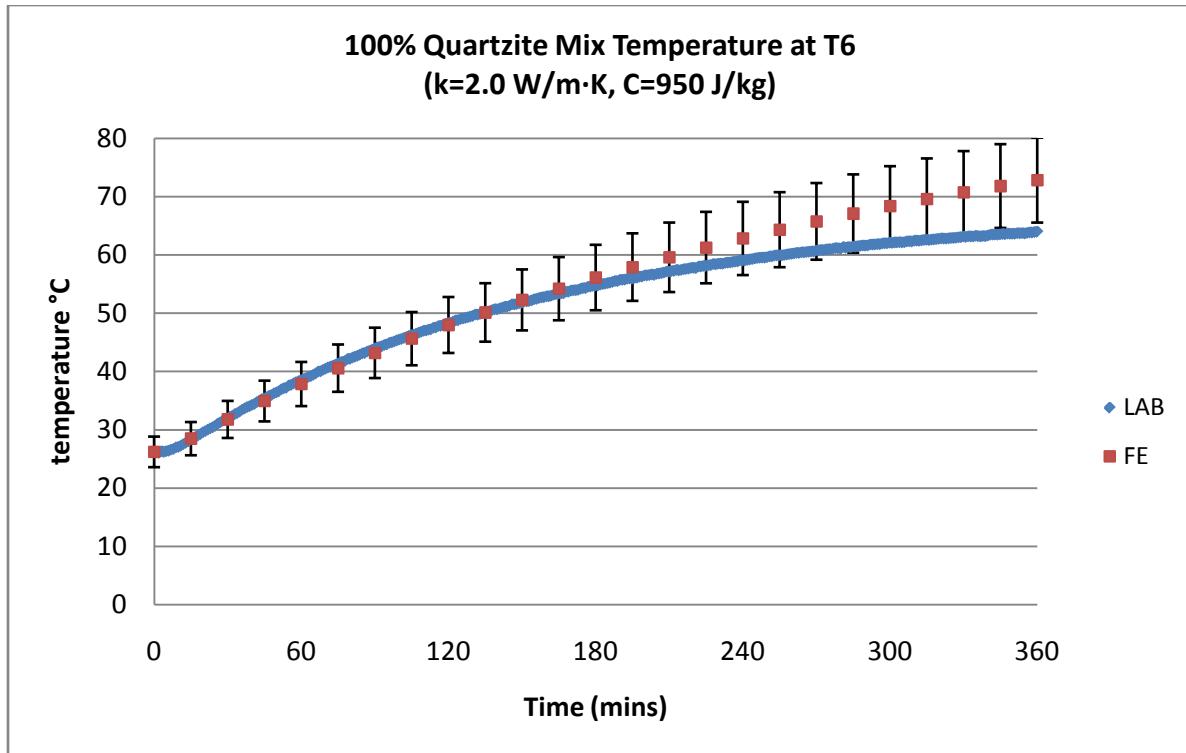


**Figure E-5 Quartzite sample temperature at T6 (finite element predicted vs. laboratory results)**

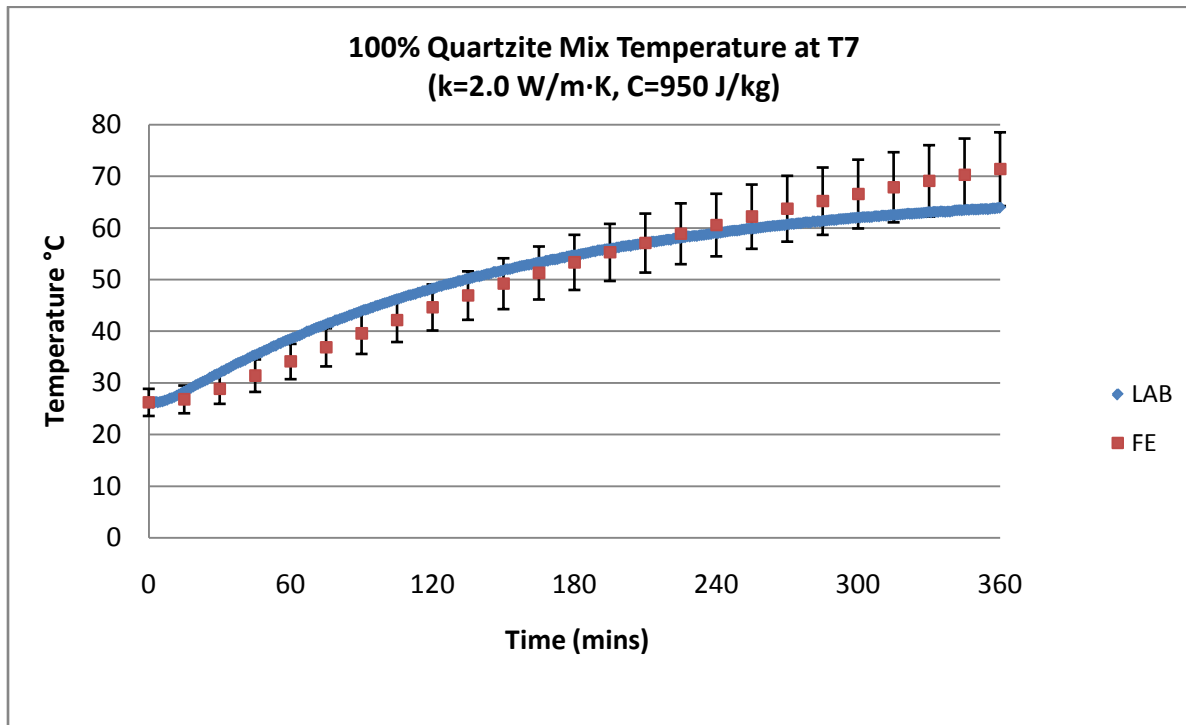


**Figure E-6 Quartzite sample temperature at T7 (finite element predicted vs. laboratory results)**



**APPENDIX G**  
**LARGE SCALE PAVEMENT (SLAB) PERPARATION**



**Figure G-1 Cart with thermocouple at the bottom**



**Figure G-2 Lay down of mix**



**Figure G-3 Compaction**



**Figure G-4 Fixing thermocouples**





**Figure G-5 Copper pipe frame**



**Figure G-6 Close-up of slab showing copper tube and thermocouples at different depths**



**Figure G-7 Completed slab ready for testing**